RICE UNIVERSITY

Synthesis and Tracking of Fluorescent and Polymerization-Propelled Single-Molecule Nanomachines

by

Jazmin Godoy Vargas

A THESIS SUBMITTED
IN PARTIAL FULFILLMENT OF THE
REQUIREMENTS FOR THE DEGREE

Doctor of Philosophy

APPROVED, THESIS COMMITTEE

James M. Tour, T.T. and W.F. Chao Professor of Chemistry, Professor of Computer Science, and Professor of Mechanical Engineering and Materials Science

Michael S. Wong, Professor of Chemical and Biomolecular Engineering and Chemistry

Angel A. Martí, Assistant Professor of Chemistry and Bioengineering

HOUSTON, TEXAS
August 2012

ABSTRACT

Synthesis and Tracking of Fluorescent and Polymerization-Propelled Single-Molecule Nanomachines

by

Jazmin Godoy Vargas

This dissertation describes the synthesis of molecular machines designed to operate on surfaces (nanocars) or in the solution phase (nanosubmarines), and the study of their diffusion using fluorescence techniques. The design of these molecular machines is aimed to facilitate monitoring of their movement and incorporation of a source of energy for propulsion.

To complement previous scanning tunneling microscopy studies of the translation of nanocars on surfaces, chapter 1 describes the synthesis of a family of fluorescently tagged nanocars. The nanocars were functionalized with a tetramethylrhodamine isothiocyanate (TRITC) fluorescent dye. Single-molecule fluorescence microscopy (SMFM) studies of one of these nanocars revealed that 25% of the nanocars moved on glass. The SMFM results also suggested that the dye hindered the mobility of the nanocars.

Seeking to improve the mobility, chapter 2 presents the synthesis of a new set of fluorescent nanocars, featuring a 4,4-difluoro-4-bora-3a,4a-diaza-*s*-indacene (BODIPY) dye embedded in their axles. The mobility of these inherently fluorescent nanocars on glass was nearly double than that of their TRITC-tagged predecessors.

Their diffusion was also studied on reactive-ion-etched glass, and amino-functionalized glass. The results showed that the mobility is affected by the substrate.

To equip the nanocars with an energy input for propulsion, two nanocars functionalized with an olefin metathesis catalyst were synthesized, as described in chapter 3. The catalytic activity of these nanocars toward ring-opening metathesis polymerization (ROMP) in solution was similar to that of their parent catalysts.

As an alternative approach to investigate if chemical propulsion through a ROMP process can be achieved at the molecular level, chapter 4 presents the synthesis of a fluorescent ROMP catalyst, termed a nanosubmarine, and the study of its diffusion using fluorescence correlation spectroscopy (FCS). FCS results showed an increase of 20 ± 7% in the diffusion constant of this nanosubmarine in presence of its fuel, *cis*,*cis*-1,5-cyclooctadiene.

Overall, the work accomplished in this dissertation constitutes a step forward toward development of easily tracked and highly mobile nanocars, and paves the way for the synthesis of truly nanosized chemically propelled molecular machines that operate in the solution phase.

Acknowledgments

I would like to sincerely thank those institutions and persons who have contributed to accomplishing the work presented in this dissertation.

Regarding institutions, I want to thank Rice University for the excellent preparation I received these four years. In particular, I want to thank the faculty and staff of the Chemistry Department, the Office of International Students and Scholars team, and the Center for Career Development staff. Also, thank you to the National Science Foundation, to the Welch Foundation, and to the NSF Penn State MRSEC program for financial support.

To Dr. Tour, my committee chair and research advisor, thank you for giving me the opportunity to work in your lab and, for all the guidance, correction, and training you have given me in all aspects of my academic formation.

Thank you to Dr. Wong and Dr. Marti, for taking the time to serve as my dissertation committee members.

Thank you to my qualifying exam committee members, Dr. Engel, Dr. Kolomeisky, and Dr. Ball, for the critical evaluation of my work and the guidance provided.

Thank you to my collaborator, Dr. Link, who directed all the fluorescence experiments. From his group, I want to thank Dr. Khatua, who conducted the single-

molecule fluorescence microscopy studies, and Lin-Yung Wang, who carried out the fluorescence correlation spectroscopy experiments.

Thank you Dr. Alemany for helping me to solve all the NMR challenges encountered during my research.

Thank you to Dr. James, Dr. Tour's lab manager, who converted my drafts into well-written manuscripts. Thank you also for the encouragement you gave me these four years Dustin. Thank you also to Polly Rocha, Dr. Tour's secretary, for taking care of me as a daughter. I will always remember your generosity toward my family.

Thank you Dr. Vives and Dr. Guerrero, my mentors in the lab, for training me in organic synthesis techniques and for all your advice during my first year at Rice; your instruction facilitated tremendously my incorporation into graduate school and into the Tour group.

Thank you to my colleagues in the Tour group for helping me with my research. In particular, thank you to the nanocars team, Pinn-Tsong, Edmund, and Victor. I have enjoyed working with you all so much.

Thank you to all the friends I have met in Houston, for making my life in graduate school much more enjoyable, and for being with me in the good and in the hard times. I came to graduate school alone, but now, thanks to you dear friends, I have a second family here in addition to my own.

Thank you to my parents, Rafael and Rosa, for your never-ending love and for supporting me to pursue my goals, even when that brought a physical separation between us. Thank you to Flavio and Andrés, my brothers, for their constant words of encouragement.

Thank you to my husband, Ciceron, for unconditional support and love, and Manuel, my precious son; both of you are my best reasons to never give up.

Above all, thank you to the Lord, my God, for every blessing received these four years, including the lab I joined.

Contents

List of Figures and Schemes

List of Tables

List of Symbols and Abbreviations

Ac	Acetyl
AFM	atomic force microscopy
ATP	adenosine triphosphate
ATR	attenuated total reflectance
Boc	*tert*-butoxycarbonyl
BODIPY	4,4-difluoro-4-bora-3a,4a-diaza-*s*-indacene
bp	boiling point
br	broad (spectral)
Bu	butyl
calcd	calculated
°C	degree Celsius
cm	centimeter(s)
cm^{-1}	wavenumbers
cod	*cis,cis*-1,5-cyclooctadiene
d	doublet
D	diffusion constant
δ	chemical shift in parts per million
DCC	*N,N'*-dicyclohexylcarbodiimide
dd	doublet of doublet
DMAP	4-(dimethylamino)pyridine
DMF	dimethylformamide
ε	extinction coefficient
eq	equation

Et	ethyl
FCS	fluorescence correlation spectroscopy
FRET	fluorescence resonance energy transfer
FTIR	Fourier transform infrared
g	gram(s)
h	hour(s)
HOMO	highest occupied molecular orbital
HRMS	high-resolution mass spectroscopy
Hz	hertz
IPA	isopropyl alcohol
J	coupling constant (in NMR spectroscopy)
KHMDS	potassium bis(trimethylsilyl)amide
L	liter(s)
λ_{abs}	maximum absorption wavelength
λ_{em}	maximum absorption wavelength
lit.	literature value
LUMO	lowest occupied molecular orbital
M	molar or moles per liter; mega
m	meter(s); mili; multiplet
MALDI	matrix-assisted desorption ionization
μ	micro
Me	methyl
Mes	2,4,6-trimethylphenyl (mesityl)
mg	milligram(s)
min	minute(s)

mol	mole(s)
mp	melting point
m/z	mass-to-charge ratio
NBS	*N*-bromosuccinimide
NHC	*N*-heterocyclic carbene
NIS	*N*-iodosuccinimide
nm	nanometer(s)
NMR	nuclear magnetic resonance
OPE	oligo(phenylene ethynylene)
p	pentet
Ph	phenyl
ppm	parts per million
%	percent
q	quartet (spectral)
ROMP	ring-opening metathesis polymerization
Φ_F	quantum yield of fluorescence
RIE	reactive ion etching
rt	room temperature
s	second(s); singlet (spectral)
SMFM	single-molecule fluorescence microscopy
STM	scanning tunneling microscopy
t	triplet (spectral)
TBAF	tetrabutylammonium fluoride
TEA	triethylamine
tert	tertiary

THF	tetrahydrofuran
TIPSA	triisopropylsilyl acetylene
TMS	trimethylsilyl
TMSA	trimethylsilyl acetylene
TOF	time-of-flight
TRITC	tetramethylrhodamine isothiocyanate
UV	ultraviolet
vis	visible

Chapter 1

Synthesis of Fluorescent Dye-Tagged Nanocars

Note: This chapter was copied in its total from a paper that I coauthored.[1] Reprinted with permission from reference 1. Copyright 2010 American Chemical Society. Some updated references were added, however.

1.1. Introduction

The construction of nanomachines that exhibit controlled movements in solution[2] have lead researchers to explore the design, synthesis and manipulation of more complex, highly functional devices that can be studied not only as ensembles, but as single entities.[3] Adapting the approach taken by biological systems, synthetic strategies often arrive at these structures via bottom-up construction, quickly generating nanometer-sized configurations from the most basic organic building blocks.[4] Concomitantly, the development of increasingly powerful imaging tools has enabled the study of the individual

rotational, translational and transportation dynamics of biological[5] and synthetic[6] nanomachines on surfaces.

Though interesting results have been obtained using other methods, [6b,6c] scanning tunneling microscopy (STM) remains unparalleled in its ability to resolve molecular-sized structures and to track the translational movement of nanoscale objects.[7] To this end, various groups have synthesized molecular motors and rotors,[8] landers,[9] wheel barrows,[10] nanowalkers,[11] and polyaromatic systems[12] for the purpose of observing their behavior on metallic surfaces. Similarly, our group has combined various nanocomponentry with molecular axles containing fullerene, *p*-carborane or organometallic wheels to construct a number of nanovehicles designed for directed motion and transport along atomically flat surfaces.[4a,13] Proof-of-concept experiments have shown, using STM, the directed movement of fullerene-wheeled nanocars on atomically flat Au(111) surfaces upon thermal and electrogradient activation.[14]

Although STM remains invaluable in the study of atomic detail and mechanism, the experimental conditions required are often less than ideal. The STM measurements are time consuming, conductive substrate surfaces must be used, and cryogenic and high-vacuum settings are often required to obtain clean images.[6b,15] Single-molecule fluorescence microscopy (SMFM), which has been widely used to track motion in biological systems,[16] offers a complementary technique to STM to study single molecules but on nonconductive surfaces. While SMFM does not have the atomic resolution of STM, nanometer localization is possible with large photon count rates, and fast measurement of distances as low as several nanometers has been realized on larger scan areas.[16,17]

To obtain accurate measurements of single molecules, it is of paramount importance to ensure that a) the molecules of interest fluoresce well and b) fluorescence from impurities, optics, and substrate surfaces is avoided.[18] Molecular design ensures that the first requirement is achieved, while the other is typically met by using excitation light with wavelengths greater than 500 nm since fewer molecules and substrates absorb in this region.[19] In our case, use of such light came with a caveat, as our previously synthesized *p*-carborane nanocars[20] do not possess absorption bands in this region. In general, molecules are tagged with a high-quantum-yield fluorescent dye to enable visualization at longer wavelengths. For our purposes, tetramethylrhodamine isothiocyanate (TRITC) was an attractive dye, as it possesses an excitation wavelength centered at the emission line of our Nd:Vanadate laser (532 nm), good quantum yield of fluorescence, and is appended to molecular structures via a simple urea formation by reaction with amines.[21] The attachment of TRITC to nanovehicular structures should afford the ability to more easily study the behavior of nanocars on nonconductive surfaces where ultra-high vacuum is not required.

In an effort to elucidate the mechanism of movement and control the directionality of nanovehicles via specific arrangements of their molecular axles and wheels, reported here are the syntheses and optical properties of five fluorescently tagged nanovehicles (Figure 1.1) specifically designed for SMFM. The molecules all bear TRITC fluorescent tags for excitation at 532 nm and *p*-carborane wheels. The main reasons for choosing *p*-carborane were 2-fold: (1) its ability to be substituted at both carbon atoms *para* to one another and (2) its stability towards many organometallic and photoinitiated processes.

As shown in Figure 1.1, nanocars **1** and **2** were designed to move along a straight trajectory due to the placement of the axles parallel to one another. Nanocar **3** was designed to move in a circular motion, a result of the axles angled towards each other. Analogous to our previous work with fullerene nanomachines, trimer **4** was designed to exhibit a pivoting motion, assessable by polarization experiments, with no translation. Due to the initial results from imaging trimer **4**,[22] nanocar **5** was designed to ascertain the effect of TRITC on wheel rotation and nanocar movement.

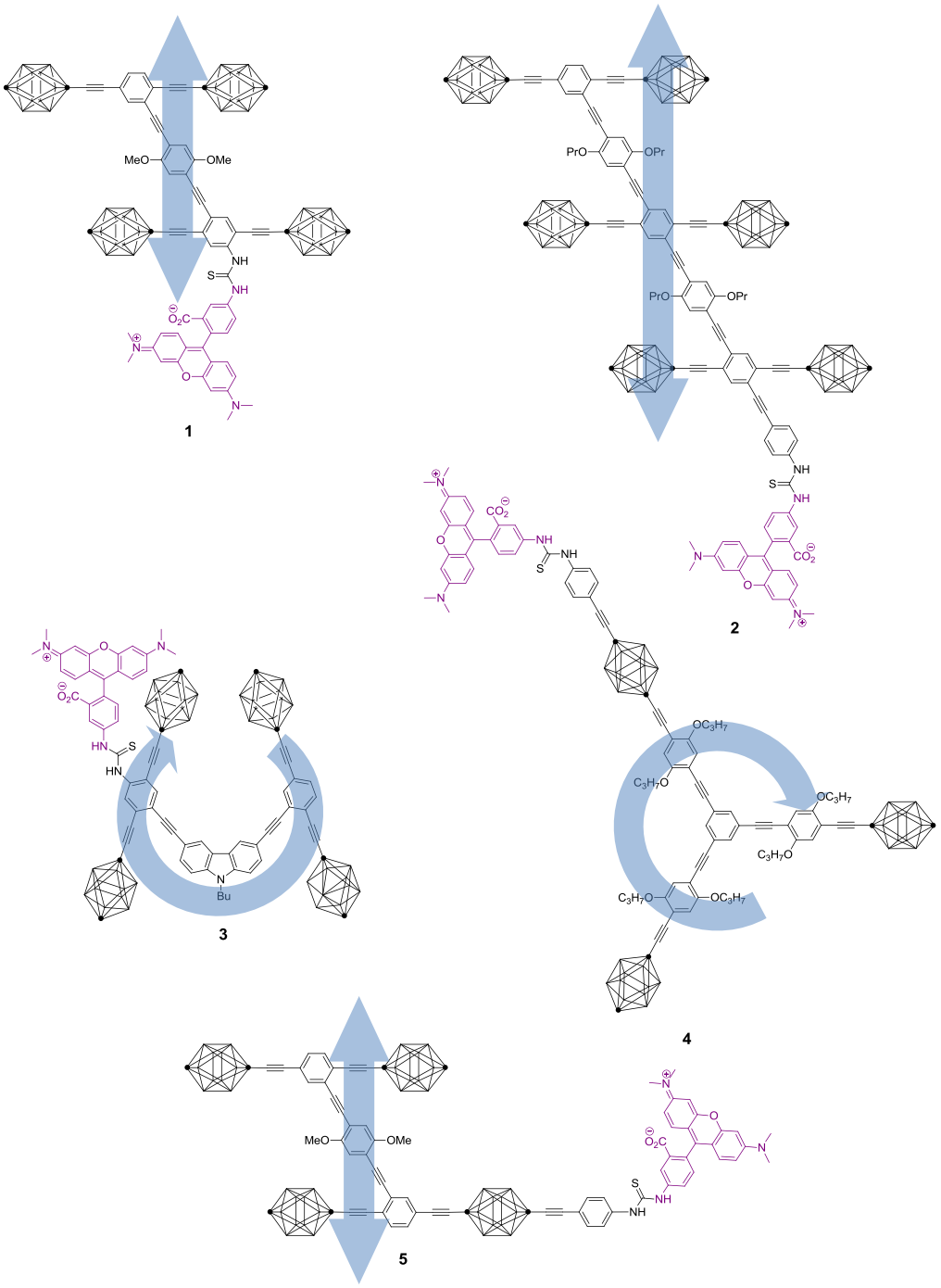

Figure 1.1.[1] The structures of the TRITC-tagged nanovehicles and their expected directional motion. Every vertex of the carborane wheel is BH except the darkened sites, where the outer (*para*) is CH and the inner (*ipso*) is an alkynyl-substituted C. Only the 5-isomer adduct of TRITC is shown.

1.2. Results and Discussion

1.2.1. Design and Synthesis

The strategy to arrive at each target adopted a convergent approach, where the inner components of each nanovehicle were synthesized and then attached to versatile *p*-carborane-containing axles. The design of nanocars **1**, **2**, and **3** dictated the use of two different molecular axles, with one axle bearing a pendant aniline for the attachment to amine-reactive TRITC. To arrive at trimer **4** and nanocar **5**, we used a convergent, symmetric approach to synthesize a late-stage intermediate, followed by statistical attachment of an extended aniline to one wheel for the purpose of TRITC tagging.

As depicted in Scheme 1.1, the synthesis of nanocar **1** began with the coupling of iodide axle **6**[23] to the methoxy-containing inner chassis **7**[24] using conventional Sonogashira conditions followed by deprotection to yield the terminal alkyne **8**. Immediate coupling with known aniline axle **9**[24] was performed to give the aniline nanocar **10**. In a final step, the aniline group of **10** was reacted with TRITC in DMF at elevated temperature, with triethylamine as base, to give target nanocar **1** in 16% yield. It is possible that the low yield was a result of steric bulk around the reacting aniline.

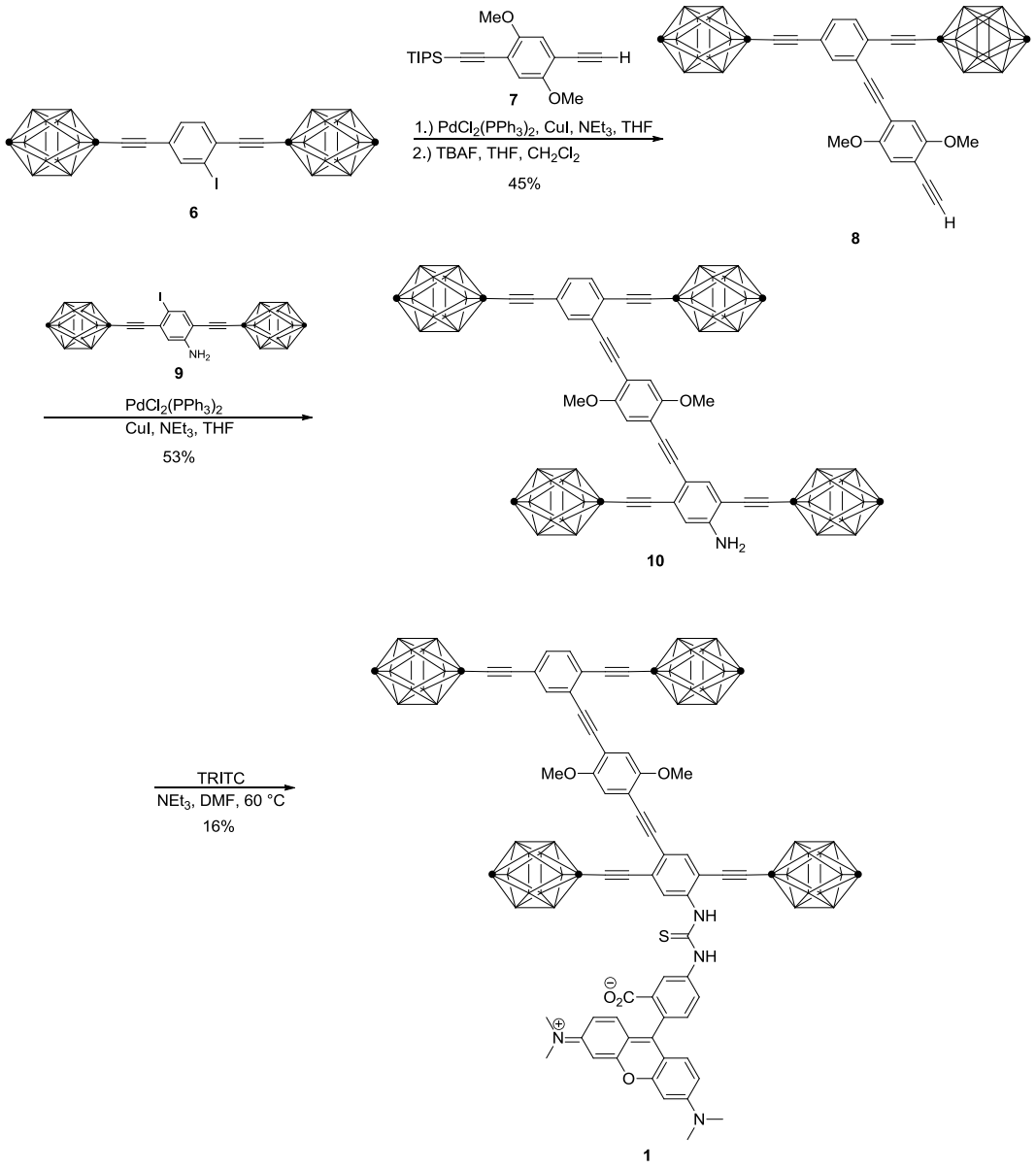

Scheme 1.1.[1] Synthesis of TRITC-tagged nanocar **1**.

SMFM results showed that the axle-tagged nanocar **1** has sufficient energy at room temperature to move along a glass surface at high rates of displacement.[22] This was an encouraging result, as the attachment of a relatively large fluorescent tag to the central

aromatic moiety of the axle of nanocar **1** demonstrated that transport on the nanoscale is not impeded by the TRITC.

The proposed mechanism[22] suggests that increasing the number of wheels (thereby increasing the surface interaction) should lead to a more controlled motion over a larger distance, with the possibility that the increase in the number of wheels would produce a concomitant decrease in the speed of the movement.

In an effort to improve controlled straight-line directionality via increased surface interaction, we synthesized an extended-chassis tagged nanovehicle with three axles and six wheels.

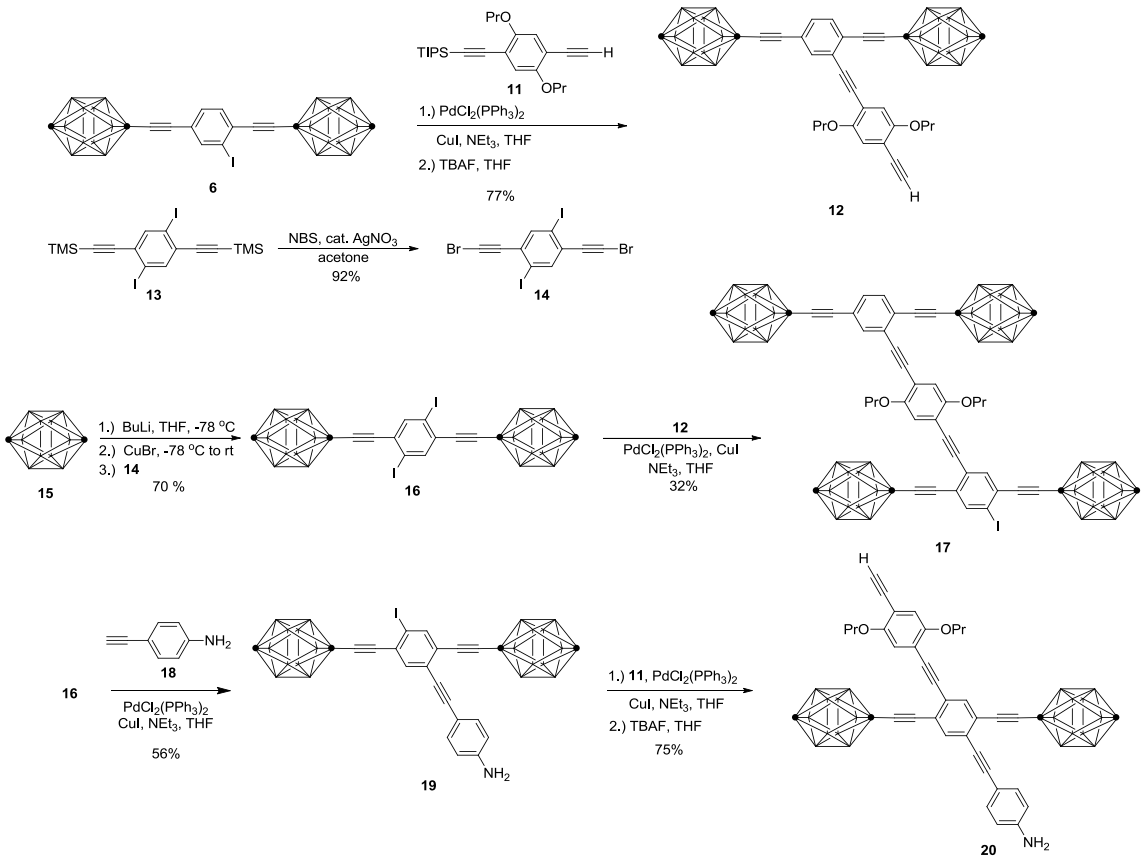

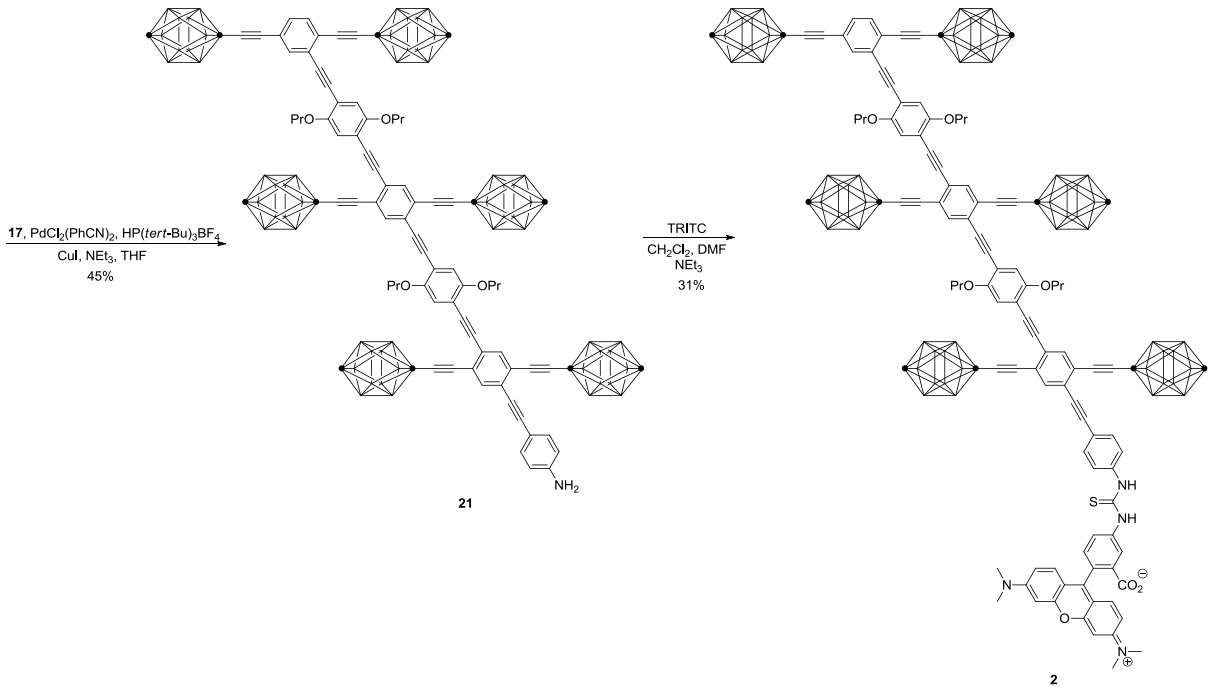

Scheme 1.2.[1] Synthesis of TRITC-tagged six-wheeled nanovehicle **2**.

As shown in Scheme 1.2, the synthesis was carried out beginning with an intermediate similar to that used for the synthesis of the four-wheeled tagged nanocar. After two straightforward steps, the half-nanocar was once again deprotected to give **12**. Separately, 1,4-diiodo-2,5-bis(trimethylsilylethynyl)benzene (**13**)[20] was subjected to desilyl bromination. The resultant alkynyl bromide **14** was coupled with *p*-carborane (**15**) via a carborane-copper adduct to give diiodide axle **16**. A statistical coupling between axle **16** and **12** gave the four-wheeled iodide nanocar **17**. It should be noted that in order to increase the solubility of the six-wheeled nanocar, the methoxy groups were replaced by more solubilizing propoxy groups. The extended aniline axle **20** was obtained in three steps starting with a statistical Sonogashira coupling between axle **16** and 4-ethynylaniline (**18**).[25] Subsequently, **19** was coupled to the chassis **11**[26] followed by deprotection to yield

the extended aniline axle with chassis **20**. A final Sonogashira coupling to four-wheeled iodo-nanocar **17** gave the six-wheeled extended aniline nanocar **21** in 45% yield. The use of the Fu-modified Sonogashira method[27] with the air-stable HP(*tert*-Bu)$_3$BF$_4$ proved to be exceedingly effective since conventional conditions using triphenylphosphine afford only a 18% yield. Room temperature attachment of the aniline to TRITC was then carried out again in DMF with triethylamine to provide the target six-wheeled tagged nanovehicle **2**.

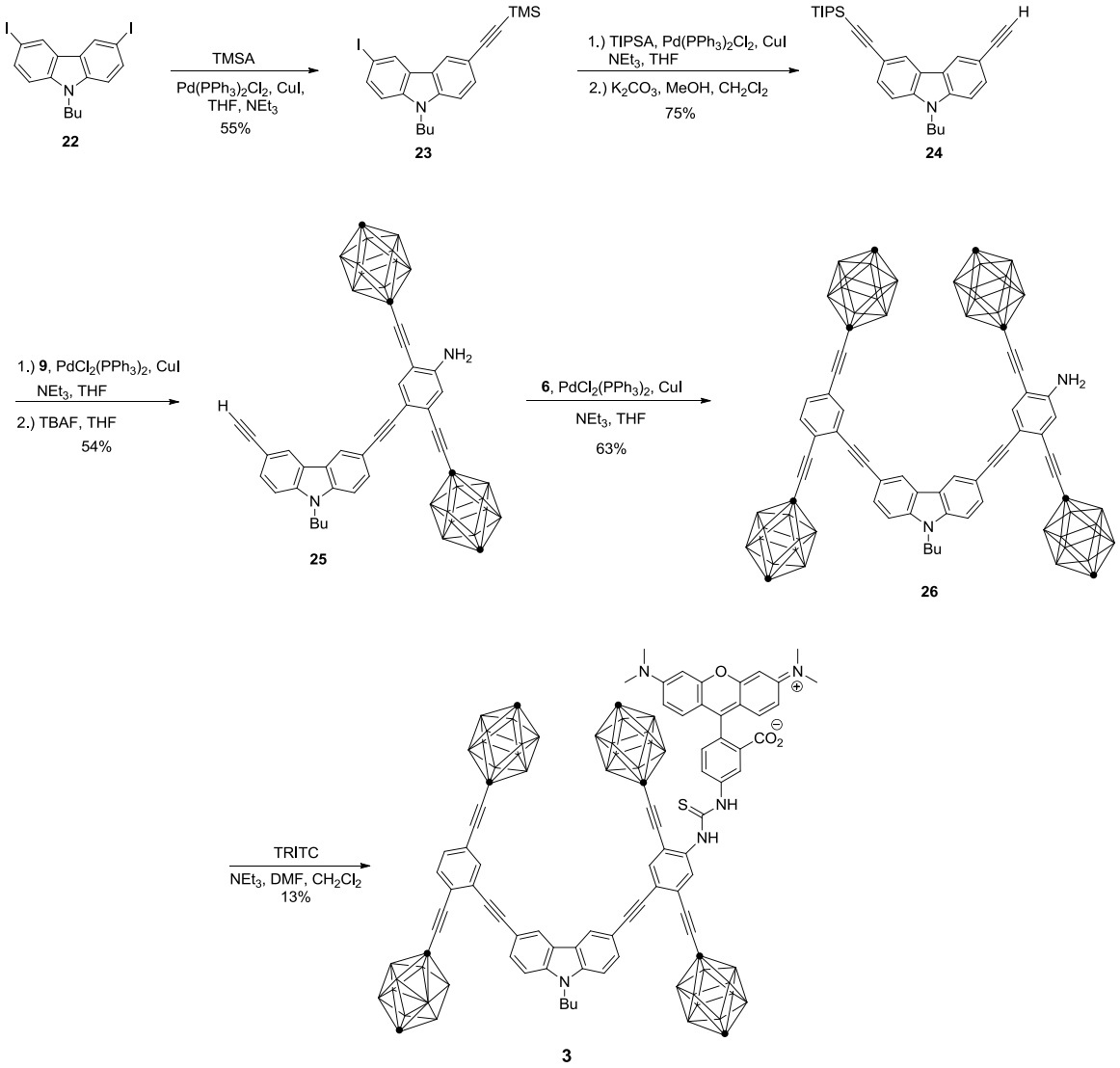

Scheme 1.3.[1] Synthesis of TRITC-tagged angled nanocar **3**.

While changing molecular design by increasing the number of axles and wheels should be a way to improve straight-line trajectory over longer distances, we also aimed to control the directionality by varying the angles of attachment to carborane-wheeled molecular components. Thus, we synthesized a nanocar with a bent chassis structure, designed to produce a circling motion (Scheme 1.3), by using a differentially substituted carbazole as the angling unit and a combination of iodide axle **6** and aniline axle **9**, the later being for the TRITC attachment. Although the expected circumference of the circle traveled by nanocar **3** would be smaller than the detection limit of our current SMFS setup, polarization anisotropy measurements have given very accurate rotational measurements, as demonstrated by previous studies on biological motors and our initial SMFS studies.[16,22] Therefore **3** was synthesized initially through two consecutive Sonogashira reactions that were carried out on the diiodocarbazole **22**.[28] The first coupling used 0.6 equiv of trimethylsilylacetylene (TMSA) to yield **23**. The coupling that followed, making use of the more robust triisopropylsilylacetylene (TIPSA), gave, after selective TMS deprotection, **24** in a combined yield of 75%. Alkyne **24** was further coupled to aniline axle **9** to give, after deprotection, the half-angled nanocar **25**. A further coupling with the iodo axle **6** gave the angled aniline nanocar **26**, that was then reacted with TRITC to give the tagged angled nanocar **3** in 13% yield. Again, the final TRITC coupling was the lowest yielding step of the sequence.

To further explore our ability to study directionality and molecular behavior, trimer **4** was designed and synthesized to have analogous properties to those of a previously studied fullerene-wheeled trimer, where the molecule undergoes no translation, but rotates about the central trialkynylated benzene.[14]

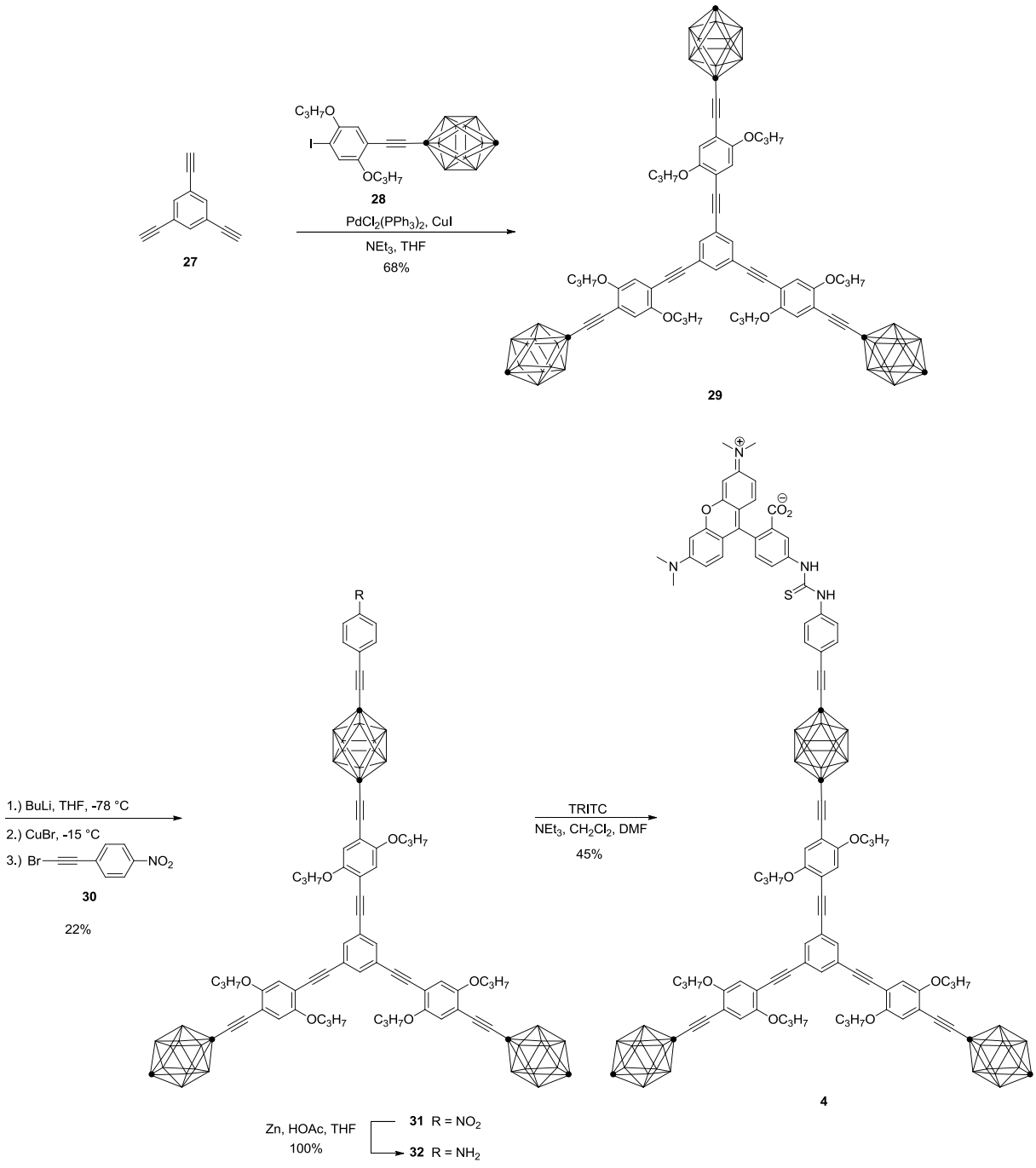

Scheme 1.4.[1] Synthesis of trimer **4**.

To synthesize trimer **4** (Scheme 1.4), we first attempted to use an early-stage statistical coupling to 1,3,5-tribromobenzene, followed by the coupling of a fully elaborated pendant aniline arm to the benzene core. This method, however, proved to be lengthy and low yielding. Using a late-stage statistical approach, trimer **4** was convergently constructed in four synthetic steps, where 1,3,5-triethynylbenzene **27**[20] was coupled to 3 equiv of known carborane arm **28**[20] to give the symmetrical trimer **29** in good yield. Initially, statistical attachment of the *p*-(bromoethynyl)nitrobenzene (**30**) unit was carried out under standard conditions for unsubstituted *p*-carborane functionalization: **29** was deprotonated using 1 equiv of *n*-butyllithium at −78 °C, followed by equilibration at room temperature for 30 min, then cooled again to −78 °C. Transmetalation was then performed by addition of CuBr and allowing the mixture to warm to room temperature, followed by coupling with the alkynyl bromide. Unfortunately, no product was obtained using this protocol and the starting material was almost totally recovered. In monosubstituted *p*-carboranes, Fox and co-workers have reported an influence of the substituent on the unsubstituted carbon.[29] Substitutions by electron-donating groups increase electron density on the *para*-carbon, following a Hammet σ_p plot with good correlation. Hence, modification of the procedure by lowering the temperature of the equilibration steps to −15 °C and increasing the equilibration times to 1 h led to formation of *p*-(bromoethynyl)nitrobenzene-substituted trimer **31** in 22% yield. The pendant nitro was then smoothly reduced using zinc powder and acetic acid in THF to provide the aniline **32** in quantitative yield. Reaction with TRITC provided fluorescently tagged trimer **4**. It should be noted that these less hindered aniline-TRITC coupling yields were considerably higher

than in the hindered aniline cases. Hence, a steric retardation on the coupling was likely the cause of the much lower yields of the nanocars **1** and **3**.

SMFM imaging of TRITC-tagged trimer **4** showed that the molecule is stationary, exhibiting no translational motion. While a lack of translational motion was expected, the molecule also failed to show any rotational movement by polarization anisotropy measurements.[22] This lack of rotation could be due to molecular design, where TRITC is attached via a pendant group emanating from one wheel, causing it to act as a brake.

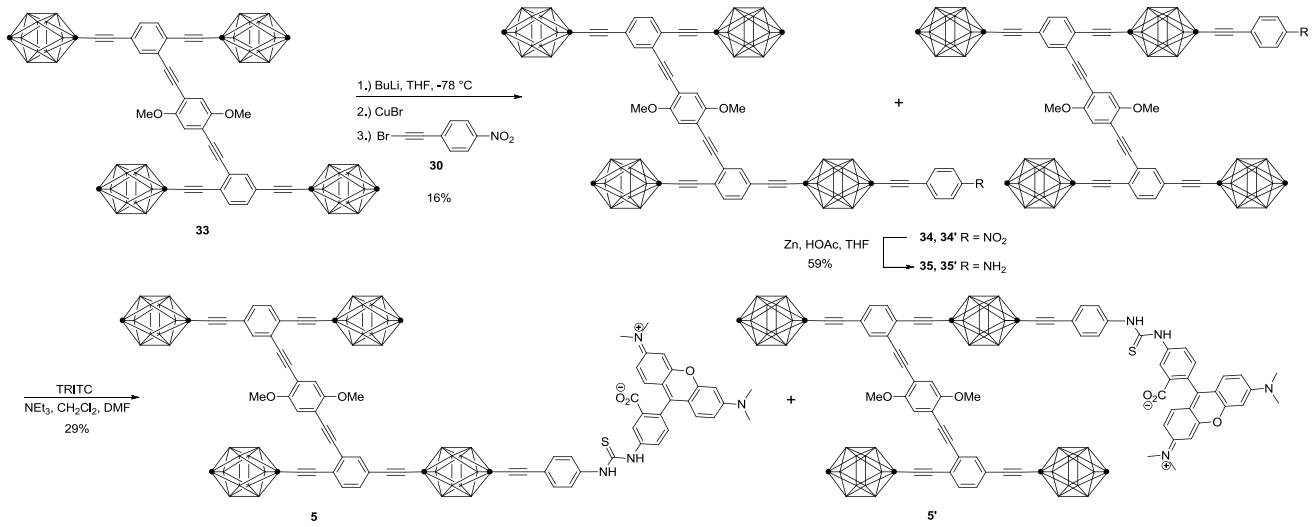

Scheme 1.5.[1] Synthesis of wheel-tagged nanocar **5**.

To test this hypothesis, we synthesized a wheel-tagged fluorescent nanocar (Scheme 1.5). Known nanocooper **33**[20] was subjected to statistical carborane substitution conditions, similar to those developed for the synthesis of the trimer, resulting in a 16% yield of **34** and **34'**; a lower yield when compared to the trimer **4** due to the statistical contribution of one extra wheel. The substitution of only one of the four wheels of nanocar **33** leads to two regioisomers, corresponding to substitution on the *ortho*- or *meta*-

positioned ethynyl carborane relative to the inner chassis. The two isomers are obtained as a 1:1 mixture that is inseparable by column chromatography. The current mechanism of translocation suggests that the two isomers should exhibit similar behavior on the glass surface, so the mixture was carried on through the rest of the synthetic sequence. Subsequent reduction to anilines **35** and **35'** and TRITC attachment gave wheel-tagged nanocars **5** and **5'** in a combined 29% yield. Initial SMFM results indicate that TRITC may indeed act as a brake, as only 5% of the nanocars exhibited translational motion, compared to 25% for nanocar **1**.

1.2.2. Optical Properties

We recently reported upon the solution-based ensemble absorption and fluorescence spectroscopy measurements of carborane-containing conjugated molecules.[20]

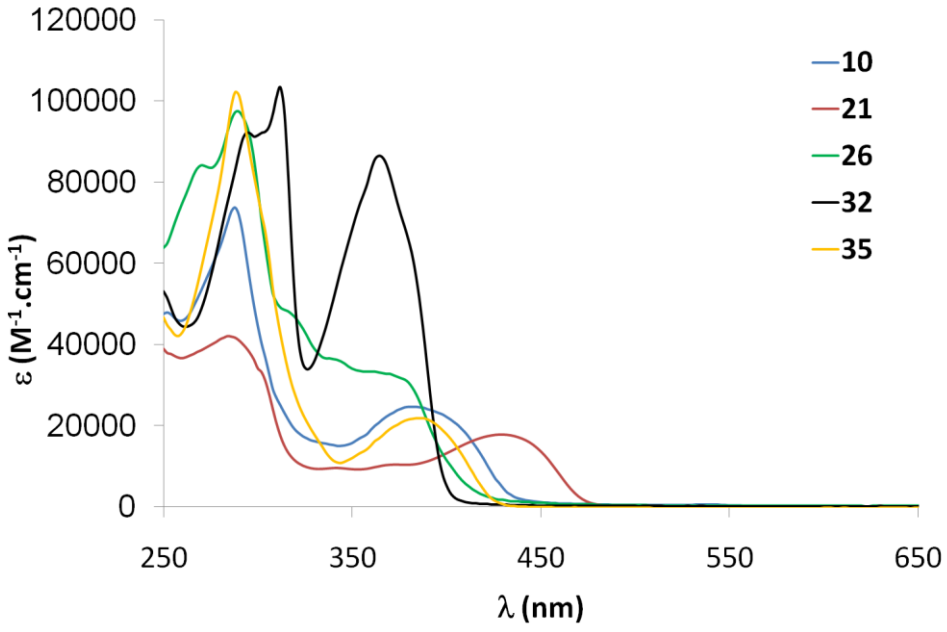

Figure 1.2.[1] UV–vis spectra of aniline substituted nanocars in $CHCl_3$.

As shown in Figure 1.2, the aniline precursors show two absorption maxima; the first one in the region λ_{max} = 288–294 and the second around 400 nm. A trend can be noted in the relative absorption energies of the alkoxy-functionalized nanovehicles, where increasing conjugation length (and the corresponding number of alkoxy units) causes a decrease in the HOMO–LUMO gap, red-shifting the λ_{max} values in the order **21 > 10** ≈ **35** > **26** > **32**. Despite the fact that the aniline precursors show relatively high quantum yield (Table 1.1), we are unable to use them in SMFM measurements, as none of these molecules can be excited at 532 nm, which our current setup requires.[22]

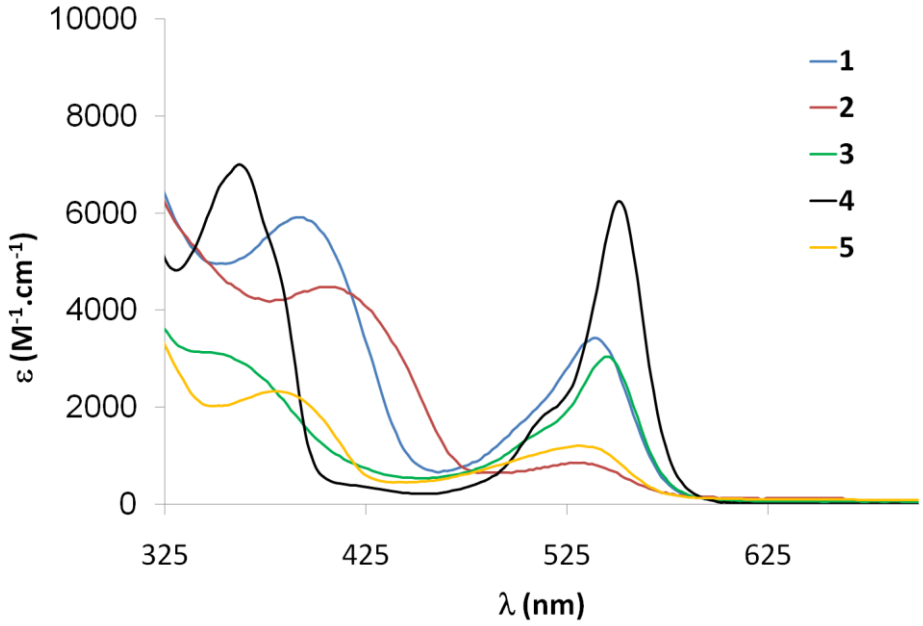

Figure 1.3.[1] UV–vis spectra of **1** – **5** in $CHCl_3$.

Although much synthetic effort is required to attach TRITC to our molecules, of paramount importance for the detection of single fluorescent molecules is the elimination of background fluorescence, in particular, fluorescence from luminescent impurities and

optical and substrate surfaces. Therefore, by using a fluorescent dye with > 500 nm wavelength excitation, we minimize undesired fluorescence, as fewer molecules and substrates are known to undergo absorption and emission in this region.[19]

As shown in the absorption spectra in Figure 1.3, upon TRITC attachment, all of the nanovehicles exhibit an absorption peak centered between 532 and 552 nm while still maintaining a UV-blue profile near-identical to the main nanovehicle structure. The absence of any vibronic structure is a clear indication that the presence of TRITC does not disturb the molecules' freedom of axle rotation in the ground state, a feature which is necessary for traversing sub-nanometer surface irregularities when related nanocars were studied on surfaces.[30]

It is interesting to note that the non-tagged aniline precursors all exhibit fluorescence quantum yields higher than those of their TRITC-tagged cousins (Table 1.1) along with very large Stokes shifts, indicating that large geometric changes occur in their excited states. Nevertheless the TRITC tagged nanocars display suitable quantum yields for SMFM studies on a glass surface, thereby fulfilling the intent of this synthetic approach.

Compound	Absorption maxima λ_{max}, (ε (M^{-1}, cm^{-1}))	λ_{em} (nm)	Φ_F[a]
1	286 (18 700), 392 (6 000), 540 (3 400)	564	0.37
2	286 (16 200), 406 (4 500), 532 (900)	554	0.22
3	286 (8 100), 546 (3 000)	564	0.40
4	312 (15 800), 362 (11 000), 552 (9 700)	569	0.47
5	288 (11 500), 380 (2300), 532 (1 200)	560	0.23
8	288 (73 800), 382 (24 600)	436	0.75
17	284 (25 000), 429 (17 800)	471	0.22
21	290 (97 000), 364 (33 100)	438	0.33
27	294 (92 000), 366 (86 100)	400	0.67
30	288 (102 200), 386 (21 800)	428	0.65

Table 1.1.[1] Optical properties of key compounds. [a]Determined in chloroform solution, ca. 1 × 10^{-7} M. Using rhodamine 6G as reference, Φ_F = 0.95 in EtOH, λ_{exc} = 488 nm. Excitation was done at the corresponding λ_{max} − 30 nm for compounds **1**-**5**. For other compounds excitation was done at λ_{max}.

1.3. Conclusions

The design and synthesis of five fluorescently tagged nanovehicles for the purpose of SMFM imaging is reported. The attachment of the TRITC fluorescent dye label to the nanovehicles was accomplished through the coupling of the isothiocyanate residue of the fluorophore with an aniline-functionalized nanovehicle. Several arrangements of axles on

the chassis were used to achieve different directional motion on the surface. Optical studies revealed that tagging with a TRITC moiety renders the nanocars suitable for SMFM studies with excitation at 532 nm.

1.4. Experimental Section

General Methods. ^{1}H NMR and ^{13}C NMR spectra were recorded at 400 or 500 and 100 or 125 MHz, respectively. Proton chemical shifts (δ) are reported in ppm downfield from tetramethylsilane (TMS). All MALDI-TOF experiments were performed using α-cyano-4-hydroxy-cinnamic acid as the matrix. FTIR spectra were recorded by deposition of the sample on a KBr plate from a CH_2Cl_2 solution using a Nicolet FTIR Infrared Microscope with ATR objective with 2 cm^{-1} slit. All reactions were performed under an atmosphere of nitrogen unless stated otherwise. Reagent grade tetrahydrofuran (THF) was distilled from sodium benzophenone ketyl. Triethylamine (TEA) and CH_2Cl_2 were distilled over CaH_2. CuBr was purified by suspension in hot MeOH and filtration. Trimethylsilylacetylene (TMSA) was donated by FAR Research Inc. or Petra Research. All other chemicals were purchased from commercial suppliers and used without further purification. Flash column chromatography was performed using 230–400 mesh silica gel from EM Science. Thin layer chromatography was performed using glass plates pre-coated with silica gel 40 F_{254} purchased from EM Science. The syntheses of compounds **6**,[23] **7**,[24] **9**,[24] **11**,[26] **13**,[20] **18**,[25] **22**,[28] **27**,[20] **28**,[20] and **33**[20] were performed according to formerly reported protocols.

General Procedure for the Coupling of a Terminal Alkyne with an Aryl Halide Using a Palladium-Catalyzed Cross-Coupling (Sonogashira) Protocol. To an oven-dried

round-bottom flask equipped with a magnetic stir bar were added the aryl halide, the terminal alkyne, $PdCl_2(PPh_3)_2$ (ca. 2 mol % per aryl halide), and CuI (ca. 4 mol % per aryl halide). A solvent system of TEA and/or THF was added depending on the substrates. Upon completion, the reaction was quenched with a saturated solution of NH_4Cl. The organic layer was then diluted with hexanes, diethyl ether or CH_2Cl_2, and washed with water or saturated NH_4Cl (1×). The combined aqueous layers were extracted with hexanes, diethyl ether, or CH_2Cl_2 (2×). The combined organic layers were dried over $MgSO_4$ and filtered, and the solvent was removed from the filtrate in vacuo to afford the crude product, which was purified by column chromatography (silica gel). Eluents and other slight modifications are described below for each compound.

General Procedure for Deprotection of TIPS-Protected Alkynes using TBAF. In a round-bottom flask equipped with a magnetic stir bar, the protected alkyne was dissolved in THF or CH_2Cl_2 ([protected alkyne] = 0.05 – 0.1 M). TBAF in THF (1.0 M, 1.1 equiv per alkyne) was added. The mixture was stirred at rt for 0.5 h or until the reaction was complete (monitored by TLC). Silica gel was added and the solvent was removed in vacuo. The resulting product loaded onto silica gel was then purified by column chromatography (silica gel as the stationary phase) to provide the product.

Compound 8. See the general procedure for the Pd/Cu coupling reaction. The materials used were **6**[23] (0.150 g, 0.28 mmol), **7**[24] (0.091 g, 0.27 mmol), $PdCl_2(PPh_3)_2$ (0.020 g, 0.028 mmol), CuI (0.012 g, 0.063 mmol), TEA (0.32 mL), and THF (4.0 mL) at rt overnight. The residue was purified by flash column chromatography in silica gel using 20% CH_2Cl_2 in hexanes; the product-containing fractions were combined, concentrated and

the residue was subjected to the general procedure for the deprotection of TIPS-protected alkynes. The materials used were the TIPS protected intermediate (0.090 g, 0.12 mmol), TBAF (0.20 mL, 1.0 M in THF) and CH_2Cl_2 (3 mL). The mixture was stirred at rt for 0.5 h, then passed through a silica plug using 30% CH_2Cl_2 in hexanes as eluent to yield **8** (0.071 g, 45%, two steps) as an off-white solid. FTIR (KBr) 2926, 2615, 1502, 1463, 1408, 1385, 1221, 1064, 1041, 785, 665 cm^{-1}; ^1H NMR (400 MHz, $CDCl_3$) δ 7.45 (d, J = 1.2 Hz, 1H), 7.22 (d, J = 8.0 Hz, 1H), 7.13 (dd, J_1 = 8.0 Hz, J_2 = 1.2 Hz, 1H), 7.04 (s, 1H), 7.01 (s, 1H), 3.97 (s, 3H), 3.89 (s, 3H), 3.44 (s, 1H), 3.40−1.45 (br m, 22H); ^{13}C NMR (100 MHz, $CDCl_3$) δ 154.5, 154.0, 135.3, 132.1, 131.0, 126.4, 123.8, 122.0, 116.2, 115.6, 113.4, 112.5, 91.8, 91.0, 90.4, 87.8, 82.8, 79.9, 77.9, 77.7, 60.3, 56.5, 56.4; EI-HRMS m/z calcd for $C_{26}H_{34}B_{20}O_2$ 595.4549, found 595.4552.

Compound 10. Terminal alkyne **8** (0.019 g, 0.031 mmol) was subjected to the general Sonogashira protocol, using **9**[24] (0.019 g, 0.034 mmol), $PdCl_2(PPh_3)_2$ (0.002 g, 0.003 mmol), CuI (0.001 g, 0.006 mmol), TEA (1 mL), and THF (5 mL) and stirred at rt overnight. The resulting residue was purified by column chromatography in silica gel with 25% CH_2Cl_2 in hexanes to give product **10** (0.017 g, 53%) as a light yellow solid. FTIR (neat) 3493, 3395, 3061, 2924, 2853, 2614, 2358, 2205, 1615, 1507, 1220, 1063, 727 cm^{-1}; ^1H NMR (400 MHz, $CDCl_3$) δ 7.47 (d, J = 1.5 Hz, 1H), 7.33 (s, 1H), 7.22 (d, J = 8 Hz, 1H), 7.13 (dd, J_1 = 8 Hz, J_2 = 1.5 Hz, 1H), 7.04 (s, 2H), 6.59 (s, 1H), 4.13 (br s, 2H), 3.98 (s, 6H), 2.6 (br m, 44H); ^{13}C NMR (100 MHz, $CDCl_3$) δ 154.0, 153.7, 147.4, 136.1, 135.3, 132.1, 130.8, 126.6, 125.1, 123.7, 121.9, 117.2, 115.5, 115.4, 115.3, 114.1, 112.2, 106.6, 92.7, 92.6, 91.6, 90.94, 90.91, 87.7, 77.9, 77.8, 74.8, 60.2, 56.3, 29.6; MALDI-TOF MS (+eV) m/z calcd for $C_{40}H_{59}B_{40}NO_2$ 1018.9, found 1019.0.

Nanocar 1. In a Schlenk tube under nitrogen, **10** (0.021 g, 0.026 mmol) was dissolved in DMF (1.0 mL) and Et_3N (0.1 mL). TRITC (5.8 mg, 0.013 mmol) in solution in DMF (1.0 mL) was added dropwise, and the mixture was heated to 60 °C, then stirred overnight in the dark. The solvents were then removed by rotary evaporation under reduced pressure. The resulting solid was purified by flash column chromatography in silica gel with 10% MeOH in CH_2Cl_2 to yield **1** as a purple solid (3 mg, 16%). FTIR (neat) 3349, 2960, 2921, 2851, 2615, 2359, 2342, 1737, 1596, 1510, 1249, 1185, 1112, 1039, 828, 803 cm^{-1}; ^1H NMR (400 MHz, $CDCl_3$) δ 7.98 (br s, 1H), 7.82 (d, J = 8.8 Hz, 1H), 7.48 (m, 1H), 7.15 (m, 6H), 6.82 (m, 2H), 6.69 (d, J = 8.6 Hz, 2H), 6.50 (d, J = 2.0 Hz, 2H), 6.42 (dd, J_1 = 7.6 Hz, J_2 = 2.0 Hz, 2H), 4.01 (s, 6H), 3.00 (s, 12H), 3.00−1.47 (br m, 44H). The material was not soluble enough for ^{13}C analysis. MALDI-TOF MS (+eV) m/z calcd 1461.9, found 1462.2.

Compound 12. See the general procedure for the Pd/Cu Sonogashira coupling reaction. The materials used were **6** (60 mg, 0.12 mmol), **11**[26] (53 mg, 0.13 mmol), $PdCl_2(PPh_3)_2$ (10 mg, 0.01 mmol), CuI (5.0 mg, 0.02 mmol), THF (10 mL), and Et_3N (5 mL) at rt overnight. The crude product was purified by column chromatography (silica gel, 10% CH_2Cl_2 in hexanes) to yield a white solid (70 mg). The product was then deprotected (see the general procedure for the removal of TMS/TIPS protecting groups). The materials used were the white solid (70 mg, 0.086 mmol), THF (10 mL), and TBAF (0.40 mL, 0.40 mmol) at rt. The resulting reaction mixture was passed through a plug of silica gel, and concentrated to afford the title compound **12** as a yellow solid (56 mg, 77%, two steps). FTIR (KBr) 2925, 2614, 1502, 1463, 1408, 1385, 1221, 1064, 1041, 785 cm^{-1}; ^1H NMR (500 MHz, $CDCl_3$) δ 7.38 (d, J = 1.6 Hz, 1H), 7.21 (d, J = 8.2 Hz, 1H), 7.12 (dd, J_1 = 8.2 Hz, J_2 = 1.6 Hz, 1H), 7.02 (s, 1H), 6.99 (s, 1H), 4.06 (t, J = 6.5 Hz, 2H), 3.97 (t, J = 6.5 Hz, 2H), 3.37 (s, 1H), 3.00−1.60 (br

m, 26H), 1.09 (m, 6H); ^{13}C NMR (126 MHz, $CDCl_3$) δ 154.2, 153.7, 135.4, 132.3, 131.0, 126.9, 123.8, 122.1, 118.0, 117.0, 114.2, 113.3, 91.8, 91.1, 91.0, 88.0, 82.7, 80.1, 78.1, 77.9, 71.25, 71.22, 69.6, 60.4, 22.85, 22.83, 18.3, 18.0, 17.9, 12.7, 12.5, 10.7, 10.6; EI-HRMS calcd for $C_{30}H_{42}B_{20}O_2$ 650.5191, found 650.5163.

Compound 14. A 25 mL round-bottom flask equipped with a magnetic stir bar was charged with **13**[20] (320 mg, 0.61 mmol) and acetone (10 mL). Then *N*-bromosuccinimide (229 mg, 1.28 mmol) and $AgNO_3$ (20 mg, 0.12 mmol) were added, in that order. The mixture was stirred in the dark at rt for 2 h, and then the solvent was removed in vacuum. The residue was passed through a silica gel plug using CH_2Cl_2 followed by Et_2O as eluents, to give **14** as a white solid (300 mg, 92%). *Caution: alkynyl bromides decompose over time and evolve HBr. Care should be taken when handling.* FTIR (neat) 3072, 2998, 2952, 2919, 2849, 1760, 1453, 1325, 1242 cm^{-1}; ^{1}H NMR (400 MHz, $CDCl_3$) δ 7.84 (s, 2H); ^{13}C NMR (100 MHz, $CDCl_3$) δ 142.4, 131.0, 99.1, 80.6, 58.1; EI-HRMS *m*/*z* calcd for $C_{10}H_2Br_2I_2$ 533.6613, found 533.6606.

Compound 16. An oven-dried 50 mL round-bottom flask equipped with a magnetic stir bar was charged with *p*-carborane (**15**) (85 mg, 0.59 mmol) and dry THF (8 mL). The solution was cooled to −78 °C and BuLi (0.24 mL, 0.60 mmol, 2.5 M in hexanes) was added dropwise. The solution was allowed to warm to room temperature and stirred for 30 min before it was cooled again at −78 °C. CuBr (121 mg, 0.84 mmol) was then added and the mixture was allowed to stir at rt for 30 min. A solution of **14** (150 mg, 0.28 mmol) in dry THF (10 mL) was added and the resulting mixture was allowed to stir overnight at rt. A few drops of water were added, and the mixture was filtered through a silica gel pad using

hexanes as the eluent. The resulting greenish solid was purified by column chromatography (silica gel, hexanes as eluent) to provide **16** (130 mg, 70%) as a white powder. FTIR (neat) 2613, 1463, 1384, 1123, 1084, 1064, 1047 cm^{-1}; ^{1}H NMR (400 MHz, $CDCl_3$) δ 7.63 (s, 2H), 3.40–1.60 (br m, 22H); ^{13}C NMR (100 MHz, $CDCl_3$) δ 141.7, 129.9, 99.7, 91.8, 79.8, 68.9, 61.0; EI-HRMS *m*/*z* calcd for $C_{14}H_{24}B_{20}I_2$ 663.1949, found 663.1944.

Compound 17. See the general procedure for the Pd/Cu Sonogashira coupling reaction. The materials used were **12** (58 mg, 0.09 mmol), **16** (98 mg, 0.15 mmol), $PdCl_2(PPh_3)_2$ (10 mg, 0.01 mmol), CuI (5.0 mg, 0.02 mmol), THF (10 mL), and Et_3N (5 mL) at rt overnight. The crude product was purified by column chromatography (silica gel, using 20% CH_2Cl_2 in hexanes) to yield **17** as a yellow solid (34 mg, 32%). FTIR (neat) 3060, 2963, 2925, 2851, 2618, 2237, 2335, 2214, 1501, 1466, 1422, 1369, 1263, 1219, 1062 cm^{-1}; ^{1}H NMR (500 MHz, $CDCl_3$) δ 7.74 (s, 1H), 7.40 (d, *J* = 1.6 Hz, 1H), 7.33 (s, 1H), 7.22 (d, *J* = 8.2 Hz, 1H), 7.14 (dd, J_1 = 8.2 Hz, J_2 = 1.6 Hz, 1H), 7.06 (s, 1H), 7.04 (s, 1H), 4.09 (t, *J* = 6.5 Hz, 4H), 3.10–1.60 (br m, 48H), 1.13 (m, 6H); ^{13}C NMR (126 MHz, $CDCl_3$) δ 153.94, 153.92, 142.0, 135.5, 135.4, 132.3, 131.0, 128.7, 127.0, 126.6, 124.8, 123.9, 122.2, 117.02, 116.98, 114.3, 113.7, 99.5, 92.4, 92.1, 91.9, 91.4, 91.2, 91.1, 88.0, 80.7, 78.2, 78.0, 77.4, 76.5, 71.22, 71.19, 69.7, 69.3, 60.9, 60.7, 60.5, 53.6, 34.9, 29.9, 22.98, 22.96, 22.88, 10.78, 10.77; MALDI-TOF MS (+eV) *m*/*z* calcd for $C_{44}H_{65}B_{40}IO_2$ 1185.8, found 1186.0.

Compound 19. See the general procedure for the Pd/Cu Sonogashira coupling reaction. The materials used were **16** (150 mg, 0.23 mmol), 4-ethynylaniline (**18**)[25] (16 mg, 0.13 mmol), $PdCl_2(PPh_3)_2$ (157 mg, 0.224 mmol), CuI (85 mg, 0.45 mmol), THF (30 mL), and Et_3N (10 mL) rt overnight. The crude product was purified by column chromatography

(silica gel, using 50% CH_2Cl_2 in hexanes) to yield **19** as a yellow solid (50 mg, 56%). ^{1}H NMR (400 MHz $CDCl_3$) δ 7.69 (s, 1H), 7.34 (d, *J* = 8.6 Hz, 2H), 7.32 (s, 1H), 6.66 (d, *J* = 8.6 Hz, 2H), 3.89 (br s, 2H), 3.10–1.60 (br m, 24H); ^{13}C NMR (100 MHz, $CDCl_3$) δ 147.5, 141.9, 134.9, 133.5, 128.4, 127.0, 124.6, 114.9, 111.9, 98.4, 97.0, 91.7, 90.9, 84.3, 80.9, 69.4, 60.7, 53.6, 29.9; EI-HRMS calcd for $C_{22}H_{30}B_{20}IN$ 652.3418, found 652.3410.

Compound 20. See the general procedure for the Pd/Cu Sonogashira coupling reaction. The materials used were **19** (30 mg, 46 μmol), **11**[26] (24 mg, 68 μmol), $PdCl_2(PPh_3)_2$ (5 mg, 5 μmol), CuI (2.5 mg, 10 μmol), THF (10 mL), and Et_3N (5 mL) at rt overnight. The crude product was purified by column chromatography (silica gel, hexanes / CH_2Cl_2 1:1) to yield a yellow solid (33 mg). The product was then deprotected (see the general procedure for the removal of TMS/TIPS protecting groups). The materials used were the white solid (33 mg, 35 μmol), THF (5 mL), and TBAF (0.10 mL, 0.10 mmol) at rt. The resulting reaction mixture was passed through a plug of silica gel, and concentrated to afford the title compound **20** as a yellow solid (26 mg, 75%, two steps). FTIR (neat) 3063, 2960, 2927, 2863, 2612, 2356, 2338, 2326, 2200, 2167, 2150, 2041, 1979, 1717, 1605, 1513, 1504, 1463, 1416, 1381, 1263, 1216, 1060 cm^{-1}; ^{1}H NMR (400 MHz $CDCl_3$) δ 7.39 (s, 1H), 7.37 (s, 1H), 7.35 (d, *J* = 8.6 Hz, 2H), 7.02 (s, 1H), 6.99 (s, 1H), 6.67 (d, *J* = 8.6 Hz, 2H), 4.06 (d, *J* = 6.5 Hz, 2H), 3.97 (d, *J* = 6.5 Hz, 2H) 3.91 (br s, 2H), 3.38 (s, 1H), 3.10–1.60 (br m, 26H), 1.09 (m, 6H); ^{13}C NMR (100 MHz, $CDCl_3$) δ 154.3, 153.8, 135.8, 135.2, 133.6, 126.6, 125.1, 123.7, 118.0, 117.0, 115.0, 114.2, 113.4, 112.0, 107.7, 92.0, 91.0, 85.0, 82.8, 80.2, 71.3, 68.2, 60.6, 22.9, 18.4, 18.0, 10.7; MALDI-TOF MS (+eV) m/z calcd for $C_{38}H_{47}B_{20}NO_2$ 765.5, found 766.6 [M + H].

Compound 21. See the general procedure for the Pd/Cu Sonogashira coupling reaction. The materials used were **17** (12 mg, 10 μmol), **20** (9 mg, 12 μmol), $PdCl_2(PhCN)_2$ (2 mg, 5 μmol), (*tert*-Bu)$_3$PHBF$_4$ (4.5 mg, 15 μmol), CuI (1 mg, 5 μmol), THF (5 mL), and Et_3N (2 mL) at 50 °C overnight. The crude product was purified by column chromatography (silica gel, using 50% CH_2Cl_2 in hexanes) to yield **21** as a fluorescent yellow solid (8.3 mg, 45%). FTIR (neat) 2925, 2857, 2612, 2480, 2359, 2332, 1725, 1655, 1460, 1377, 1257, 1066, 1036 cm^{-1}; ^{1}H NMR (500 MHz, $CDCl_3$) δ 7.42 (s, 2H), 7.40 (m, 3H), 7.36 (d, J = 8.6 Hz, 2H), 7.23 (d, J = 8.2 Hz, 1H), 7.14 (dd, J_1 = 8.2 Hz, J_2 = 1.6 Hz, 1H), 7.07 (s, 1H), 7.06 (br s, 3H), 6.68 (d, J = 8.6 Hz, 2H), 4.10 (t, J = 6.5 Hz, 8H), 3.91 (br s, 2H), 3.10–1.60 (br m, 74H), 1.13 (m, 12H); ^{13}C NMR (126 MHz, $CDCl_3$) δ 154.0, 153.9, 153.9, 147.5, 135.8, 135.5, 135.2, 133.6, 132.3, 127.0, 126.5, 125.9, 125.1, 123.9, 123.8, 123.7, 123.6, 122.2, 117.0, 114.9, 114.2, 113.9, 112.0, 97.5, 92.9, 92.3, 92.2, 91.2, 91.1, 91.0, 85.1, 71.2, 69.6, 60.5, 59.1, 53.6, 29.9, 23.3, 23.0, 22.9, 14.4, 14.3, 11.8, 10.8; MALDI-TOF MS (+eV) m/z calcd for $C_{82}H_{111}B_{60}NO_4$: 1822.5, found: 1823.6 [M + H].

Compound 2. In a Schlenk tube under nitrogen the aniline nanocar **21** (7 mg, 4 μmol) was dissolved in CH_2Cl_2 (1.0 mL) and Et_3N (0.1 mL). TRITC (1.7 mg, 4 μmol) in solution in DMF (1.0 mL) was added dropwise and the mixture stirred overnight at rt in the dark. The solvents were then removed by rotary evaporation under reduced pressure. The resulting solid was purified by column chromatography (silica gel, using 10% MeOH in CH_2Cl_2) to yield **2** as a purple solid (2.7 mg, 31%). FTIR (neat) 3349, 3193, 2919, 2851, 2609, 2362, 2338, 2158, 1979, 1716, 1661, 1610, 1510, 1451, 1410, 1372, 1216, 1177, 1104, 1062 cm^{-1}; ^{1}H NMR (400 MHz, $CDCl_3$) δ 8.28 (s, 2H), 7.66 (d, J = 9.1 Hz, 2H), 7.49 (d, J = 8.5 Hz, 1H), 7.47 (s, 1H), 7.09–7.03 (m, 5H), 6.99–6.97 (m, 2H), 6.69 (d, J = 8.9 Hz, 2H),

6.56–6.50 (m, 4H), 6.34–6.33 (m, 2H), 6.31 (d, *J* = 2.5 Hz, 1H), 6.02 (s 1H), 3.38 (t, *J* = 6.5 Hz, 8H), 3.08 (br s, 12H), 3.00–1.47 (br m, 74H), 1.13 (m, 12H). The material was not soluble enough for ^{13}C analysis. MALDI-TOF MS (+eV) *m*/*z* calcd for $C_{107}H_{132}B_{60}N_4O_7S$ 2266.9, found 2267.4.

Compound 23. See the general procedure for the Pd/Cu Sonogashira coupling reaction. The materials used were carbazole **22**[28] (3.54 g, 7.46 mmol), TMSA (0.64 mL, 4.48 mmol), $PdCl_2(PPh)_3$ (157 mg, 0.22 mmol), CuI (85 mg, 0.45 mmol), THF (30 mL), and Et_3N (10 mL) at rt overnight. The crude product was purified by column chromatography (silica gel, using 10% CH_2Cl_2 in hexanes) to yield **23** as a yellow solid (1096 mg, 55%). FTIR (neat) 3204, 3060, 2960, 2930, 2869, 2353, 2323, 2153, 1858, 1628, 1590, 1478, 1434, 1384, 1345, 1286, 1251, 1210, 1174, 1151, 1130, 1062, 1051, 1012, 897, 839, 803 cm^{-1}; ^1H NMR (400 MHz, $CDCl_3$) δ 8.34 (d, *J* = 1.7 Hz, 1H), 8.16 (d, *J* = 1.4 Hz, 1H), 7.69 (dd, J_1 = 8.6 Hz, J_2 = 1.7 Hz, 1H), 7.57 (dd, J_1 = 8.5 Hz, J_2 = 1.6 Hz, 1H), 7.28 (d, *J* = 8.5 Hz, 1H), 7.16 (d, *J* = 8.6 Hz, 1H), 4.22 (t, *J* = 8.0 Hz, 2H), 1.80 (quint, *J* = 7.5 Hz, 2H), 1.34 (sext, *J* = 7.5 Hz, 2H), 0.92 (t, *J* = 7.4 Hz, 3H), 0.29 (s, 9H); ^{13}C NMR (100 MHz, $CDCl_3$) δ 140.3, 140.1, 134.4, 130.4, 129.6, 125.1, 124.9, 121.6, 113.9, 111.2, 108.9, 106.5, 92.3, 82.0, 43.2, 31.2, 20.7, 14.0, 0.4; EI-HRMS *m*/*z* calcd for $C_{21}H_{24}INSi$ 445.0717, found 445.0723.

Compound 24. See the general procedure for the Pd/Cu coupling reaction. The materials used were **23** (1.07 g, 2.4 mmol), TIPSA (1.1 mL, 4.95 mmol), $PdCl_2(PPh_3)_2$ (84 mg, 0.12 mmol), CuI (46 mg, 0.24 mmol), TEA (10 mL), and THF (30 mL) at rt overnight. The residue was purified by flash column chromatography in silica gel with 5% CH_2Cl_2 in hexanes; the product-containing fractions were combined and concentrated. The TMS-

protected intermediate (983 mg, 1.97 mmol) was dissolved in 30 mL of a 1:1 mixture of THF and MeOH. Then K_2CO_3 (542 mg, 3.92 mmol) was added and the mixture was stirred at rt for 1.5 h. Then it was passed through a silica plug using 30% CH_2Cl_2 in hexanes as eluent to yield **24** (763 mg, 75%, 2 steps) as a yellow oil. FTIR (neat) 3311, 3042, 2954, 2942, 2886, 2863, 2721, 2359, 2329, 2147, 2099, 1870, 1678, 1628, 1602, 1478, 1466, 1378, 1351, 1289, 1251, 1213, 1151, 1133, 1068, 998, 918, 883, 803 cm^{-1}; ^1H NMR (400 MHz, $CDCl_3$) δ 8.23 (d, *J* = 1.2 Hz, 1H), 8.19 (d, *J* = 1.4 Hz, 1H), 7.60 (d, *J* = 1.5 Hz, 1H), 7.57 (d, *J* = 1.5 Hz, 1H), 7.31 (d, *J* = 7.1 Hz, 1H), 7.29 (d, *J* = 7.1 Hz, 1H), 4.26 (t, *J* = 8.0 Hz, 2H), 3.06 (s, 1H), 1.81 (quint, *J* = 8.0 Hz, 2H), 1.34 (sext, *J* = 8.0 Hz, 2H), 1.17 (s, 21 H), 0.92 (t, *J* = 8.0 Hz, 3H); ^{13}C NMR (100 MHz, $CDCl_3$) δ 140.6, 140.4, 130.2, 129.9, 124.8, 124.6, 122.3, 122.2, 114.3, 112.6, 108.9, 108.8, 108.2, 88.3, 84.7, 75.3, 43.0, 31.0, 20.4, 18.7, 13.8, 11.4; EI-HRMS *m*/*z* calcd for $C_{29}H_{37}NSi$ 427.2698, found 427.2695.

Compound 25. See the general procedure for the Pd/Cu coupling reaction. The materials used were **24** (30 mg, 69.6 μmol), **9**[24] (32 mg, 58.0 μmol), $PdCl_2(PPh_3)_2$ (6 mg, 8.7 μmol), CuI (3.3 mg, 17.4 μmol), TEA (1 mL), and THF (3 mL) at rt overnight. The residue was purified by flash column chromatography in silica gel with 20% CH_2Cl_2 in hexanes; the product-containing fractions were combined and concentrated. The product was then deprotected (see the general procedure for the removal of TMS/TIPS protecting groups). The materials used were the yellow solid (38 mg, 44.0 μmol), THF (5 mL), and TBAF (0.33 mL, 0.33 mmol) at rt. Then it was passed through a silica plug using 20% CH_2Cl_2 in hexanes as eluent to yield **25** (19.5 mg, 54%, 2 steps) as a yellow solid. FTIR (neat) 3487, 3393, 3308, 3060, 2957, 2925, 2871, 2606, 2362, 2329, 2226, 2208, 2105, 1613, 1596, 1498, 1478, 1381, 1357, 1286, 1210, 1151, 1127, 1062, 1006, 971, 886, 806, 753 cm^{-1}; ^1H NMR

(400 MHz, $CDCl_3$) δ 8.28 (dd, J_1 = 12.0 Hz, J_2 = 4.0 Hz, 2H), 7.60 (dd, J_1 = 12.0 Hz, J_2 = 4.0 Hz, 2H), 7.36 (t, J = 8.0 Hz, 2H), 7.31 (s, 1H), 6.61 (s, 1H), 4.30 (t, J = 8.0 Hz, 2H), 4.09 (s, 2H), 3.30–1.50 (br m, 25H), 1.42 (quart, J = 8.0 Hz, 2H), 0.96 (t, J = 8.0 Hz, 3H); ^{13}C NMR (100 MHz, $CDCl_3$) δ147.2, 140.9, 140.6, 135.7, 130.2, 129.7, 125.3, 125.1, 124.4, 122.7, 122.6, 117.6, 116.3, 114.3, 112.8, 109.1, 106.9, 92.9, 90.1, 85.6, 85.0, 78.4, 75.5, 75.2, 60.3, 43.1, 31.3, 20.7, 14.0; MALDI-TOF MS (+eV) m/z calcd for $C_{34}H_{42}B_{20}N_2$ 694.9, found 695.5.

Compound 26. See the general procedure for the Pd/Cu Sonogashira coupling reaction. The materials used were **25** (60 mg, 86.0 μmol), **6**[23] (42 mg, 78.0 μmol), $PdCl_2(PPh)_3$ (5.5 mg, 7.8 μmol), CuI (3.0 mg, 3.0 μmol), THF (4.5 mL), and Et_3N (1.5 mL) at rt overnight. The crude product was purified by column chromatography (silica gel, using 25% CH_2Cl_2 in hexanes) to yield **26** as a yellow solid (54 mg, 63%). FTIR (neat) 3493, 3390, 3066, 3010, 2927, 2654, 2609, 2362, 2323, 2207, 2158, 1610, 1590, 1493, 1460, 1384, 1351, 1286, 1239, 1210, 1148, 1127, 1062, 1004, 968, 877, 806 cm^{-1}; ^{1}H NMR (400 MHz, $CDCl_3$) δ 8.37 (dd, J_1 = 12.0 Hz, J_2 = 4.0 Hz, 2H), 7.66 (dd, J_1 = 12.0 Hz, J_2 = 1.7 Hz, 1H), 7.64 (dd, J_1 = 12.0 Hz, J_2 = 4.0 Hz, 1H), 7.41 (m, 3H), 7.24 (s, 1H), 7.24 (d, J = 4.0 Hz, 1H), 7.11 (dd, J_1 = 8.0 Hz, J_2 = 4.0 Hz, 1H), 6.62 (s, 1H), 4.33 (t, J = 8.0 Hz, 2H), 4.08 (br s, 2H), 3.40–1.40 (br m, 48H), 0.99 (t, J = 7.4 Hz, 3H); ^{13}C NMR (100 MHz, $CDCl_3$) δ 147.2, 141.0, 140.6, 135.6, 134.8, 132.4, 130.4, 129.7, 129.5, 127.4, 125.3, 124.7, 123.9, 122.9, 122.8, 122.0, 117.6, 116.4, 114.4, 113.4, 109.4, 109.2, 106.8, 96.5, 93.0, 92.8, 91.0, 90.1, 87.8, 85.6, 85.3, 78.4, 78.3, 78.2, 75.2, 69.9, 69.4, 60.5, 43.4, 31.4, 29.9, 20.8, 14.3, 14.1; MALDI-TOF MS (+eV) m/z calcd for $C_{48}H_{66}B_{40}N_2$ 1103.4, found 1104.0.

Compound 3. In a Schlenk tube under nitrogen, the aniline nanocar **26** (19 mg, 17.2 μmol) was dissolved in CH_2Cl_2 (1.0 mL) and Et_3N (0.1 mL). TRITC (8 mg, 17.2 μmol) in solution in DMF (1.0 mL) was added dropwise and the mixture stirred overnight at 50 °C in the dark. The solvents were then removed under reduced pressure. The resulting solid was purified by column chromatography (silica gel, using 10% MeOH in CH_2Cl_2) to yield **3** as a purple solid (3.3 mg, 13%). *Note: It was not possible to obtain a clean ^{1}H NMR spectrum of **3** where all expected signals were observable due to the small amount prepared; however, the presence of the desired compound was confirmed by MALDI MS.* FTIR (neat) 3343, 3060, 2925, 2854, 2618, 2356, 2338, 2209, 1711, 1596, 1493, 1463, 1410, 1348, 1266, 1216, 1189, 1127, 1104, 1062, 930, 827 cm^{-1}; ^{1}H NMR (400 MHz, $CDCl_3$) δ 7.80 (d, J = 8.5 Hz, 1H), 7.70 (dd, J_1 = 6.0 Hz, J_2 = 3.5 Hz, 2H), 7.53 (dd, J_1 = 6.0 Hz, J_2 = 3.5 Hz, 2H), 7.47 (s, 1H), 7.30 (s, 2H), 7.22 (s, 2H), 7.12 (m, 5H), 7.05 (s, 1H), 6.80 (m, 3H), 6.73 (d, J = 8.5 Hz, 1H), 4.22 (m, 2H), 3.35 (s, 12H). The material was not soluble enough for ^{13}C analysis. MALDI-TOF MS (+eV) m/z calcd for $C_{73}H_{87}B_{40}N_5O_3S$ 1547.0, found 1548.2 [M + H].

Compound 29. Trialkyne **27**[20] (0.100 g, 0.667 mmol) was subjected to the general Sonogashira protocol using **28**[20] (0.978 g, 2.00 mmol), $PdCl_2(PPh_3)_2$ (0.126 g, 0.179 mmol), CuI (0.066 g, 0.346 mmol), TEA (3.0 mL), and THF (10.0 mL) and the mixture was stirred at rt overnight. The resulting residue was purified by column chromatography with 25% CH_2Cl_2 in hexanes to give **29** (0.557 g, 68%) as a light yellow solid. FTIR (KBr) 2963, 2613, 1579, 1502, 1423, 1218, 1061 cm^{-1}; ^{1}H NMR (400 MHz, $CDCl_3$) δ 7.57 (s, 3H), 6.89 (s, 3H), 6.76 (s, 3H), 3.92 (t, J = 5.2 Hz, 6H), 3.87 (t, J = 5.2 Hz, 6H), 3.15–1.90 (br m, 33H), 1.82 (m, 12H), 1.08 (m, 18H); ^{13}C NMR (100 MHz, $CDCl_3$) δ 154.5, 153.7, 134.2, 124.3, 117.2, 117.1,

114.5, 112.5, 93.5, 91.0, 87.1, 76.2, 71.4, 71.1, 22.9, 22.8, 10.8, 10.7; MALDI-TOF MS (+eV) m/z calcd for $C_{60}H_{84}B_{30}O_6$ 1226.0, found 1226.0.

Compound 30. 1-Nitro-4-trimethylsilylethynylbenzene (2.19 g, 10.00 mmol) was combined with $AgNO_3$ (0.340 g, 2.00 mmol), *N*-bromosuccinimide (1.80 g, 10.1 mmol) and acetone (100 mL). The mixture was stirred for 2 h at rt in the dark, and poured onto a pad of silica gel. The pad was then eluted with 40% CH_2Cl_2 in hexanes and the solvents removed to yield **30** (2.37 g, 91%) as a light yellow solid. *Caution: alkynyl bromides decompose over time and evolve HBr. Care should be taken when handling.* FTIR (KBr) 3105, 2196, 1772, 1698, 1591, 1508, 1346, 1192, 853, 748 cm^{-1}; ^1H NMR (500 MHz, $CDCl_3$) δ 8.18 (d, J = 8.8 Hz, 2H), 7.58 (d, J = 8.8 Hz, 2H); ^{13}C NMR (126 MHz, $CDCl_3$) δ 147.5, 133.0, 129.7, 123.8, 78.6, 56.6; EI-HRMS m/z calcd for $C_8H_4BrNO_2$ 224.9425, found 224.9419.

Compound 31. Trimer **29** (0.40 g, 0.33 mmol) was added to an oven-dried, three-neck round-bottom flask, followed by THF (5 mL). The mixture was cooled to −78 °C, and BuLi (2.5 M in hexanes, 0.13 mL, 0.033 mmol) was added dropwise. The mixture was allowed to stir at −15 °C for 1 h, followed by cooling to −78 °C. To the blue mixture was then added CuBr (0.061 g, 0.424 mmol), followed by warming to −15 °C and stirring for 1 h. Alkynyl bromide **30** (0.096 g, 0.424 mmol) was then added all at once as a solid, and the mixture was allowed to warm to rt and stirred overnight. The reaction was quenched by addition of 1 drop of water, followed by elution through a Celite pad with CH_2Cl_2. The resulting residue was then purified using flash chromatography with 25% CH_2Cl_2 in hexanes as eluent to give product **31** (0.098 g, 22%) as a light yellow solid. FTIR (KBr) 2963, 2925, 2875, 2855, 2615, 1579, 1502, 1467, 1423, 1387, 1343, 1276, 1218, 1062,

1017, 989 cm^{-1}; ^1H NMR (400 MHz, $CDCl_3$) δ 8.14 (d, *J* = 7.2 Hz, 2H), 7.57 (s, 3H), 7.47 (d, *J* = 6.8 Hz, 2H), 6.89 (s, 3H), 6.76 (s, 3H), 3.92 (t, *J* = 5.2 Hz, 6H), 3.86 (t, *J* = 5.2 Hz, 6H), 3.20–1.90 (br m, 33H), 1.81 (m, 12H), 1.07 (m, 18H); ^{13}C NMR (100 MHz, $CDCl_3$) δ 154.5, 153.7, 147.8, 134.2, 133.1, 128.2, 124.3, 124.2, 123.7, 117.19, 117.17, 117.1, 117.0, 114.8, 114.5, 93.7, 93.5, 91.1, 87.1, 71.40, 71.37, 71.14, 71.07, 29.9, 22.9, 22.8, 10.8; MALDI-TOF MS (+eV) *m*/*z* calcd for $C_{68}H_{87}B_{30}NO_8$ 1371.0, found 1371.0.

Compound 32. To a round bottom flask with stir bar was added trimer **31** (0.074 g, 0.054 mmol), Zn powder (0.353 g, 5.39 mmol), 1 drop AcOH, and THF (3.0 mL). The mixture was allowed to stir for 1 h and the reaction quenched by elution through a Celite pad with CH_2Cl_2. The resulting residue was then purified using flash chromatography with 25% CH_2Cl_2 in hexanes as eluent to give product **32** (0.072 g, 100%) a light yellow solid. FTIR (neat) 3568, 3386, 2964, 2934, 2876, 2614, 2364, 2229, 1619, 1605, 1578, 1501, 1422, 1386, 1276, 1217, 1062, 1015 cm^{-1}; ^1H NMR (400 MHz, $CDCl_3$) δ 7.57 (s, 3H), 7.11 (d, *J* = 8.7 Hz, 2H), 6.89 (s, 3H), 6.75 (s, 3H), 6.53 (d, *J* = 8.7 Hz, 2H), 3.92 (t, *J* = 6.5 Hz, 6H), 3.86 (t, *J* = 6.2 Hz, 6H), 3.30–1.60 (br m, 46H), 1.06 (t, *J* = 7.4 Hz, 18H); ^{13}C NMR (100 MHz, $CDCl_3$) δ 154.49, 154.48, 153.7, 134.2, 133.5, 124.3, 117.2, 117.11, 117.09, 115.7, 114.7, 114.5, 112.5, 93.6, 87.1, 76.8, 76.2, 71.4, 71.1, 29.9, 22.9, 22.8, 10.76, 10.75; MALDI-TOF MS (+eV) *m*/*z* calcd for $C_{68}H_{90}B_{30}NO_6$ 1341.0, found 1342.1 [M + H].

Trimer 4. Into a Schlenk tube under nitrogen, trimer **32** (15 mg, 0.011 mmol) was dissolved in CH_2Cl_2 (1 mL) and TEA (0.1 mL). TRITC (5 mg, 0.011 mmol) in solution in DMF (1 mL) was added dropwise, and the mixture was stirred overnight in the dark at rt. The solvents were removed by rotary evaporation. The resulting residue was then purified

using flash chromatography with 10% MeOH in CH_2Cl_2 as eluent to give **4** (9 mg, 45%) as a purple solid. FTIR (neat) 3350, 2961, 2924, 2853, 2615, 2369, 1596, 1500, 1421, 1365, 1349, 1218, 1188 cm^{-1}; ^1H NMR (400 MHz, $CDCl_3$) δ 8.05 (br s, 1H), 7.89 (d, J = 8.8 Hz, 1H), 7.74 (br s, 1H), 7.58 (m, 1H), 7.52 (s, 3H), 7.20 (m, 4H), 7.05 (d, J = 9.5 Hz, 1H), 6.85 (s, 3H), 6.72 (dd, J_1 = 8.3 Hz, J_2 = 2.0 Hz, 2H), 6.71 (s, 3H), 6.67 (d, J = 2.0 Hz, 2H), 3.88 (t, J = 6.5 Hz, 6H), 3.82 (t, J = 6.5 Hz, 6H), 3.21 (s, 12H), 3.00–1.47 (br m, 33H), 1.77 (m, 12H), 1.02 (m, 18H). The material was not soluble enough for ^{13}C analysis. MALDI-TOF MS (+eV) m/z calcd for $C_{93}H_{110}B_{30}N_4O_6S$ 1784.1, found 1785.1 [M + H].

Compound 34. A Schlenk tube equipped with a magnetic stir bar was charged with **33**[20] (80 mg, 80 μmol) and dry THF (3 mL). The solution was cooled to -30 °C and BuLi (32 μL, 80 μmol, 2.5 M in hexanes) was added. The solution was allowed to stir at −30°C for 15 min before CuBr (17 mg, 118 μmol) was added and the mixture was allowed to stir at −30°C for 15 min. **30** (18 mg, 80 μmol) was added and the resulting mixture was allowed to stir at rt for 16 h. A few drops of water were added, and the mixture was filtered through a silica gel pad using CH_2Cl_2 as the eluent. The resulting greenish solid was purified by column chromatography (silica gel, using 50% CH_2Cl_2 in hexanes) to provide a mixture of **34** and **34'** as a white powder (15 mg, 16%). FTIR (neat) 3063, 3010, 2960, 2927, 2854, 2609, 2362, 2344, 2209, 1593, 1528, 1501, 1450, 1407, 1378, 1348, 1278, 1257, 1219, 1133, 1059, 1039, 1012, 853, 830 cm^{-1}; ^1H NMR (400 MHz, $CDCl_3$) δ 8.14 (d, J = 9.0 Hz, 2H), 7.49–7.45 (m, 4H), 7.26–7.23 (m, 2H), 7.17–7.15 (m, 2H), 7.07–7.05 (m, 2H), 4.00 (m, 6H), 3.20–1.60 (br m, 44H); ^{13}C NMR (100 MHz, $CDCl_3$) δ 154.27, 154.23, 147.82, 135.53, 133.03, 132.35, 132.28, 131.20, 128.11, 128.06, 126.81, 126.68, 124.26, 124.01, 123.70, 122.39, 122.17, 121.85, 115.82, 113.62, 113.56, 113.40, 11.37, 92.23, 91.18, 92.04, 91.34, 91.17,

91.02, 90.89, 90.85, 90.78, 90.08, 88.18, 88.05, 87.60, 79.61, 79.51, 78.50, 78.42, 78.10, 78.04, 69.69, 69.33, 60.53, 56.66; MALDI-TOF MS (+eV) m/z calcd for $C_{48}H_{61}B_{40}NO_4$ 1148.4, found 1148.7.

Compound 35. A Schlenk tube equipped with a magnetic stir bar was charged with **34** (14 mg, 12 μmol), Zn powder (79 mg, 1.21 mmol), 1 drop AcOH and THF (3.0 mL). The mixture was allowed to stir at 30 °C for 15 min. The resulting greenish solid was purified by column chromatography (silica gel, hexanes / CH_2Cl_2 1:1) to provide a mixture of **35** and **35'** as a white powder (8 mg, 59%). FTIR (neat) 3484, 3387, 3060, 2919, 2851, 2609, 2356, 2326, 2220, 1719, 1602, 1504, 1460, 1407, 1384, 1284, 1224, 1180, 1145, 1062, 1045, 1012, 892, 868, 830 cm^{-1}; ^1H NMR (400 MHz, $CDCl_3$) δ 7.48–7.49 (m, 2H), 7.23 (d, J = 8.1 Hz, 2H), 7.14 (dd, J_1 = 8.1 Hz, J_2 = 1.6 Hz, 2H), 7.11-7.06 (m, 4H), 6.54–6.51 (m, 2H), 4.00 (m, 6H), 3.81 (br s, 2H), 3.20–1.60 (br m, 44H); ^{13}C NMR (100 MHz, $CDCl_3$) δ 154.23, 147.49, 135.54, 133.51, 132.33, 131.16, 126.73, 124.04, 123.97, 122.14, 115.81, 114.65, 113.51, 113.47, 113.40, 110.49, 110.40, 92.15, 92.13, 91.19, 90.96, 90.93, 88.01, 69.69, 69.34, 60.52, 56.65; MALDI-TOF MS (+eV) m/z calcd for $C_{48}H_{63}B_{40}NO_2$ 1118.5, found 1118.9.

Compound 5. In a Schlenk tube under nitrogen, the aniline nanocar **35** (8 mg, 7 μmol) was dissolved in CH_2Cl_2 (1.0 mL) and Et_3N (0.1 mL). TRITC (3 mg, 7 μmol) in DMF (1.0 mL) was added dropwise and the mixture was stirred overnight at rt in the dark. The solvents were then removed by rotary evaporation under reduced pressure. The resulting solid was purified by column chromatography (silica gel, 10% MeOH in CH_2Cl_2) to yield a mixture of **5** and **5'** as a purple solid (3.1 mg, 29%). FTIR (neat) 3337, 3060, 2922, 2854, 2612, 2362, 2338, 1711, 1593, 1578, 1504, 1460, 1410, 1381, 1260, 1219, 1180, 1104,

1062, 1045, 1009, 847 cm^{-1}; ^1H NMR (400 MHz, $CDCl_3$) δ 7.95 (br s, 1H), 7.82 (d, *J* = 8.8 Hz, 1H), 7.74 (d, *J* = 8.8 Hz, 1H), 7.58 (d, *J* = 8.9 Hz, 1H), 7.49–7.48 (m, 3H), 7.15–7.05 (m, 5H), 6.98 (d, *J* = 8.4 Hz, 2H), 6.82 (m, 2H), 6.72 (d, *J* = 8.6 Hz, 1H), 6.46–6.40 (m, 4H), 4.01 (br s, 6H), 3.00 (br s, 12H), 3.00–1.47 (br m, 43H). The material was not soluble enough for ^{13}C analysis. MALDI-TOF MS (+eV) *m/z* calcd for $C_{73}H_{84}B_{40}N_4O_5S$ 1561.9, found 1562.0.

Supporting Information. ^1H and ^{13}C NMR spectra of new compounds.

1.5. References

1. Vives, G.; Guerrero, J. M.; Godoy, J.; Kathua, S.; Wang, Y.-P.; Kiappes, J. L.; Link, S.; Tour, J. M. *J. Org. Chem.* **2010**, *75*, 6631-6643.
2. For examples of early work see Balzani, V.; Credi, A.; Venturi, M. *Molecular Devices and Machines: Concepts and Perspectives for the Nanoworld*; Wiley-VCH: Weinheim, Germany, 2008.
3. For a comprehensive review of molecular machine work see Kay, E. R.; Leigh, D. A.; Zerbetto, F. *Angew. Chem. Int. Ed.* **2007**, *46*, 72-191.
4. For recent reviews of synthetic approaches see: a) Vives, G.; Tour, J. M. *Acc. Chem. Res.* **2009**, *42*, 473-487. b) Delius, M. V.; Leigh, D. A. *Chem. Soc. Rev.* **2011**, *40*, 3656-3676. c) Silvi, S.; Venturi, M.; Credi, A. *Chem. Comm.* **2011**, *47*, 2483-2489. c) Vives, G.; Tour, J. M. *Acc. Chem. Res.* **2009**, *42*, 473-487.
5. a) Takano, H.; Kenseth, J. R.; Wong, S.-S.; O'Brien, J. C.; Porter, M. D. *Chem. Rev.* **1999**, *99*, 2845-2890. b) Soong, R. K.; Bachand, G. D.; Neves, H. P.; Olkhovets, A. G.; Craighead, H. G.; Montemagno, C. D. *Science* **2000**, *290*, 1555-1558. c) Bachand, G. D.;

Soong, R. K.; Neves, H. P.; Olkhovets, A. G.; Craighead, H. G. Montemagno, C. D. *Nano Lett.* **2001**, *1*, 42-44. d) Park, H.; Toprak, E.; Selvin, P. R. *Quarterly Reviews of Biophysics* **2007**, *40*, 87-111.

6. a) Rosei, F.; Schunack, M.; Naitoh, Y.; Jiang, P.; Gourdon, A.; Laegsgaard, E.; Stensgaard, I.; Joachim, C.; Besenbacher, F. *Prog. Surf. Sci*. **2003**, *71*, 95-146. b) Tinnefeld, P.; Sauer, M. *Angew. Chem. Int. Ed.* **2005**, *44*, 2642-2671. c) Sasaki, T.; Guerrero, J. M.; Leonard, A. D.; Tour, J. M. *Nano Research* **2008**, *5*, 412-419.
7. a) Grill, L. *J. Phys.: Condens. Matter* **2008**, *20*, 0053001.
8. a) Manzano, C.; Soe, W.-H.; Wong, H. S.; Ample, F.; Gourdon, A.; Chandrasekhar, N.; Joachim, C. *Nature Mat.* **2009**, *8*, 576-579. b) Michl, J.; Sykes, E. C. H. *ACS Nano* **2009**, *3*, 1042-1048. c) Kudernac, T.; Ruangsupapichat, N.; Parschau, M.; Macia, B.; Katsonis, N.; Harutyunyan, S. R.; Ernst, K.-H.; Feringa, B. L. *Nature*, **2011**, *479*, 208-211.
9. a) Rosei, F.; Schunack, M.; Jiang, P.; Gourdon, A.; Legsgaard, E.; Stensgaard, I.; Joachim, C.; Besenbacher, F. *Science* **2002**, *296*, 328-331. b) Moresco, F.; Gourdon, A. *Proc. Natl. Acad. Sci. U. S. A.* **2005**, *102*, 8809-8814. c) Yu, M.; Kalashnyk, N.; Barattin, R.; Benjalal, Y.; Hliwa, M.; Bouju, X.; Gourdon, A.; Joachim, C.; Lægsgaard, E.; Besenbacher, F.; Linderoth, T. R. *Chem. Comm.* **2010**, *46*, 5545-5547.
10. a) Grill, L.; Rieder, K.-H.; Moresco, F.; Jimenez-Bueno, G.; Wang, C.; Rapenne, G.; Joachim, C. *Surf. Sci.* **2005**, *584*, L153-L158. b) Jimenez-Bueno, G.; Rapenne, G. *Tetrahedron* **2007**, *63*, 7018-7026.
11. Kwon, K.-Y.; Wong, K. L.; Pawin, G.; Bartels, L.; Stolbov, S.; Rahman, T. S. *Phys. Rev. Lett.* **2005**, *95*, 166101-166104.

12. Gimzewski, J. K.; Joachim, C.; Schlittler, R. R.; Langlais, V.; Tang, H.; Johannsen, I. *Science* **1998**, *281*, 531. b) Gross, L.; Rieder, K.–H.; Moresco, F.; Stojkovic, S. M.; Gourdon, A.; Joachim, C. *Nat. Mater.* **2006**, *4*, 892.
13. a) Vives, G.; Kang, J.; Kelly, K. F.; Tour, J. M. *Org. Lett.* **2009**, *11*, 5602-5605. b) Villagomez, C. J.; Sasaki, T.; Tour, J. M.; Grill, L. *J. Am. Chem. Soc.* **2010**, *132*, 16848-16854. c) Chiang, P.-T.; Mielke, J.; Godoy, J.; Guerrero, J. M.; Alemany, L. B.; Villagomez, C. J.; Saywell, A.; Grill, L.; Tour, J. M. *ACS Nano* **2012**, *6*, 592–597.
14. Shirai, Y.; Osgood, A. J.; Zhao, Y.; Kelly, K. F.; Tour, J. M. *Nano Lett.* **2005**, *5*, 2330-2334.
15. a) Eigler, D. M.; Lutz, C. P.; Rudge, W. E. *Nature* **1991**, *352*, 600-603. b) Anderson, H. *Angew. Chem. Int. Ed.* **2000**, *39*, 2451-2453.
16. a) Haustein, E.; Schwille, P. *Methods* **2003**, *29*, 153–166. b) Yildiz, A.; Forkey, J. N.; McKinney, S. A.; Ha, T.; Goldman, Y. E.; Selvin, P. R. *Science* **2003**, *300*, 2061-2065. c) Yildiz, A.; Tomishige, M.; Vale, R. D.; Selvin, P. R. *Science* **2004**, *303*, 676-678. d) Qiu, W.; Derr, N. D.; Goodman, B. S.; Villa, E.; Wu, D.; Shih, W.; Reck-Peterson, S. L. *Nat. Struct. Mol. Biol.* **2012**, *19*, 193-201. e) DeWitt, M. A.; Chang, A. Y.; Combs, P. A.; Yildiz, A. *Science* **2012**, *335*, 221-225.
17. Thompson, R. E.; Larson, D. R.; Webb, W. W. *Biophys. J.* **2002**, *82*, 2775-2783.
18. Rueda, D.; Walter, N. G. *J. Nanosci. Nanotechnol.* **2005**, *5*, 1990-2000.
19. a) Telford, W. G.; Murga, M.; Hawley, T.; Hawley, R.; Packard, B.; Komoriya, A.; Haas, F.; Hubert, C. *Cytometry A* **2005**, *68A*, 36–44. b) Van Hoof, D.; Pinkse, M. W. H.; Ward-Van Oostwaard, D.; Mummery, C. L.; Heck, A. J. R.; Krijgsveld, J. *Nature Methods* **2007**, *4*, 678-679. c) Perfetto, S. P.; Roederer, M. *Cytometry A* **2007**, *71A*, 73–79.

20. Morin, J.–F.; Sasaki, T.; Shirai, Y.; Guerrero, J. M.; Tour, J. M. *J. Org. Chem.* **2007**, *72*, 9481-9490.

21. a) Corrie, J. E. T. ; Craik, J. S. *J. Chem. Soc., Perkins Trans.* **1994**, 2967-2973. b) Buchynskyy, A. ; Kempin, U.; Vogel, S. ; Hennig, L. ; Findeisen, M.; Müller, D.; Giesa, S.; Knoll, H.; Welzel, P. *Eur. J. Org. Chem.* **2002**, 1149-1162. c) Hernando, J.; van der Schaaf, M.; van Dijk, E. M. H. P.; Sauer, M.; García-Parajó, M. F.; van Hulst, N. F. *J. Phys. Chem. A* **2003,** *107,* 43-52. d) Reizelman, A.; Wigchert, S. C. M.; del-Bianco, C.; Zwanenburg, B. *Org. Biol. Chem.* **2003**, *1*, 950-959. e) Sørensen, M. D.; Martins, R.; Hindsgaul, O. *Angew. Chem. Int. Ed.* **2007**, *46*, 2403-2407.

22. Khatua, S.; Guerrero, J. M.; Claytor, K.; Vives, G.; Kolomeisky, A. B.; Tour, J. M.; Link, S. *ACS Nano* **2009**, *3*, 351-356.

23. Morin, J.–F.; Shirai, Y.; Tour, J. M. *Org. Lett.* **2006**, *8*, 1713-1716.

24. Sasaki, T.; Tour, J. M. *Tetrahedron Lett.* **2007**, *48*, 5821-5824.

25. Maya, F.; Chanteau, S. H.; Cheng, L.; Stewart, M. P.; Tour, J. M. *Chem. Mat*. **2005**, *17*, 1331-1345.

26. Lindner, E.; Zong, R.; Eichele, K.; Ströbele, M. *J. Organomet. Chem.* **2002**, *660*, 78-84.

27. Netherton, M. R.; Fu, G. C. *Org. Lett.* **2001**, *3*, 4295-4298.

28. Zhao, T.; Liu, Z.; Song, Y.; Xu, W.; Zhang, D.; Zhu, D. *J. Org. Chem*. **2006**, *71*, 7422-7432.

29. Fox, M. A.; MacBride, J. A. H.; Peace, R. J.; Wade, K. *J. Chem. Soc., Dalton Trans.* **1998**, 401-411.

30. Shirai, Y.; Osgood, A.; Zhao, Y.; Yao, Y.; Saudan, L.; Yang, H.; Yu-Hung, C.; Alemany, L. B.; Sasaki, T.; Morin, J.-F.; Guerrero, J. M.; Kelly, K. F.; Tour, J. M. *J. Am. Chem. Soc.* **2006**, *128*, 4854-4864.

1.6. Experimental Contributions Section

My contributions to the experimental work described in this chapter are the following: synthesis and characterization of nanocar **3**, as well as measurement of the optical properties of the five fluorescently labeled nanocars and their aniline precursors. Jason Guerrero conceived the project and synthesized nanocars **1** and **2**. Guillaume Vives synthesized nanocars **4** and **5**. Saumyakanti Khatua developed the correction file used for the fluorescence spectra. Yu-Pu-Wang and J. L. Kiappes provided assistance with the syntheses of several nanocar precursors. Benaiah E. Tour and Pin-Lei E. Chu synthesized axles **6** and **9**, respectively.

Chapter 2

Synthesis and Fluorescence Imaging of BODIPY-Based Nanocars

Note: This chapter was copied in large part from two papers that I coauthored.[1,2] Reprinted with permission from references 1 and 2. Copyright 2010 American Chemical Society.

2.1. Introduction

The control of motion at the molecular level stands as a challenge for scientists. Nature gives the supreme example of such control when the synchronization of motion of individual molecules leads to intricate biological functions.[3] Unfortunately, the use of natural molecular machines for *ex vivo* applications is intrinsically limited due to unfavorable environmental perturbations.[4] Much effort has been devoted toward the design, synthesis and operation of synthetic molecular machines. As a consequence, a large

variety of nanostructures have been made to operate either in solution, in the solid state or mounted on surfaces.[5]

Our group has focused on the study of restricted rolling motion to control the translation of individual molecules along atomically flat surfaces. Incorporation of either C_{60}-fullerene,[6] *p*-carborane[7] or a ruthenium complex[8] as molecular wheels in flexible oligo(phenylene ethynylene) (OPE) chassis has afforded a collection of molecular vehicles termed nanocars.[9]

Most nanocars have been designed to be observed and tracked using scanning tunneling microscopy (STM) since it offers unparalleled atomic resolution.[10] Exploration of other single-molecule imaging tools, however, is essential in order to observe movement of nanomachines on non-conductive surfaces. Single-molecule fluorescence microscopy (SMFM) is a good alternative. Even though its resolution is limited by diffraction, nanometer localization of individual fluorophores has become possible.[11]

As described in chapter 1, a family of five fluorescently-tagged nanocars was synthesized, intended for imaging through SMFM.[12] The nanocars were functionalized with a tetramethylrhodamine fluorescent tag to allow excitation with a Nd:Vn laser (532 nm) with good fluorescence quantum yields. The motion of one of the nanocars was monitored on a glass surface at ambient conditions.[13] The nanocars moved at an average speed of 4 nm/s at room temperature. However, only 25% of the nanocars studied showed motion, suggesting that the fluorophore might interfere with the nanocar motion by blocking some of the molecules. In addition, the synthesis of the tagged-nanocars presented some drawbacks, such as lengthy routes and low-yielding attachment of the fluorescent label. Consequently, a new set of intrinsically fluorescent nanocars was designed to obviate the

need for a pendant fluorescent tag. We envisioned that removal of the large pendant fluorophore might lead to an increase in the fraction of moving molecules.

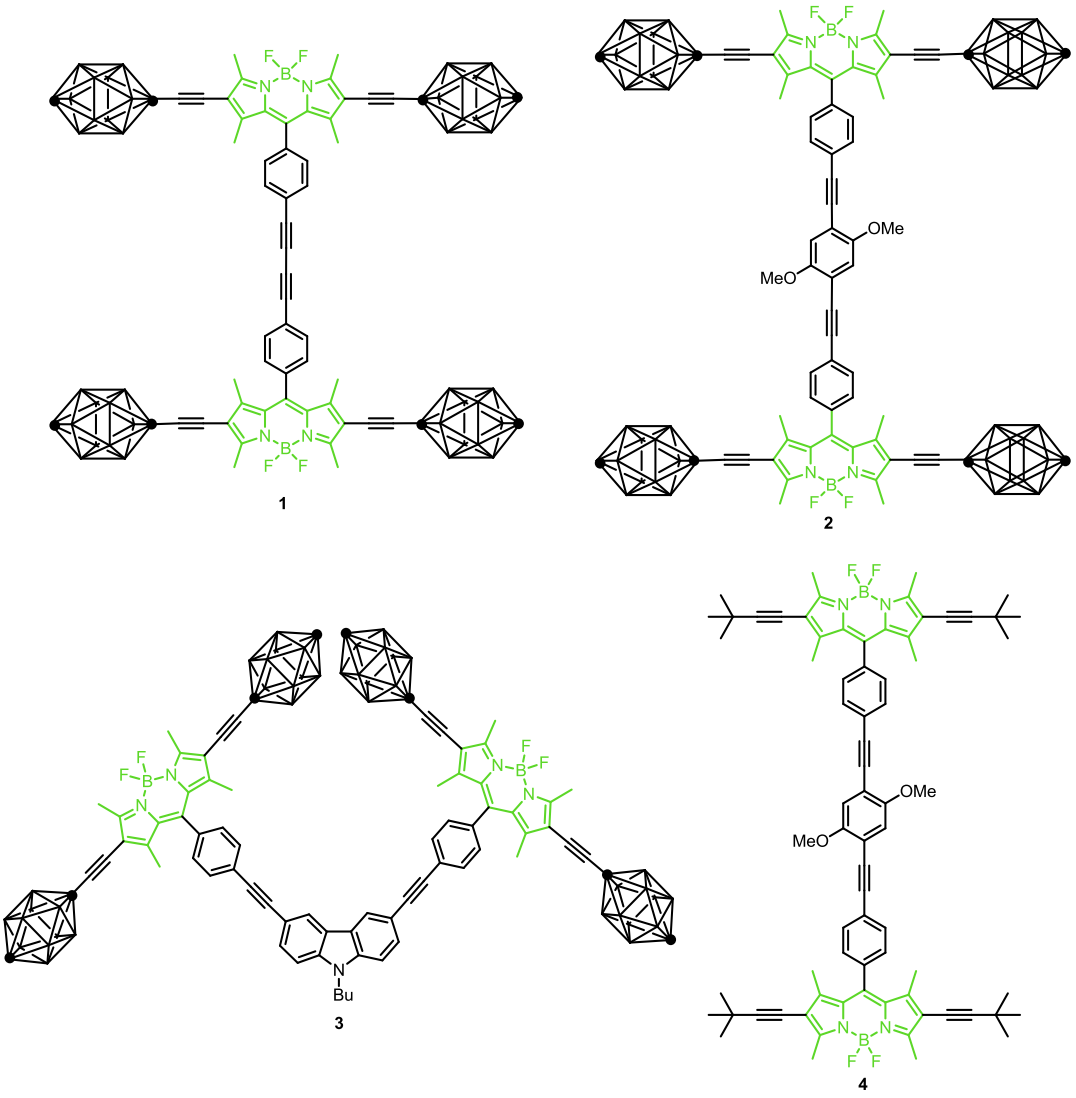

Figure 2.1. (Modified from reference 1). Structure of BODIPY-based nanocars **1-3** and analogue **4**. Every vertex of the carborane wheel is BH except the darkened sites, where the outer (*para*) is CH and the inner (*ipso*) is alkynyl-substituted C.

A modular and convergent route was used to synthesize fluorescent nanocars **1-3** and the analogue **4** that each incorporate a 4,4-difluoro-4-bora-3a,4a-diaza-*s*-indacene (BODIPY) core[14] in their axles (Figure 2.1). The BODIPY moiety is a versatile fluorophore; BODIPY-based chromophores tend to exhibit good thermal and photochemical stability, high fluorescence quantum yields, intense absorption profiles, tunability of absorption range and good solubility in most organic solvents.[15] Furthermore, the geometry of the core yields nanocars where the chassis is perpendicular to the axles, leading to only one conformation on the surface, in contrast to the previous 'Z-shaped' chassis obtained from OPE-axle-based nanocars.[9]

The mobility of nanocar **2** was studied on three surfaces: plasma cleaned, reactive ion etched, and amine-functionalized glass. Using single-molecule fluorescence spectrocsopy, the percentage of moving nanocars and their diffusion constants were determined for each substrate.

2.2. Results and Discussion

2.2.1. Synthesis of Nanocars

Nanocars **1** and **2** were designed to move in a straight line on sufaces while nanocar **3** is expected to exhibit circular surface motion that could be detected by measuring the polarization anisotropy distribution.[16] In order to confirm the importance of the *p*-carborane wheels in translational motion, nanocar analogue **4**, bearing *tert*-butyl groups instead of the *p*-carborane clusters, was also designed and synthesized.

Our synthetic strategy was based upon the realization that nanocars **1-3** (Figure 2.1) could be assembled by coupling two units of a BODIPY-containing axle with the appropriate inner portion or via a homocoupling. By incorporating the fluorophore in the axle, a modular synthesis of nanocars with various chassis is accessible. The *tert*-butyl-substituted analogue **4** could be analogously assembled using a different axle. Both axles were synthesized from known BODIPY **5**[17] using the 2,6-acetylenic functionalization first explored by Ziessel.[18]

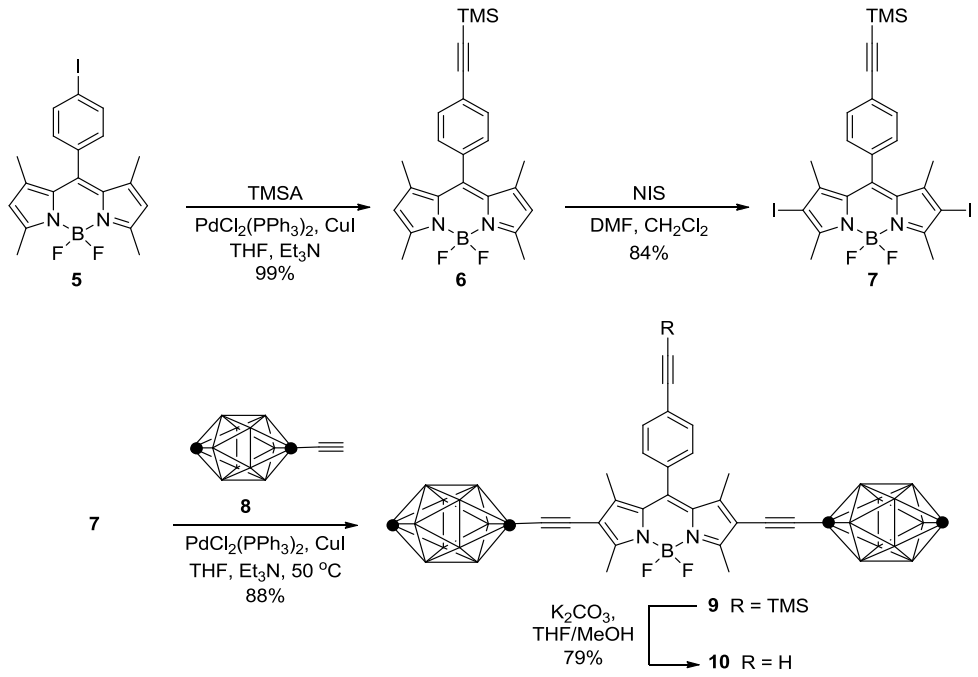

Scheme 2.1.[1] Synthesis of axle **10**.

The synthesis of axle **10** (Scheme 2.1) started with a Sonogashira coupling reaction between BODIPY **5** and trimethylsilylacetylene (TMSA) that afforded **6**. Double iodination of the BODIPY core in **6** using *N*-iodosuccinimide (NIS) gave **7**. Diiodide **7** was then subjected to a double Sonogashira coupling with 1-ethynyl-*p*-carborane **8**[19] to give **9**, which upon TMS deprotection afforded axle **10**. Fluoride sources were avoided for

deprotection since they are known to give lower yields due to partial destruction of the BODIPY core.[20] It is noteworthy that, in our experience, reaction times longer than 1.5 h with the K_2CO_3/MeOH system also reduce the yield and lead to formation of unknown byproducts. In summary, axle **10** was prepared in four steps from BODIPY **5** with an overall yield of 58%.

Nanocar **1** was assembled by palladium-catalyzed homocoupling of axle **10** in the presence of air (Scheme 2.2). The reaction was complete in 10 min and the product was obtained in high yield. In contrast, Eglinton-Glaser conditions[21] led only to decomposition of **10**, probably due to substitution of the boron by the Cu(II) required in the process.[22]

Axle **10** was also used in the final assembly of nanocars **2** and **3** (Scheme 2.2). Synthesis of nanocar **2** was accomplished through Sonogashira coupling between 1,4-diiodo-2,5-dimethoxybenzene (**11**)[23] and three equivalents of **10** to give **2** using typical coupling conditions. A methoxy substituted benzene was used as the inner portion to allow easier purification away from the byproduct nanocar **1**. Similarly, to obtain nanocar **3**, 9-butyl-3,6-diiodo-9H-carbazole (**12**)[24] was coupled with three equivalents of axle **10** to give the desired nanocar **3**.

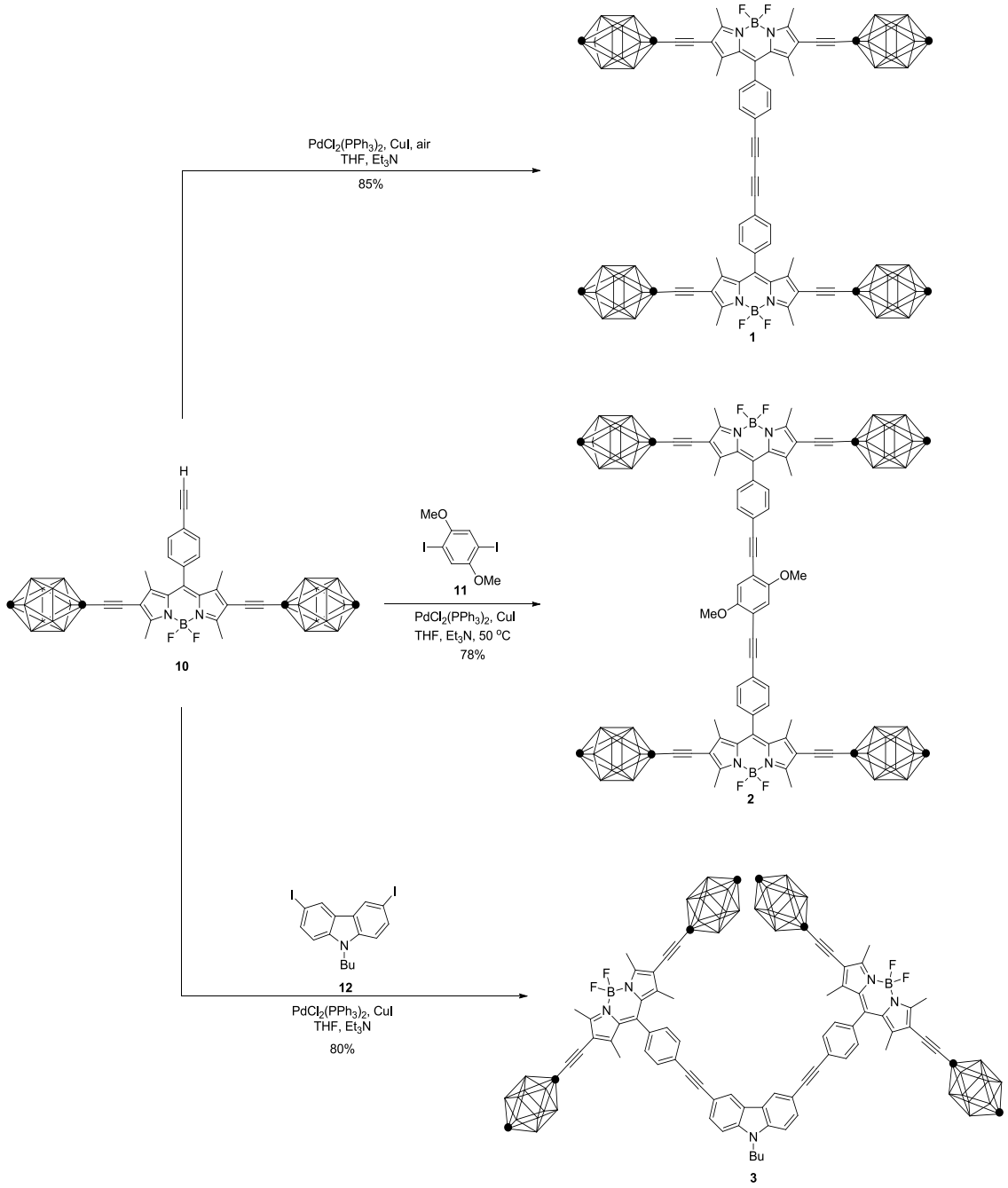

Scheme 2.2. (Modified from reference 1). Synthesis of nanocars **1**–**3**.

In order to address the importance of the carborane wheels in translational motion, their replacement by a non-wheel-like group was desired. Introduction of small alkyl chains was considered since they are not expected to significantly modify the fluorescence

of the BODIPY core. Lacking the wheel-like structure of *p*-carborane, an alkyl-substituted analogue would also enable us to evaluate the influence of the *p*-carborane on the absorption and emission properties of the BODIPY core. To prepare analogue **4**, bisiodide **7** was coupled with 3,3-dimethyl-1-butyne to give the TMS-protected axle **13**. After nearly quantitative deprotection, the free alkyne **14** was subjected to the final coupling with **11** to give the nanocar analogue **4** in excellent yield (Scheme 2.3).

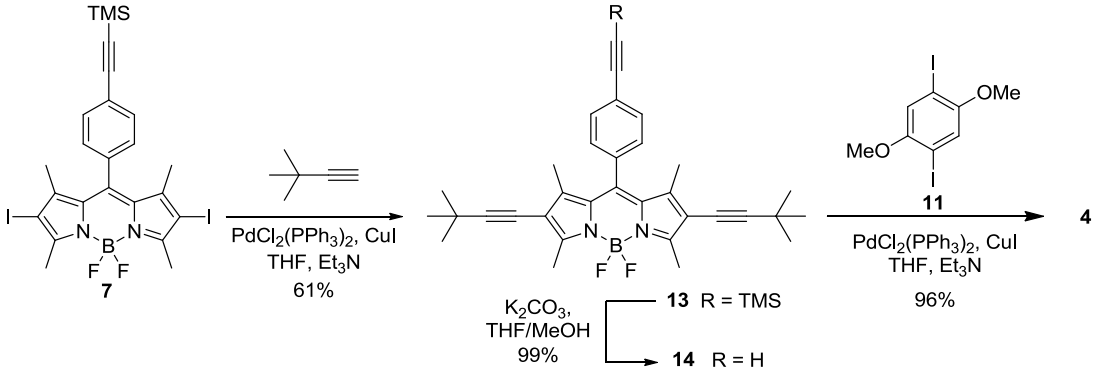

Scheme 2.3.[1] Synthesis of nanocar analogue **4**.

The efficiency of the coupling reactions to obtain **1**–**3** suggests that the BODIPY-containing axle **10** is a versatile building block to prepare even more complex nanocars by varying the inner portion.

2.2.2. Synthesis of a Trimer

To evaluate the importance of a car-like arrangement of the carborane wheels to observe translational motion, we also synthesized a BODIPY trimer in which only two of its three carborane wheels are aligned.

Trimer **16** (Scheme 2.4) was synthesized in two steps. First, a double iodination of BODIPY **5** using NIS provided **15**. Next, triiodide **15** reacted with1-ethynyl-*p*-carborane **8** under conventional Sonogashira coupling conditions to afford trimer **16**.

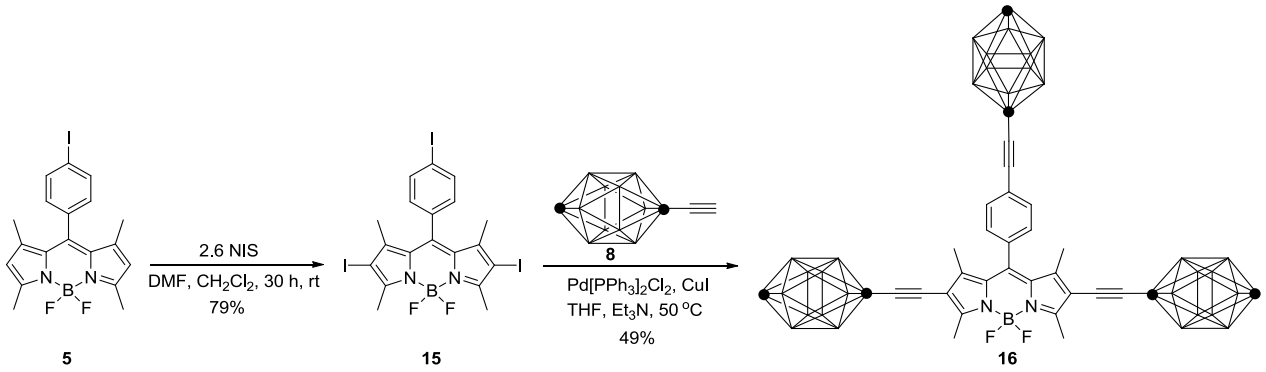

Scheme 2.4.[2] Synthesis of trimer **16**.

2.2.3. Optical Properties

The optical properties of the nanocars, the trimer, and some precursors were investigated by UV−vis and fluorescence spectroscopy (Table 2.1). The photophysical behavior of some of the compounds reported here was particularly interesting given that there was no previous report of carborane−BODIPY diads.[25] The absorption spectrum of all compounds exhibit a strong $S_0 \rightarrow S_1$ (π–π^*) transition located between 504 and 564 nm with variable extinction coefficients depending on the substitution pattern. The molecules with two BODIPY units have the largest extinction coefficients due to the extension in the conjugated system. The *tert*-butyl substituted compounds are slightly bathochromically shifted compared to their carboranyl-susbstituted analogues, probably due to the stronger electron-donating character of the *tert*-butyl groups.

compd	λ_{abs} (nm)	ε ($M^{-1}cm^{-1}$)	λ_{em} (nm)	Φ_F[a]
1	554	123 000	571	0.69
2	552	181 000	569	0.70
3	552	191 000	567	0.79
4	564	144 000	586	0.59
6	504	70 000	514	0.46
7	538	90 000	552	0.04
9	552	109 000	567	0.82
10	552	116 000	567	0.85
13	564	59 000	586	0.58
14	564	69 000	586	0.62
16	552	83 000	568	0.85

Table 2.1.[1] Optical properties of all compounds. [a]Determined in chloroform solution, ca. 1 × 10^{-7} M. Using rhodamine 6G as reference, Φ_F = 0.95 in EtOH, λ_{exc} 488 nm. Excitation was done at the corresponding λ_{max} – 30 nm wavelength.

Diiodo BODIPY **7** exhibits very low fluorescence quantum yield, in part due to efficient intersystem crossing caused by the heavy iodine atom, leading to a low lying triplet state.[26] The fluorescence was restored, however, upon introduction of the alkynyl carborane wheels or the alkynyl *tert*-butyl groups and was retained after the final assembly. The presence of the carboranes enhanced the quantum yields (compare **10** with **14** and **2** with **4**). The fluorescence quantum yields of nanocars **1**–**3** are slightly smaller than that of the BODIPY axle **10** possibly due to partial through-bond energy transfer between the two BODIPY units.

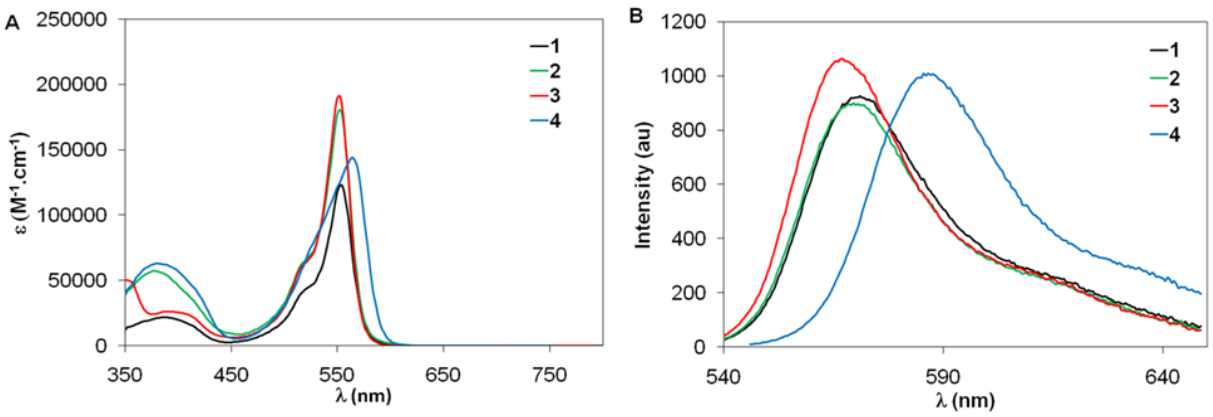

Figure 2.2. (Modified from reference 1). Absorption and emission spectra of **1–4 .** (A) UV–vis absorption spectra of **1–4** in $CHCl_3$. (B) Fluorescence spectra of **1–4** in $CHCl_3$. Excitation done at λ_{max} −30 nm.

Since our current SMFM setup requires excitation of the molecules with a 514 nm laser, it was a prerequisite for the nanocars to exhibit reasonable absorption at this wavelength. As depicted in Figure 2.2, both nanocars, analogue, and trimer (**1**-**4** and **16**) absorb in this region. Furthermore, the high fluorescence quantum yields of the three nanocars and the trimer make them particularly well-suited for imaging by SMFS at the excitation wavelengths.

2.2.4. Fluorescence Microscopy

The mobility of nanocar **2** was studied on three substrates: plasma cleaned glass, reactive ion etched glass, and amine-functionalized glass. Nanocars were deposited on different substrates by spin coating them from a 10^{-12} M solution in chloroform. The mobility of individual nanocars **2** was determined from time-lapsed confocal fluorescence images. Figure 2.3A shows the first of a series of images taken for nanocars dispersed on

plasma cleaned glass coverslips. The bright spots in the fluorescence image correspond to individual nanocars. As illustrated in Figure 2.3B, two-dimensional trajectories of the nanocar motion were computed from the entire series of images taken over the same area using a single-molecule tracking algorithm that can account for fluorescence blinking and bleaching.[27] The single-molecule trajectories were each analyzed to give a two-dimensional diffusion constant (Figure 2.3C), enabling a quantitative comparison between different nanocars and surfaces.

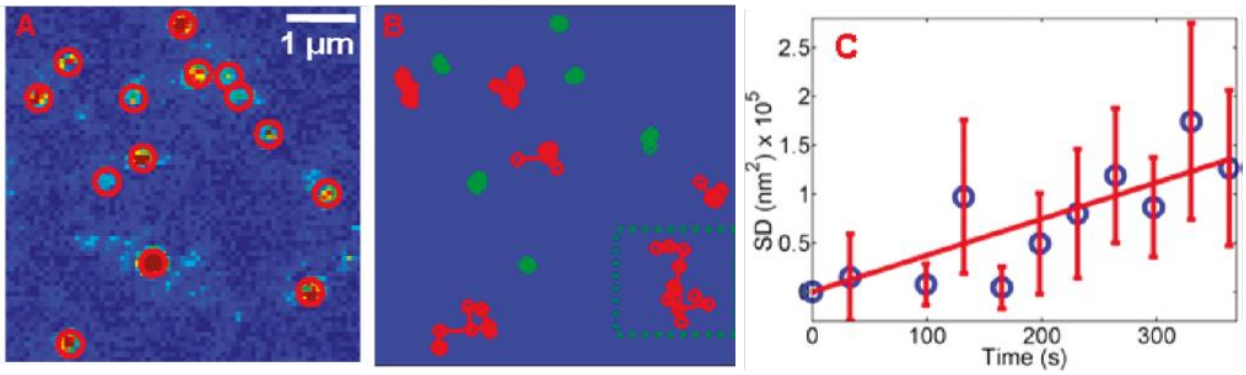

Figure 2.3. (Modified from reference 2). Fluorescence images of nanocar **2** on glass. (A) First of a time series of fluorescence images for single nanocars on a plasma-cleaned glass substrate. Individual nanocars indicated by the red circles were identified based on a threshold intensity. (B) XY trajectories of the nanocars identified in panel A. Trajectories colored red and green indicate "moving" and "stationary" nanocars, respectively. (C) Squared displacements SD versus time t calculated from the single nanocar trajectory surrounded by the green dotted square in panel B. A linear fit according to SD = $4Dt$ gives a diffusion constant of $D = 4.6\times10^{-16}$ m^2/s.

On plasma cleaned glass, 45% (126 out of 279) of nanocars **2** showed motion. This percentage was nearly double than the fraction of moving TRITC-tagged nanocars **17** (Figure 2.4), which were studied under identical conditions.[13] Removal of the TRITC tag might have contributed to the increase in moving molecules. However, it is difficult to quantify that contribution due to the profound structural differences between nanocars **17** and **2**; the zwitterionic nature of TRITC can promote electrostatic interactions of the nanocar with the glass surface; also, the 'Z-shaped' chassis of nanocar **17** leads to more possible conformations on a surface than the linear chassis of nanocar **2**.

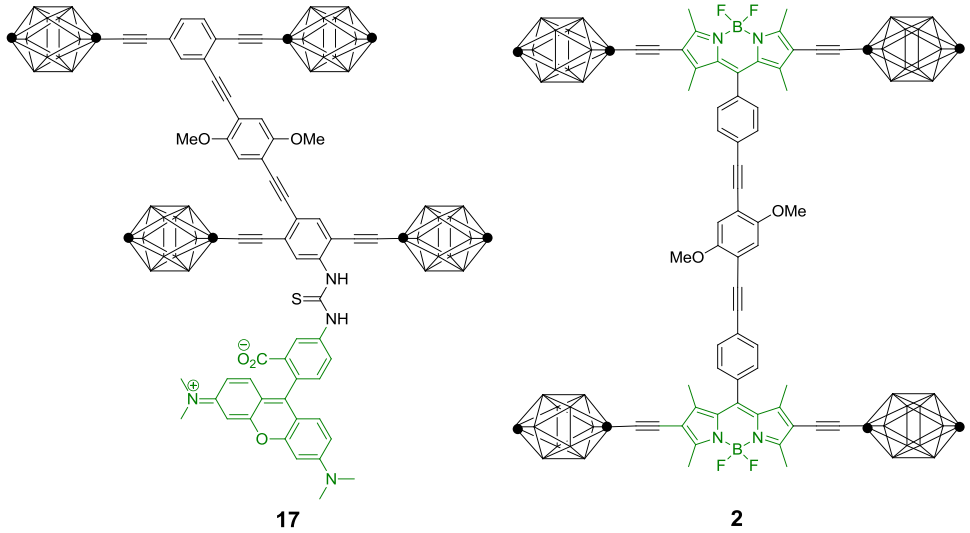

Figure 2.4.[2] Structures of the TRITC-tagged (**17**) and BODIPY-based (**2**) nanocars. Every vertex on the *p*-carboranes is BH, except the black dots, where the outer (*para*) is CH and the inner (*ipso*) is alkynyl-substituted C.

Although the fraction of moving molecules increased, the magnitude of *D* was similar for nanocars **17** and **2** (Figure 2.5A). These results suggest that, although structurally different, a common feature between nanocars **17** and **2** must account for the similarity. Since both **17** and **2** contain four *p*-carborane wheels, it is possible that the

magnitude of *D* in moving nanocars is mainly governed by the interactions between the substrate and the nanocar wheels.

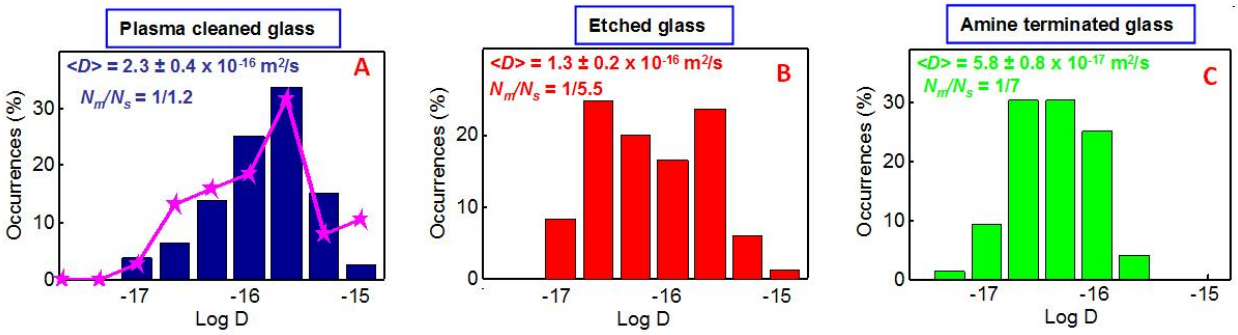

Figure 2.5. (Modified from reference 2). Distribution of single-molecule diffusion constants of nanocar **2** on three different substrates. (A) Distribution of single-molecule diffusion constants *D* for the moving BODIPY nanocars **2** on glass (bars). For comparison, the histogram of diffusion constants for TRITC-tagged nanocar **17** with carborane wheels moving on a glass surface is also included (line). The mean diffusion constants are nearly identical with D=2.4×10^{-16} m^2/s and D=2.2×10^{-16}m^2/s, for nanocars **2** and **17**, respectively. (B,C) Histograms of diffusion constants for nanocars on reactive ion-etched and amine-terminated glass. N_m and N_s are the number of moving and stationary nanocars, respectively.

To test if the movement for the majority of the nanocars was consistent with a rolling-type motion, the mobility of BODIPY-based trimer **16** (Figure 2.6) was studied. Under the same experimental conditions, it was found that only ~10% of the trimers moved on glass. Because of the perpendicular orientation of the third wheel, a rolling-type motion was hindered, as was predicted. The opposite trend is expected for motion by

hopping or slipping due to the decrease in the number of wheels and hence surface interaction.

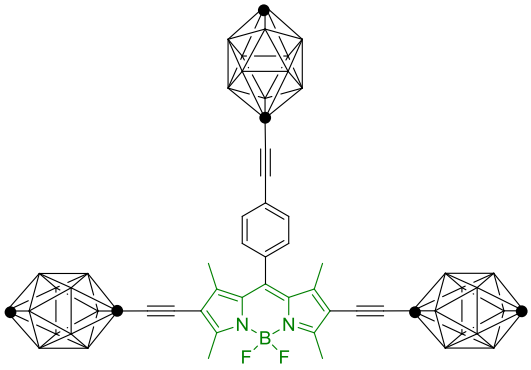

16

Figure 2.6. Structure of trimer **16**.

To investigate the impact of surface roughness and nanocar-substrate interactions on the mobility, nanocar **2** was then studied on reactive ion etching (RIE) treated glass and Vectabond™ treated glass (Figure 2.5B and 2.5C, respectively). Based on atomic force microscopy (AFM) analysis, the RIE process increased the average surface roughness (R_a) from 0.4 ± 0.1 nm in intact glass to 2.6 ± 0. 2 nm in etched glass. Vectabond™ was utilized to functionalize the glass surface with amine groups.[28] A significant decrease in the fraction of moving nanocars and their diffusion constants took place in both surfaces. Only 18% of the molecules moved on RIE-etched glass, while on Vectabond™-functionalized glass the percentage dropped to 13%.

The results from RIE-etched glass showed that an increase in surface roughness decreases the fraction of moving molecules. Some molecules might become lodged in the surface irregularities. Therefore, the lack of motion by almost half the nanocars **2** on plasma cleaned glass might be due, at least partially, to surface irregularities.

In the Vectabond™ treated glass, AFM showed holes as big as 50 nm in diameter and 5 nm in height, most likely due to uneven functionalization of the glass. However, these holes constitute less than 3% of the total surface area. The rest of the surface has an R_a similar to untreated glass. Consequently, a different factor should be responsible of the remarkable drop in moving molecules and in their diffusion constant. On glass, carborane can form hydrogen bonds of the type B–H···O (~ 1.1 kcal/mol for hydroxyl-terminated glass)[29] with the surface. On the other hand, amines can form unusual dihydrogen bonds of the type B–H···H–N (2.1 – 5 kcal/mol)[30,31] with boranes and carboranes. Therefore, the surface-carborane interactions are stronger in the Vectabond™ treated glass than in intact glass, which might account for the lower fraction of moving molecules and smaller diffusion constant.

2.3. Conclusions

In summary, the synthesis of three BODIPY-containing highly fluorescent nanocars, one analogue, and a trimer was achieved using a modular approach that involves a versatile BODIPY containing axle. The nanocars were prepared in five steps with overall yields of 49%, 45%, and 46% for **1**, **2**, and **3**, respectively. Electronic spectroscopic studies revealed that the nanocars exhibit absorption centered around 550 nm and have high fluorescence quantum yields.

Through the study of the motion of BODIPY-based nanocar **2** in glass, we have shown that a significant improvement in the number of moving molecules can be achieved

with an intrinsically fluorescent nanocar. Furthermore, we found that both the surface roughness and the interaction strength between the nanocar wheels and the substrate are important factors in determining the percentage of moving nanocars and their speeds. When changing the surface from hydroxyl to amine termination, the speed decreased 2-fold from 4.2 to 2.1 nm/s.

2.4. Experimental Section

General Methods. ^{1}H NMR and ^{13}C NMR spectra were recorded at 400 or 500 and 100 or 125 MHz, respectively. Chemical shifts (δ) are reported in ppm from tetramethylsilane (TMS). Mass spectrometry was performed at Rice University or the University of South Carolina Mass Spectrometry Laboratory. All MALDI-TOF experiments were performed using alpha cyano-4-hydroxy-cinnamic acid as the matrix. FTIR spectra were recorded using a Nicolet FTIR Infrared Microscope with ATR objective with 2 cm^{-1} slit. Melting points were not recorded since the compounds did not melt below 200 °C. Reagent grade tetrahydrofuran (THF) was distilled from sodium benzophenoneketyl. Triethylamine (Et_3N), dichloromethane (CH_2Cl_2) and 1,2-dichloroethane were distilled from CaH_2 under N_2 atmosphere. Hexanes were distilled. Optima grade chloroform ($CHCl_3$) was used. THF and Et_3N were degassed with a stream of argon for 30 min before being used in the Sonogashira coupling reactions. 2,4-dimethylpyrrole was distilled from CaH_2 under nitrogen atmosphere. Trimethylsilylacetylene (TMSA) was donated by FAR Research Inc. or Petra Research. All other chemicals were purchased from commercial suppliers and used without further purification. Flash column chromatography was performed using 230-400 mesh silica gel from EM Science. Thin layer chromatography (TLC) was performed

using aluminum plates pre-coated with silica gel 60 F_{254} 0.20 mm layer thickness purchased from Sigma Aldrich. The synthesis of 1-ethynyl-p-carborane **8**,[17] 1,4-diiodo-2,5-dimethoxybenzene **11**[23] and 9-butyl-3,6-diiodo-9H-carbazole **12**[24] was performed according to the literature procedures.

Spectroscopic Measurements. Absorption spectra were recorded on a Shimadzu UV-3101PC spectrophotometer. UV–vis spectra have 2 nm slit. The fluorescence emission spectra were obtained in a Perkin Elmer LS50B instrument, using $CHCl_3$ solutions exposed to air with absorbance between 0.01 – 0.06. Two emission spectra were recorded for each compound and the two quantum yields obtained were then averaged. All fluorescence spectra were corrected. Excitation was done at the corresponding λ_{max} - 30 nm wavelength. Rhodamine 6G was used as the reference (ϕ_{ref} = 0.95 in EtOH, λ_{exc} = 488 nm).[32] The fluorescence quantum yields were calculated from eq. 1. *F* denotes the integral of the corrected fluorescence spectrum, *A* is the absorbance at the excitation wavelength and *n* is the refractive index of the medium.

$$\Phi_{\text{exp}} = \Phi_{\text{ref}} \frac{F\{1-\exp(-A_{\text{ref}}\ln 10)\}n^2}{F_{\text{ref}}\{1-\exp(-A\ln 10)\}{n_{\text{ref}}}^2} \quad (2.1)$$

General Procedure for the Coupling of a Terminal Alkyne with an Aryl Iodide Using a Palladium-Catalyzed Cross-Coupling (Sonogashira) Protocol. To an oven-dried round bottom flask or Schlenk tube equipped with a magnetic stir bar were added the aryl halide, the terminal alkyne, $PdCl_2(PPh_3)_2$ (ca. 5 mol% per aryl halide) and CuI (ca. 10 mol% per aryl halide). A solvent system of THF:Et_3N 3:1 was well-degassed under argon for 30 min prior to addition to the reaction mixture. Upon completion, the reaction was quenched with a saturated solution of NH_4Cl. The organic layer was then diluted with CH_2Cl_2 (2×) and

washed with water or saturated NH_4Cl (1×). The combined aqueous layers were extracted with CH_2Cl_2 (2×). The combined organic layers were dried over $MgSO_4$, filtered, and the solvent was removed from the filtrate in vacuo to afford the crude product, which was purified by column chromatography (silica gel). Eluents and other slight modifications are described below for each compound.

BODIPY 5.[17] (Modified procedure[33]). *p*-iodobenzoyl chloride (2238 mg, 8.4 mmol) was added to an oven-dried 250 ml round bottom flask and then was dissolved in freshly distilled 1,2-dichloroethane (150 mL). Freshly distilled 2,4-dimethylpyrrole (1.7 mL, 16.8 mmol) was added via syringe. After 13 hr at reflux, the mixture was cooled to room temperature and then triethylamine (6.0 mL, 42.6 mmol) was added. Borontrifluoride etherate (9.0 mL, 72.24 mmol) was added after stirring the mixture 10 min. The mixture was heat at reflux for 2 h. The solvent was removed in vacuo and the residue was purified on a silica gel column using 3-5% EtOAc in hexanes as eluent to give **5** as an orange solid with metallic luster (901 mg, 2.00 mmol, 24%). ^{1}H NMR (400 MHz, $CDCl_3$, ppm) δ 7.85 (d, 2H *J* = 8.0 Hz), 7.05 (d, 2H *J* = 8.0 Hz), 5.99 (s, 2H), 2.55 (s, 6H), 1.42 (s, 6H).

TMS-protected BODIPY 6. See the general procedure for the Pd/Cu coupling reaction. The materials used were **5** (437 mg, 0.97 mmol), $Pd[PPh_3]_2Cl_2$ (34 mg, 0.048 mmol), CuI (19 mg, 0.097 mmol), THF (8 mL) and Et_3N (3 mL). TMSA (0.17 mL, 1.17 mmol) was added via syringe and the mixture was stirred at room temperature for 16 h. The residue was purified by flash column chromatography (silica gel, 20% CH_2Cl_2 in hexanes) to provide **6** (405 mg, 0.964 mmol, 99%) as an orange solid. FTIR (neat) 3089, 3045, 2960, 2925, 2851, 2320, 2161, 1537, 1513, 1463, 1407, 1307, 1245, 1183, 1156 cm^{-1}; ^{1}H NMR

(400 MHz, $CDCl_3$, ppm) δ 7.60 (d, 2H *J* = 8.0 Hz), 7.24 (d, 2H *J* = 8.0 Hz), 5.98 (s, 2H), 2.55 (s, 6H), 1.40 (s, 6H), 0.28 (s, 9H); ^{13}C NMR (100 MHz, $CDCl_3$, ppm) δ 156.0, 143.2, 140.9, 135.4, 132.9, 131.3, 128.3, 124.1, 121.5, 104.4, 96.0, 14.82, 14.80, 0.1; EI-HRMS *m*/*z* calcd for $C_{24}H_{27}BF_2N_2Si$ 420.1995, found 420.2005.

Diiodo BODIPY 7. A 100 mL round-bottom flask equipped with a magnetic stir bar was charged with **6** (850 mg, 2.02 mmol), 30 mL of CH_2Cl_2 and 10 mL of DMF. *N*-iodosuccinimide (1136 mg, 5.05 mmol) was added and the orange solution was stirred at room temperature for 21 h. A red solution was obtained. The CH_2Cl_2 was removed in vacuum and the residue was treated with 100 mL of water. The mixture was then extracted with Et_2O (100 mL × 3). The combined organic fractions were mixed with 50 mL of CH_2Cl_2 and then dried with $MgSO_4$. The solvent was removed in vacuum and the residue was purified by flash column chromatography (silica gel, 40% CH_2Cl_2 in hexanes) to provide **7** (1.14 g, 1.70 mmol, 84%) as a red solid. FTIR (neat) 2951, 2916, 2848, 2359, 2318, 2153, 1525, 1443, 1404, 1345, 1301, 1245, 1171 cm^{-1}; ^1H NMR (400 MHz, $CDCl_3$, ppm) δ 7.63 (d, 2H *J* = 8.0 Hz), 7.21 (d, 2H *J* = 8.0 Hz), 2.64 (s, 6H), 1.41 (s, 6H), 0.29 (s, 9H); ^{13}C NMR (125 MHz, $CDCl_3$, ppm) δ 157.3, 145.4, 140.6, 135.0, 133.2, 131.3, 128.1, 124.8, 104.1, 96.7, 86.1, 17.4, 16.3, 0.12; EI-HRMS *m*/*z* calcd for $C_{24}H_{25}BF_2I_2N_2Si$ 671.9936, found 671.9938.

TMS-protected axle 9. See the general procedure for the Pd/Cu coupling reaction. The materials used were **7** (400 mg, 0.59 mmol), **8** (300 mg, 1.78 mmol), $Pd[PPh_3]_2Cl_2$ (42 mg, 0.06 mmol) and CuI (23 mg, 0.12 mmol), THF (7.5 mL) and Et_3N (2.5 mL). The mixture was stirred at 50 °C for 7 h. The crude was purified by column chromatography (silica gel, 20% CH_2Cl_2 in hexanes as eluent) to provide **9** (396 mg, 0.53 mmol, 88%) as a red solid.

FTIR (neat) 3060, 2957, 2922, 2895, 2854, 2603, 2238, 2158, 1528, 1481, 1392, 1319, 1260, 1186 cm^{-1}; ^{1}H NMR (400 MHz, $CDCl_3$, ppm) δ 7.59 (d, 2H *J* = 8.0 Hz), 7.12 (d, 2H *J* = 8.0 Hz), 3.20-1.50 (br m, 28H), 1.32 (s, 6H), 0.29 (s, 9H); ^{13}C NMR (100 MHz, $CDCl_3$, ppm) δ 159.1, 145.4, 142.3, 134.2, 133.1, 131.0, 127.9, 124.8, 114.7, 104.0, 96.7, 93.3, 72.1, 70.0, 59.9, 13.7, 0.08; EI-HRMS *m/z* calcd for $C_{32}H_{47}B_{21}F_2N_2Si$ 752.5588, found 752.5597.

Axle 10. A 100 mL round-bottom flask equipped with a magnetic stir bar was charged with **9** (360 mg, 0.48 mmol), 15 mL of MeOH and 15 mL of THF. K_2CO_3 was added (99 mg, 0.72 mmol) and the mixture was stirred at room temperature for 1 h. The reaction was quenched with 30 mL of 15% NH_4Cl and then extracted with CH_2Cl_2 (50 mL × 2). The combined organic fractions were dried with $MgSO_4$ and evaporated in vacuum. The residue was purified by column chromatography (silica gel, 20% CH_2Cl_2 in hexanes) to provide **10** (256 mg, 0.38 mmol, 79%) as a red solid. FTIR (neat) 3276, 3061, 2952, 2925, 2854, 2226, 2158, 1521, 1481, 1396, 1319, 1259, 1183 cm^{-1}; ^{1}H NMR (400 MHz, $CDCl_3$, ppm) δ 7.61 (d, 2H *J* = 8.0 Hz), 7.15 (d, 2H *J* = 8.0 Hz), 3.21 (s, 1H), 3.18-1.60 (br m, 28H), 1.33 (s, 6H); ^{13}C NMR (125 MHz, $CDCl_3$, ppm) δ 159.2, 145.4, 142.1, 134.7, 133.3, 131.0, 128.1, 123.9, 114.8, 93.3, 82.8, 79.3, 72.1, 70.0, 60.0, 13.7; EI-HRMS *m/z* calcd for $C_{29}H_{39}B_{21}F_2N_2$ 680.5195, found 680.5199.

Nanocar 1. Axle **10** (8 mg, 0.012 mmol), $Pd[PPh_3]_2Cl_2$ (2 mg, 2.8 μmol), CuI (1.1 mg, 6 μmol), THF (3 mL) and Et_3N (1 mL) were added to a Schlenk tube open to air. The mixture was stirred for 10 min at room temperature. Since axle **10** was consumed according to TLC, the solvent was removed. The residue was purified by column chromatography (silica gel, 30% $CHCl_3$ in hexanes) to provide nanocar **1** (6.8 mg, 0.005

mmol, 85%) as a red solid. FTIR (neat) 3060, 2922, 2654, 2612, 2359, 2323, 2238, 1528, 1479, 1389, 1319, 1260, 1183 cm^{-1}; ^{1}H NMR (400 MHz, $CDCl_3$, ppm) δ 7.67 (d, 4H *J* = 8.0 Hz), 7.20 (d, 4H *J* = 8.0 Hz), 3.30-1.58 (br m, 56H), 1.35 (s, 12H); ^{13}C NMR (100 MHz, $CDCl_3$, ppm) δ 159.4, 145.3, 141.8, 135.3, 133.6, 130.9, 128.3, 123.3, 114.9, 93.4, 81.4, 75.5, 72.0, 69.9, 60.0, 13.7; MALDI m/z calcd for $C_{58}H_{76}B_{42}F_4N_4$ 1359.3, found 1359.1.

Nanocar 2. See the general procedure for the Pd/Cu coupling reaction. The materials used were axle **10** (28 mg, 41.0 μmol), 1,4-dimethoxy-2,5-diiodobenzene **11** (5.7 mg, 14.6 μmol), $Pd[PPh_3]_2Cl_2$ (1 mg, 1.4 μmol) and CuI (0.5 mg, 2.7 μmol). 3 mL of a 3:1 THF:Et_3N mixture were added inside a dry box. The mixture was stirred at 50 ºC for 6 h. The solvent was removed in vacuum and the resultant solid was purified by column chromatography in silica gel (25-35% $CHCl_3$ in hexanes). Nanocar **2** was obtained (17.5 mg, 11.4 μmol, 78%) as a red solid. FTIR (neat) 3063, 2957, 2919, 2851, 2612, 2365, 2323, 2238, 1722, 1531, 1460, 1395, 1322, 1263, 1186 cm^{-1}; ^{1}H NMR (400 MHz, $CDCl_3$, ppm) δ 7.70 (d, 4H *J* = 8.0 Hz), 7.18 (d, 4H *J* = 8.0 Hz), 7.09 (s, 2H) 3.95 (s, 6H), 3.30-1.58 (br m, 56H), 1.36 (s, 6H); ^{13}C NMR (125 MHz, $CDCl_3$, ppm) δ 159.2, 154.2, 145.4, 142.3, 134.2, 132.8, 131.0, 128.0, 124.8, 115.8, 114.7, 113.4, 94.4, 93.3, 87.6, 72.1, 70.0, 60.0, 56.7, 13.7; MALDI m/z calcd for $C_{66}H_{84}B_{42}F_4N_4O_2$ 1495.4, found 1495.2.

Nanocar 3. See the general procedure for the Pd/Cu coupling reaction. The materials used were **10** (64 mg, 0.09 mmol), 9-butyl-3,6-diiodo-9H-carbazole **12** (15 mg, 0.03 mmol), $Pd[PPh_3]_2Cl_2$ (4.5 mg, 0.006 mmol) and CuI (2.5 mg, 0.013 mmol). 2.5 mL of a 3:1 THF:Et_3N mixture were added inside a dry box. The mixture was stirred at room temperature for 14 h. The solvent was removed in vacuo and the resultant solid was

purified by column chromatography (silica gel using 10-25% CH_2Cl_2 in hexanes) to provide **3** (40 mg, 0.025 mmol, 80%) as a red solid. FTIR (neat) 3060, 2957, 2922, 2857, 2606, 2359, 2321, 2229, 2209, 1528, 1478, 1392, 1319, 1263, 1183 cm^{-1}; ^1H NMR (400 MHz, $CDCl_3$, ppm) δ 8.33 (d, 2H *J* = 4.0 Hz), 7.71 (m, 6H), 7.44 (d, 2H *J* = 8.0 Hz), 7.19 (d, 4H *J* = 8.0 Hz), 4.34 (t, 2H, *J* = 7.0 Hz), 3.20-1.60 (br m, 60H), 1.40 (s, 12H), 1.00 (t, 3H, *J* = 7.0 Hz); ^{13}C NMR (125 MHz, $CDCl_3$, ppm) δ 159.1, 145.5, 142.6, 141.0, 133.6, 132.6, 131.1, 130.1, 128.0, 125.5, 124.6, 122.7, 114.7, 113.6, 109.5, 93.3, 92.8, 87.2, 72.1, 70.0, 68.2, 59.9, 44.0, 31.3, 25.8, 20.8, 14.1, 13.75, 13.70; MALDI *m/z* calcd for $C_{74}H_{92}B_{42}F_4N_5$ 1581.6, found 1581.2.

TMS-protected axle 13. See the general procedure for the Pd/Cu coupling reaction. The materials used were **7** (188 mg, 0.28 mmol), 3,3-dimethyl-1-butyne (0.1 mL, 0.84 mmol), $Pd[PPh_3]_2Cl_2$ (19.5 mg, 27.9 μmol), CuI (11 mg, 56.0 μmol), THF (6 mL) and Et_3N (2 mL). The mixture was stirred at room temperature for 12 h. The crude was purified by column chromatography (silica gel using 25-30% CH_2Cl_2 in hexanes) to provide **13** (99 mg, 0.17 mmol, 61%) as a red solid. FTIR (neat) 2966, 2925, 2863, 2603, 2326, 2288, 2164, 1531, 1469, 1398, 1360, 1263, 1198 cm^{-1}; ^1H NMR (500 MHz, $CDCl_3$, ppm) δ 7.60 (d, 2H *J* = 8.0 Hz), 7.19 (d, 2H *J* = 8.0 Hz), 2.59 (s, 6H), 1.43 (s, 6H), 1.27 (s, 18H), 0.29 (s, 9H); ^{13}C NMR (125 MHz, $CDCl_3$, ppm) δ 158.3, 143.3, 141.0, 135.2, 133.0, 130.8, 128.3, 124.4, 117.1, 106.2, 104.3, 96.2, 70.9, 31.4, 28.5, 13.7, 13.6, 0.1; EI-HRMS *m/z* calcd for $C_{36}H_{43}BF_2N_2Si$ 580.3263, found 580.3257.

Free Axle 14. A 25 mL round-bottom flask equipped with a magnetic stir bar was charged with **13** (85 mg, 0.15 mmol), 5 mL of MeOH and 5 mL of THF. K_2CO_3 was added (24 mg, 0.17 mmol) and the mixture was stirred at room temperature for 1 h. The reaction was

quenched with 10 mL of 15% NH_4Cl and then extracted with CH_2Cl_2 (20 mL × 2). The combined organic fractions were dried with $MgSO_4$ and evaporated in vacuo. The residue was purified by column chromatography (silica gel, 40% CH_2Cl_2 in hexanes) to provide **14** (74 mg, 0.14 mmol, 99%) as a red solid. FTIR (neat) 3272, 2969, 2925, 2866, 2329, 2288, 2226, 2117, 1525, 1466, 1395, 1363, 1257, 1201, 1163 cm^{-1}; ^1H NMR (500 MHz, $CDCl_3$, ppm) δ 7.62 (d, 2H *J* = 8.0 Hz), 7.22 (d, 2H *J* = 8.0 Hz), 3.19 (s, 1H), 2.60 (s, 6H), 1.43 (s, 6H), 1.27 (s, 18H); ^{13}C NMR (125 MHz, $CDCl_3$, ppm) δ 158.3, 143.2, 140.8, 135.5, 133.1, 130.8, 128.4, 123.4, 117.1, 106.3, 83.0, 78.9, 70.9, 31.4, 28.5, 13.7, 13.6; EI-HRMS m/z calcd for $C_{33}H_{35}BF_2N_2$ 508.2862, found 508.2861.

Nanocar analogue 4. See the general procedure for the Pd/Cu coupling reaction. The materials used were **14** (60 mg, 0.12 mmol), 1,4-dimethoxy-2,5-diiodobenzene **11** (18 mg, 0.046 mmol), $Pd[PPh_3]_2Cl_2$ (3 mg, 4.0 μmol) and CuI (1.5 mg, 8.0 μmol). 3 mL of a 3:1 THF:Et_3N mixture were added inside a dry box. The mixture was stirred at room temperature for 12 h. The solvent was removed in vacuo and the resultant solid was purified by column chromatography (silica gel, 50% - 70% $CHCl_3$ in hexanes) to provide **4** (51 mg, 0.044 mmol, 96%) as a red solid. FTIR (neat) 2966, 2919, 2857, 2326, 2226, 1531, 1466, 1395, 1366, 1313, 1260, 1195 cm^{-1}; ^1H NMR (400 MHz, $CDCl_3$, ppm) δ 7.71 (d, 4H *J* = 8.0 Hz), 7.25 (d, 4H *J* = 8.0 Hz), 7.09 (s, 2H), 3.95 (s, 6H), 2.61 (s, 12H), 1.45 (s, 12H), 1.28 (s, 36H); ^{13}C NMR (125 MHz, $CDCl_3$, ppm) δ 158.4, 154.3, 143.2, 141.1, 135.1, 132.7, 130.9, 128.4, 124.4 , 117.1, 115.8, 113.5, 106.3, 94.7, 87.3, 70.9, 56.8, 31.5, 28.4, 13.72, 13.68; MALDI m/z calcd for $C_{74}H_{76}B_2F_4N_4O_2$ 1151.0, found 1150.7.

BODIPY 15: A 25 mL round-bottom flask equipped with a magnetic stir bar was charged with BODIPY **5** (100 mg, 0.22 mmol), 5 mL of CH_2Cl_2, and 5 mL of DMF. *N*-iodosuccinimide (130 mg, 0.58 mmol) was added and the orange solution was stirred at room temperature for 30 hours. A red solution was obtained. The CH_2Cl_2 was removed under vacuum and the residue was treated with 10 mL of water. The mixture was then extracted with Et_2O (25 mL × 3). The combined organic fractions were mixed with 20 mL of CH_2Cl_2 and then dried with $MgSO_4$. The solvent was removed under vacuum and the residue was purified by flash column chromatography (silica gel, 40% CH_2Cl_2 in hexanes) to provide **15** (123 mg, 0.17 mmol, 79%) as a red solid. FTIR (neat) 2957, 2918, 2850, 2360, 2341, 1539, 1400, 1190, 1181 cm^{-1}; ^1H NMR (400 MHz, $CDCl_3$, ppm) δ 7.88 (d, 2H, J = 8.0 Hz), 7.02 (d, 2H, J = 8.0 Hz), 2.64 (s, 6H), 1.43 (s, 6H); ^{13}C NMR (100 MHz, $CDCl_3$, ppm) δ 157.4, 145.3, 139.9, 138.9, 134.5, 131.2, 129.9, 95.6, 86.2, 17.5, 16.3; EI-HRMS m/z calcd for $C_{19}H_{15}BF_2I_3N_2$ $[M-H]^-$ 701.8428, found 700.8439.

BODIPY-based trimer 16: A Schlenk tube equipped with a magnetic stir bar was filled with **15** (100 mg, 0.14 mmol), **8** (110 mg, 0.64 mmol), $Pd[PPh_3]_2Cl_2$ (10 mg, 14.2 μmol), CuI (5.5 mg, 28.4 μmol), THF (9 mL), and Et_3N (3 mL). The solvent mixture of THF:Et_3N = 3:1 was well-degassed under argon for 30 minutes prior to addition of the reactants. The solution was then stirred overnight at 50 °C. The reaction was quenched with a saturated solution of NH_4Cl. The organic layer was then diluted with CH_2Cl_2 (2×). The aqueous layer was extracted with CH_2Cl_2 once. The combined organic layers were dried over $MgSO_4$. The solvent was removed under vacuum and the residue was purified by column chromatography (silica gel, 30-35% $CHCl_3$ in hexanes) to provide **16** (57 mg, 0.069

mmol, 49%) as a red solid. FTIR (neat) 3066, 2922, 2852, 2609, 2360, 2342, 1537, 1476, 1394, 1319, 1261, 1186, 1057, 1013 cm^{-1}; ^{1}H NMR (500 MHz, $CDCl_3$, ppm) δ 7.43 (d, 2H, *J* = 8.0 Hz), 7.09 (d, 2H, *J* = 8.0 Hz), 3.3–1.7 (br m, 39H), 1.28 (s, 6H); ^{13}C NMR (125 MHz, $CDCl_3$, ppm) δ 159.2, 145.3, 141.9, 134.8, 133.0, 130.9, 128.0, 123.0, 114.7, 93.3, 87.3, 78.3, 72.0, 70.0, 69.3, 60.6, 59.9, 13.7 (overlap of two **C**H_3); EI-HRMS *m/z* calcd for $C_{31}H_{48}{}^{11}B_{25}{}^{10}B_6F_2N_2$ $[M-H]^-$ 821.6819, found 821.6856.

Experimental Microscope Setup. Single nanocars were deposited on different substrates by spin coating them from a 10^{-12} mol/L solution in chloroform (Sigma Aldrich) at 3000 rpm for 60 s. Glass coverslips (Fisher Scientific) were cleaned in oxygen plasma (Harrick Plasma) before spin coating. After the exposure to the oxygen plasma the glass surface was hydroxyl-terminated. Hydroxyl-terminated, but roughened glass substrates were prepared by reactive ion etching (Trion Technology) using the following conditions: 5 sccm O_2, 10 sccmCF_4, 100 WRF power, 30 mTorr total pressure. For the Vectabond treatment of the glass, plasma-cleaned glass coverslips were immersed into Vectabond reagent solution (Vector Laboratories, 20 μL/ml in acetone) for 5 min.[28] The coverslips were then taken out of the Vectabond solution and rinsed with molecular biology grade water (Thermo Scientific) for 30 s and dried under nitrogen. The Vectabond treatment changes the surface functionality from hydroxyl- to amine-terminated. All solvents used in these experiments were of spectroscopic grade and were used as received. Blank tests were always performed before nanocar deposition to test for fluorescence impurities from the solvent and the substrate. Single-molecule fluorescence images were taken with a home-built confocal microscope consisting of a 514 nm Ar^+ laser (Modu-Laser) as the excitation source, an inverted microscope (Zeiss Axiovert 200), a xyz piezo scanning stage

(Physik Instrumente), an oil-immersion objective lens (Zeiss Fluar), and two avalanche photodiodes (Perkin-Elmer). The nanocars were excited using circularly polarized light with a power of 500 nW. Fluorescence was separated from the laser excitation using appropriate dichroic and notch filters. The fluorescence images were formed by scanning the sample across the focused laser beam with the scanning stage. Image dimensions were 10 μm × 10 μm and consisted of 128 × 128 pixels with an integration time of 1ms/pixel. The S/N ratio was comparable for all substrates, suggesting that the results were not influenced by different degrees of fluorescence quenching through nanocar surface interactions. All experiments were repeated at least three times starting every measurement with the preparation of the substrates, nanocar deposition, and fluorescence imaging. The average diffusion constants obtained for each measurement were used to calculate the reported errors.

Supporting Information. ^{1}H and ^{13}C NMR spectra of new compounds, time-lapse fluorescent images, and AFM images of the different substrates.

2.5. References

1. Godoy, J.; Vives, G.; Tour, J. M. *Org. Lett.* **2010**, *12*, 1464-1467.
2. Kathua, S.; Godoy, J.; Tour, J. M.; Link, S. *J. Phys. Chem. Lett.* **2010**, *1*, 3288-3291.
3. Schliwa, M., Ed. *Molecular Motors*; Wiley-VCH: Germany, 2003.
4. Huang, T. J.; Juluri, B. K. *Nanomedicine* **2008**, *3*, 107–124.
5. Kay, E. R.; Leigh, D. A.; Zerbetto, F. *Angew. Chem. Int. Ed.* **2007**, *46*, 72–191.
6. Shirai, Y.; Osgood, A. J.; Zhao, Y.; Kelly, K. F.; Tour, J. M. *Nano Lett.* **2005**, *5*, 2330–2334.

7. a) Morin, J-F.; Sasaki, T.; Shirai, Y.; Guerrero, J. M.; Tour, J. M. *J. Org. Chem.* **2007**, *72*, 9481–9490. b) Vives, G.; Kang, J.; Kelly, K. F.; Tour, J. M. *Org. Lett.* **2009**, *11*, 5602-5605.
8. Vives, G.; Tour, J. M. *Tetrahedron Lett.* **2009**, *50*, 1427–1430.
9. Vives, G.; Tour, J. M. *Acc. Chem. Res.* **2009**, *42*, 473–487.
10. Grill, L. *J. Phys. Condens. Matter* **2008**, *20*, 053001–053019.
11. a) Yildiz, A.; Forkey, J. N.; McKinney, S. A.; Ha, T.; Goldman, Y. E.; Selvin, P. R. *Science* **2003**, *300*, 2061-2065. b) Yildiz, A.; Tomishige, M.; Vale, R. D.; Selvin, P. R. *Science* **2004**, *303*, 676-678. c) Qiu, W.; Derr, N. D.; Goodman, B. S.; Villa, E.; Wu, D.; Shih, W.; Reck-Peterson, S. L. *Nat. Struct. Mol. Biol.* **2012**, *19*, 193-201. d) DeWitt, M. A.; Chang, A. Y.; Combs, P. A.; Yildiz, A. *Science* **2012**, *335*, 221-225.
12. Vives, G.; Guerrero, J. M.; Godoy, J.; Kathua, S.; Wang, Y.-P.; Kiappes, J. L.; Link, S.; Tour, J. M. *J. Org. Chem.* **2010**, *75*, 6631-6643.
13. Khatua, S.; Guerrero, J. M.; Claytor, K.; Vives, G.; Kolomeisky, A. B.; Tour, J. M.; Link, S. *ACS Nano* **2009**, *3*, 351–356.
14. Treibs, A.; Kreuzer, F. – H. *Liebigs Ann. Chem.* **1968**, *718*, 208–223.
15. a) Ulrich, G.; Ziessel, R.; Harriman, A. *Angew. Chem. Int. Ed.* **2008**, *47*, 1184–1201.; b) Loudet, A.; Burgess, K. *Chem. Rev.* **2007**, *107*, 4891–4932.
16. Ha, T.; Laurence, T. A.; Chemla, D. S.; Weiss, S. *J. Phys. Chem. B* **1999**, *103*, 6839–6850.
17. Burghart, A.; Kim, H.; Welch, M. B.; Thoresen, L. H.; Reibenspies, J.; Burgess, K.; Bergstroem, F.; Johansson, L. B.-A. *J. Org. Chem.* **1999**, *64*, 7813–7819.
18. Bonardi, L.; Ulrich, G.; Ziessel, R. *Org. Lett.* **2008,** *10*, 2183–2186.

19. Fox, M. A.; Cameron, A. M.; Low, P. J.; Paterson, M. A. J.; Batsanov, A. S.; Goeta, A. E.; Rankin, D. W. H.; Robertson, H. E.; Schirlin, J. T. *Dalton Trans.* **2006**, *29*, 3544–3560.

20. Wan, C. – W.; Burghart, A.; Chen, J.; Bergström, F.; Johansson, L. B.-Å.; Wolford, M. F.; GyumKim, T.; Topp, M. R.; Hochstrasser, R. M.; Burgess, K. *Chem. Eur. J*. **2003**, *9*, 4430–4441.

21. Eglinton, G.; McCrae, W. *Adv. Org. Chem.* **1963***, 4,* 225–328.

22. Maeda, H.; Hasegawa, M.; Hashimoto, T.; Kakimoto, T.; Nishio, S.; Nakanishi, T. *J. Am. Chem. Soc.* **2006**, *128,* 10024–10025.

23. Waybright, S. M.; Singleton, C. P.; Wachter, K.; Murphy, C. J.; Bunz, U. H. F. *J. Am. Chem. Soc.* **2001**, *123*, 1828–1833.

24. Zhao, T.; Liu, Z.; Song, Y.; Xu, W.; Zhang, D.; Zhu, D. *J. Org. Chem.* **2006**, *71*, 7422–7432.

25. After publication of our results (ref. 1) two other types of BODIPY-carborane dyads have been reported. a) Ziessel, R.; Ulrich, G.; Olivier, J.–H.; Bura, T.; Sutter, A. *Chem. Comm.* **2010**, *46*, 7978–7980. b) Hablot, D.; Sutter, A.; Retailleau, P.; Ziessel, R. *Chem.–Eur. J.* **2012**, *18*, 1890–1895.

26. Yogo, T.; Urano, Y.; Ishitsuka, Y.; Maniwa, F.; Nagano, T. *J. Am. Chem. Soc.* **2005**, *127*, 12162–12163.

27. Claytor, K.; Khatua, S.; Guerrero, J. M.; Tcherniak, A.; Tour, J. M.; Link, S. *J. Chem. Phys*. **2009**, *130*, 164710-1–164710-9.

28. Taylor, N. J.; Darugar, Q.; Kourentzi, K.; Willson, R. C.; Landes, C. F. *Biochem. Biophys. Res. Commun.* **2008**, *373*, 213–218.

29. Andrews, P. C.; Hardie, M. J.; Raston, C. L. *Coord. Chem. Rev.* **1999**, *189*, 169-198.

30. Fanfrlik, J.; Lepsik, M.; Horinek, D.; Havlas, Z.; Hobza, P. *ChemPhysChem* **2006**, *7*, 1100-1105.

31. Patwari, G. N. *J. Phys. Chem. A* **2005**, *109*, 2035-2038.

32. Magde, D.; Wong, R.; Seybold, P. G. *Photochem. Photobiol*. **2002**, *75*, 327−334.

33. Chen, J.; Burghart, A.; Wan, C-W.; Thai, L.; Ortiz, C.; Reibenspies, J.; Burgess, K. *Tetrahedron Lett*. **2000**, *41*, 2303−2307. b) Chen, J.; Burghart, A.; Derecskei-Kovacs, A.; Burgess, K. *J. Org. Chem*. **2000**, *65*, 2900−2906.

2.6. Experimental Contributions Section

My contributions to the experimental work described in this chapter are the following: I conceived the project and conducted the synthesis of all the molecules. Guillaume Vives supervised the synthetic strategy and calculated the fluorescence quantum yields. Saumyakanti Khatua carried out the single-molecule fluorescence spectroscopy experiments.

Chapter 3

Toward Chemical Propulsion: Synthesis of ROMP–Propelled Nanocars

Note: This chapter was copied in its total from a paper that I coauthored.[1] Reprinted with permission from reference 1. Copyright 2011 American Chemical Society.

3.1. Introduction

In the current trend of miniaturization of devices, science and engineering on the nanoscale offers new possibilities for the design and synthesis of functional materials.[2] In contrast to the "top-down" approach that is currently reaching its limits, nanoscale engineering is also driven by a "bottom-up" approach. Nanomachines are promising new entities that are designed to exhibit controlled mechanical motion resembling their macroscopic analogues.[3–5] Among the most important tasks for molecular machines is the directed motion and transport of nanocargo.

We have recently developed a family of nanovehicles that resemble their macroscopic analogues, with the goal of transporting nanocargo in a controlled manner on surfaces.[6,7] These so-called nanocars are composed of a chassis connected to axles terminated by molecular wheels. The first generation nanocar bearing C_{60} wheels showed thermally activated translational motion and pivoting on a gold surface.[8,9] The translational motion occurred perpendicular to the axles. The directionality of the translation was possible due to the rolling action of the molecular wheels. However, in order to obtain unidirectional motion, the nanocar must consume energy from an external source since latent thermal energy only leads to two-dimensional Brownian motion.[3]

The goal of the present work is to synthesize a nanomachine that can convert energy inputs into controlled unidirectional motion on a surface. In the first examples of such control, the electric field gradient of a scanning tunneling microscope tip was successfully used to attract a nanocar in a forward-rolling motion.[8] Also, a nanocar incorporating a light-powered Feringa motor[10] and a diazobenzene-based nanoworm[11] have already been described. However, investigation of other sources of energy, such as the thrust that can be developed from the energy released during a chemical reaction, would permit the synthesis of a family of nanovehicles that can be operated using various stimuli. For example, biological nanomachines such as myosin or ATP synthase commonly use the energy liberated by a chemical reaction (generally the hydrolysis of ATP) to bias Brownian motion into unidirectional motion. Alternatively, artificial chemically powered nanomotors working in solution have recently been described.[12] These nanomotors are bimetallic nanorods that use the catalytic dismutation of hydrogen peroxide for propulsion in solution.

Inspired both by nature and artificial systems, in this work, we have investigated the functionalization of *p*-carborane-wheeled nanocars with Ru based metathesis catalysts for potential propelling by a ring-opening metathesis polymerization (ROMP).

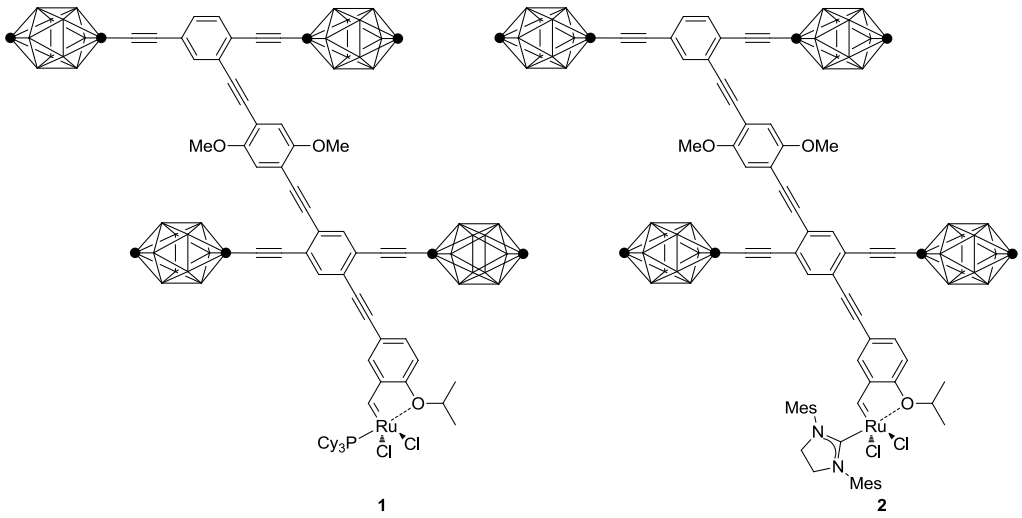

Figure 3.1.[1] Ru-based metathesis catalyst nanocars **1** and **2**. Every vertex of the carborane wheel is BH except the darkened sites, where the outer (*para*) is CH and the inner (*ipso*) is alkynyl-substituted C.

Three main methods have been previously explored to attach a metathesis catalyst to a support.[13] Permanent binding can be achieved by exchange of the anionic ligands or *via* modification of the N-heterocyclic carbene (NHC) ligand, whereas temporary attachment can be accomplished by a benzylidene moiety. In this report, we present the synthesis and catalytic activity toward ROMP of two modified Hoveyda–Grubbs metathesis catalysts, **1** and **2**, bound to a carborane-wheeled nanocar by a benzylidene moiety (Figure 3.1). By feeding the nanocar with a cyclic strained alkene such as norbornene, a ROMP should occur

on the surface and the energy liberated might provide the thrust to propel the nanocar (Figure 3.2).

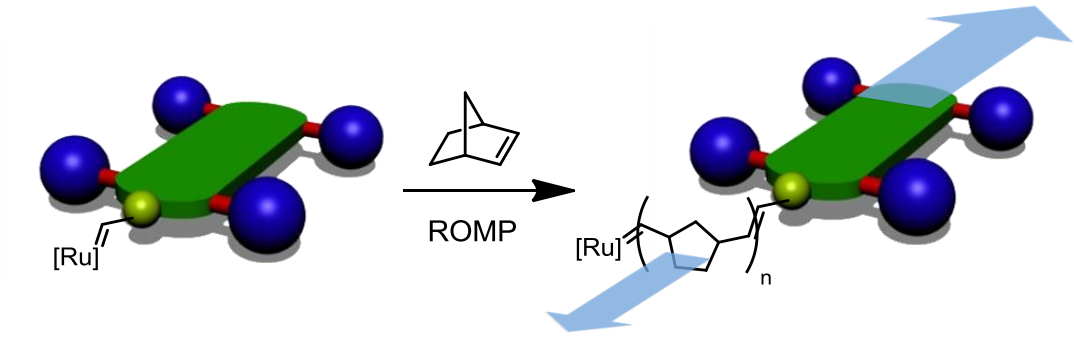

Figure 3.2.[1] Proposed propulsion scheme for a nanocar composed of four wheels (blue) connected to a chassis (green) by two axles (red), and bearing a ruthenium-based ROMP catalyst. By addition of norbornene, a ROMP should occur at the ruthenium site leading to a polymer growth on one end of the nanocar. In the process, the energy liberated might propel the nanocar. Concurrently, the ruthenium catalyst and the nanocar will move away from each other (blue arrows).

3.2. Results and Discussion

3.2.1. Design and Synthesis

The syntheses of nanocars **1** and **2** are based on a modular approach using a styryl-substituted nanocar as a common intermediate. To synthesize the precursor of the isopropoxy styryl fragment, 5-iodosalicylaldehyde was alkylated with 2-iodopropane in the presence of Cs_2CO_3 to give **3**. A Sonogashira coupling between iodide **3** and trimethylsilylacetylene (TMSA) gave protected alkyne **4** which, after deprotection with K_2CO_3 in MeOH, afforded **5** (Scheme 3.1).

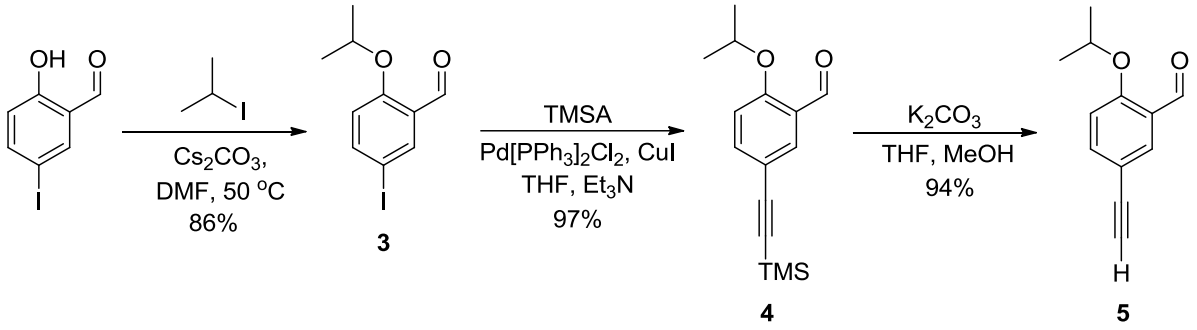

Scheme 3.1.[1] Synthesis of isoproxy benzaldehyde **5**.

The nanocar moiety was first assembled by a statistical coupling between alkyne **6**[14] and axle **7**.[14] Coupling of the resultant iodide nanocar **8** with alkyne **5** afforded aldehyde nanocar **9** in good yield. Finally, styryl-substituted nanocar **10** was obtained by olefination of aldehyde **9** under conventional Wittig conditions (Scheme 3.2).

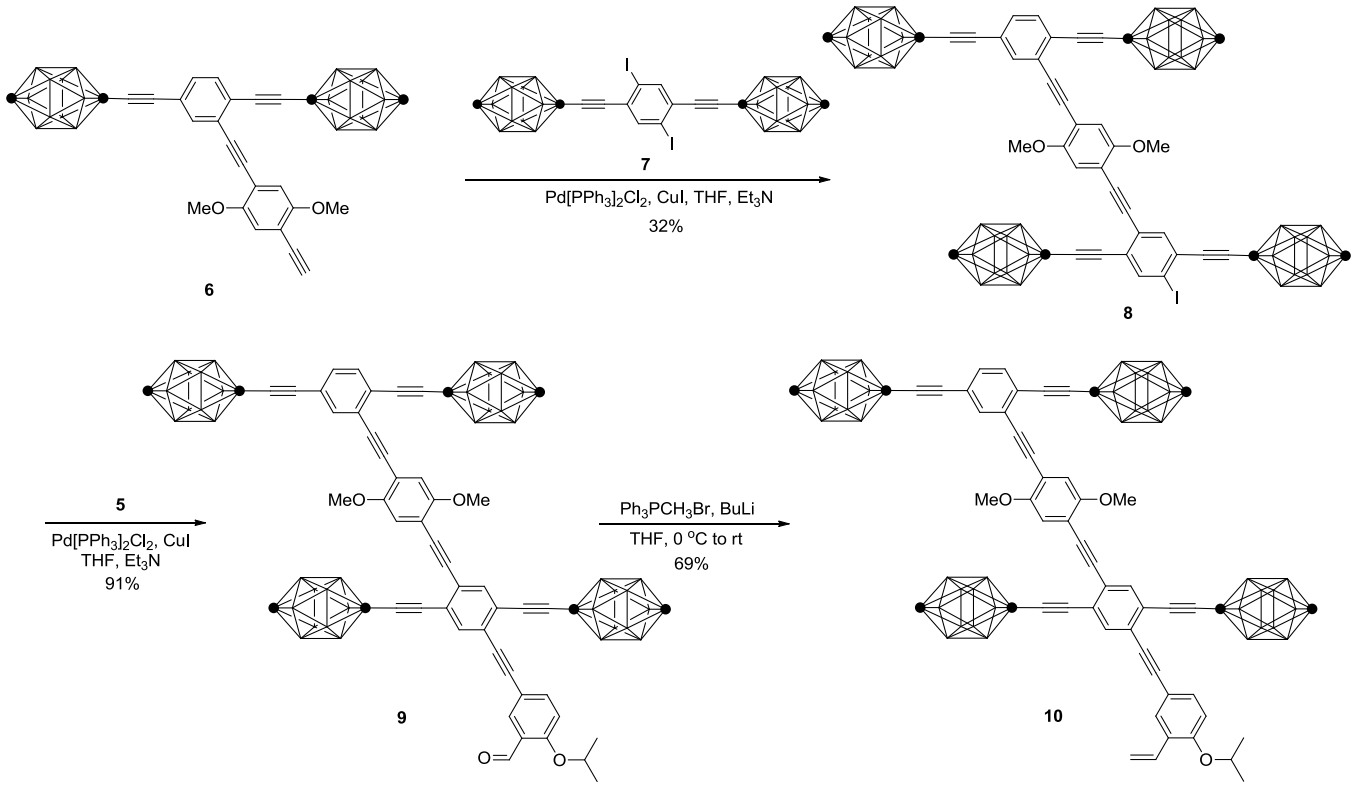

Scheme 3.2.[1] Synthesis of styryl-substituted nanocar **10**.

With styryl-substituted nanocar **10** in hand, we proceeded to the preparation of the catalysts using a ligand exchange procedure (Scheme 3.3).[15] Nanocar **10** was treated with Grubbs first-generation **11**[16] or second-generation catalyst **12**[17] in CH_2Cl_2 at 40 °C for 2 h in presence of CuCl as a phosphine scavenger. ^{1}H NMR analysis of the crude reaction indicated the formation of only one benzylidene-containing species. The other major compound in the mixture was unreacted nanocar **10**. After chromatographic purification on silica gel, phosphine-containing complex **1** was obtained in 63% yield whereas NHC-substituted complex **2** was obtained in 53% yield. Although the complexes were stored in a glovebox, they were both air- and moisture-stable. A catalyst solution prepared in $CDCl_3$ under ambient conditions did not show changes by ^{1}H NMR after 3 days.

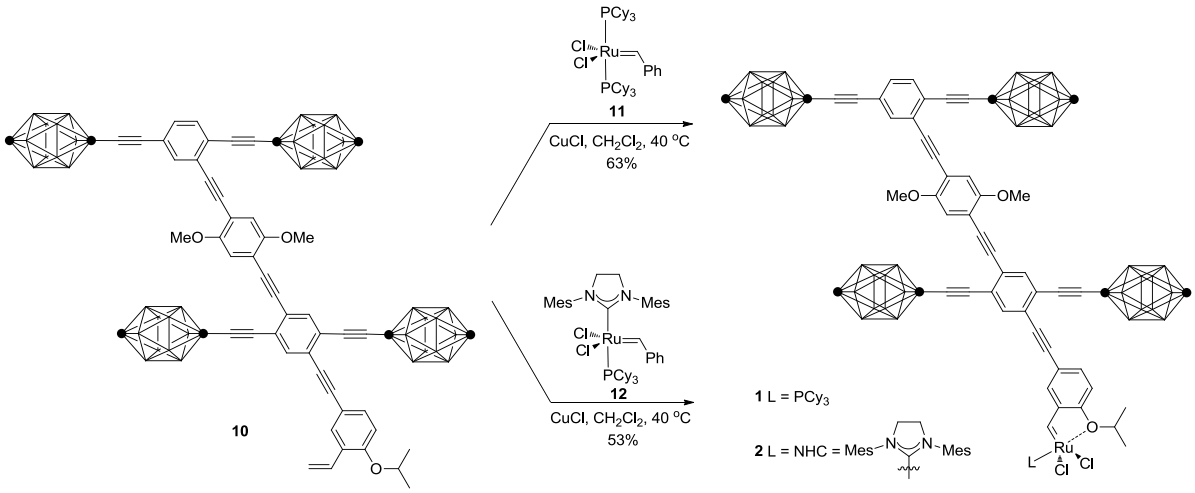

Scheme 3.3.[1] Final assembly of nanocars **1** and **2**.

NMR spectroscopic data were consistent with a typical Hoveyda–Grubbs Ru complex.[18] The alkylidene proton in the phosphine-containing complex **1** was observed in the ^{1}H spectrum as a doublet at 17.40 ppm with J_{PH} = 4.4 Hz, whereas the benzylidene

carbene ^{13}C signal was observed at 277.4 ppm. The presence of the phosphine ligand was confirmed by the ^{31}P NMR signal observed at 60.16 ppm. In the case of the NHC substituted complex **2**, the benzylidene proton was observed in the ^{1}H spectrum as a broad singlet at 16.61 ppm and the benzylidene carbene ^{13}C resonated at 295.0 ppm. The isopropoxy methine protons were observed at 5.33 and 4.96 ppm for **1** and **2**, respectively.

3.2.2. Catalytic Activity

The catalytic activity of **1** and **2** toward ROMP of 1,5-cyclooctadiene (cod) was tested according to the standard procedure developed by Grubbs (Figure 3.3).[19,20] In that system, cod was selected partially due to its relatively slow polymerization rate, compared to more highly strained cyclic olefins such as norbornene, which facilitates monitoring of the reaction by NMR spectroscopy.

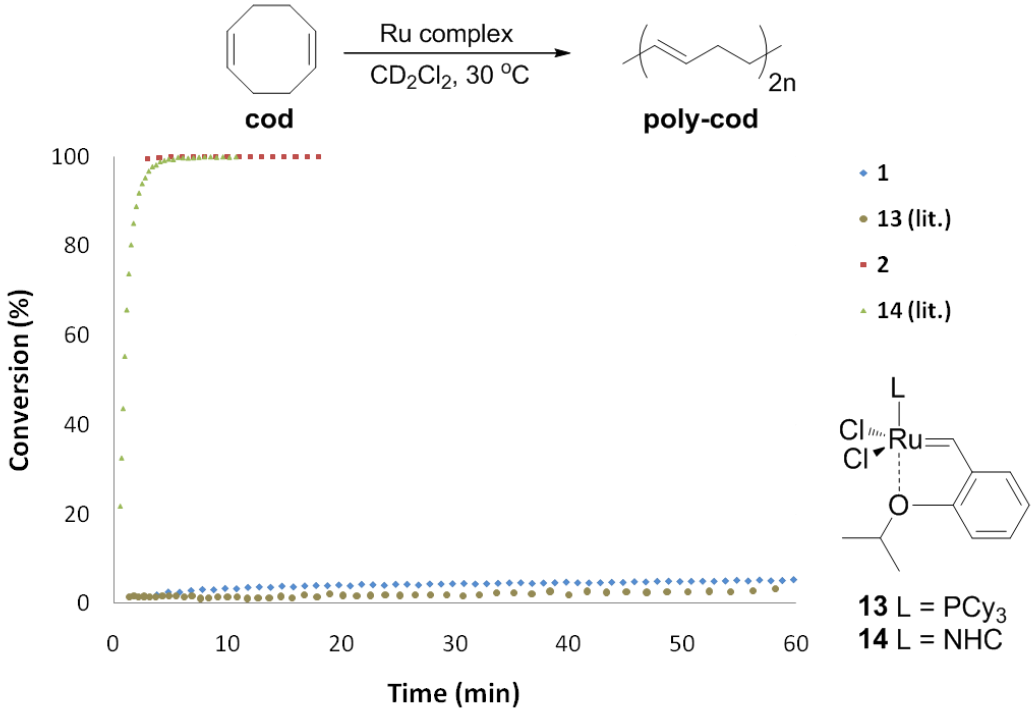

Figure 3.3.[1] ROMP activity of **1** and **2** versus their unsubstituted analogues **13** and **14**.

Only 5% conversion was observed using the phosphine-containing complex **1** as catalyst during the 60 min that the reaction was monitored. Low activity was expected for **1**, however, given that its parent Hoveyda–Grubbs catalyst **13** exhibits 4% conversion under those conditions. On the other hand, nearly complete conversion was observed with the NHC substituted complex **2** when the first spectrum was taken at 3 min. This complex had comparable activity to its parent catalyst **14**.

The activation of oxygen-chelated ruthenium catalysts by electron-withdrawing groups has been well established.[21] One of the most prominent examples is the nitro-substituted complex **15** (Table 3.1) reported by Grela and co-workers. The catalytic activity of **15** toward a variety of olefin metathesis processes is remarkably higher than that of **14**.[22] They reasoned that the electron-withdrawing nitro group would weaken the *i*PrO–Ru chelation and therefore facilitate initiation of the catalytic cycle. Comparison of NMR data between **15** and its parent catalyst **14** further supports their conclusion (Table 3.1).

	δ (ppm) in $CDCl_3$			
cmpd	**C_a**	**H_a**	**C_b**	**H_b**
2	76.2	4.96	295.0	16.61
14	74.9	4.89	296.8	16.56
15	77.6	4.98	291.2	16.47

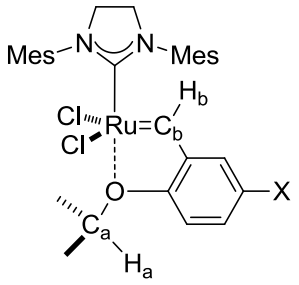

2 X = Nanocar moiety
14 X = H
15 X = NO_2

Table 3.1.[1] Comparison of NMR data of complexes **2**, **14**, and **15**.

The *i*PrO methine proton (H_a) and carbon (C_a) of **15** are shifted downfield compared to **14**, whereas the benzylidene carbene carbon (C_b) and proton (H_b) are shifted upfield. Similarly, the *i*PrO carbon and proton signals of NHC-substituted nanocar **2** are shifted downfield, whereas its benzylidene carbene carbon is shifted upfield, although the benzylidene proton is shifted downfield. Therefore, it is possible that the sp-linked nanocar chassis slightly decreases the availability of the isopropoxy-ether lone pair to bind the ruthenium and thereby might cause a subtle enhancement of the catalytic activity of **2** with respect to **14**, though the data obtained are too close to make any conclusive assessments.

Due to the low conversion observed with cod, the catalytic activity of phosphine containing nanocar **1** toward ROMP was also tested with a more reactive substrate (Scheme 3.4). With norbornene, a highly viscous mixture was obtained within a few minutes, indicating a high degree of polymerization. According to the ratio of the integrals of the vinyl protons in the ring-opened polynorbornene, the polymer obtained was, as expected,

predominantly *trans* (84%).

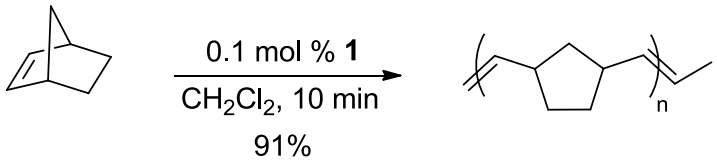

Scheme 3.4.[1] ROMP of norbornene catalyzed by **1**.

These results show that both norbornene and 1,5- cyclooctadiene might be usable as chemical fuels for the ROMP-propelled motion of nanocars **1** and **2** on a surface. Designing

the imaging reaction chamber remains a challenge, however. We further tried, unsuccessfully, to prepare the nanocar such that the Ru catalyst would remain permanently bound to the nanocar during and after polymerization.[23]

3.3. Conclusions

In summary, we have synthesized potentially chemically powered nanocars based on olefin metathesis catalysts. We demonstrated that stable yet highly active modified Hoveyda–Grubbs catalyst nanocars **1** and **2** can be prepared using a ligand exchange process on the benzylidene moiety. Their high activity toward ROMP in solution makes them good candidates for surface-initiated ROMP that will permit evaluation of polymer growth to propel the motion of the nanocar.

3.4. Experimental Section

General Methods. ^{1}H NMR and ^{13}C NMR spectra were recorded at 400 or 500 and 100 or 125 MHz, respectively. Chemical shifts (δ) are reported in ppm from residual signal of $CDCl_3$ (δ 7.26 ppm). ^{31}P NMR spectra were recorded at 202 MHz. Chemical shifts of the phosphorus resonances were determined relative to 85% phosphoric acid as the external standard (H_3PO_4: δ 0.0 ppm). All MALDI-TOF experiments were performed using alpha cyano-4-hydroxy-cinnamic acid as the matrix in positive ion mode (+eV). FTIR spectra were recorded using a Nicolet FTIR Infrared Microscope with ATR objective with 2 cm^{-1} slit. Melting points of compounds **3**, **4** and **5** were recorded on a MEL-TEMP Electrothermal melting point apparatus. The other solid compounds did not melt below 200 °C. Reagent

grade tetrahydrofuran (THF) was distilled from sodium benzophenoneketyl. Triethylamine (Et_3N) and dichloromethane (CH_2Cl_2) were distilled from CaH_2 under N_2 atmosphere. THF and Et_3N were degassed with a stream of argon for 30 min before being used in Sonogashira coupling reactions. *cis*,*cis*-1,5-Cyclooctadiene was distilled from CaH_2 under a nitrogen atmosphere. Trimethylsilylacetylene (TMSA) was donated by FAR Research Inc. or Petra Research. All other chemicals were purchased from commercial suppliers and used without further purification. The reactions were conducted under nitrogen atmosphere. Flash column chromatography was performed using 230-400 mesh silica gel from EM Science for all compounds except for nanocars **1** and **2**, which were purified using 40-63 μm Geduran silica gel 60 from EMD Chemicals. Thin layer chromatography (TLC) was performed using aluminum plates pre-coated with silica gel 60 F_{254} 0.20 mm layer thickness purchased from Sigma-Aldrich. The syntheses of **6**[14] and **7**[14] were performed according to reported protocols.

General Procedure for the Coupling of a Terminal Alkyne with an Aryl Iodide Using a Palladium-Catalyzed Cross-Coupling (Sonogashira) Protocol. To an oven-dried round-bottom flask or Schlenk tube equipped with a magnetic stir bar were added the aryl halide, the terminal alkyne, $PdCl_2(PPh_3)_2$ (ca. 5 mol% per aryl halide) and CuI (ca. 10 mol% per aryl halide). A solvent system of THF:Et_3N 3:1 was well-degassed under argon for 30 min prior to addition to the reaction mixture. Upon completion, the reaction was quenched with a saturated solution of NH_4Cl. The organic layer was then diluted with CH_2Cl_2 (2×) and washed with water or saturated NH_4Cl (1×). The combined aqueous layers were extracted with CH_2Cl_2 (2×). The combined organic layers were dried over $MgSO_4$, filtered, and the

solvent was removed from the filtrate *in vacuo* to afford the crude product, that was purified by column chromatography.

Compound 3. A Schlenk tube equipped with a magnetic stir bar was charged with 5-iodosalicyladehyde (823 mg, 3.32 mmol), cesium carbonate (2.14 g, 6.64 mmol), and DMF (30 mL). Then isopropyl iodide (1.2 mL, 11.6 mmol) was added and the mixture stirred overnight at 50 °C. The reaction was quenched with water (50 mL), and then was extracted with diethyl ether (50 mL). The organic layer was washed with water (50 mL ×5). After drying the organic layer with $MgSO_4$, the solvent was removed *in vacuo* to give **3** as a white solid (824 mg, 86%): mp 54–56 °C. FTIR (neat) 3338, 3092, 3059, 2977, 2860, 2758, 2545, 2482, 2362, 2053, 1877, 1831, 1780, 1677, 1609, 1582, 1463, 1423, 1404, 1390, 1382, 1372, 1352, 1335, 1272, 1237, 1183, 1142, 1105 cm^{-1}; ^1H NMR (400 MHz, $CDCl_3$, ppm) δ 10.35 (s, 1H), 7.08 (d, 1H, J = 2.4 Hz), 7.76 (dd, 1H, J_1 = 8.8 Hz, J_2 = 2.4 Hz), 6.77 (d, 1H, J = 8.8 Hz), 4.65 (sep, 1H, J = 6.0 Hz), 1.39 (d, 6H, J = 6.0 Hz); ^{13}C NMR (125 MHz, $CDCl_3$, ppm) δ 188.8, 160.3, 144.1, 137.2, 127.6, 116.6, 82.8, 71.7, 22.1, 1.2; EI-HRMS m/z calcd for $C_{10}H_{11}IO_2$ 289.9804, found 289.9803.

Compound 4. See the general procedure for the Pd/Cu coupling reaction. The materials used were **3** (824 mg, 2.84 mmol), $Pd(PPh_3)_2Cl_2$ (60 mg, 0.085 mmol), CuI (32 mg, 0.17 mmol), THF (18 mL), and Et_3N (6 mL). TMSA (0.81 mL, 5.68 mmol) was added via syringe and the mixture was stirred at rt overnight. The residue was purified by flash column chromatography (silica gel, 40% CH_2Cl_2 in hexanes) to provide **4** as a light-yellow solid (715 mg, 2.74 mmol, 97%): mp 56–58 °C. FTIR (neat) 3655, 3334, 3047, 2963, 2900, 2876, 2765, 2512, 2325, 2188, 2153, 2011, 1979, 1943, 1879, 1799, 1678, 1603, 1569,

1482, 1410, 1393, 1384, 1374, 1354, 1273, 1247, 1217, 1178, 1159, 1138, 1115, 1101 cm^{-1}; ^1H NMR (500 MHz, $CDCl_3$, ppm) δ 10.39 (s, 1H), 7.90 (d, 1H, J = 2.4 Hz), 7.56 (dd, 1H, J_1 = 8.8 Hz, J_2 = 2.4 Hz), 6.89 (d, 1H, J = 8.4 Hz), 4.66 (sep, 1H, J = 6.0 Hz), 1.38 (d, 6H, J = 6.0 Hz), 0.22 (s, 9H); ^{13}C NMR (125 MHz, $CDCl_3$, ppm) δ 189.3, 160.4, 138.9, 132.4, 125.5, 115.6, 113.9, 103.91, 93.8, 71.5, 22.1, 0.11; EI-HRMS m/z calcd for $C_{15}H_{20}O_2Si$ 260.1233, found 260.1228.

Compound 5. A 50 mL round-bottom flask equipped with a magnetic stir bar was charged with **4** (80 mg, 0.307 mmol), MeOH (5 mL), and THF (5 mL). K_2CO_3 was added (100 mg, 1.00 mmol) and the mixture was stirred at room temperature for 2 h. The reaction was quenched with 15% NH_4Cl (20 mL) and then extracted with CH_2Cl_2 (20 mL ×2). The combined organic fractions were dried with $MgSO_4$ and evaporated *in vacuo*. The residue was purified by column chromatography (silica gel, 40% CH_2Cl_2 in hexanes) to provide **5** as a white solid (54 mg, 0.29 mmol, 94%): mp 84–85 °C. FTIR (neat) 3343, 3258, 3046, 2988, 2491, 2912, 2874, 2764, 2101, 1911, 1822, 1680, 1602, 1565, 1485, 1450, 1417, 1388, 1351, 1335, 1282, 1250, 1212, 1183, 1164, 1131, 1113, 1104 cm^{-1}; ^1H NMR (500 MHz, $CDCl_3$, ppm) δ 10.41 (s, 1H), 7.93 (d, 1H, J = 2.0 Hz), 7.60 (dd, 1H, J_1 = 9.0 Hz, J_2 = 2.0 Hz), 6.93 (d, 1H, J = 9.0 Hz), 4.69 (sep, 1H, J = 6.0 Hz), 3.01 (s, 1H), 1.40 (d, 6H, J = 6.5 Hz); ^{13}C NMR (125 MHz, $CDCl_3$, ppm) δ 189.3, 160.7, 139.2, 132.5, 125.6, 114.5, 114.1, 82.6, 76.9, 71.6, 22.1; EI-HRMS m/z calcd for $C_{12}H_{12}O_2$ 188.0837, found 188.0838.

Compound 8. See the general procedure for the Pd/Cu Sonogashira coupling reaction. The materials used were **6**[24] (257 mg, 0.43 mmol), **7**[24] (477 mg, 0.72 mmol), $PdCl_2(PPh_3)_2$ (25 mg, 36.0 μmol), CuI (14.0 mg, 72 μmol), THF (45 mL), and Et_3N (15 mL) at

rt overnight. The crude product was purified by column chromatography (silica gel, 20% CH_2Cl_2 in hexanes) to yield **8** as a yellow solid (154 mg, 32%). FTIR (neat) 3062, 2825, 2854, 2611, 2360, 2212, 2212, 1726, 1595, 1504, 1487, 1463, 1411, 1362, 1281, 1221, 1140, 1064, 1042 cm^{-1}; ^1H NMR (500 MHz, $CDCl_3$) δ 7.74 (s, 1H), 7.47 (d, 1H, J = 1.0 Hz), 7.41 (s, 1H), 7.23 (d, 1H, J = 8.0 Hz), 7.14 (dd, 1H, J_1 = 8.0 Hz, J_2 = 1.5 Hz), 7.06 (d, 1H, J = 6.5 Hz), 3.99 (s, 6H), 3.20−1.60 (br m, 44H); ^{13}C NMR (125 MHz, $CDCl_3$) δ 154.3, 142.0, 135.5, 135.4, 132.3, 131.2, 128.6, 126.7, 126.3, 124.9, 124.0, 122.2, 115.9, 115.8, 113.8, 113.2, 99.7, 92.3, 92.1, 92.0, 91.5, 91.21, 91.17, 90.9, 88.1, 80.7, 78.1, 78.0, 77.2, 76.5, 69.7, 69.3, 69.1, 60.9, 60.7, 60.5, 56.7, 56.6; MALDI-TOF MS (+eV) m/z calcd for $C_{40}H_{57}B_{40}IO_2$ 1129.2, found 1129.6.

Compound 9. See the general procedure for the Pd/Cu Sonogashira coupling reaction. The materials used were **8** (84 mg, 0.074 mmol), **5** (28 mg, 0.15 mmol), $PdCl_2(PPh_3)_2$ (5.0 mg, 7.1 μmol), CuI (2.5 mg, 13.1 μmol), THF (10 mL), and Et_3N (10 mL) at rt overnight. The crude product was purified by column chromatography (silica gel, 5% EtOAc in hexanes) to yield **9** as a yellow solid (80 mg, 91%). FTIR (neat) 3063, 2978, 2864, 2610, 2213, 1688, 1603, 1504, 1464, 1412, 1386, 1271, 1221, 1184, 1138, 1109, 1063, 1043, 1007 cm^{-1}; ^1H NMR (400 MHz, $CDCl_3$, ppm) δ 10.48 (s, 1H), 8.03 (d, 1H, J = 2.4 Hz), 7.68 (dd, 1H, J = 8.8 Hz, J = 2.0 Hz), 7.49 (s, 1H), 7.48 (d, 1H, J = 1.6 Hz), 7.44 (s, 1H), 7.23 (d, 1H, J = 8.4 Hz), 7.14 (dd, 1H, J_1 = 8.0 Hz, J_2 = 1.6 Hz), 7.07 (m, 2H), 7.03 (d, 1H, J = 9.2 Hz), 4.77 (sep, 1H, J = 6.0 Hz), 4.00 (s, 6H), 3.20−1.60 (br m, 44H), 1.45 (d, 6H, J = 6.5 Hz); ^{13}C NMR (125 MHz, $CDCl_3$) δ 189.2, 160.9, 154.28, 154.26, 138.8, 135.8, 135.5, 135.43, 135.39, 132.47, 132.34, 131.18, 130.49, 127.90, 127.86, 126.7, 125.8, 125.7, 124.04, 124.00, 123.96, 122.2, 115.8, 114.9, 114.2, 113.7, 113.4, 95.1, 92.4, 92.3, 92.1, 91.5, 91.3, 91.2, 90.9, 88.0,

86.2, 78.1, 78.0, 77.3, 71.7, 69.4, 60.5, 56.7, 29.9, 22.2; MALDI-TOF MS (+eV) *m*/*z* calcd for $C_{52}H_{68}B_{40}O_4$ 1189.5, found 1189.8.

Compound 10. $MePPh_3Br$ (217 mg, 0.61 mmol) was dried at 60 °C *in vacuo* for 2 h in a 50 mL round-bottom flask equipped with a magnetic stir bar. THF was added (20 mL) and the resultant suspension was cooled to 0 °C. BuLi (2.5 M in hexane, 0.24 mL, 0.61 mmol) was added dropwise and the mixture was stirred for 30 min at 0 °C. A yellow solution was obtained. Only 5.0 mL of this solution were transferred via syringe to a solution of compound **9** (120 mg, 0.101 mmol) in THF (10 mL) cooled to 0 °C. The mixture was allowed to warm at rt and stirred overnight. The solvent was removed. The crude product was purified by column chromatography (silica gel, 15% CH_2Cl_2 in hexanes) to yield **10** as a yellow solid (84 mg, 69%). FTIR (neat) 3062, 2964, 2612, 2211, 1689, 1600, 1504, 1464, 1411, 1385, 1279, 1242, 1221, 1111, 1064, 1043 cm^{-1}; ^1H NMR (500 MHz, $CDCl_3$) δ 7.70 (d, 1H, *J* = 2.0 Hz), 7.49 (d, 1H, *J* = 0.5 Hz), 7.48 (d, 1H, *J* = 1.0 Hz), 7.44 (s, 1H), 7.39 (dd, 1H, J_1= 8.6 Hz, J_2 = 2.0 Hz), 7.23 (dd, 1H, J_1 = 8.0 Hz, J_2 = 0.5 Hz), 7.14 (dd, 1H, J_1 = 8.1 Hz, J_2 = 1.6 Hz), 7.09−7.00 (m, 3H), 6.88 (d, 1H, *J* = 8.7 Hz), 5.85 (dd, 1H, J_1 = 17.8 Hz, J_2 = 1.1 Hz), 5.33 (dd, 1H, J_1 = 11.2 Hz, J_2 = 1.2 Hz), 4.63 (sep, 1H, *J* = 6.0 Hz), 4.00 (s, 6H), 3.20−1.60 (br m, 44H), 1.39 (d, 6H, *J* = 6.0 Hz); ^{13}C NMR (125 MHz, $CDCl_3$) δ 156.1, 154.3, 135.8, 135.5, 135.4, 132.6, 132.3, 131.3, 131.2, 130.6, 128.3, 126.7, 126.4, 125.3, 124.0, 123.9, 123.8, 122.2, 115.84, 115.80, 115.3, 114.5, 113.7, 113.6, 113.5, 96.7, 92.2, 91.2, 91.0, 88.0, 85.4, 78.2, 78.0, 77.8, 71.0, 69.6, 69.4, 60.6, 56.7, 22.4; MALDI-TOF MS (+eV) *m*/*z* calcd for $C_{53}H_{70}B_{40}O_3$ 1187.6, found 1187.8.

Nanocar Catalyst 1. A 10 mL round-bottom flask equipped with a magnetic stir bar and condenser was charged with Ru complex **11**[16] (11.5 mg, 13.9 μmol) and CuCl (4.0 mg, 40.0 μmol). Then CH_2Cl_2 (0.5 mL) was added, immediately followed by addition of a solution of nanocar **10** (15.0 mg, 12.6 μmol) in CH_2Cl_2 (2.5 mL). The resulting solution was stirred at 40 °C for 2 h. The solvent was removed in vacuum, and the residue was purified (Geduran silica gel, 40% then 70% CH_2Cl_2 in hexanes) to afford **1** as a brownish solid (14.0 mg, 63%). Five milligrams of starting material **10** was recovered: FTIR (neat) 3059, 2928, 2852, 2611, 2361, 1688, 1594, 1504, 1450, 1411, 1386, 1262, 1221, 1181, 1101, 1063, 1043, 1008 cm^{-1}; ^1H NMR (500 MHz, $CDCl_3$) δ 17.40 (d, 1H, J_{PH} = 4.4 Hz), 7.91 (d, 1H, J = 2.0 Hz), 7.79 (dd, 1H, J_1 = 8.6 Hz, J_2 = 2.0 Hz), 7.50 (s, 1H), 7.48 (d, 1H, J = 1.0 Hz), 7.46 (s, 1H), 7.23 (d, 1H, J = 8.0 Hz), 7.13 (m, 2H), 7.07 (d, 2H, J = 3.0 Hz), 5.33 (septet, 1H, J = 6.0 Hz), 4.00 (s, 6H), 3.20–1.70 (br m, 83H); ^{13}C NMR (125 MHz, $CDCl_3$) δ 277.4, 154.29, 154.26, 153.4, 144.0, 135.9, 135.7, 135.5, 132.9, 132.5, 132.3, 131.2, 126.7, 126.1, 125.8, 125.7, 125.6, 124.04, 123.96, 123.93, 122.2, 117.2, 115.8, 113.8, 113.7, 113.4, 94.9, 92.4, 92.2, 92.1, 91.3, 91.2, 90.9, 88.0, 86.7, 78.1, 78.0, 77.8, 76.7, 71.7, 69.7, 69.5, 69.3, 60.5, 56.6, 36.1, 35.9, 30.3, 29.9, 28.0, 27.9, 26.4, 22.4, 22.2; ^{31}P NMR (202 MHz, $CDCl_3$) δ 60.16 (s). It was not possible to obtain mass spectrometry characterization of this compound; MALDI-TOF, ESI, and EI methods were attempted.

Nanocar Catalyst 2. A 10 mL round-bottom flask equipped with a magnetic stir bar and condenser was charged with Ru complex **12**[17] (7.5 mg, 8.8 μmol) and CuCl (4.0 mg, 40.4 μmol). Then CH_2Cl_2 (0.5 mL) was added, immediately followed by addition of a solution of nanocar **10** (10.0 mg, 8.0 μmol) in CH_2Cl_2 (2.5 mL). The resulting solution was stirred at 40 °C for 2 h. The solvent was removed in vacuum, and the residue was purified

(Geduran silica gel, 40% then 60% CH_2Cl_2 in hexanes) to afford **2** as an olive green solid (7.0 mg, 53%). One milligram of starting material **10** was recovered: FTIR (neat) 3054, 2966, 2924, 2856, 2611, 2210, 1950, 1725, 1593, 1488, 1463, 1412, 1385, 1262, 1220, 1162, 1134, 1102, 1063, 1040 cm^{-1}; ^1H NMR (500 MHz, $CDCl_3$) δ 16.61 (s, 1H), 7.70 (dd, 1H, J_1 = 8.5 Hz, J_2 = 2.0 Hz), 7.49 (s, 1H), 7.48 (d, 1H, J = 1.0 Hz), 7.42 (s, 1H), 7.23 (d, 1H, J = 8.5 Hz), 7.15 (dd, 1H, J_1 = 8.5 Hz, J_2 = 2.0 Hz), 7.11–7.07 (m, 7H), 6.86 (d, 1H, J = 9.0 Hz), 4.96 (septet, 1H, J = 6.0 Hz), 4.19 (s, 4H), 4.00 (s, 6H), 3.20–1.70 (br m, 62H), 1.31 (d, 6H, J = 6.0 Hz); ^{13}C NMR (125 MHz, $CDCl_3$) δ 295.0, 210.6, 154.3, 153.0, 145.4, 139.3, 135.8, 135.6, 133.2, 132.4, 131.2, 129.7, 126.7, 126.0, 125.64, 125.55, 124.14, 124.07, 123.9, 122.2, 117.0, 115.8, 113.7, 113.4, 95.1, 92.4, 92.24, 92.18, 91.5, 91.3, 91.2, 91.0, 88.0, 86.1, 78.1, 78.0, 77.8, 76.2, 69.7, 69.5, 69.3, 60.6, 60.5, 56.7, 51.8, 29.9, 21.3. It was not possible to obtain mass spectrometry characterization of this compound. MALDI-TOF, ESI, and EI methods were tried.

ROMP of 1,5-cyclooctadiene.[19] CD_2Cl_2 was freeze/pump/thawed three times. *cis*,*cis*-1,5-Cyclooctadiene was distilled over CaH_2 immediately prior the polymerization reaction. As reported by Grubbs,[19] in our experience, aged cyclooctadiene gave considerably lower rates. ^1H NMR spectra were collected at 500 MHz. Inside a glovebox, an NMR tube with a septum/screw cap was charged with catalyst solution (0.40 μmol) and CD_2Cl_2 to give a total volume of 0.80 mL. The solution was equilibrated at 30 °C in the NMR probe. The sample was then ejected to add *cis*,*cis*-1,5-cyclooctadiene (50 μL, 0.40 mmol) *via* syringe. A series of spectra were collected over an appropriate period of time. The degree of conversion to polymer was determined by comparing the ratio of the integrals of the methylene protons in the starting material, δ 2.36 (m) with those in the product, δ 2.09 br

(m), δ 2.04 (br m). The integration that **1** and **2** exhibit in this region was neglected since a 1000:1 ratio of *cis,cis*-1,5-cyclooctadiene/catalyst was used.

Supporting Information. ^{1}H and ^{13}C NMR spectra of new compounds and tables of ROMP results.

3.5. References

1. Godoy, J.; Vives, G.; Tour, J. M. *ACS Nano* **2011**, *5*, 85-90.
2. Balzani, V.; Venturi, M.; Credi, A. *Molecular Devices and Machines: Concepts and Perspectives for the Nanoworld*; Wiley-VCH: Weinheim, Germany, 2008.
3. Kay, E. R.; Leigh, D. A.; Zerbetto, F. *Angew. Chem., Int. Ed.* **2007**, *46*, 72–191.
4. Kottas, G. S.; Clarke, L. I.; Horinek, D.; Michl, J. *Chem. Rev.* **2005**, *105*, 1281–1376.
5. Rapenne, G. *Org. Biomol. Chem.* **2005**, *3*, 1165–1169.
6. Shirai, Y.; Morin, J.-F.; Sasaki, T.; Guerrero, J. M.; Tour, J. M. *Chem. Soc. Rev.* **2006**, *35*, 1043–1055.
7. Vives, G.; Tour, J. M. *Acc. Chem. Res.* **2009**, *42*, 473–487.
8. Shirai, Y.; Osgood, A. J.; Zhao, Y.; Kelly, K. F.; Tour, J. M. *Nano Lett.* **2005**, *5*, 2330–2334.
9. Shirai, Y.; Osgood, A. J.; Zhao, Y.; Yao, Y.; Saudan, L.; Yang, H.; Chiu, Y.-H.; Alemany, L. B.; Sasaki, T.; Morin, J.-F.; *et al. J. Am. Chem. Soc.* **2006**, *128*, 4854–4864.
10. Morin, J.-F.; Shirai, Y.; Tour, J. M. *Org. Lett.* **2006**, *8*, 1713–1716.
11. Sasaki, T.; Tour, J. M. *Org. Lett.* **2008**, *10*, 897–900.
12. Mirkovic, T.; Zacharia, N. S.; Scholes, G. D.; Ozin, G. A. *ACS Nano* **2010**, *4*, 1782–1789.
13. Deshmukh, P. H.; Blechert, S. *Dalton Trans.* **2007**, 2479–2491.

14. Vives, G.; Guerrero, J. M.; Godoy, J.; Khatua, S.; Wang, Y.-P.; Kiappes, J. L.; Link, S.; Tour, J. M. *J. Org. Chem.* **2010**, *75*, 6631–6643.
15. Garber, S. B.; Kingsbury, J. S.; Gray, B. L.; Hoveyda, A. H. *J. Am. Chem. Soc.* **2000**, *122*, 8168–8179.
16. Schwab, P.; Grubbs, R. H.; Ziller, J. W. *J. Am. Chem. Soc.* **1996**, *118*, 100–110.
17. Scholl, M.; Ding, S.; Lee, C. W.; Grubbs, R. H. *Org. Lett.* **1999**, *1*, 953–956.
18. Kingsbury, J. S.; Harrity, J. P. A.; Bonitatebus, P. J.; Hoveyda, A. H. *J. Am. Chem. Soc.* **1999**, *121*, 791–799.
19. Ritter, T.; Hejl, A.; Wenzel, A. G.; Funk, T. W.; Grubbs, R. H. *Organometallics* **2006**, *25*, 5740–5745.
20. We measured the activity of complexes **11** and **12** to ensure our experimental setup afforded results comparable to those reported. See Supporting Information for details.
21. Tzur, E.; Szadkwoska, A.; Ben-Asuly, A.; Makal, A.; Goldberg, I.; Wózniak, K.; Grela, K.; Lemcoff, N. G. *Chem.–Eur. J.* **2010**, *16*, 8726–8737.
22. Michrowska, A.; Bujok, R.; Harutyunyan, S.; Sashuk, V.; Dolgonos, G.; Grela, K. *J. Am. Chem. Soc.* **2004**, *126*, 9318–9325.
23. For details on that approach, see the Supporting Information of reference 1.

3.6. Experimental Contributions Section

My contributions to the experimental work described in this chapter are the synthesis and characterization of all the molecules, and the study of the catalytic activity of the

nanocars. Guillaume Vives conceived of the project and synthesized nanocar intermediates **3**, **4**, **5**, and **8**.

Chapter 4

A Polymerization-Propelled 'Nanosubmarine': Synthesis and Diffusion Studies

4.1. Introduction

The synthesis of micro- and nano-sized motors has attracted much interest in recent years.[1] Concomitantly, a number of chemically propelled nanomotors have been developed to operate in solution.[2] Interesting examples of these include bimetallic nanorods that use the catalytic dismutation of H_2O_2 to induce translational movement,[3] and silica particles equipped with a H_2O_2 disproportionation catalyst.[4] In these systems, small by-product molecules are produced during the propulsion.

An attractive alternative is to explore in synthetic systems the potential of a polymerization process to propel motion at the nanoscale, given that this

mechanism of propulsion is already present in nature. For example, the movement of the bacterium *listeria monocytogenes* is driven by the polymerization of actin.[5] Indeed, it was recently demonstrated that gold-silica Janus particles functionalized with a ring-opening metathesis polymerization (ROMP) catalyst can be propelled by a polymerization process.[6] Upon addition of the cyclic olefin norbornene, the diffusion constant of the particles increased up to 70%. These particles, however, are approximately 500 nm in diameter. Similarly, the size of the other nanomotors described above spans from several hundreds of nanometers to a few microns. Hence, to the best our knowledge, chemically propelled synthetic nanomotors that are truly molecule sized have not been reported.

The purpose of the present work was to investigate if chemical propulsion through a ROMP process can be achieved at the molecular level in the solution phase. Our hypothesis was that the diffusion constant of a ROMP catalyst would increase during catalysis. One method to monitor the diffusion of molecules in solution is fluorescence correlation spectroscopy (FCS).[7] Therefore, to test our hypothesis using FCS to monitor movement, it was necessary to prepare a fluorescent ROMP catalyst (Figure 4.1).

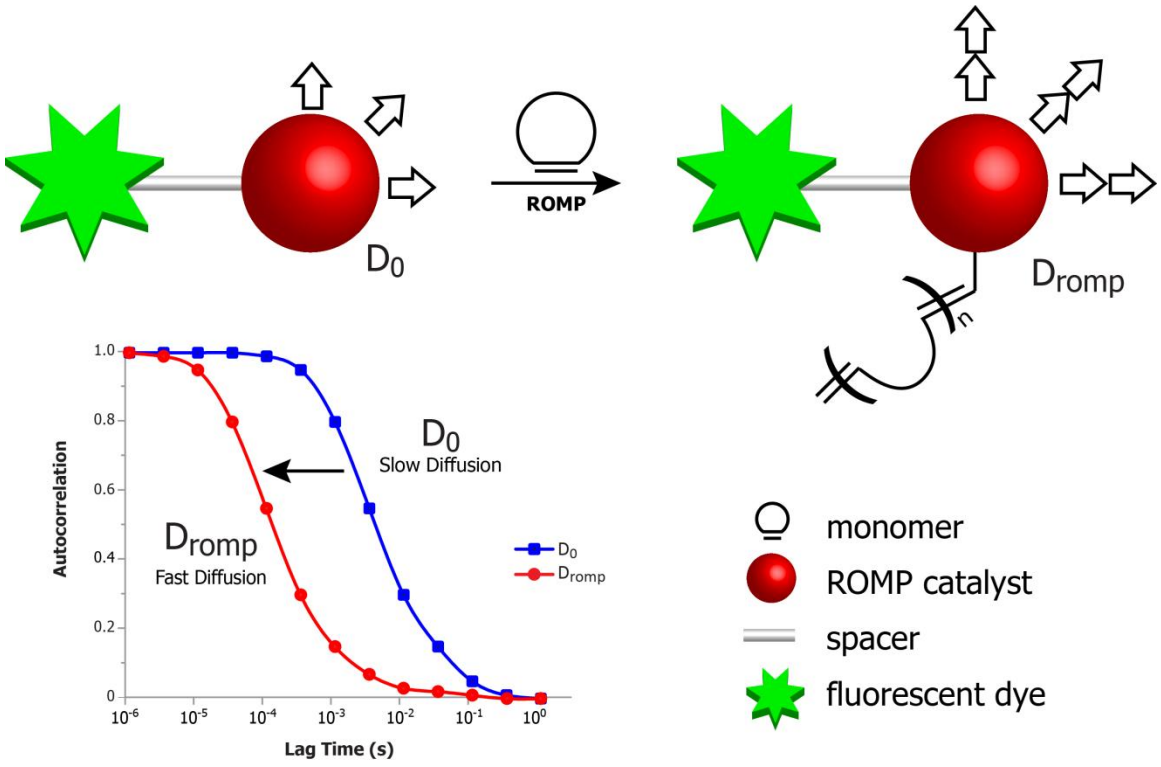

Figure 4.1. Proposed propulsion scheme for a fluorescent ROMP catalyst. Upon addition of cyclic olefin, a ROMP process should occur and the energy released may be sufficient to propel the catalyst, thereby increasing its diffusion constant (D) from D_0 to D_{romp}, as detected using FCS. A decrease in lag time in the autocorrelation curve denotes an increase in diffusion constant.

A number of different types of ROMP catalysts have been developed; the Ru-based Hoveyda-Grubbs type (Figure 4.2) was selected for this study, due to its high catalytic activity and relatively higher stability toward air/moisture when compared to other types of catalyst.[8]

As described in section 3.1 of the previous chapter, there are three main approaches commonly used to functionalize a Hoveyda-Grubbs catalyst.[9] Of those,

functionalization at the N-heterocyclic carbene (NHC) ligand is the most widely used, since the NHC is not exchanged during the ROMP process, thereby providing permanent tagging. For this reason the present work focused on the preparation of Hoveyda-Grubbs ROMP catalysts dye-tagged at the NHC ligand.

4.2. Results and Discussion

4.2.1. Design and Synthesis

The initial targets of fluorescently labeled ROMP catalysts are presented in Figure 4.2. They feature a 4,4-difluoro-4-bora-3a,4a-diaza-*s*-indacene (BODIPY)[10] dye attached to the ruthenium complex through the NHC ligand. It was envisioned that catalysts **1** and **2** could be prepared through a ligand exchange reaction between the 1st generation Hoveyda-Grubbs catalyst (**3**)[11] and the corresponding carbenes of imidazolium salts **4** and **5**, respectively. The difference between **1** and **2** is the distance between the BODIPY core and the catalytic center. The ethynyl phenyl spacer of **1** was removed in **2**, to evaluate the effect of the alkyne on the formation of the NHC carbene.

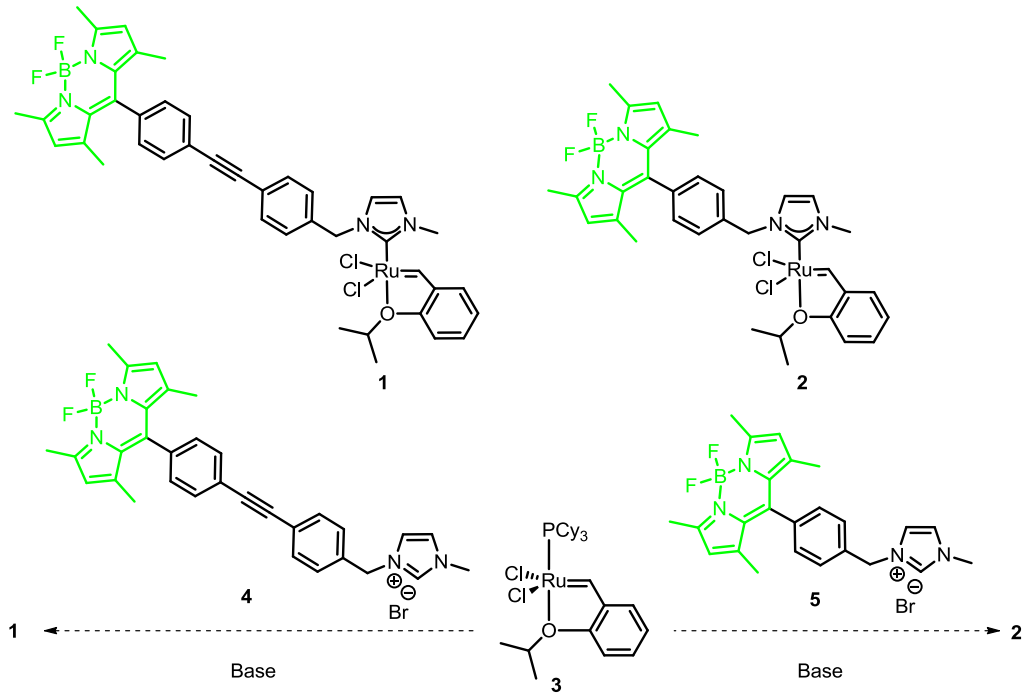

Figure 4.2. Structure of the fluorescent Hoveyda-Grubbs catalysts **1** and **2** and the final step of the proposed synthesis.

The synthesis of BODIPY imidazolium salt **4** started with a Sonogashira coupling between BODIPY **6**[12] and 4-ethynylbenzyl alcohol[13] (Scheme 4.1). The resultant benzylic alcohol **7** reacted with PBr_3 in presence of catalytic DMF to substitute the hydroxyl group with a bromide. Finally, alkylation of the benzylic bromide in **8** with 1-methylimidazole afforded **4** in excellent yield.

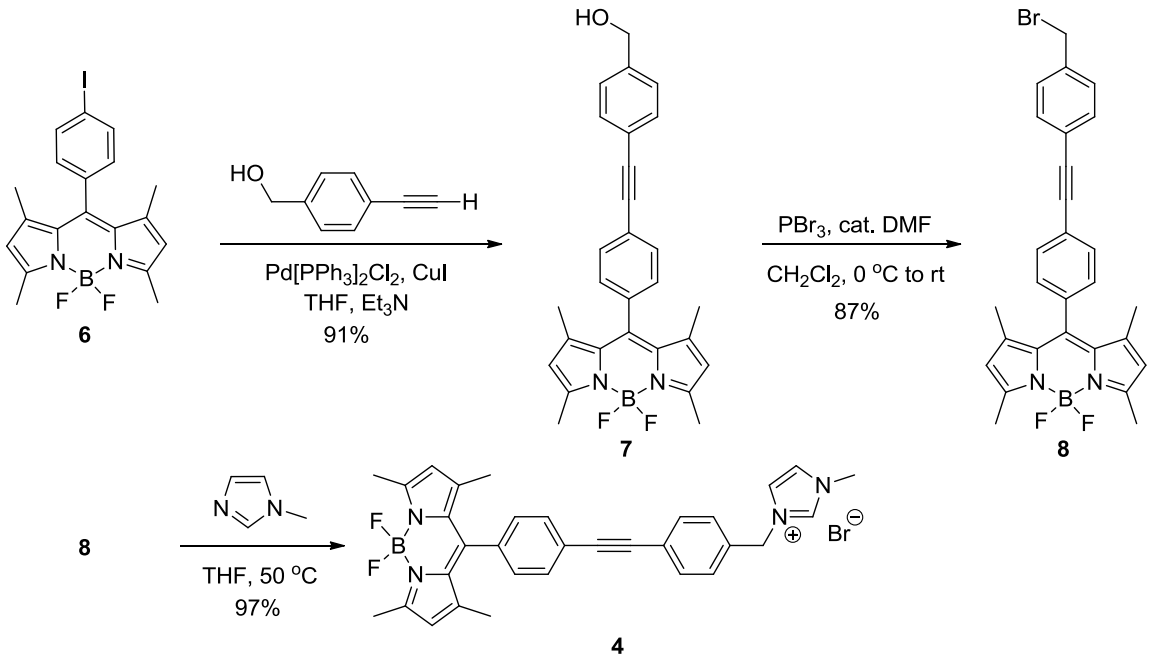

Scheme 4.1. Synthesis of BODIPY imidazolium salt **4**.

The synthesis of **5** followed a similar approach (Scheme 4.2). BODIPY **9**[14] was treated with PBr_3 to give the benzylic bromide **10**. Then, imidazolium salt **5** was obtained in high yield by alkylation of **10** with 1-methylimidazole.

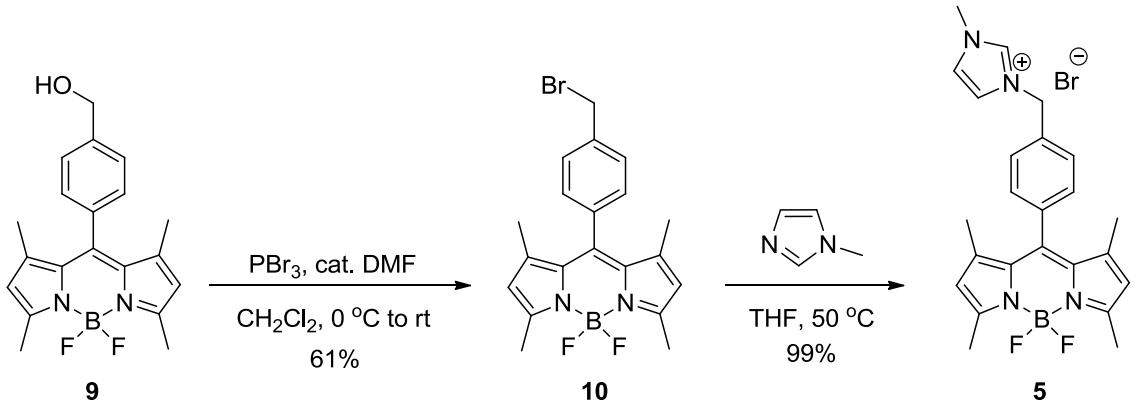

9

Scheme 4.2. Synthesis of BODIPY imidazolium salt **5**.

With imidazolium salts **4** and **5** in hand, the formation of the corresponding carbenes and subsequent ligand exchange with **3** was investigated (Scheme 4.3). Although many of the common methods to generate NHC carbenes[14] were tried, in all the experiments the imidazolium salts decomposed and no desired product was detected. The failed approaches included a two step process in which **4** or **5** were initially reacted with the first generation Grubbs catalyst (**11**)[16] expecting to produce an intermediate NHC Grubbs catalyst that bears a phosphine ligand. Then a second ligand exchange with 2-isopropoxystyrene was attempted to produce the desired ether-chelate complex. However, the diazonium salts decomposed and no desired product was obtained.

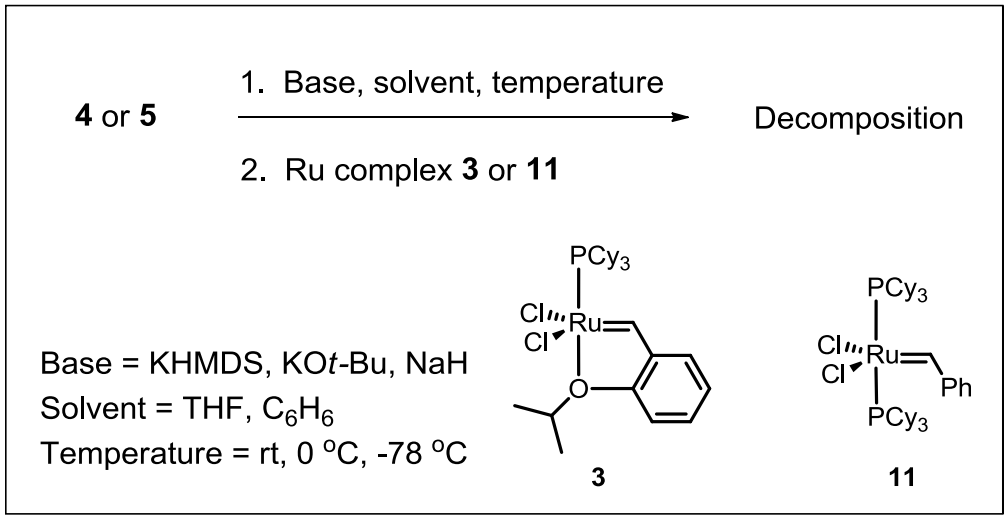

Scheme 4.3. Failed syntheses of BODIPY-tagged Hoveyda-Grubbs catalysts.

Although the cause for the decomposition of the BODIPY imidazolium salt was unclear, it was observed that the decomposition occurred during preparation of the NHC carbene. Hence, a new strategy was devised in which no NHC carbene would be generated in presence of BODIPY. The new target, **12**, was synthesized in four straightforward steps from previously reported compounds (Scheme 4.4). BODIPY **6** was coupled with 4-ethynylbenzoic acid[17] under conventional Sonogashira coupling conditions. The crude BODIPY carboxylic acid was esterified with pentafluorophenol in the presence of *N*,*N*'-dicyclohexylcarbodiimide (DCC) to give BODIPY pentafluorophenol ester **13**. Separately, Boc-protected Hoveyda-Grubbs complex **14**[18] was deprotected with hydrogen chloride. Finally, to obtain **12**, BODIPY ester **13** was coupled with the catalyst terminal amine through formation of an amide bond.

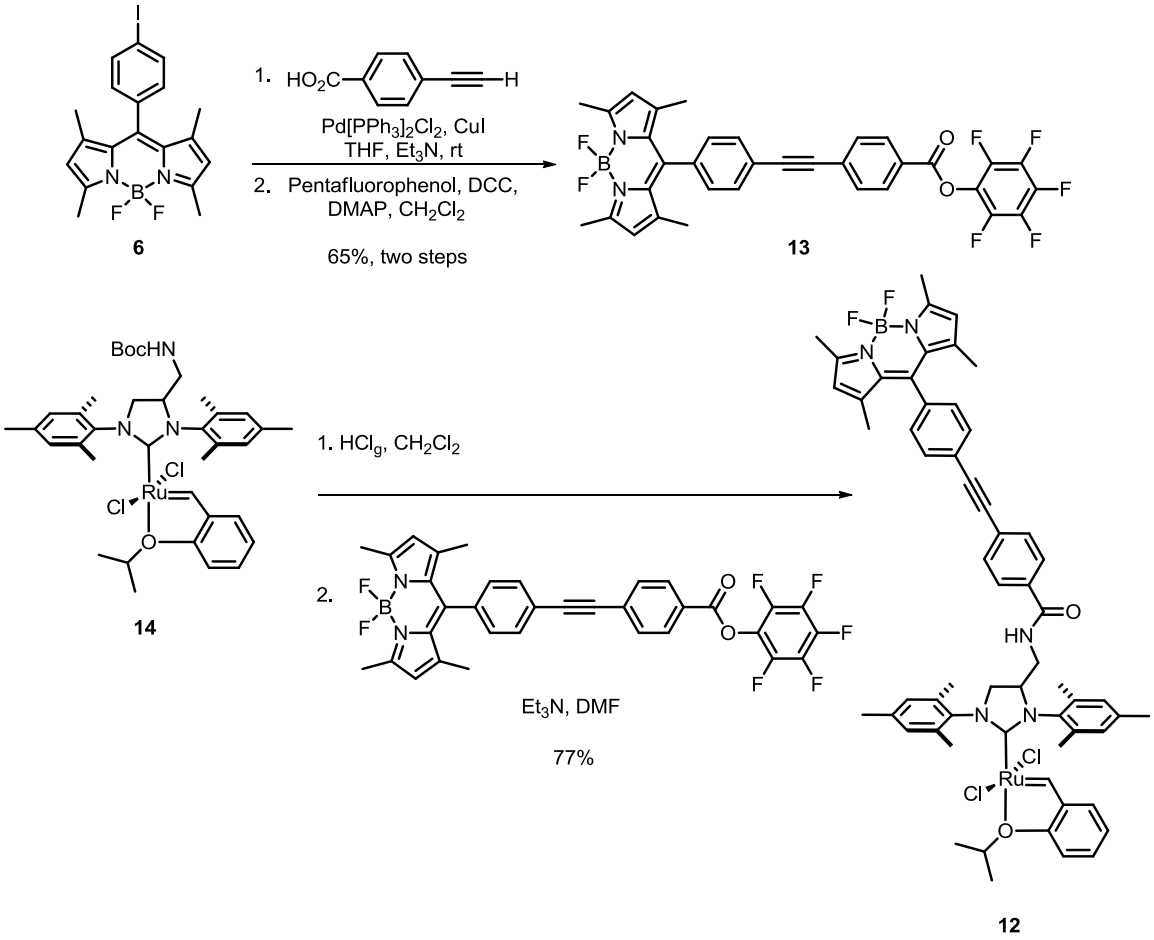

Scheme 4.4. Synthesis of BODIPY Hoveyda-Grubbs catalyst **12**.

4.2.2. Optical Properties

Since our current FCS setup requires excitation of the molecules with a 514 or 532 nm laser, it was a prerequisite that the BODIPY catalyst **12** exhibit adequate absorption at either of those wavelengths. As depicted in Figure 4.3A, **12** absorbs strongly in this region, with its λ_{max} = 504 nm (ε = 72 000 $M^{-1}cm^{-1}$, in CH_2Cl_2).

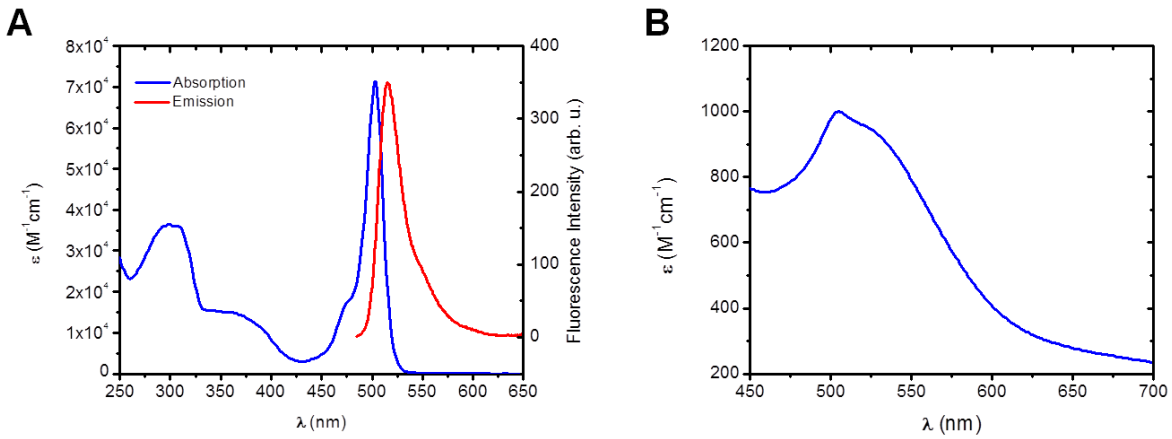

Figure 4.3. Absorption and emission spectra of **12** and absorption spectrum of **11**. A) UV–vis absorption (blue line) and emission (red line) spectra of **12** in CH_2Cl_2. B) UV–vis absorption spectrum of the 1st generation Grubbs catalyst (**11**) in CH_2Cl_2.

A second requirement was an acceptable fluorescence quantum yield (Φ_F). In dichloromethane, the fluorescence quantum yield of **12** was 0.22. This value is significantly smaller than the fluorescence quantum yield of the precursor BODIPY **6** (Φ_F = 0.46, in CH_2Cl_2).[19] The drop in the fluorescence of **12** compared to **6** could be due to fluorescence resonance energy transfer (FRET). Ru-based metathesis catalysts, including Hoveyda-Grubbs type, exhibit absorption bands that span across the 500 nm region, where BODIPY emits (Figure 4.3B). Therefore, upon excitation of the BODIPY core, the energy could be transferred to the Ru center and then released in a nonradiative process. The quenching effect of Ru-based complexes has been exploited to do a comparative study of the affinity of the Ru complex toward alkanes, alkenes and alkynes.[20] The time-dependent fluorescence quenching of dye-tagged alkanes, alkenes and alkynes was monitored as a function of the association

with different Ru-based complexes. Nonetheless, a Φ_F = 0.22 is sufficient for FCS studies, therefore **12** had sufficient optical properties.

4.2.3. Catalytic Activity

The catalytic activity of **12** toward ROMP was evaluated in accordance with the standard protocol developed by Grubbs[21] (Table 4.1). To carry out that polymerization test, an NMR tube with a septum-capped screw cap (model 27093, Sigma-Aldrich) was charged with a solution of complex **12** in CD_2Cl_2. The solution was equilibrated at 30 °C in the NMR probe. The monomer, *cis*,*cis*-1,5-cyclooctadiene (cod), was then injected into the NMR tube *via* syringe after ejecting the NMR tube from the instrument. A series of ^{1}H NMR spectra were collected over a short period of time. The degree of conversion of cod to polymer was determined by comparing the ratio of the integrals of the methylene protons in the starting material to those in the product.

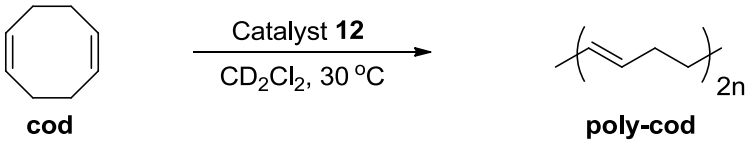

Time (min)	% conversion
4.2	96.8
5.2	98.9
6.4	99.6
7.4	99.8
8.6	99.9
9.6	99.9
10.8	99.9
11.8	99.9

Table 4.1. ROMP of *cod* catalyzed by **12**.

One of the reasons for choosing cod in the procedure developed by Grubbs was its relatively slow polymerization rate when compared to more highly strained cyclic olefins such as norbornene. Indeed, 96.8% of the cod had reacted by the time the first spectrum was collected at 4.2 min (Table 4.1). The high activity of **12** was

similar to its parent second generation Hoveyda-Grubbs catalyst (**15**)[22] (Figure 4.4), which afforded 98.9% conversion of cod at 4.1 min.[20]

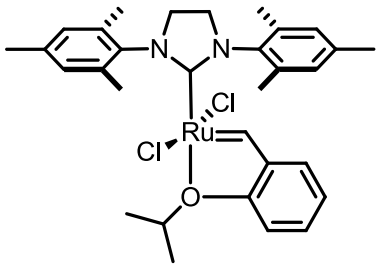

15

Figure 4.4. Structure of the second generation Hoveyda-Grubbs catalyst.

In addition to being a highly active catalyst, **12** is stable under inert conditions. The catalytic activity of a sample that was stored inside a glove box over two months remained unchanged. The high catalytic activity along with the above discussed optical properties made **12** an excellent candidate to study the potential of a polymerization process to induce motion at the molecular level, using FCS.

4.2.4. Fluorescence Correlation Spectroscopy

The solvent plays a crucial role in FCS experiments. It not only provides the environment for the diffusion of the molecules under study, but it can drastically impact the overall outcome of the experiment, as shown in the present study.

The first solvent selected for this study was *p*-xylene, since aromatic solvents are widely used in ROMP reactions. In addition, its high boiling point (138 °C) was desirable to minimize evaporation during the measurements, given that the current experimental setup uses only 40 μL of sample and that volume needs to remain

constant for ~ 5 min. Despite intense efforts, however, it was not possible to obtain reliable information about the dynamics of **12** in this solvent. The most likely reason was the closeness of the refractive index (n) of p-xylene (1.49) to that of glass (~1.50). In FCS experiments, the incident laser first passes through the glass of the sample holder, and then the instrument tries to focus where the refractive index changes. If there is no significant change in refractive index, the laser will not focus properly and thereby no consistent data will be obtained. For this reason it was necessary to use a solvent with $n \leq 1.45$.

The next solvent selected was isopropyl alcohol (IPA), with n = 1.37. The focusing issues were solved, and the conditions were optimized to monitor the diffusion of **12** before and after addition of cod. The optimum concentration of **12** was ~ 2 nM in IPA. Under these conditions, the calculated three-dimensional diffusion constant (D_t) was (2.1 ± 0.2) × 10^{-10} m^2/s (Figure 4.5). Next, to study the effect of a ROMP process on the diffusion of **12**, different concentrations of cod were added: 0.1 M, 0.5 M, or 1 M. However, there was no change detected in the diffusion of **12** upon addition of cod, as shown in Figure 4.5 for 0.1 M cod.

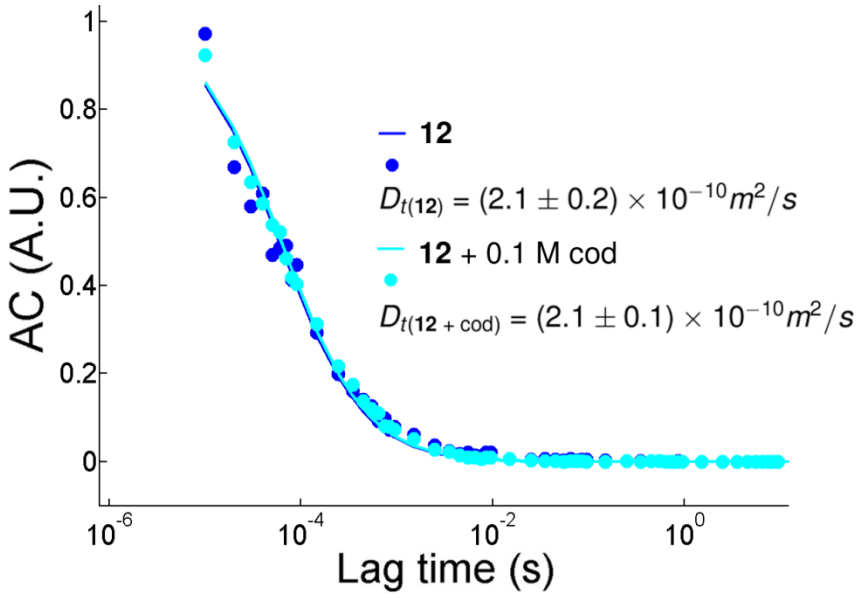

Figure 4.5. Autocorrelation curves of **12** as a 2 nM solution in IPA, before (dark blue) and after addition of cod (light blue).

Seeking to understand why the D_t of **12** remained unchanged upon addition of cod, a polymerization test was conducted under conditions identical to those used in the FCS experiments. Using ^{1}H NMR to assess the degree of polymerization, it was found that only 14% of the monomer had reacted after 5 min, the typical time required to complete the FCS measurements.

A possible reason for the poor polymerization observed was potential decomposition of **12** due to oxygen and/or moisture. Increasing the concentration of **12** was not an option since the approximation of single-molecule detection would not be valid, so instead the low concentration of **12** was maintained and a non-fluorescent ROMP catalyst was added to serve as a sacrificial substrate to oxygen and/or moisture. The second generation Hoveyda-Grubbs catalyst (**15**) was chosen,

since its catalytic activity is very similar to that of **12**. In order to optimize its fluorescence detection, the concentration of **12** was increased from 2 nM in the initial system to 20 nM, due to the quenching effect of the Hoveyda-Grubbs catalyst **15** that was discussed in section 4.2. The composition of the new FCS sample was therefore: 0.47 mM of **15**, 20 nM of **12**, and for the polymerization experiments, 0.47 M of cod.

As shown in Figure 4.6, the D_t of **12** decreased significantly after addition of cod. Two reasons that would account for the decrease would be 1) an increase in the particle size due to the growing polymer chain bound to the catalyst, and/or 2) an increase in the viscosity of the medium.

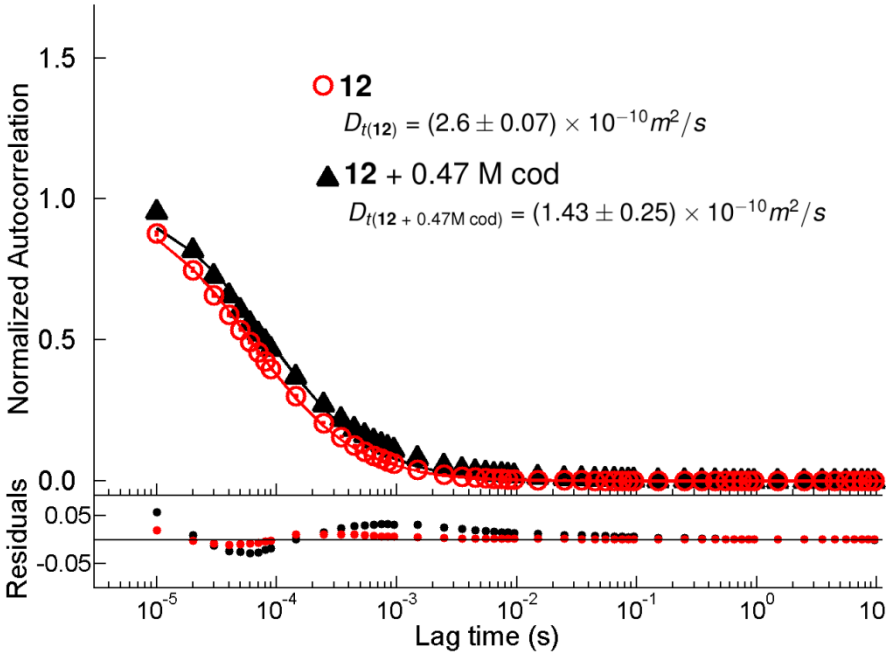

Figure 4.6. Autocorrelation curves of **12** as a 20 nM solution in IPA, before (red) and after addition of cod (black).

To assess the impact of the viscosity increase on the diffusion of **12**, the diffusion of BODIPY **6** was studied. The FCS sample contained 0.47 mM of **15**, ~ 1 nM of BODIPY **6**, and for the polymerization experiments, 0.47 M of cod. As expected, the diffusion coefficient of **6** decreased; before adding cod, D_t = (1.42 ± 0.28) x 10^{-10} m^2/s, but upon addition of cod D_t dropped to (0.75 ± 0.13) x 10^{-10} m^2/s. Using these data to correct the diffusion due to the increase in viscosity, there was an apparent increase in the diffusion coefficient of **12** during the ROMP process (Figure 4.7), but the large standard deviation of the experiments with cod prevented the confident rendering of a conclusion. An interesting observation was the formation of a polymer film in the sample holder during the FCS measurements. If the polymer was precipitating from the solution, it is possible that the heterogeneity of the system was the cause of the large variability in the results. For this reason a different solvent, in which the polymer would be soluble, was used in the next experiments.

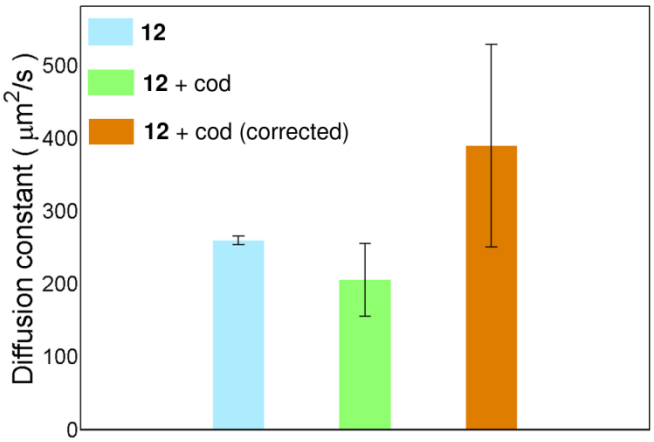

Figure 4.7. Effect of adding cod on the diffusion coefficient of **12** in IPA. The data in orange was calculated from the data in green after correcting for the viscosity change. The error bars correspond to the standard deviation of the data.

The solvent selected was 1,2-dichloroethane; halogenated solvents are commonly used in ROMP reactions. In addition, its refractive index (1.44) and boiling point (84 °C) made it a good candidate for the FCS studies. The sample composition was 0.47 mM of **15**, 2 nM of **12**, and in the polymerization experiments, 0.47 M of cod. The polymer that formed was highly soluble and the system remained homogeneous during the ROMP process. As a result, the standard deviation was reduced (Figure 4.8).

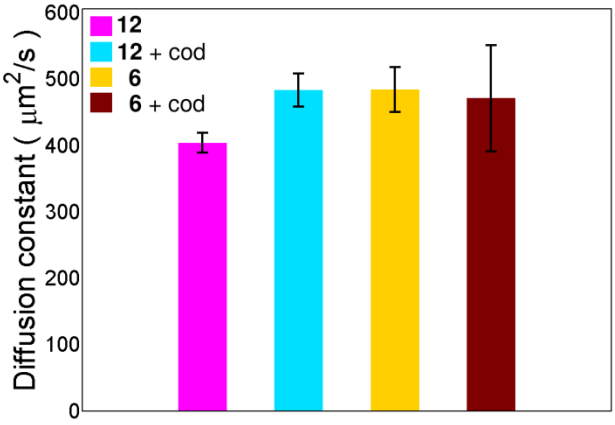

Figure 4.8. Effect of adding cod on the diffusion coefficients of **12** and **6** in 1,2-dichloroethane. The error bars correspond to the standard deviation of the data.

Most importantly, the diffusion of **12** increased upon addition of cod (Table 4.2) by 20 ± 7%, even without correction for the viscosity increase. The diffusion of BODIPY **6** was also studied under these conditions. Although no significant change

was observed in its average diffusion, the standard deviation was still considerable large and therefore the experiment needs to be repeated to confirm the results.

Sample	D_t [(μm)^2 s^{-1}]	# of measurements
BODIPY **6**	484 ± 34	6
BODIPY **6** + cod	472 ± 68	4
12	404 ± 15	6
12 + cod	483 ± 25	9

Table 4.2. Effect of adding cod on the diffusion coefficient of **12** and **6** in 1,2-dichloroethane.

Although the mechanism of propulsion is still unknown, these results show that catalyst **12** is indeed propelled by the ROMP process, thereby acting as a 'nanosubmarine'. However, there are several items that need to be addressed to complete this study. Those include a comprehensive study of the effect of monomer concentration, use of more reactive monomers, addition of a ROMP inhibitor, characterization of the polymer formed, and study of the propulsion mechanism.

4.3. Conclusions

In summary, a fluorescent Hoveyda-Grubbs catalyst (**12**) was synthesized and utilized to explore, *via* FCS, the potential of a ROMP process to provide a molecule with sufficient energy for self-propulsion in solution. The catalytic activity

of this complex toward ROMP was found to be similar to that of its non-fluorescent analogue **15**. In addition, by choosing a suitable solvent (1,2-dichloroethane) and catalyst/monomer concentration, preliminary results showed an increase of 20 ± 7% in the diffusion constant of this nanosubmarine in presence of its fuel, cod. These results pave the way toward development of truly nanosized chemically propelled molecular machines that operate in the solution phase.

4.4. Experimental Section

General Methods. ^{1}H NMR and ^{13}C NMR spectra were recorded at 400 or 500 and 100 or 125 MHz, respectively. Proton chemical shifts (δ) are reported in ppm downfield from tetramethylsilane (TMS). MALDI-TOF of **12** was performed using 2-[(2*E*)-3-(4-*tert*-butylphenyl)-2-methylprop-2-enylidene]malononitrile (DCTB) as the matrix. FTIR spectra were recorded by deposition of the sample on a KBr plate from a CH_2Cl_2 solution using a Nicolet FTIR Infrared Microscope with ATR objective with 2 cm^{-1} slit. All reactions were performed under an atmosphere of nitrogen unless stated otherwise. Reagent grade tetrahydrofuran (THF) and diethyl ether (Et_2O) were distilled from sodium benzophenone ketyl. Triethylamine (TEA) and CH_2Cl_2 were distilled over CaH_2. 2,4-Dimethylpyrrole was distilled from CaH_2 under a nitrogen atmosphere. *cis,cis*-1,5-Cyclooctadiene was distilled from CaH_2 under a nitrogen atmosphere. All other chemicals were purchased from commercial suppliers and used without further purification. Flash column chromatography was performed using 230–400 mesh silica gel from EM Science, except for catalyst **12**,

which was purified using 40-63 μm Geduran silica gel 60 from EMD Chemicals. Thin layer chromatography was performed using glass plates pre-coated with silica gel 40 F_{254} purchased from EM Science. The syntheses of compounds **6**,[12] 4-ethynylbenzyl alcohol,[13] 4-ethynylbenzoic acid,[17] **9**,[14] and **14**,[18] were performed according to formerly reported protocols.

General Procedure for the Coupling of a Terminal Alkyne with an Aryl Halide Using a Palladium-Catalyzed Cross-Coupling (Sonogashira) Protocol. To an oven-dried round-bottom flask or screw cap tube equipped with a magnetic stir bar were added the aryl halide, the terminal alkyne, $PdCl_2(PPh_3)_2$ or $PdCl_2(PhCN)_2$ (ca. 2 mol % per aryl halide), CuI (ca. 4 mol % per aryl halide), and in the case of using $PdCl_2(PhCN)_2$, also ca. 4 mol % per aryl halide of HP(*tert*-Bu)$_3$. A solvent system of TEA and/or THF was added depending on the substrates. Upon completion, the reaction was quenched with a saturated solution of NH_4Cl. The organic layer was then diluted with diethyl ether or CH_2Cl_2, and washed with water or saturated NH_4Cl (1×). The combined aqueous layers were extracted with hexanes, diethyl ether, or CH_2Cl_2 (2×). The combined organic layers were dried over $MgSO_4$ and filtered, and the solvent was removed from the filtrate *in vacuo* to afford the crude product, which was purified by column chromatography (silica gel). Eluents and other slight modifications are described below for each compound.

General Procedure for Deprotection of TIPS-Protected Alkynes using TBAF. In a round-bottomed flask equipped with a magnetic stir bar, the protected alkyne was dissolved in THF ([protected alkyne] = 0.05 – 0.1 M). TBAF in THF (1.0

M, 1.1 equiv per alkyne) was added. The mixture was stirred at rt for 0.5 h or until the reaction was complete (monitored by TLC). The reaction was quenched with a saturated solution of NH_4Cl. The organic layer was then diluted with ethyl acetate. The organic layer was dried over $MgSO_4$ and filtered, and the solvent was removed from the filtrate in vacuo to afford the crude product, which was purified by column chromatography (silica gel).

4-Ethynylbenzyl alcohol.[13] See the general procedure for the Pd/Cu coupling reaction. A screw cap tube was used. The materials used were 4-bromobenzyl alcohol (0.280 g, 1.50 mmol), TIPSA (0.50 mL, 2.25 mmol), $PdCl_2(PhCN)_2$ (57.5 mg, 0.15 mmol), CuI (28.0 mg, 0.15 mmol), HP(*tert*-Bu)$_3$ (87.0 mg, 0.30 mmol), TEA (10.0 mL), and THF (10.0 mL) at 70 °C overnight. The residue was purified by flash column chromatography in silica gel using 20% ethyl acetate in hexanes; the product-containing fractions were combined, concentrated and the residue was subjected to the general procedure for the deprotection of TIPS-protected alkynes. The materials used were the TIPS protected intermediate (349 mg, 1.2 mmol), and TBAF (1.8 mL, 1.0 M in THF). The mixture was stirred at rt for 3 h. The crude terminal alkyne was purified in a silica gel column using 30% ethyl acetate in hexanes as eluent to yield 4-ethynylbenzyl alcohol (131 mg, 0.99 mmol, 67%, two steps) as a brown oil. ^{1}H NMR (400 MHz, $CDCl_3$) δ 7.49 (d, *J* = 8.0 Hz, 2H), 7.32 (d, *J* = 8.0 Hz, 2H), 4.70 (s, 2H), 3.07 (s, 1H).

BODIPY 7. See the general procedure for the Pd/Cu coupling reaction. The materials used were BODIPY **6**[12] (610 mg, 1.35 mmol), 4-ethynylbenzyl alcohol[13]

(269 mg, 2.03 mmol), $PdCl_2(PPh_3)_2$ (47.4 mg, 0.07 mmol), CuI (26.0 mg, 0.135 mmol), TEA (20.0 mL), and THF (60.0 mL) at rt overnight. The residue was suspended in 35 mL of MeOH. The suspension was heated using an oil bath until the mixture started boiling. The heating was then turned off, and the mixture was allowed to cool inside the oil bath. The resultant solid was filtered under vacuum and washed with cold EtOH. After drying the product in vacuum, BODIPY **7** was obtained as an orange solid (556 mg, 1.22 mmol, 91%). FTIR (neat) 3558, 3116, 3066, 3039, 2954, 2919, 2874.5, 2842, 2786, 2730, 2680, 2347, 2223, 1926, 1619, 1540, 1501.5, 1466, 1401, 1366, 1298,1266, 1183, 1157, 1086, 1039, 968, 824, 765, 703 cm^{-1}; ^1H NMR (400 MHz, $CDCl_3$) δ 7.67 (d, *J* = 8.4 Hz, 2H), 7.56 (d, *J* = 8.0 Hz, 2H), 7.38 (d, *J* = 8.0 Hz, 2H), 7.29 (d, *J* = 8.0 Hz, 2H), 5.99 (s, 2H), 4.74 (d, *J* = 5.6 Hz, 2H), 2.56 (s, 6H), 1.43 (s, 6H); ^{13}C NMR (100 MHz, $CDCl_3$) δ 155.99, 143.23, 141.64, 141.03, 135.17, 132.53, 132.05, 131.42, 128.44, 127.11, 124.31, 122.23, 121.58, 90.82, 88.87, 65.14, 14.82; EI-HRMS *m/z* calcd for $C_{28}H_{25}BF_2N_2ONa$ $[M + Na]^+$ 477.1921, found 477.1925.

BODIPY 8. A 100 mL round-bottom flask equipped with a magnetic stir bar was charged with **7** (260 mg, 0.57 mmol) and CH_2Cl_2 (50 mL). The resultant solution was cooled to 0 °C using an ice bath. Then DMF (0.5 mL) was added via syringe, followed by PBr_3 (0.86 mL, 1.0 M in CH_2Cl_2). The mixture was allowed to warm to rt without removal of the ice bath, and then it was stirred at rt overnight. The solvent was removed in vacuum. The residue was dissolved in CH_2Cl_2 (10 mL); a white solid that formed was removed by filtration. Silica gel was added to the filtered solution,

and after solvent removal, the silica-bound product was purified in a column of silica gel using 5% then 40% ethyl acetate in hexanes as eluent. BODIPY **8** was obtained as an orange solid (256 mg, 0.49 mmol, 87%). FTIR (neat) 3119, 3066, 3034, 2960, 2922, 2851, 2739, 2680, 2347, 2129, 1926, 1546, 1534, 1513, 1498.5, 1460, 1437, 1410, 1363, 1307, 1189, 1154, 1110, 1077, 1051, 974, 818, 762, 703 cm^{-1}; ^{1}H NMR (400 MHz, $CDCl_3$) δ 7.66 (d, *J* = 8.4 Hz, 2H), 7.53 (d, *J* = 8.4 Hz, 2H), 7.40 (d, *J* = 8.0 Hz, 2H), 7.30 (d, *J* = 8.4 Hz, 2H), 5.99 (s, 2H), 4.51 (s, 2H), 2.56 (s, 6H), 1.43 (s, 6H); ^{13}C NMR (100 MHz, $CDCl_3$) δ 156.02, 143.22, 140.97, 138.40, 135.36, 132.58, 132.24, 131.42, 129.39, 128.48, 124.13, 123.18, 121.61, 90.44, 89.67, 33.10, 14.83; EI-HRMS *m/z* calcd for $C_{28}H_{25}BBrF_2N_2$ $[M + H]^+$ 517.1283, found 517.1262.

Compound 4. A 50 mL round-bottom flask equipped with a magnetic stir bar was charged with **8** (291 mg, 0.56 mmol), THF (9.0 mL), and 1-methylimidazole (90 μL, 1.12 mmol), in that order. The mixture was stirred at 50 °C overnight. Then the mixture was cooled to rt, and filtered *in vacuo*. The orange solid obtained was washed with Et_2O (5 mL, 4×) and dried under vacuum, to give imidazolium salt **4** as a bright orange solid (326 mg, 0.54 mmol, 97%). FTIR (neat) 3626, 3452, 3381, 3143, 3028, 2975, 2919, 2860, 2727, 2374, 2347, 2217.5, 2035, 1908, 1625, 1616, 1546, 1510, 1466, 1398, 1363, 1304, 1257, 1186, 1157, 1118.5, 1080, 1039, 971, 833, 815, 765, 700 cm^{-1}; ^{1}H NMR (400 MHz, DMSO-d6) δ 9.24 (s, 1H), 7.81 (d, *J* = 8.0 Hz, 2H), 7.73 (s, 2H), 7.66 (d, *J* = 8.0 Hz, 2H), 7.48 (d, *J* = 8.0 Hz, 2H), 7.46 (d, *J* = 8.0 Hz, 2H), 6.21 (s, 2H), 5.48 (s, 2H), 3.87 (s, 3H), 2.46 (s, 6H), 1.39 (s, 6H); ^{13}C NMR (125 MHz, DMSO-d6) δ 155.18, 142.59, 140.91, 136.86, 135.69, 134.49, 132.28,

131.99, 130.43, 128.66, 128.52, 124.09, 122.94, 122.41, 122.31, 121.54, 89.93, 89.36, 51.41, 35.93, 14.24, 14.15; EI-HRMS *m*/*z* calcd for $C_{32}H_{30}BF_2N_4$ $[M - Br]^+$ 519.2518, found 519.2532.

Compound 10. A 50 mL round-bottom flask equipped with a magnetic stir bar was charged with **9**[14] (260 mg, 0.57 mmol) and CH_2Cl_2 (15 mL). The resultant solution was cooled to 0 °C using an ice bath. DMF (0.15 mL) was added *via* syringe, followed by PBr_3 (0.63 mL, 1.0 M in CH_2Cl_2). The mixture was allowed to warm to rt without removal of the ice bath, and then it was stirred at rt overnight. The solvent was removed *in vacuo*. The residue was dissolved in ethyl acetate (20 mL) and water (20 mL). The aqueous layer was extracted with ethyl acetate (3×). The combined organic layers were dried over $MgSO_4$ and filtered, and the solvent was removed from the filtrate *in vacuo* to afford the crude product as an orange solid. Purification was done by column chromatography in silica gel using 20% ethyl acetate in hexanes as eluent. Compound **10** was obtained as a bright orange solid (106 mg, 0.25 mmol, 61%). FTIR (neat) 3101, 3039.5, 2978, 2963, 2927.5, 2863, 2730, 2677, 2497, 2377, 2347, 2306, 2123, 1728, 1625, 1613.5, 1540, 1501.5, 1469, 1437, 1407, 1366, 1304, 1263, 1180, 1151, 1048, 965, 809, 753, 709 cm^{-1}; ^1H NMR (400 MHz, $CDCl_3$) δ 7.50 (d, *J* = 8.0 Hz, 2H), 7.28 (d, *J* = 8.0 Hz, 2H), 5.98 (s, 2H), 4.82 (d, *J* = 3.2 Hz, 2H), 2.56 (s, 6H), 1.39 (s, 6H); ^{13}C NMR (100 MHz, $CDCl_3$) δ 155.88, 143.22, 141.09, 139.26, 135.31, 131.50, 130.00, 128.68, 121.54, 32.80, 14.80, 14.68; EI-HRMS *m*/*z* calcd for $C_{20}H_{20}BBrF_2N_2Na$ $[M + Na]^+$ 439.0784, found 439.0767.

Compound 5. A 25 mL round-bottom flask equipped with a magnetic stir bar was charged with **10** (208 mg, 0.50 mmol), THF (8.0 mL), and 1-methylimidazole (80 μL, 1.00 mmol), in that order. The mixture was stirred at 50 °C overnight. Then the mixture was cooled to rt, and filtered in vacuum. The orange solid obtained was washed with Et_2O (5 mL, 4×) and dried under vacuum, to give imidazolium salt **5** as a bright orange solid (247 mg, 0.49 mmol, 99%). FTIR (neat) 3458, 3381, 3143, 3095.5, 2983.5, 2922, 2374, 2344, 2026, 1622, 1546, 1501.5, 1463, 1410, 1369, 1307, 1180, 1148, 1051, 974, 847, 803, 762, 730 cm^{-1}; ^1H NMR (400 MHz, DMSO-d6) δ 9.26 (s, 1H), 7.75 (s, 2H), 7.55 (d, *J* = 7.6 Hz, 2H), 7.46 (d, *J* = 7.2 Hz, 2H), 6.18 (s, 2H), 5.55 (s, 2H), 3.89 (s, 3H), 2.45 (s, 6H), 1.31 (s, 6H); ^{13}C NMR (100 MHz, DMSO-d6) δ 155.06, 142.64, 141.21, 136.99, 136.03, 134.31, 130.59, 128.84, 128.52, 124.25, 122.23, 121.49, 51.38, 35.97, 14.22, 14.08; EI-HRMS *m*/*z* calcd for $C_{24}H_{26}BF_2N_4$ $[M - Br]^+$ 419.2219, found 419.2217.

BODIPY 13. See the general procedure for the Pd/Cu coupling reaction. The materials used were BODIPY **6**[12] (349 mg, 0.77 mmol), 4-ethynylbenzoic acid[17] (170 mg, 1.16 mmol), $PdCl_2(PPh_3)_2$ (27.0 mg, 38.0 μmol), CuI (15.0 mg, 77.0 μmol), TEA (5.0 mL), and THF (15.0 mL) at rt overnight. The crude product (348 mg), pentafluorophenol (135 mg, 0.73 mmol), DMAP (5 mg, 0.04 mmol), and DCC (224 mg, 1.08 mmol) were added to a 50 mL round-bottom flask equipped with a magnetic stir bar. CH_2Cl_2 (12 mL) was added *via* syringe, and the mixture was stirred overnight at rt. The solvent was removed *in vacuo*, and the residue was purified on a silica gel column using 5%, then 30% ethyl acetate in hexanes.

Pentafluorophenol ester **13** was obtained as an orange solid (316 mg, 0.50 mmol, 65% over two steps). FTIR (neat) 3499, 3361, 3101, 2998, 2954, 2925, 2857, 2733, 2668, 2462, 2347, 2220, 1761, 1540, 1513, 1463, 1404, 1372, 1298, 1236, 1186, 1151, 1077, 1045, 974, 824, 709 cm^{-1}; ^{1}H NMR (400 MHz, $CDCl_3$) δ 8.21 (d, *J* = 8.0 Hz, 2H), 7.72 (d, *J* = 8.4 Hz, 4H), 7.34 (d, *J* = 8.0 Hz, 2H), 6.01 (s, 2H), 2.57 (s, 6H), 1.44 (s, 6H); ^{13}C NMR (125 MHz, $CDCl_3$) δ 162.24, 156.13, 143.13, 140.67, 136.05, 132.76, 132.18, 131.34, 130.93, 129.71, 128.64, 126.61, 123.45, 121.65, 93.04, 89.71, 14.82. The chemical shifts of the four different types of carbons on the C_6F_5 ring are not reported because the extensive one-bond and long-range $^{13}C–^{19}F$ couplings make the individual signals too weak and broad to interpret with any confidence. EI-HRMS *m*/*z* calcd for $C_{34}H_{22}BF_7N_2O_2Na$ $[M + Na]^+$ 657.1588, found 657.1561.

Complex 12. Inside a nitrogen-filled glove box, a 10 mL round-bottom flask equipped with a magnetic stir bar was charged with **14**[18] (50 mg, 66 μmol). CH_2Cl_2 (3 mL) was added and the flask was capped with a septum. The seal of the septum was reinforced with Teflon tape and the flask was taken out of the glove box. Hydrogen chloride was bubbled into the flask for 1 h. The HCl was generated by drop-wise addition of conc. H_2SO_4 to NH_4Cl. Then the mixture was stirred 2 h at rt. The solvent was removed by rotary evaporation. Next, the flask was charged with BODIPY **13**. Under a nitrogen atmosphere, DMF (2.5 mL) and Et_3N (0.2 mL) were added, and the mixture was stirred at rt overnight. The solvent was removed in vacuum (using a Schlenk line with a dry ice trap, not by rotary evaporation) at 40 °C. The residue was dissolved in degassed CH_2Cl_2 and purified under ~ anaerobic

conditions[23] in a silica gel column (Geduran, see General Methods). In ~ anaerobic chromatography, the column was packed under a stream of nitrogen, and the solvents used as eluents (diethyl ether and pentane) were degassed prior to use with a sparge of nitrogen for 30 min. The product was eluted under nitrogen and it was collected in a round-bottom flask previously purged with nitrogen and equipped with a magnetic stir bar and a nitrogen sparge. The eluant was removed using a Schlenk line with a dry ice trap (not by rotary evaporation). Unreacted BODIPY **13** was removed using 50% distilled Et_2O in pentane, then pure Et_2O was used to elute the desired product. Complex **12** was obtained as a dark brown solid (56 mg, 50 μmol, 77%). FTIR (neat) 3343, 2963, 2922, 2854, 2733, 2379.5, 2344, 2321, 2049.5, 1979, 1946, 1923, 1840, 1554, 1475, 1440, 1398, 1378, 1310, 1263, 1198, 1157, 1083, 983, 853 cm^{-1}; ^1H NMR (500 MHz, CD_2Cl_2) δ 16.40 (s, 1H), 7.76 (br s, 2H), 7.69 (d, J = 6.8 Hz, 2H), 7.57 (d, J = 7.2 Hz, 3H), 7.33 (d, J = 6.8 Hz, 2H), 7.16 (br s, 1H), 7.10 (br s, 1H), 7.08 (br s, 1H), 6.99–6.98 (m, 1H), 6.92 (d, J = 5.2 Hz, 2H), 6.87 (d, J = 6.4 Hz, 1H), 6.035 (s, 2H), 4.94 (m, 1H), 4.68 (br s, 1H), 4.32 (t, J = 8.8 Hz, 1H), 3.955 (dd, J_1 = 6.4 Hz, J_2 = 8.8 Hz, 2H), 3.68 (br s, 1H), 2.90–2.80 (br m, 3H), 2.52 (s, 6H), 2.41 (br m, 15H), 1.45 (s, 6H), 1.28 (br d, J = 8.8 Hz, 6H); ^{13}C NMR (125 MHz, CD_2Cl_2) δ 297.09, 216.07, 167.26, 156.23, 152.62, 145.47, 143.76, 141.46, 139.88, 139.69, 135.80, 133.91, 132.98, 132.09, 131.66, 130.98, 130.54, 130.40, 130.06, 128.94, 127.89, 126.72, 124.17, 122.91, 122.84, 121.84, 113.49, 91.40, 90.19, 75.74, 64.25, 42.67, 21.50, 21.36, 14.85; MALDI-TOF MS (+eV) m/z calcd for $C_{60}H_{63}BCl_2F_2N_5O_2Ru$ 1106.9, found 1106.5.

Spectroscopic Measurements. Absorption spectra were recorded on a Shimadzu UV-3101PC spectrophotometer. UV–vis spectra have 2 nm slit. The fluorescence emission spectra were obtained in a Perkin Elmer LS50B instrument, using dichloromethane solutions exposed to air with absorbance between 0.01 – 0.06. Two emission spectra were recorded for each compound and the two quantum yields obtained were then averaged. All fluorescence spectra were corrected. Excitation was done at the corresponding λ_{max} − 30 nm wavelength. Rhodamine 6G was used as the reference (ϕ_{ref} = 0.95 in EtOH, λ_{exc} = 488 nm). The fluorescence quantum yield of **12** was calculated from eq. 1. *F* denotes the integral of the corrected fluorescence spectrum, *A* is the absorbance at the excitation wavelength and *n* is the refractive index of the medium.

$$\Phi_{exp} = \Phi_{ref} \frac{F\{1- \exp(-A_{ref}\ln 10)\}n^2}{F_{ref}\{1-\exp(-A\ln 10)\}n_{ref}{}^2} \quad (4.1)$$

ROMP of 1,5-cyclooctadiene.[21] Dichloromethane-d2 was freeze/pump/ thawed three times. Cod was distilled over CaH_2 immediately prior the polymerization reaction. As reported by Grubbs,[21] we too found that aged cod gave considerably lower rates. ^{1}H NMR spectra were collected at 500 MHz. Inside a glove box, an NMR tube with a septum/screw-cap (model 27093, Sigma-Aldrich) was charged with catalyst solution (0.40 μmol) and CD_2Cl_2 to give a total volume of 0.80 mL. The solution was equilibrated at 30 °C in the NMR probe. The sample was then ejected from the NMR instrument to add cod (50 μL, 0.40 mmol) *via* syringe. A series of spectra were collected over an appropiate period of time. The degree of

conversion to polymer was determined by comparing the ratio of the integrals of the methylene protons in the starting material at δ 2.36 (m) with those in the product at δ 2.09 br (m), δ 2.04 (br m).

Calculation of Diffusion Constants using FCS. FCS records the fluorescence fluctuations from a single light-emitting source in a small open volume and transforms the time traces into autocorrelation curves via the correlation analysis. The intensity of the autocorrelation as a function of lagtime (τ) can be expressed in terms of experimental parameters as:

$$G(\tau) = \frac{1}{V_{eff}<C>} \cdot \frac{1}{\left(1+\frac{\tau}{\tau_D}\right)} \cdot \frac{1}{\left(1+\left(\frac{r_0}{z_0}\right)^2\left(\frac{\tau}{\tau_D}\right)\right)^{1/2}} \quad (4.2)$$

where V_{eff} is volume, r_0 is beam waist, z_0 is beam height, τ_D is characteristic diffusion time, and $<C>$ is analyte concentration. The experimental characteristic diffusion time can thus be obtained by fitting the autocorrelation curves with the above equation. Finally, the three-dimensional diffusion coefficient (D) can be calculated using the following equation:

$$\tau_D = \frac{r_0^2}{4D} \quad (4.3)$$

Optical Setup for FCS. FCS was performed using a home-built inverted confocal microscope (Observer.D1, Zeiss). The light from a 532 nm laser (Verdi-6, Coherent Inc.) is collimated and expanded to overfill the back aperture of a microscope objective (Fluar, Zeiss:100×, NA = 1.3). The beam was circularly

polarized using a λ/4 waveplate (Newport). The laser power was attenuated to ~ 150 nW using neutral density filters (Thorlabs). This power gives a signal to background ratio of ~ 10, yet ensured negligible heating of the sample. The focal plane of the objective is set to approximately ~ 6 μm inside the solution to avoid excessive scattered light from the glass–water interface. Polystyrene fluorospheres (100 nm in diameter, Molecular Probes) are used for alignment and calibration of the focal volume. The fluorescence is collected in the backward direction and redirected to a 50 μm pinhole (Thorlabs) before focusing onto an avalanche photodetector (SPCM-AQRH, Perkin-Elmer).

Supporting Information. ^{1}H and ^{13}C NMR spectra of new compounds.

4.5. References

1. Balzani, V.; Credi, A.; Venturi, M. *Molecular Devices and Machines: Concepts and Perspectives for the Nanoworld*; Wiley-VCH: Weinheim, Germany, 2008.
2. a) Mirkovic, T.; Zacharia, N. S.; Scholes, G. D.; Ozin, G. A. *ACS Nano* **2010**, *4*, 1782–1789. b) Mirkovic, T.; Zacharia, N. S.: Scholes, G. D.; Ozin, G. A. *Small* **2010**, *6*, 159–167. c) Paxton, W. F.; Sundararajan, S.; Mallouck, T. E.; Sen, A. *Angew. Chem., Int. Ed.* **2006**, *45*, 5420–5429. d) Wang, J. *ACS Nano* **2009**, *3*, 4–9.

3. a) Laocharœnsuk, R.; Burdick, J.; Wang, J. *ACS Nano* **2008**, *2*, 1069–1075. b) Paxton, W. F.; Kistler, K. C.; Olmeda, C. C.; Sen, A.; Angelo, S. K.; Cao, Y.; Mallouk, T. E.; Lammert, P. E.; Crespi, V. H. *J. Am. Chem. Soc.* **2004**, *126*, 13424–13431. c) Manesh, K. M.; Cardona, M.; Yuan, R.; Clark, M.; Kagan, D.; Balasubramanian, S.; Wang, J. *ACS Nano* **2010**, *4*, 1799–1804.
4. Heureux, N.; Lusitani, F.; Browne, W. R.; Pshenichnikov, M. S.; van Loosdrecht, P. H. M.; Feringa, B. L. *Small* **2008**, *4*, 476–480.
5. Smith, G. A.; Portnoy, D. A. *Trends Microbiol*. **1997**, *5*, 272–276.
6. Pavlick, R. A.; Sengupta, S.; McFadden, T.; Zhang, H.; Sen, A. *Angew. Chem., Int. Ed.* **2011**, *50*, 9374-9377.
7. Tcherniak, A.; Reznick, C.; Link, S.; Landes, C. F. *Anal. Chem.* **2009**, *81*, 746–754.
8. Samojlowicz, C.; Bieniek, M.; Grela, K. *Chem. Rev.* **2009**, *109*, 3708–3742.
9. Deshmukh, P. H.; Blechert, S. *Dalton Trans.* **2007**, 2479–2491.
10. a) Treibs, A.; Kreuzer, F.–H. *Liebigs Ann. Chem.* **1968**, *718*, 208–223. b) Loudet, A.; Burgess, K. *Chem. Rev.* **2007**, *107*, 4891–4932.
11. Kingsbury, J. S.; Harrity, J. P. A.; Bonitatebus, P. J.; Hoveyda, A. H. *J. Am. Chem. Soc.* **1999**, *121*, 791–799.
12. Godoy, J.; Vives, G.; Tour, J. M. *Org. Lett.* **2010**, *12*, 1464–1467.
13. Percec, V.; Rudick, J. G.; Peterca, M.; Wagner, M.; Obata, M.; Mitchell, C. M.; Cho, W.–D.; Balagurusamy, V. S. K.; Heiney, P. A. *J. Am. Chem. Soc.* **2005**, *127*, 15257–15264.

14. Yue, Y.; Guo, Y.; Xu, J.; Shao, S. *New J. Chem.* **2011**, *35*, 61–64. For full characterization of **9** see: Matsumoto, T.; Urano, Y.; Takahashi, Y.; Mori, Y.; Terai, T.; Nagano, T.; *J. Org. Chem.* **2011**, *76*, 3616–3625.
15. Vougioukalakis, G. C.; Grubbs, R. H. *Chem. Rev*. **2010**, *110*, 1746–1787.
16. Schwab, P.; Grubbs, R. H.; Ziller, J. W. *J. Am. Chem. Soc.* **1996**, *118*, 100–110.
17. Jones, L. F.; Cochrane, M. E.; Koivisto, B. D.; Leigh, D. A.; Perlepes, S. P.; Wernsdorfer, W.; Brechin, E. K. *Inorg. Chim. Acta* **2008**, *361*, 3420–3426.
18. Lo, C.; Ringenberg, M. R.; Gnandt, D.; Wilson, Y.; Ward, T. R. *Chem. Comm.* **2011**, *47*, 12065–12067
19. Chen, J.; Burghart, A.; Wan, C-W.; Thai, L.; Ortiz, C.; Reibenspies, J.; Burgess, K. *Tetrahedron Lett*. **2000**, *41*, 2303–2307.
20. Kim, K. H.; Ok, T.; Lee, K.; Lee, H.-S.; Chang, K. T.; Ihee, H.; Sohn, J.-H.; *J. Am. Chem. Soc.* **2010**, *132*, 12027–12033.
21. Ritter, T.; Hejl, A.; Wenzel, A. G.; Funk, T. W.; Grubbs, R. H. *Organometallics* **2006**, *25*, 5740–5745.
22. (a) Garber, S. B.; Kingsbury, J. S.; Gray, B. L.; Hoveyda, A. H. *J. Am. Chem. Soc.* **2000**, *122*, 8168-8179. (b) Gessler, S.; Randl, S.; Blechert, S. *Tetrahedron Lett.* **2000**, *41*, 9973-9976.
23. Exactly as described in Jordan, J. P.; Grubbs, R. H. *Angew. Chem. Int. Ed.* **2007**, *46*, 5152–5155.

4.6. Experimental Contributions Section

My contributions to the experimental work described in this chapter are the following: synthesis and characterization of the fluorescent catalyst, as well as measurement of its optical properties and catalytic activity. Lin-Yung Wang carried out the FCS experiments. E. Loïc Samuel made figure 4.1.

Supporting Information

Supporting Information of

Chapter 1

Synthesis of Fluorescent Dye-Tagged Nanocars

^{1}H and ^{13}C NMR spectra of all new compounds

Figure S1.1. ^{1}H NMR spectrum of **8** (400 MHz, $CDCl_3$).

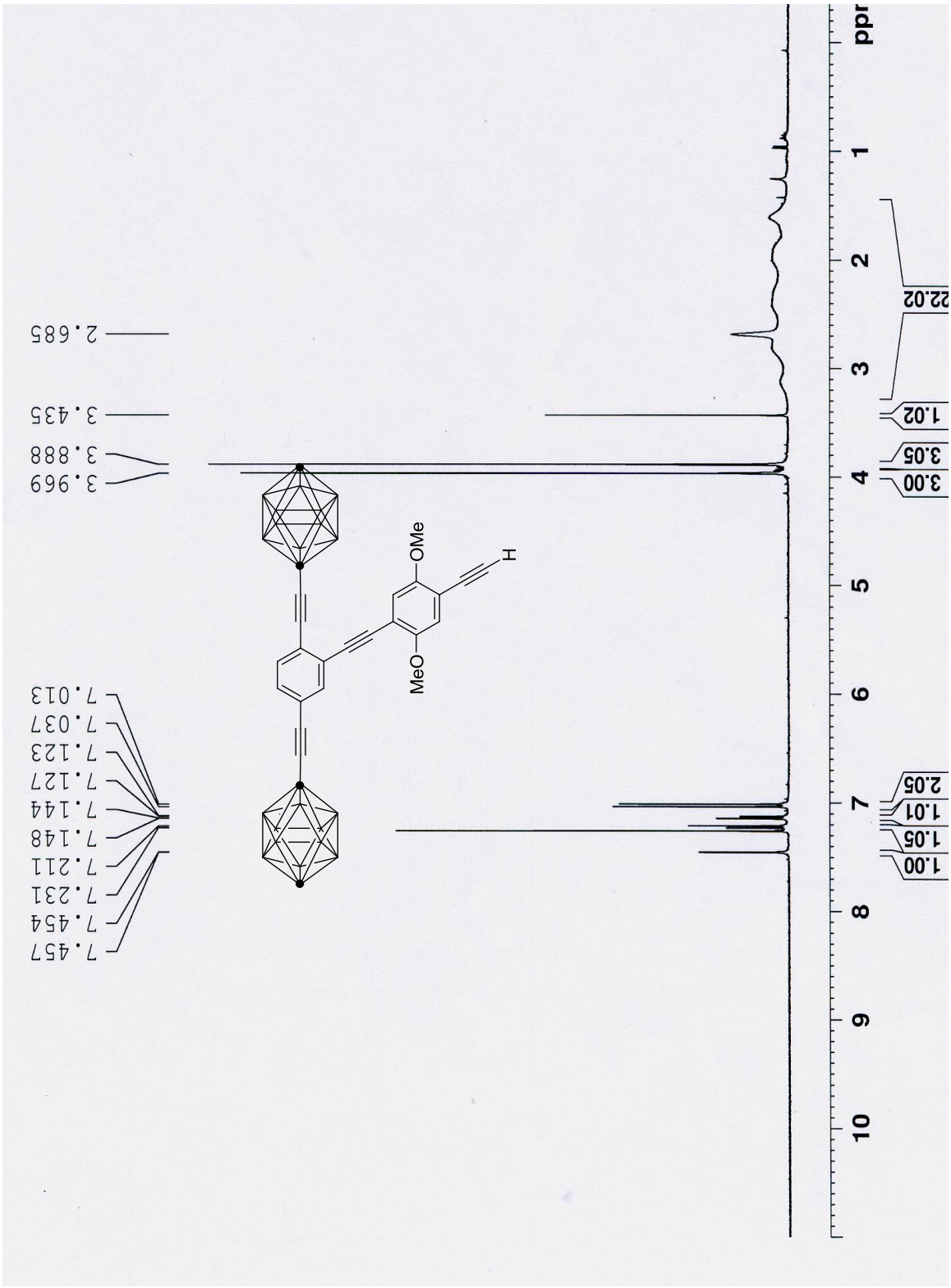

Figure S1.2. ^{13}C NMR spectrum of **8** (100 MHz, $CDCl_3$).

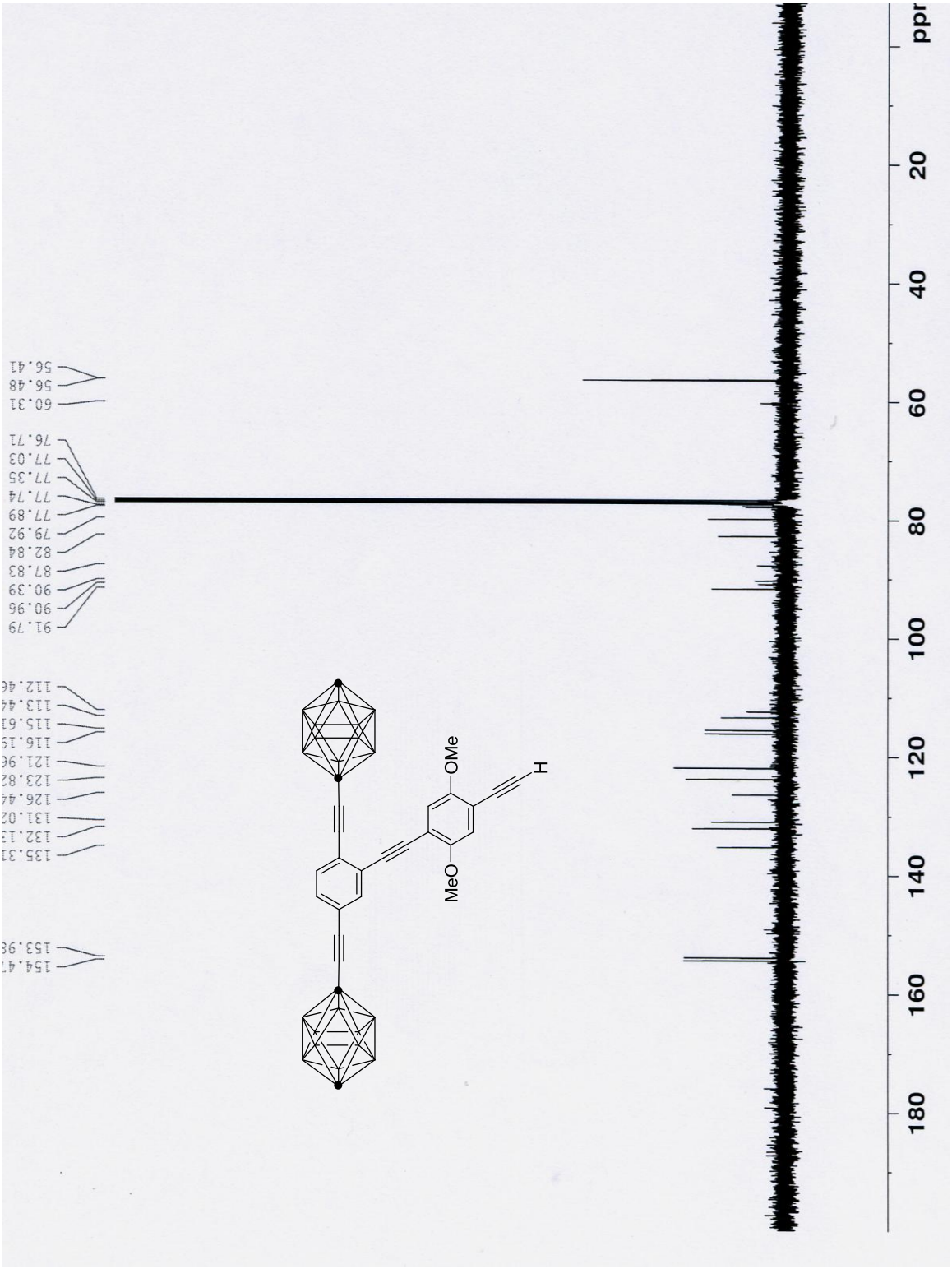

Figure S1.3. ^{1}H NMR spectrum of **10** (400 MHz, $CDCl_3$).

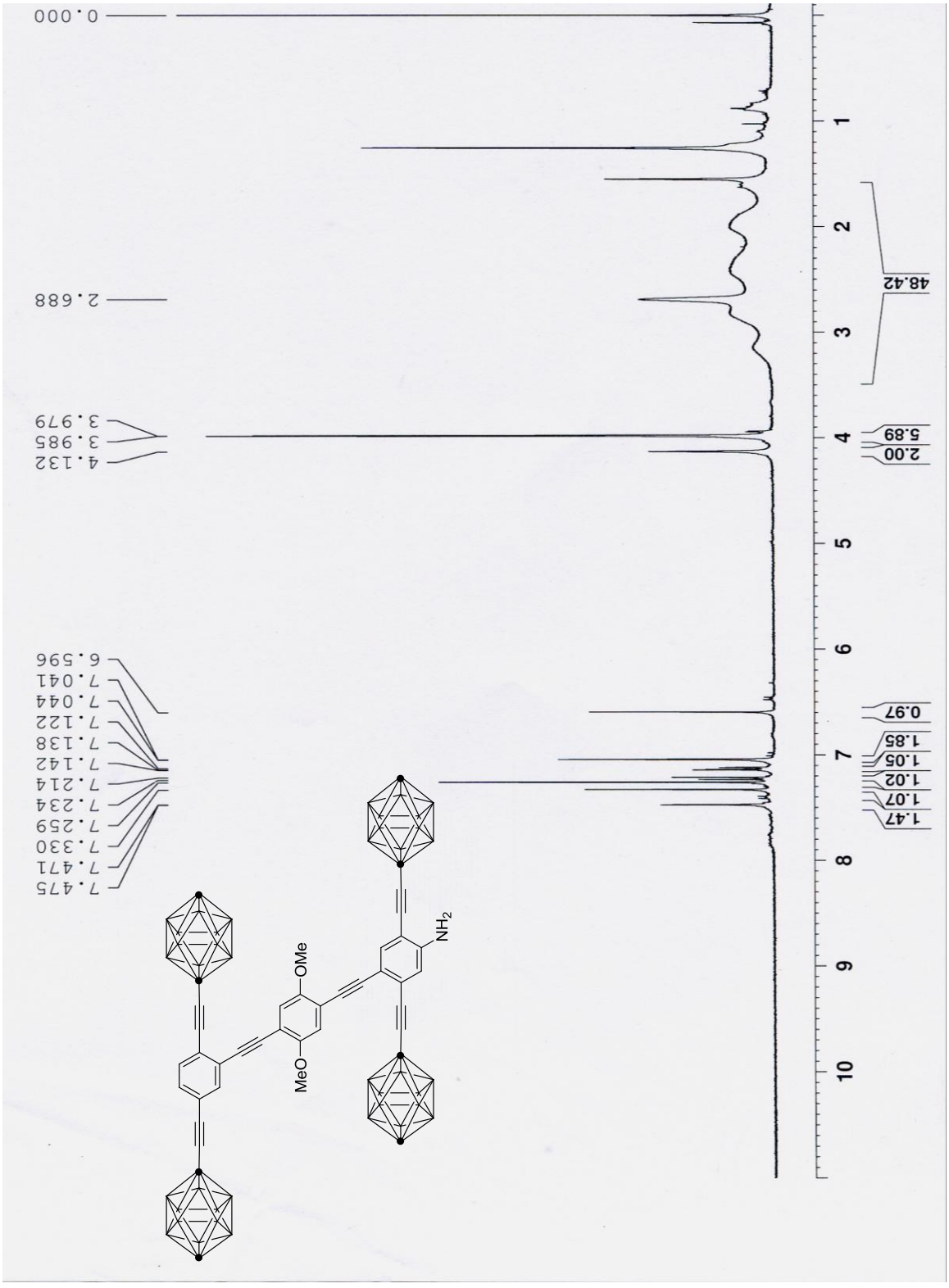

Figure S1.4. ^{13}C NMR spectrum of **10** (100 MHz, $CDCl_3$).

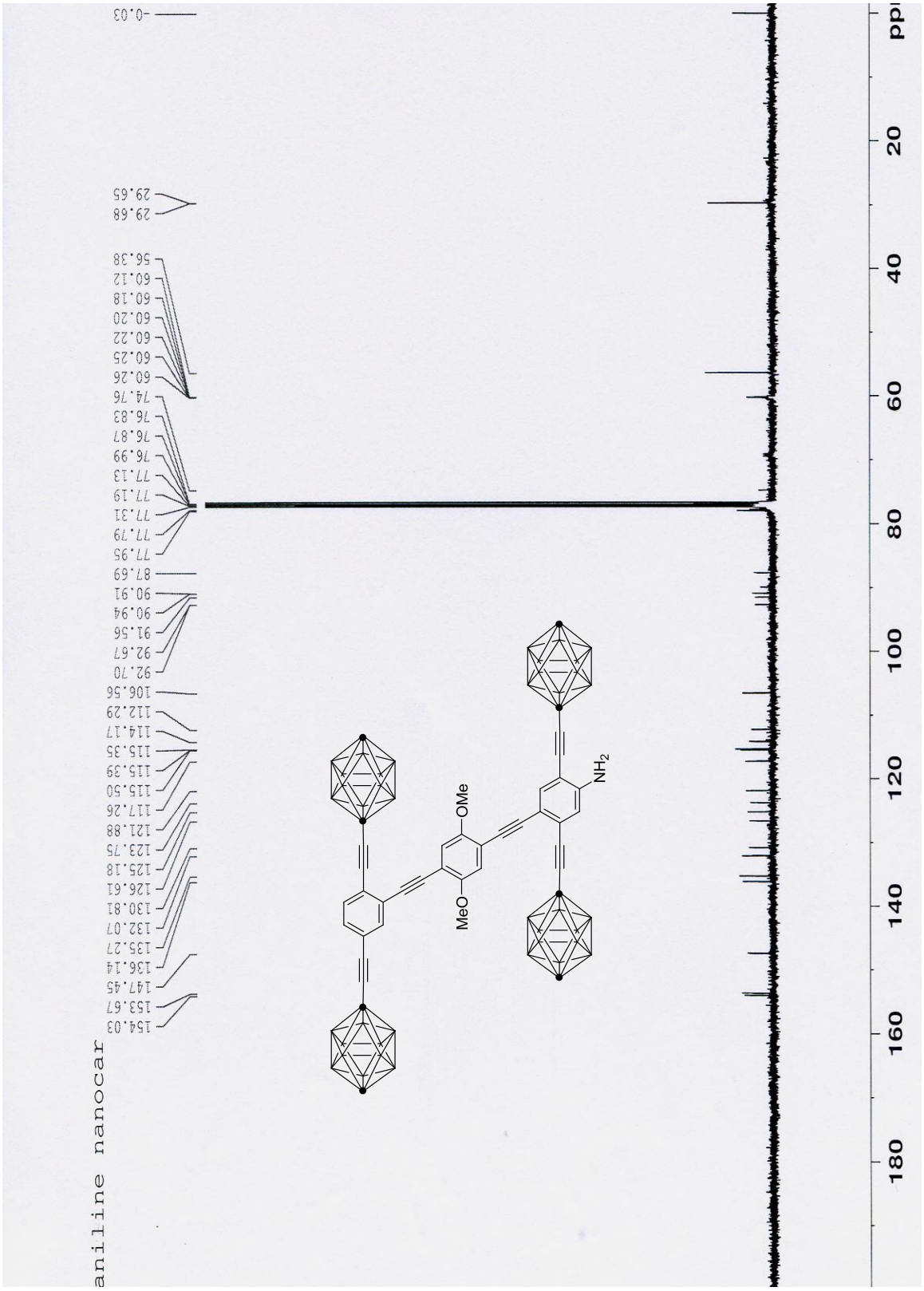

Figure S1.5. ^{1}H NMR spectrum of **1** (400 MHz, $CDCl_3$).

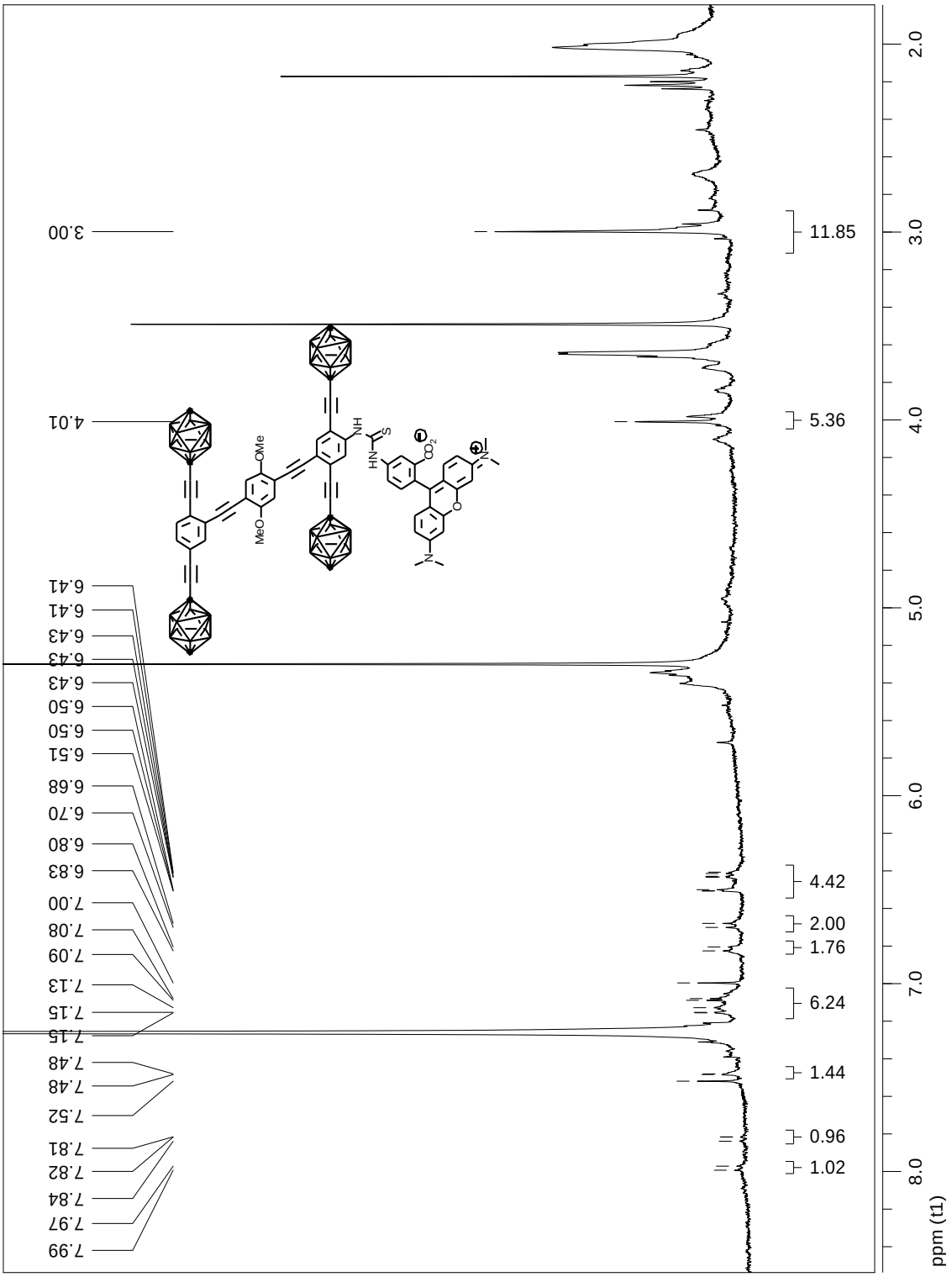

Figure S1.6. ^{1}H NMR spectrum of **12** (500 MHz, $CDCl_3$).

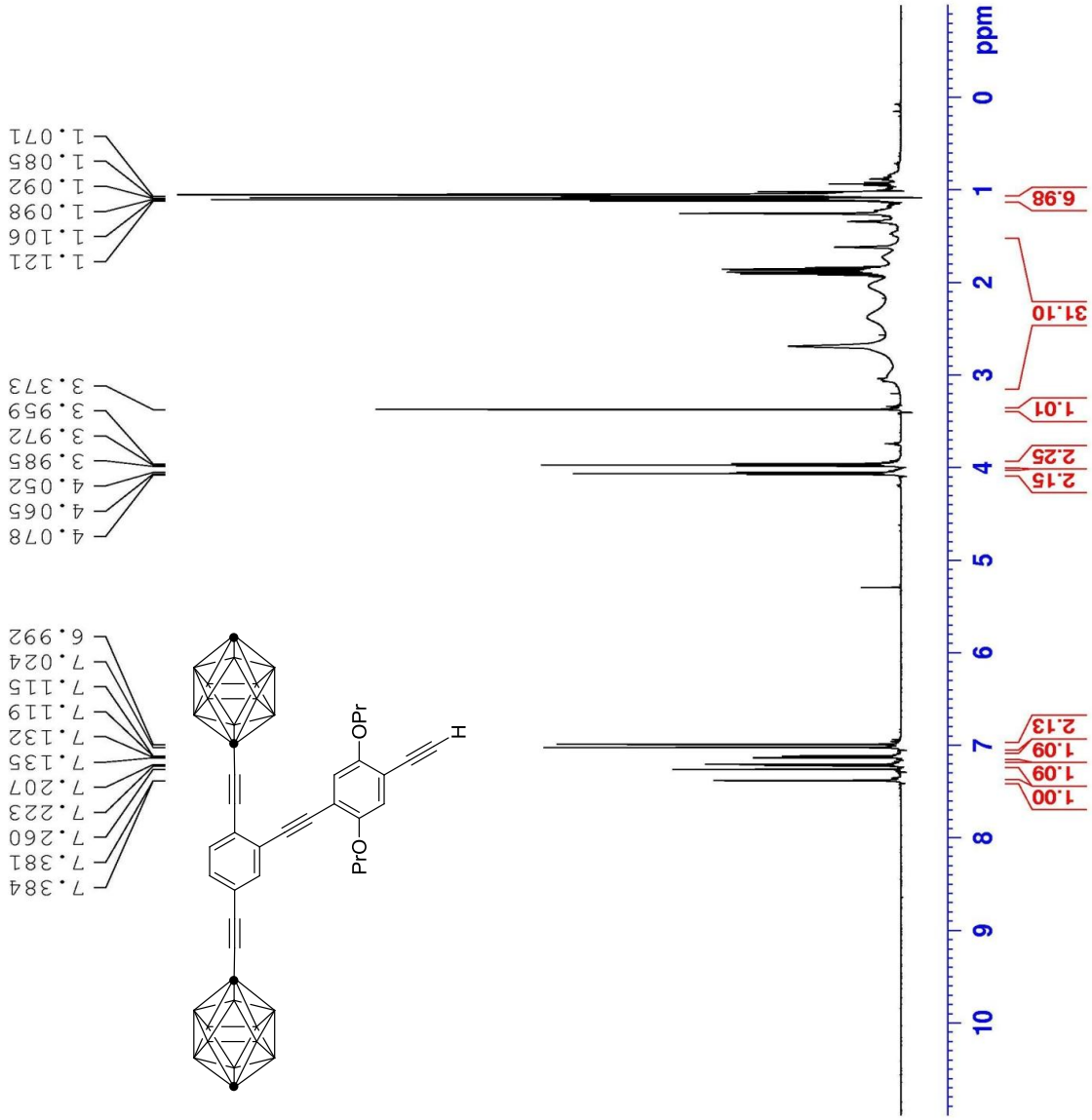

Figure S1.7. ^{13}C NMR spectrum of **12** (125 MHz, $CDCl_3$).

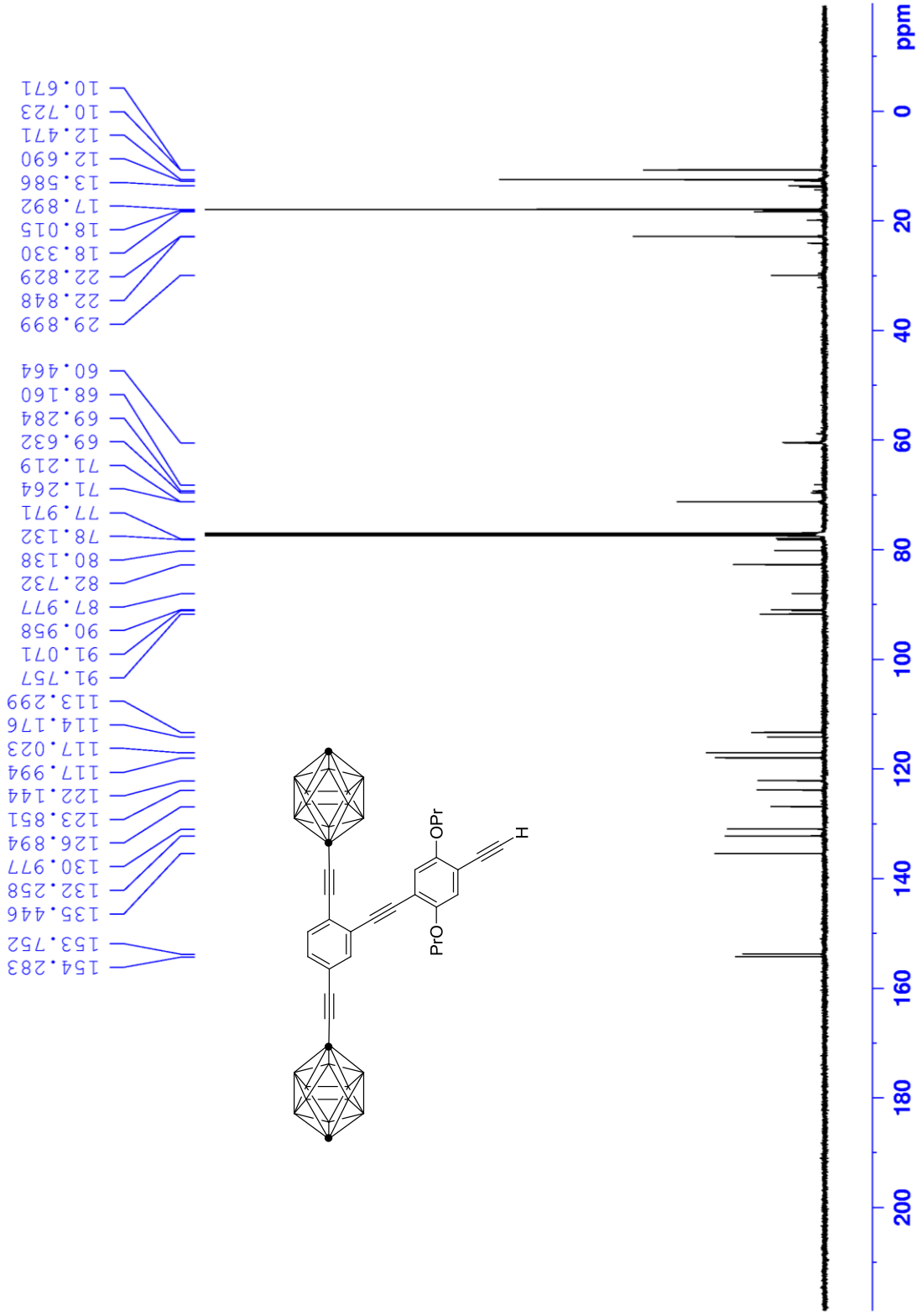

Figure S1.8. ^{1}H NMR spectrum of **14** (400 MHz, $CDCl_3$).

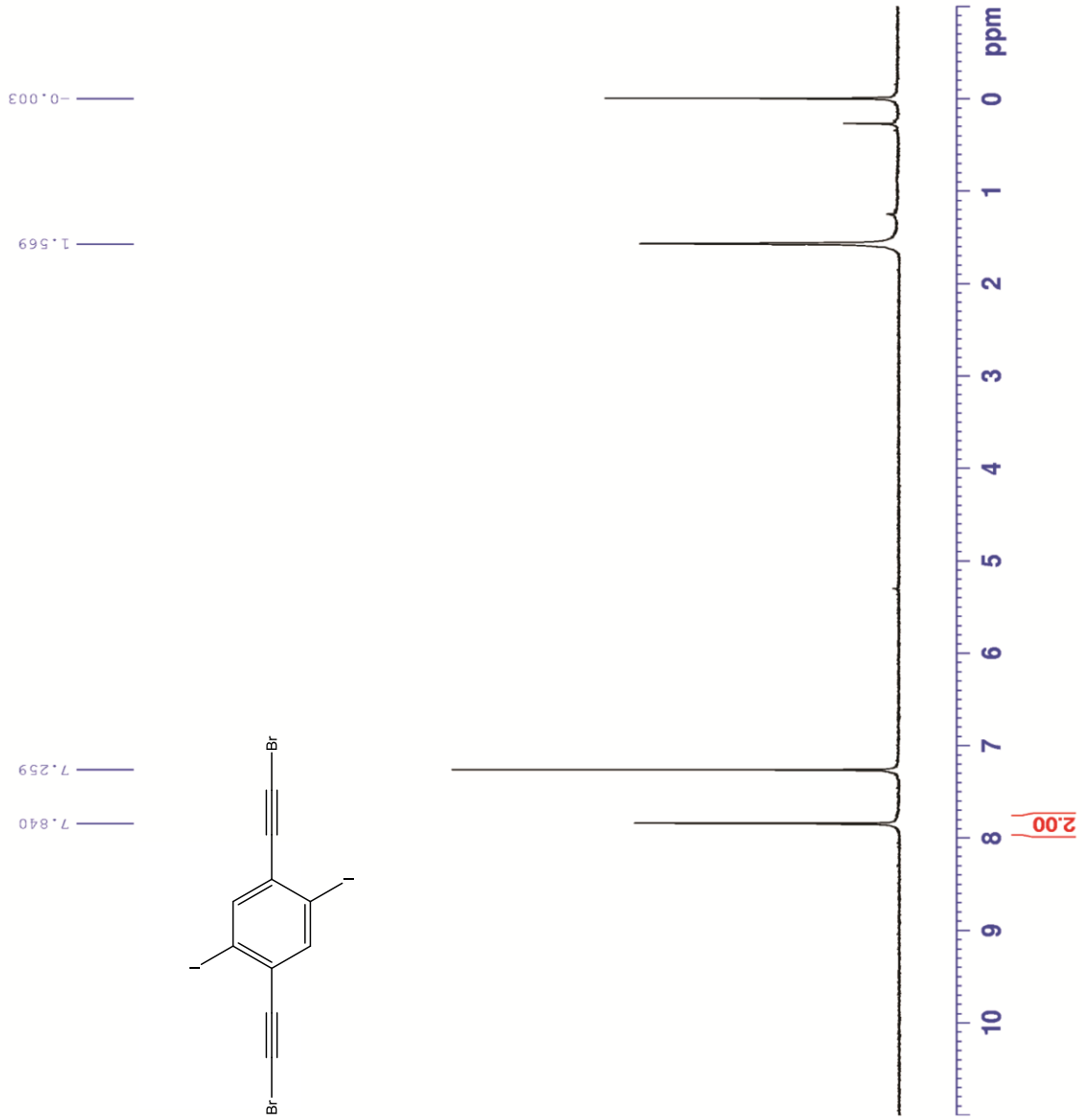

Figure S1.9. ^{13}C NMR spectrum of **14** (100 MHz, $CDCl_3$).

Figure S1.10. ^{1}H NMR spectrum of **16** (400 MHz, $CDCl_3$).

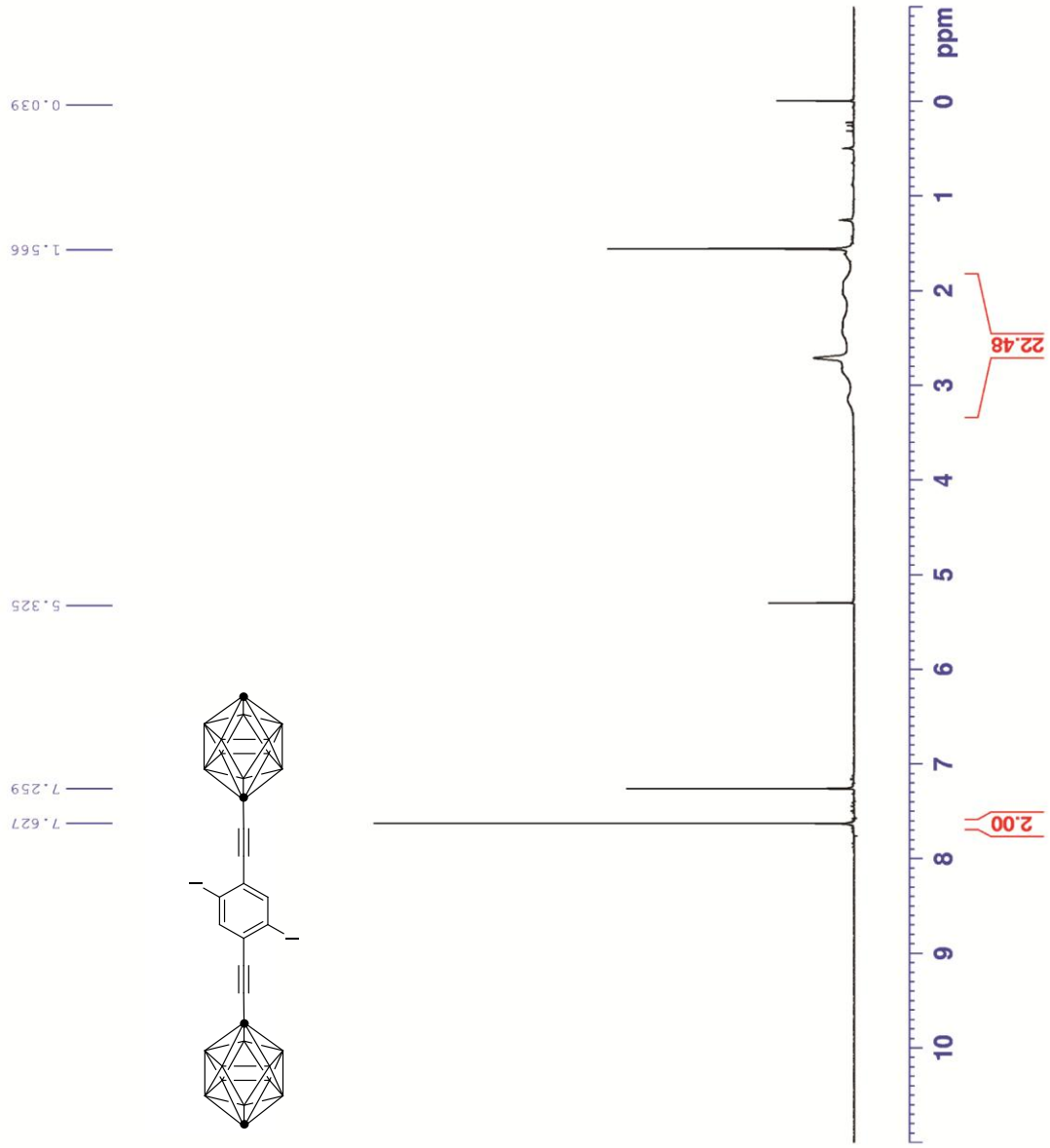

Figure S1.11. ^{13}C NMR spectrum of **16** (100 MHz, $CDCl_3$).

Figure S1.12. ^{1}H NMR spectrum of **17** (500 MHz, $CDCl_3$).

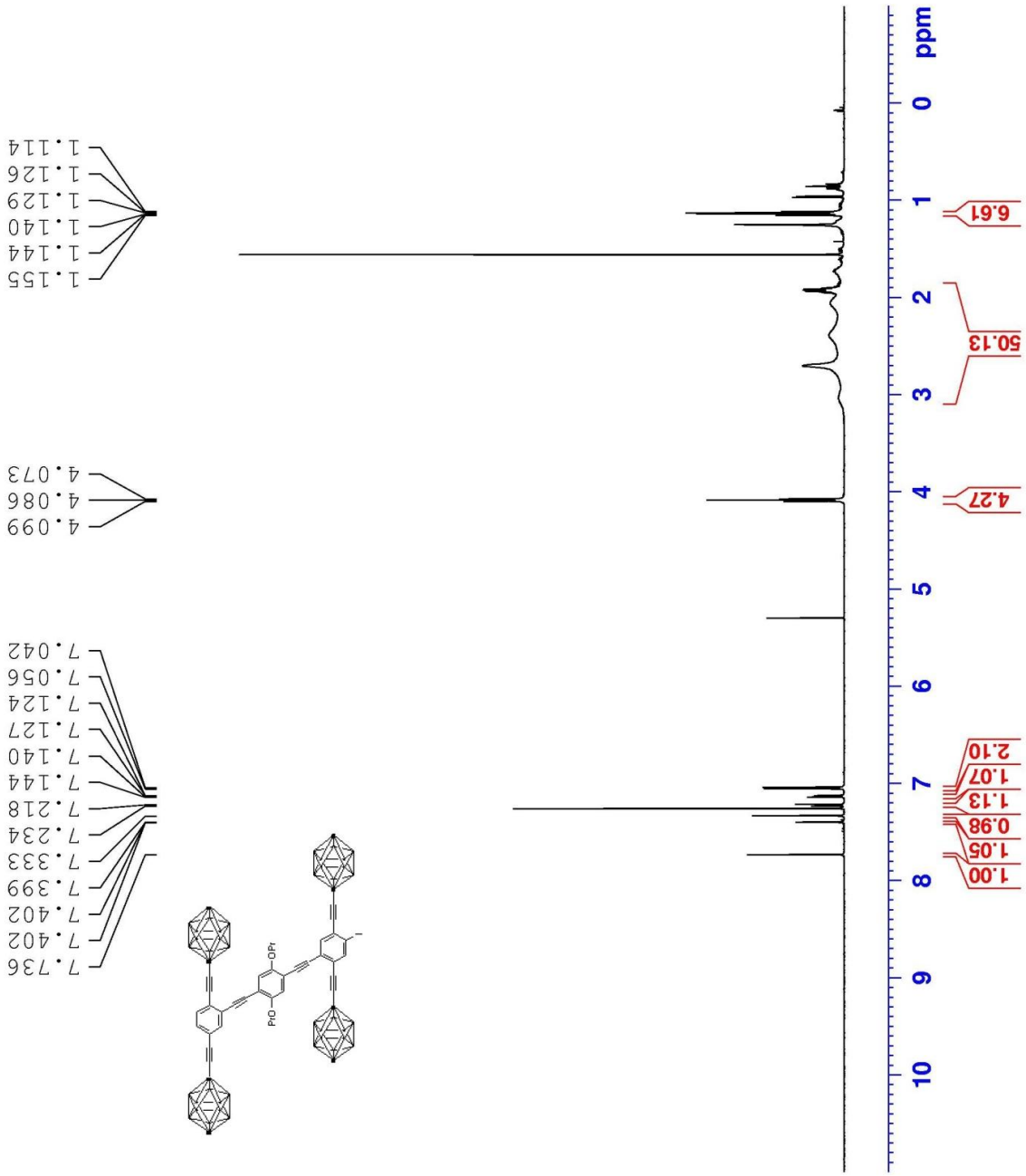

Figure S1.13. ^{13}C NMR spectrum of **17** (125 MHz, $CDCl_3$).

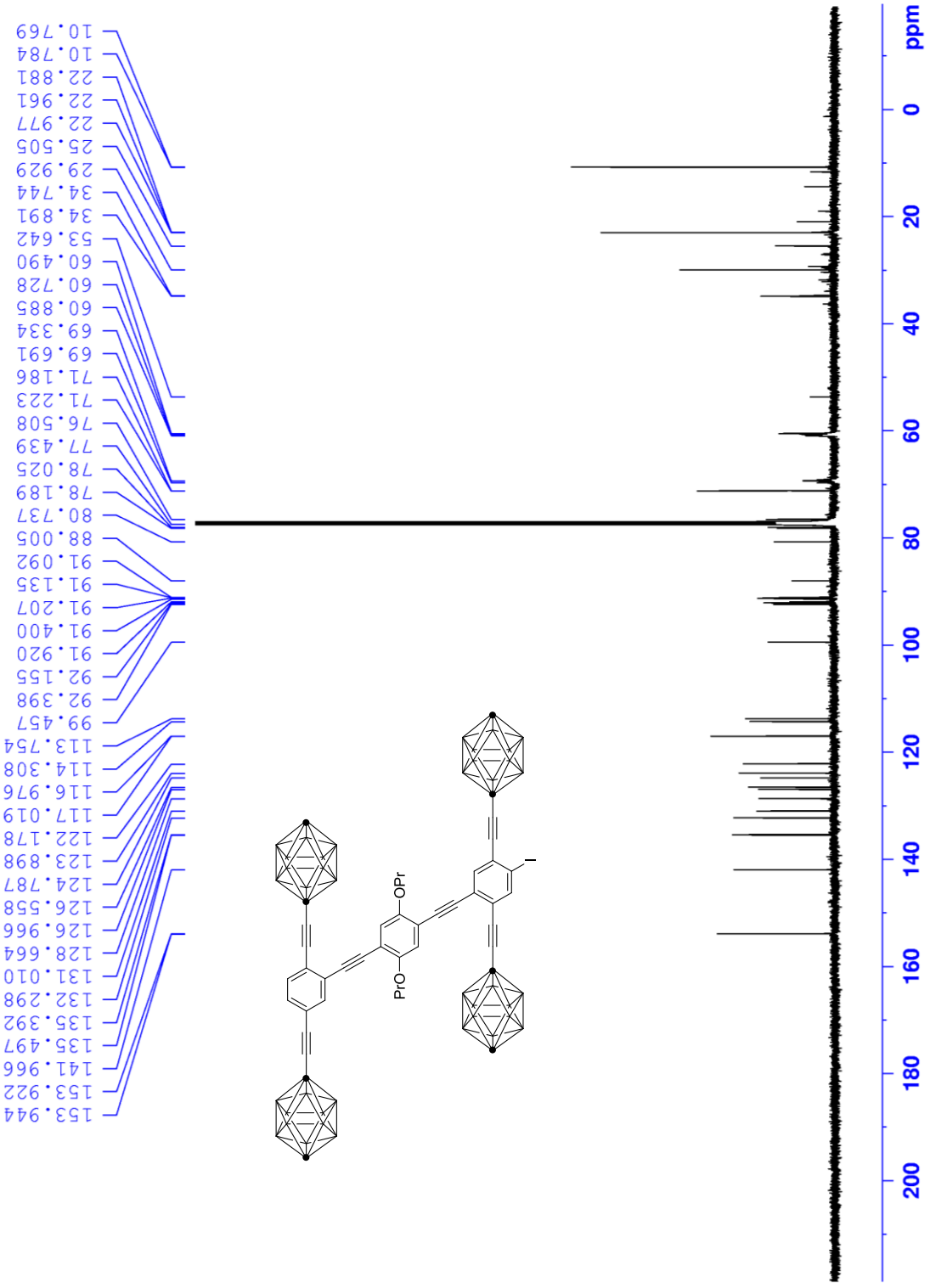

Figure S1.14. ^{1}H NMR spectrum of **19** (400 MHz, $CDCl_3$).

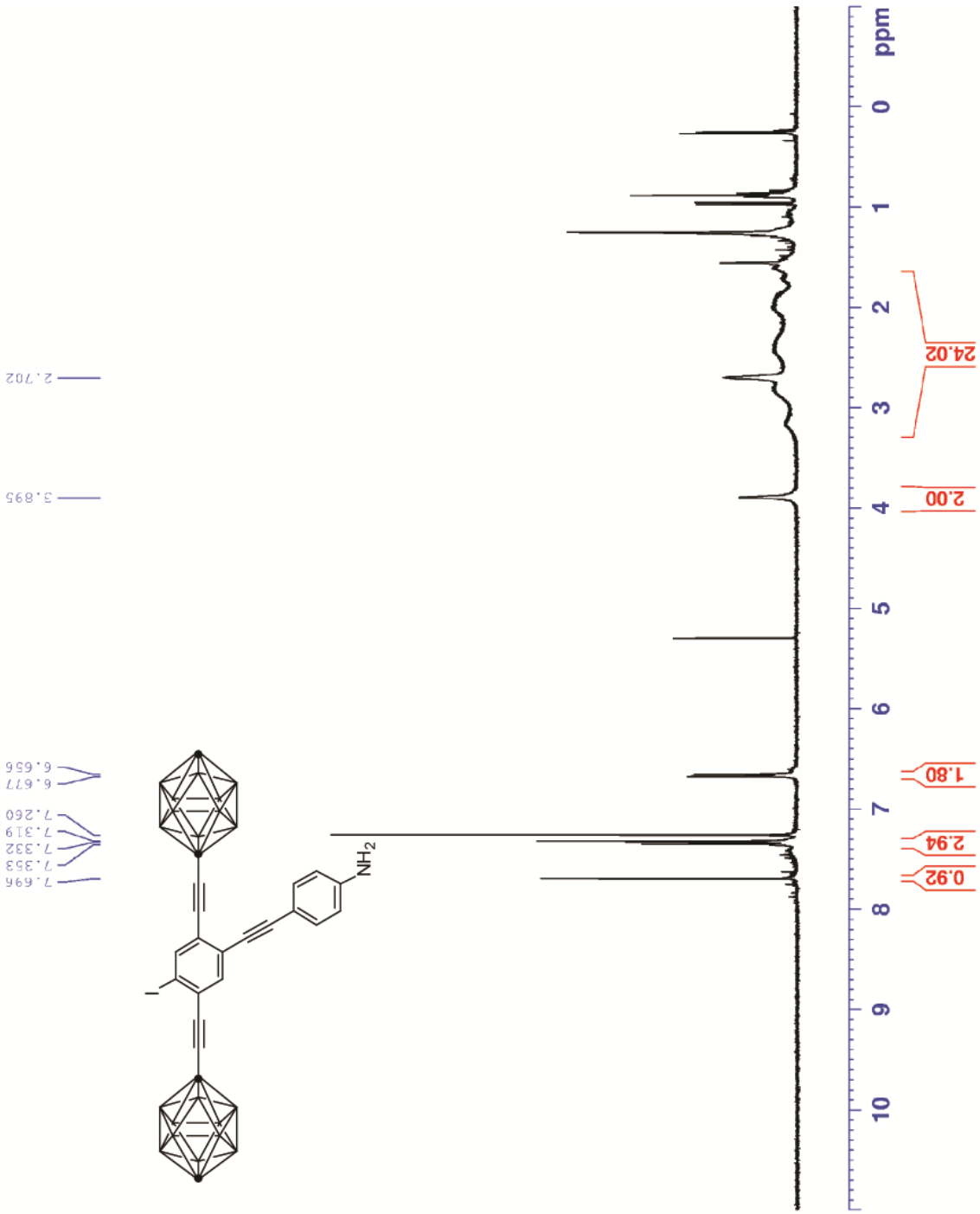

Figure S1.15. ^{13}C NMR spectrum of **19** (100 MHz, $CDCl_3$).

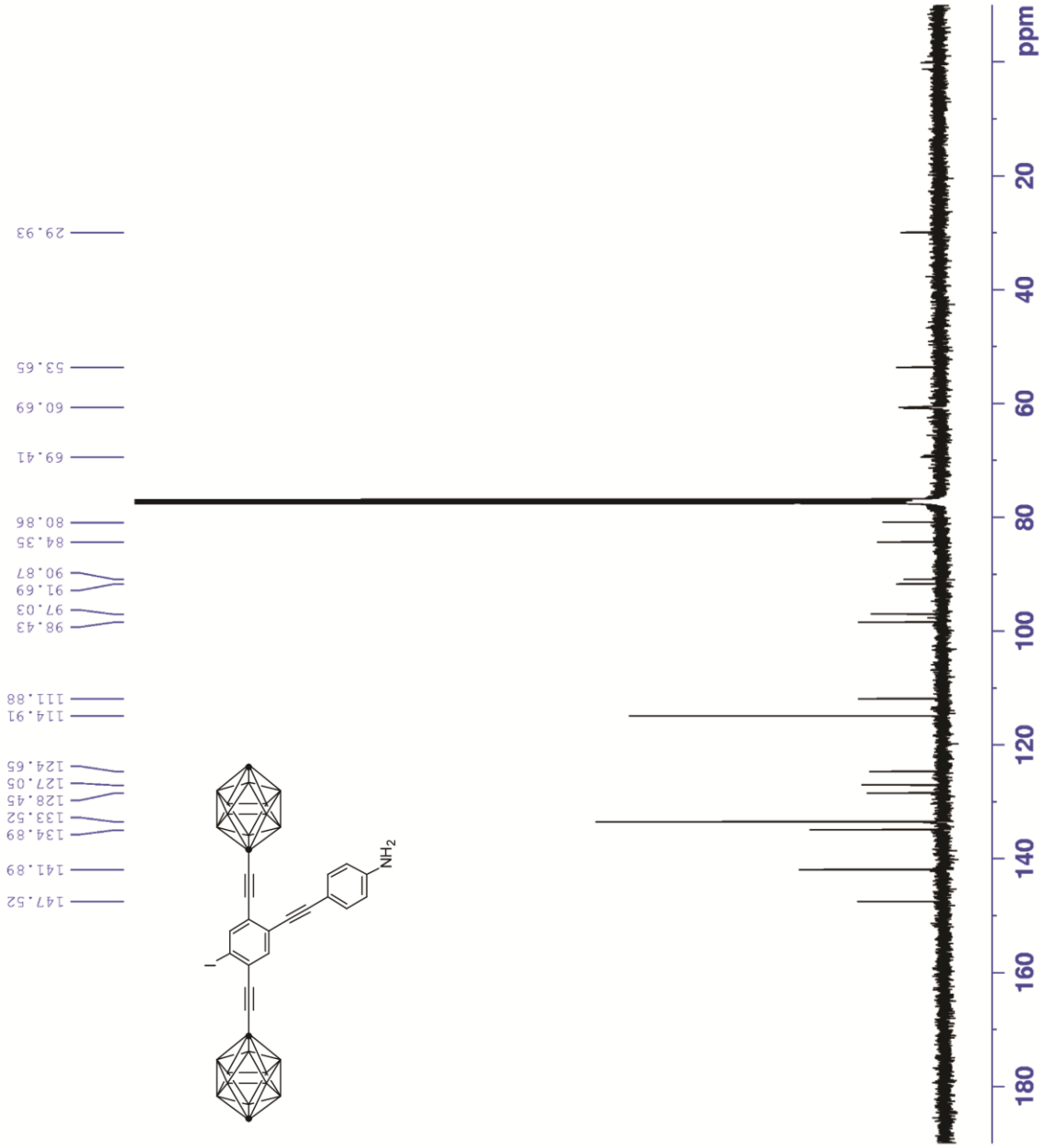

Figure S1.16. ^{1}H NMR spectrum of **20** (400 MHz, $CDCl_3$).

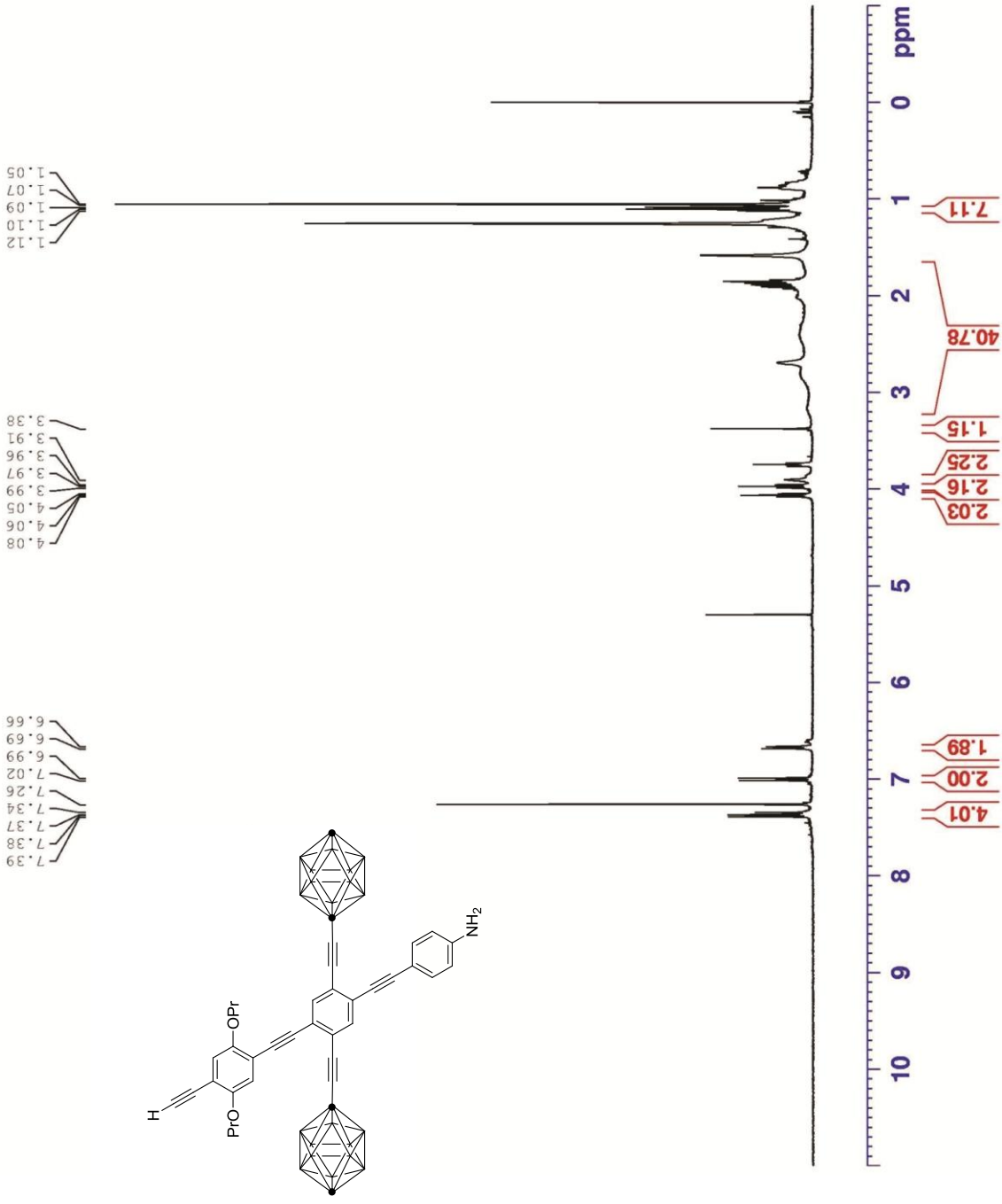

Figure S1.17. ^{13}C NMR spectrum of **20** (100 MHz, $CDCl_3$).

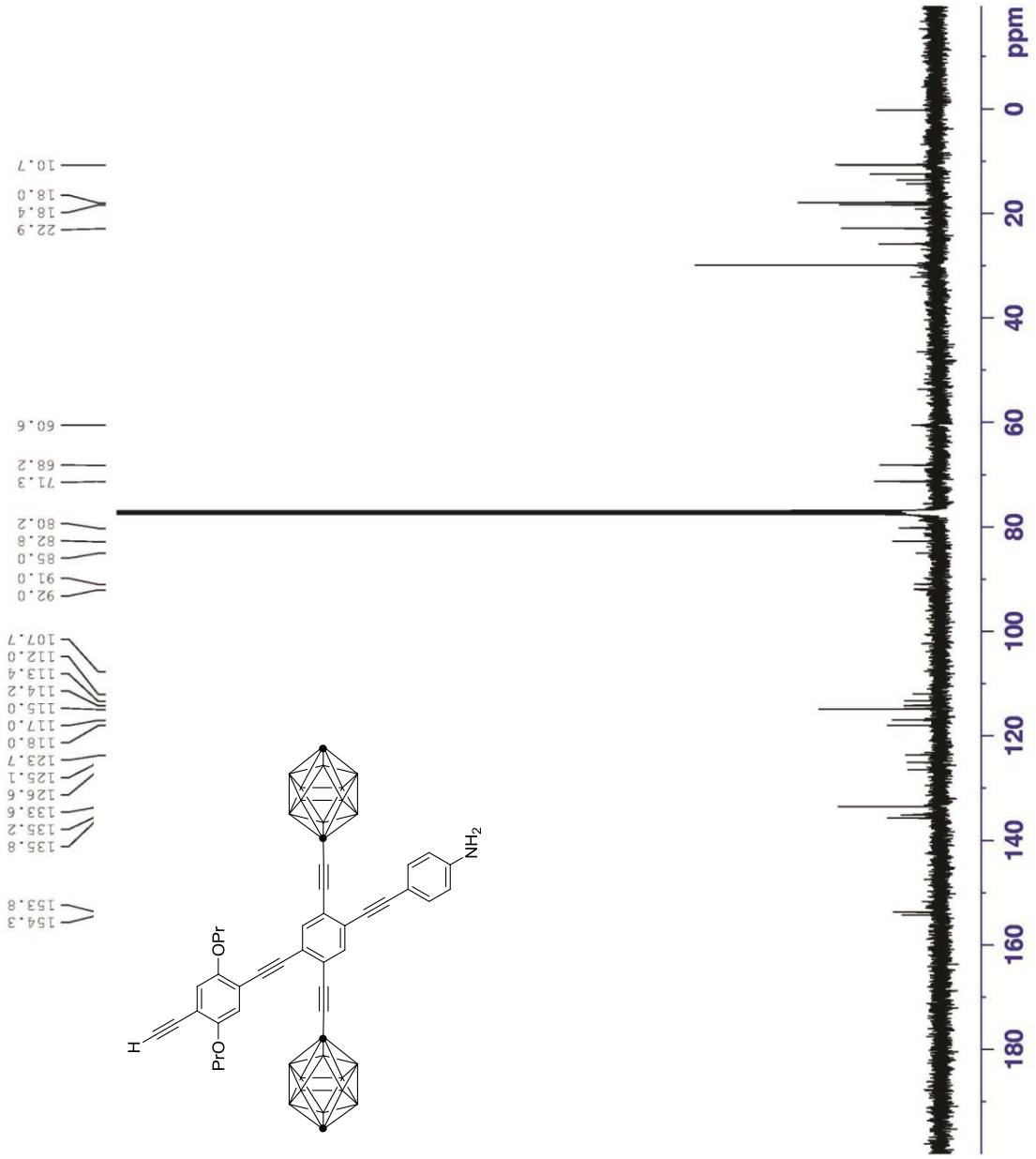

Figure S1.18. ^{1}H NMR spectrum of **21** (500 MHz, $CDCl_3$).

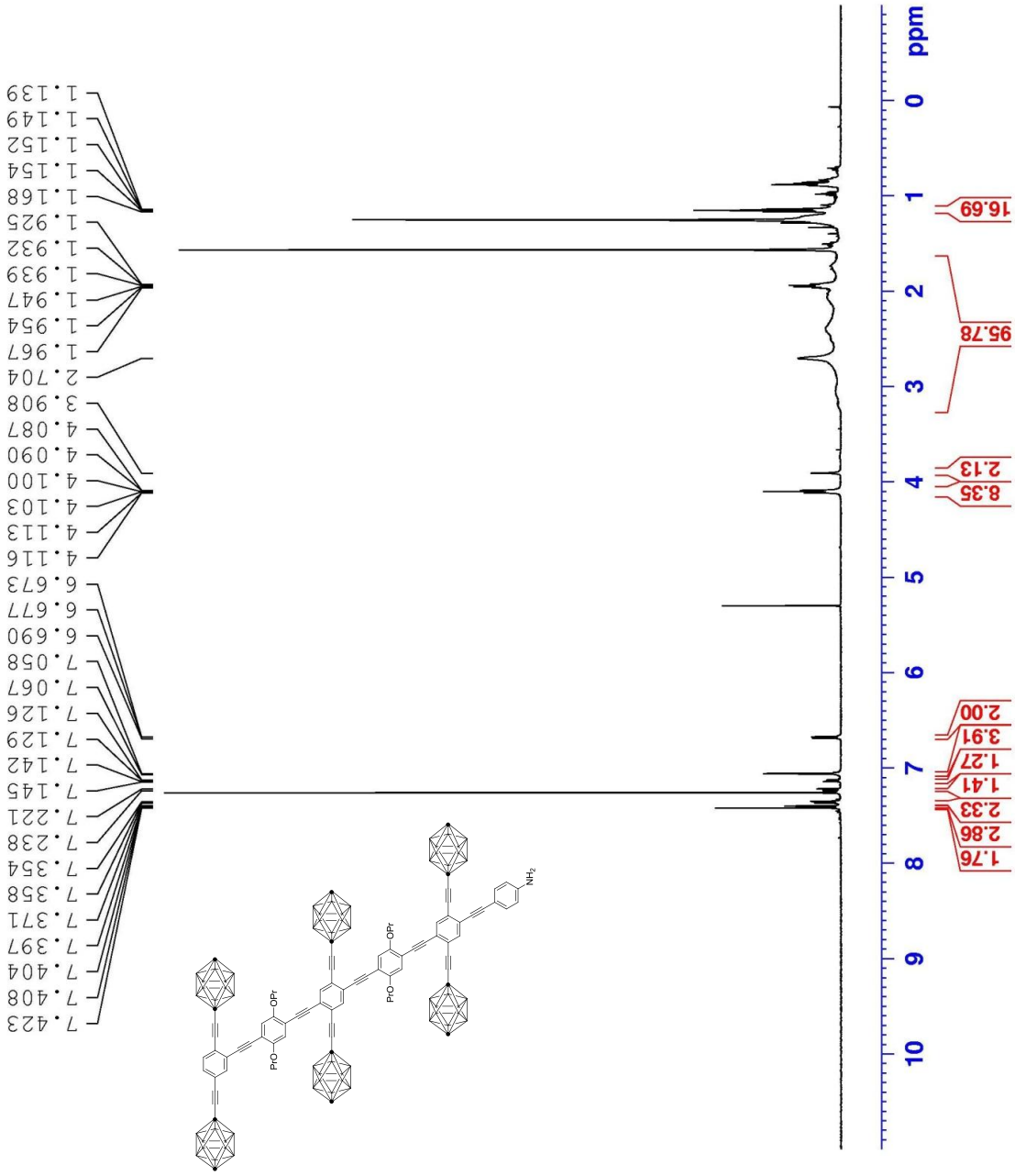

Figure S1.19. ^{13}C NMR spectrum of **21** (125 MHz, $CDCl_3$).

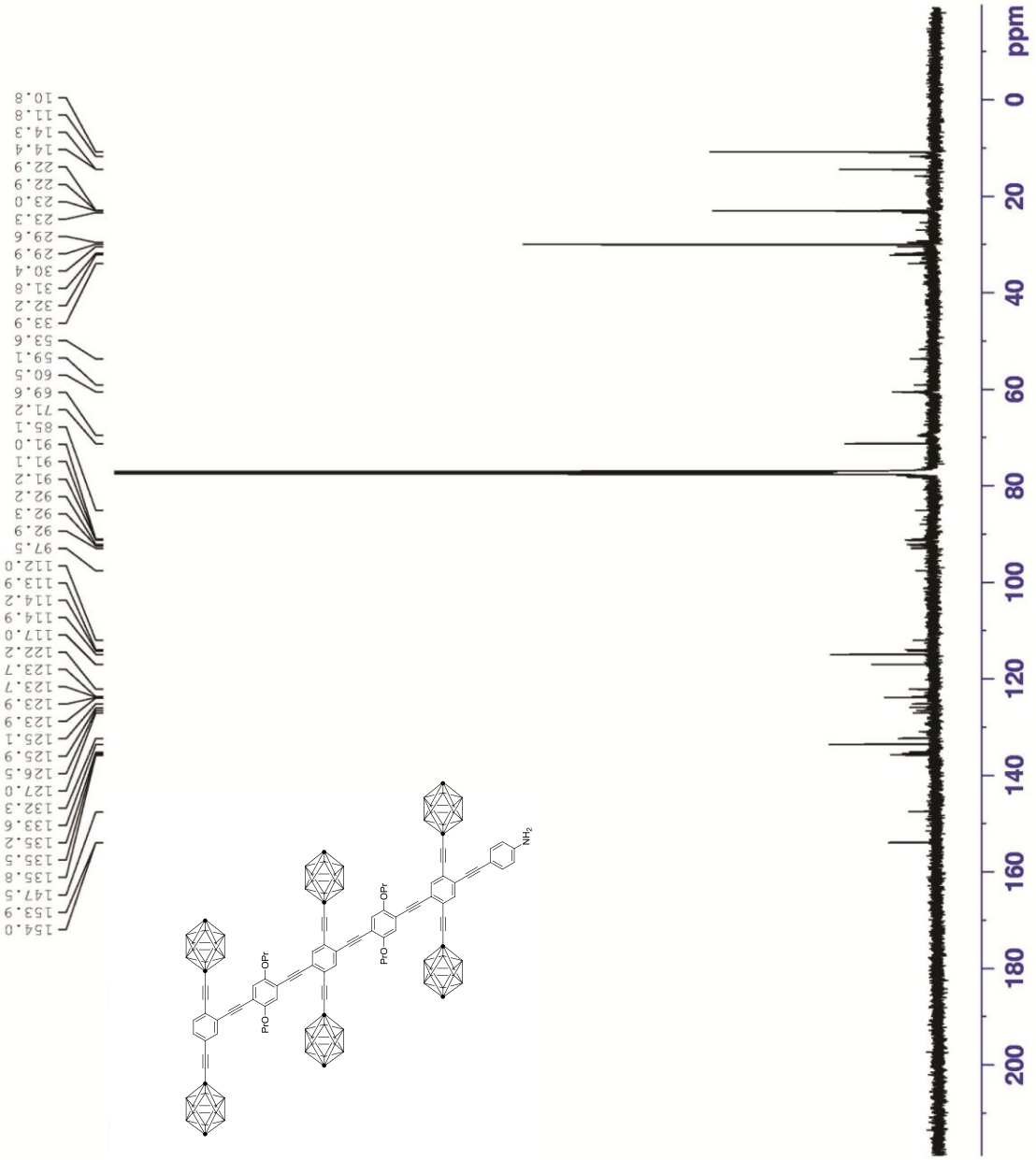

Figure S1.20. ^{1}H NMR spectrum of **2** (400 MHz, $CDCl_3$).

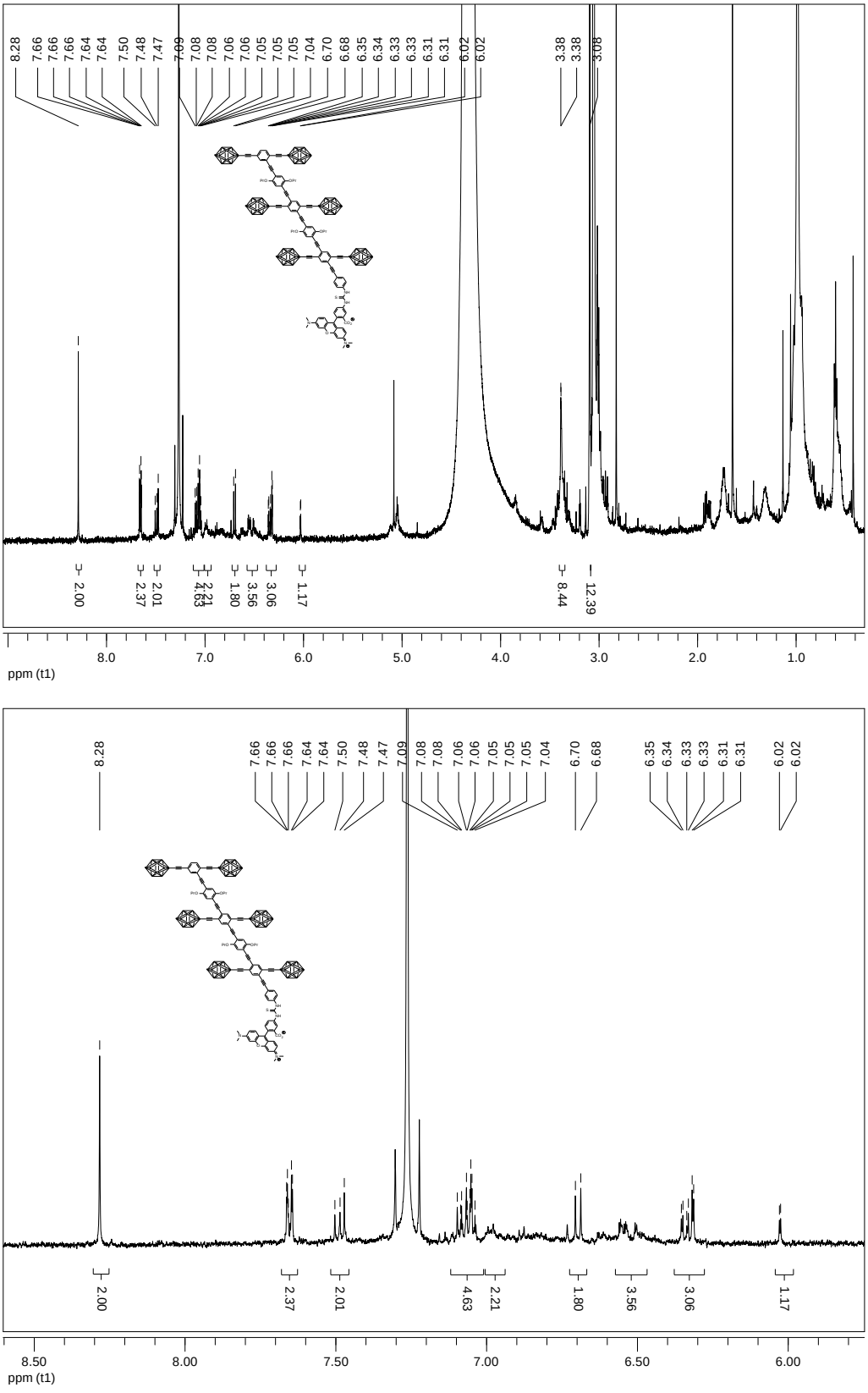

Figure S1.21. ^{1}H NMR spectrum of **23** (400 MHz, $CDCl_3$).

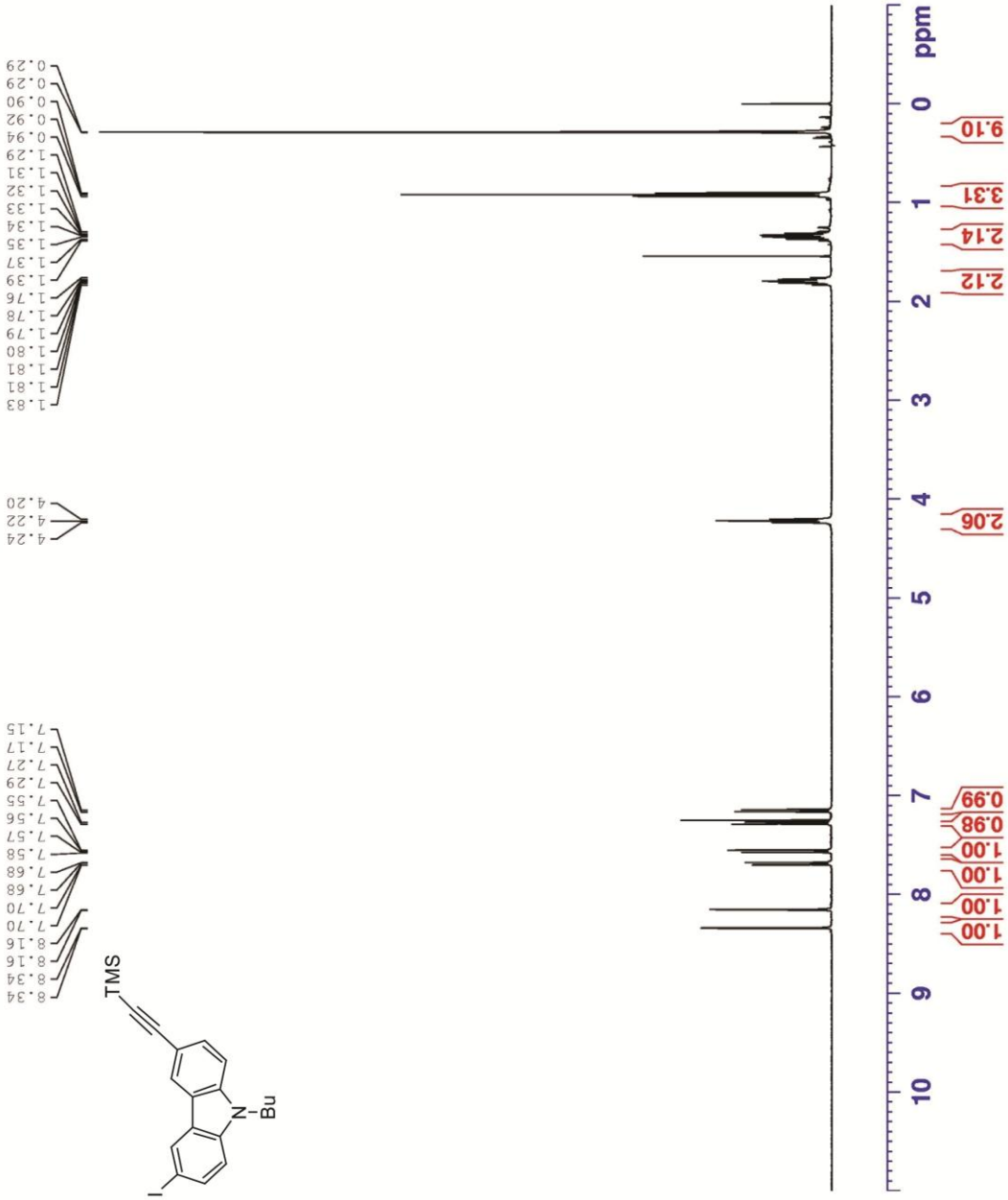

Figure S1.22. ^{13}C NMR spectrum of **23** (100 MHz, $CDCl_3$).

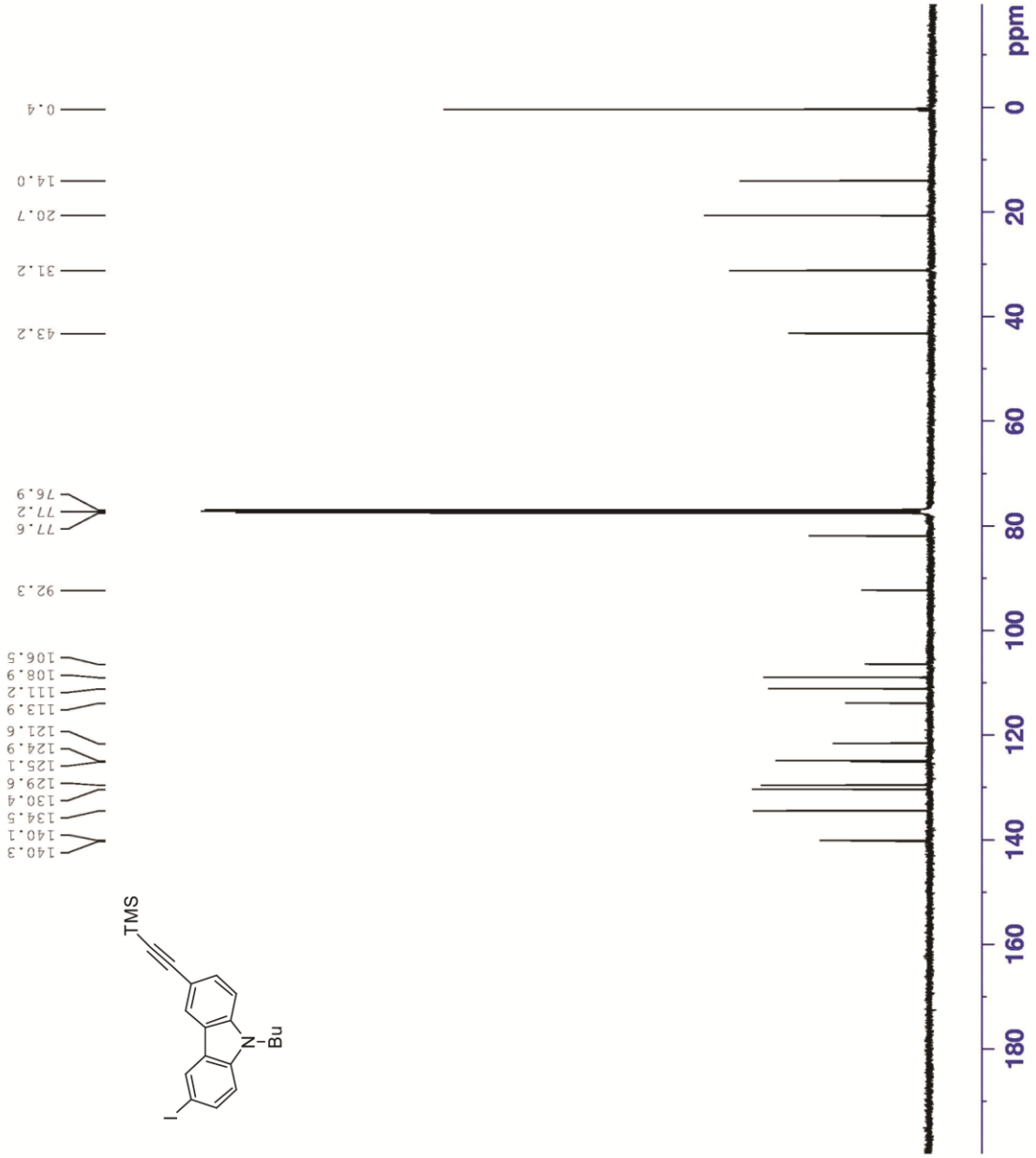

Figure S1.23. ^{1}H NMR spectrum of **24** (400 MHz, $CDCl_3$).

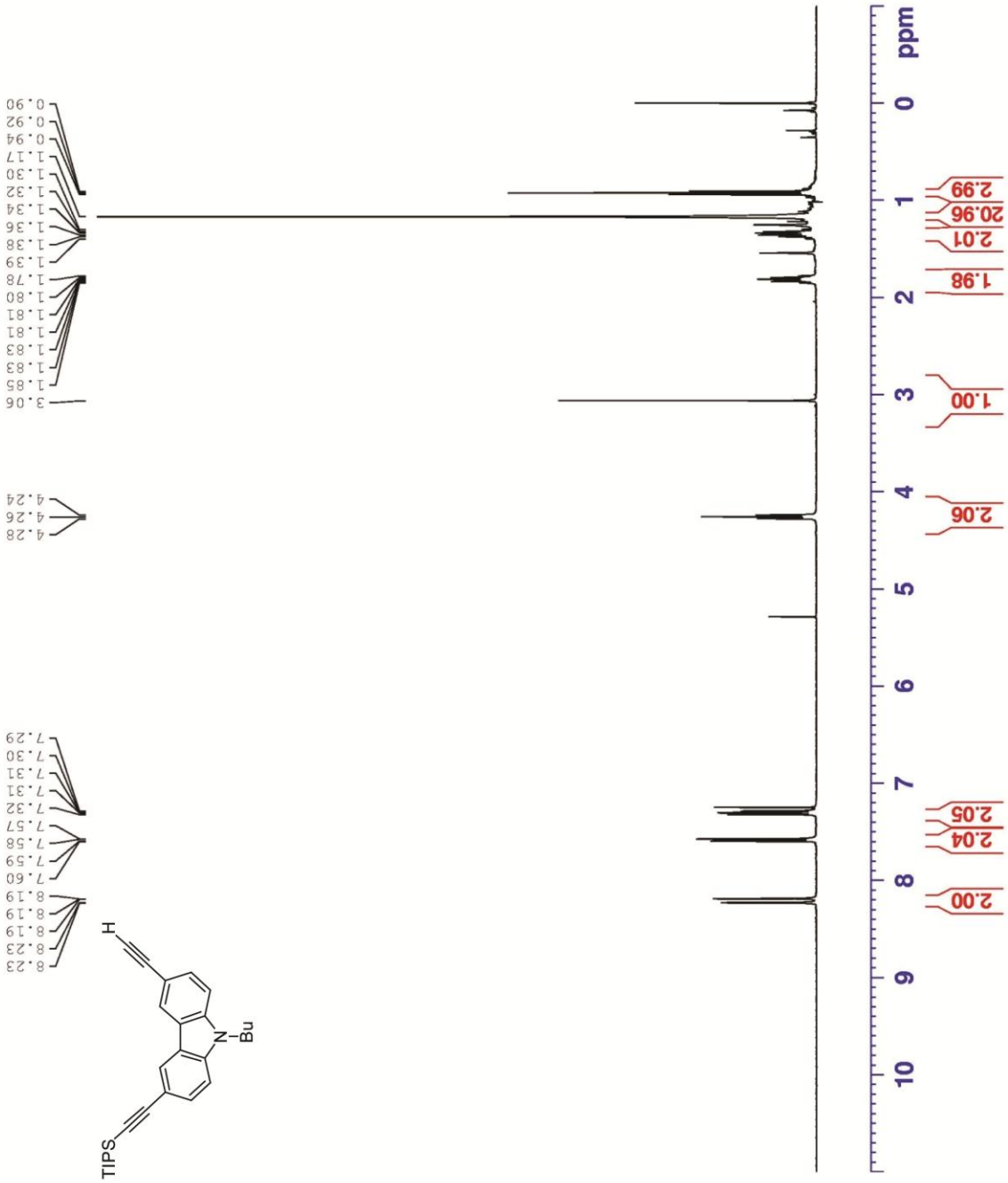

Figure S1.24. ^{13}C NMR spectrum of **24** (100 MHz, $CDCl_3$).

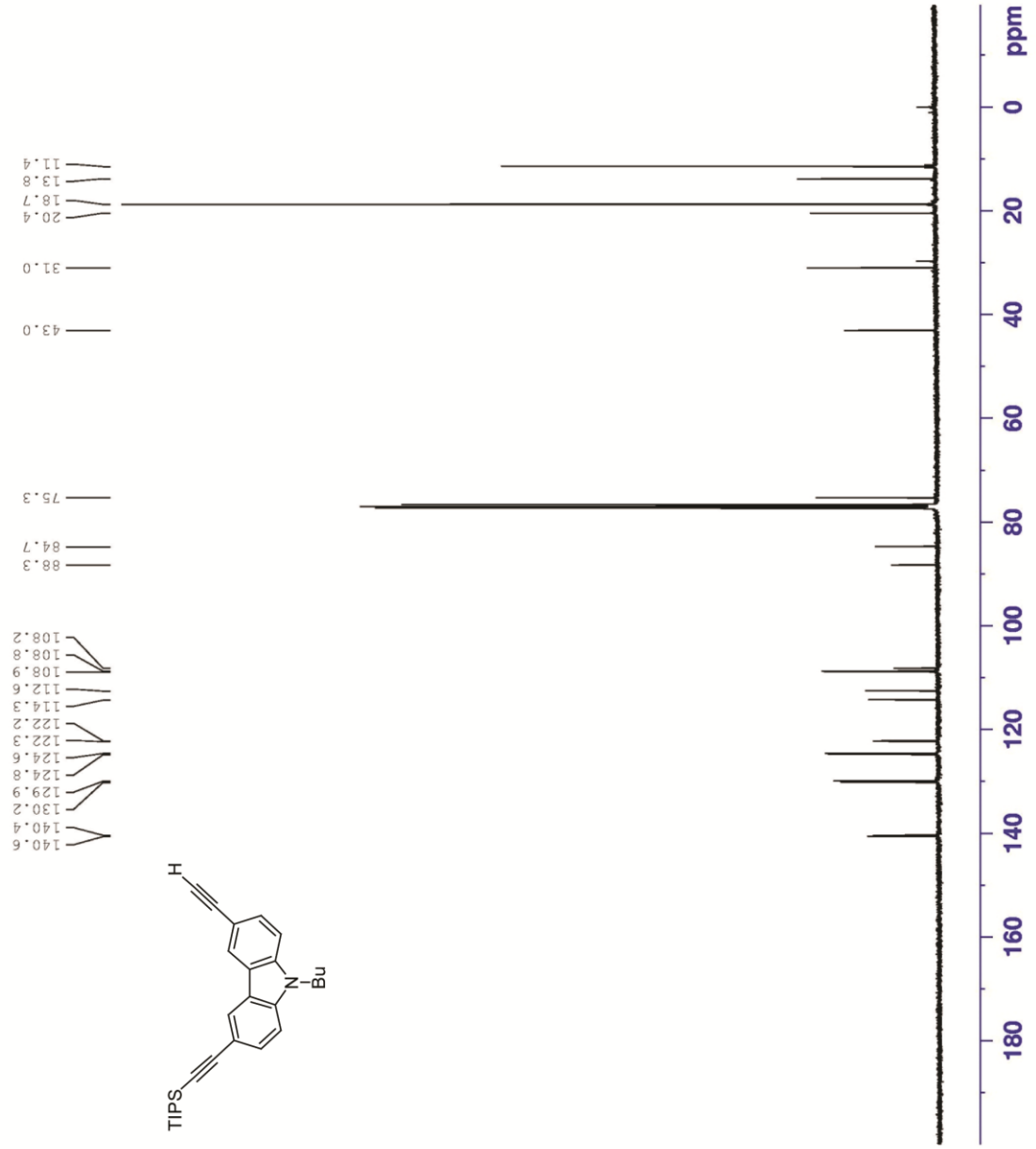

Figure S1.25. ^{1}H NMR spectrum of **25** (400 MHz, $CDCl_3$).

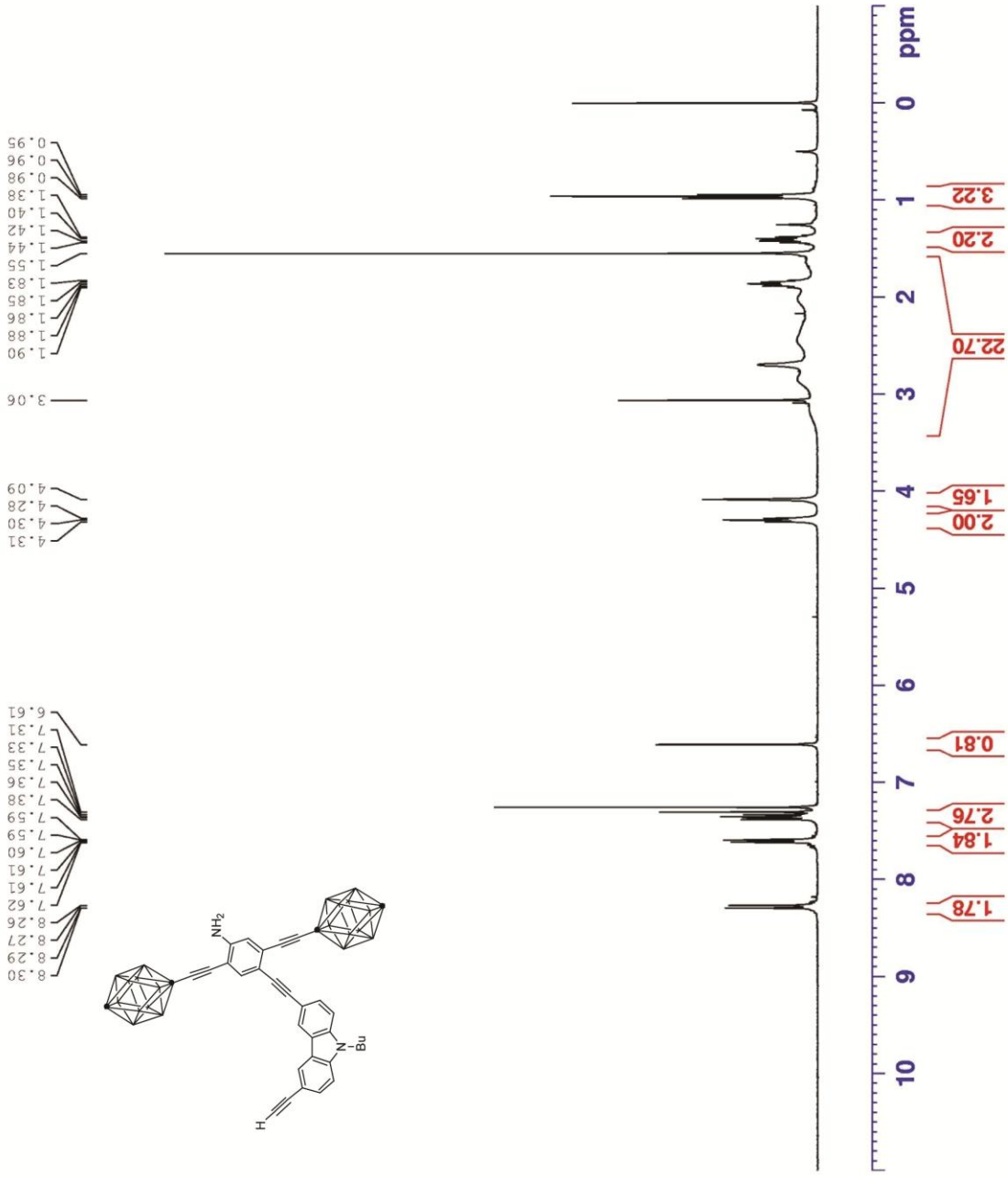

Figure S1.26. ^{13}C NMR spectrum of **25** (100 MHz, $CDCl_3$).

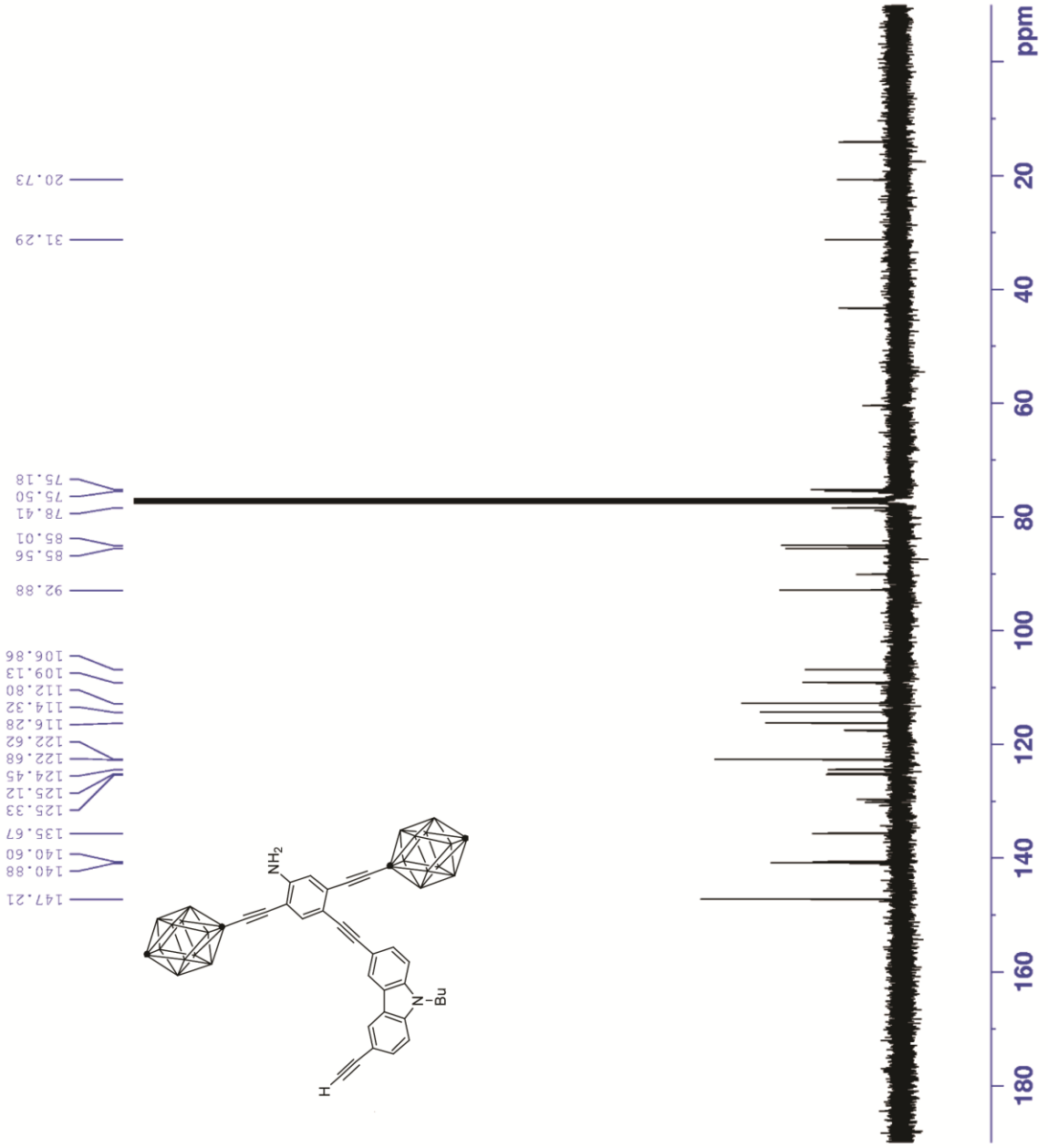

Figure S1.27. ^{1}H NMR spectrum of **26** (400 MHz, $CDCl_3$).

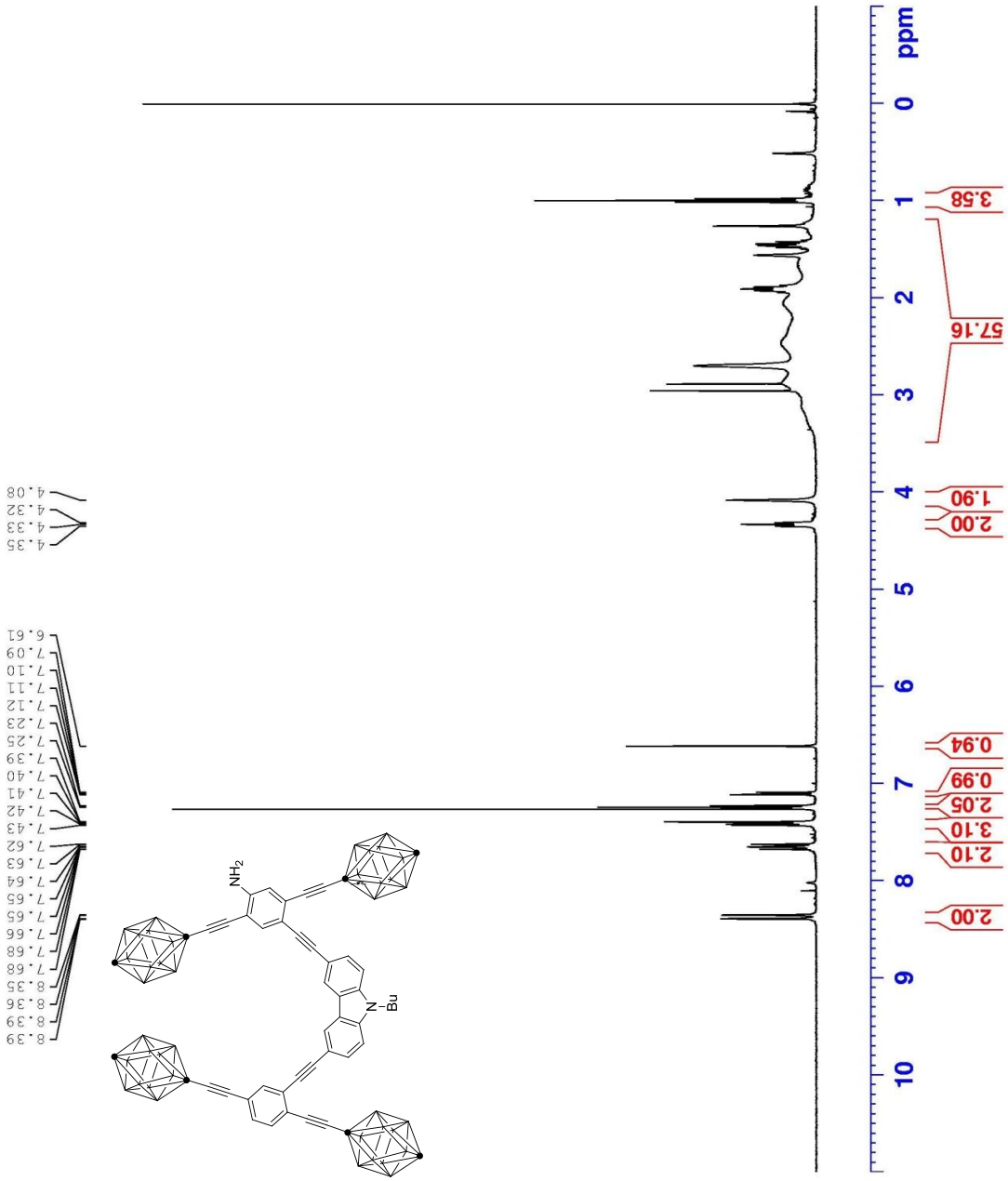

Figure S1.28. ^{13}C NMR spectrum of **26** (100 MHz, $CDCl_3$).

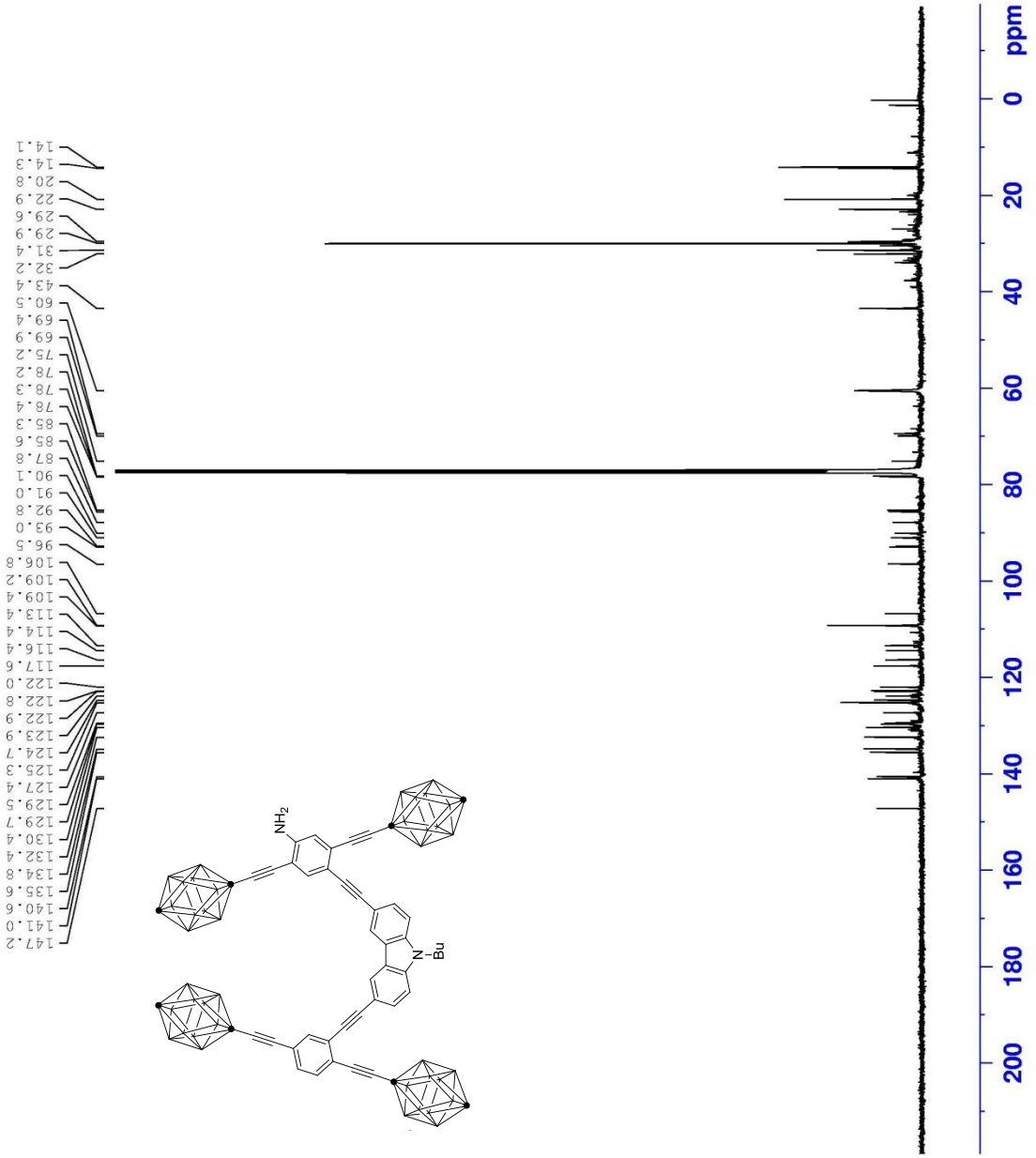

Figure S1.29. ^{1}H NMR spectrum of **3** (500 MHz, $CDCl_3$).

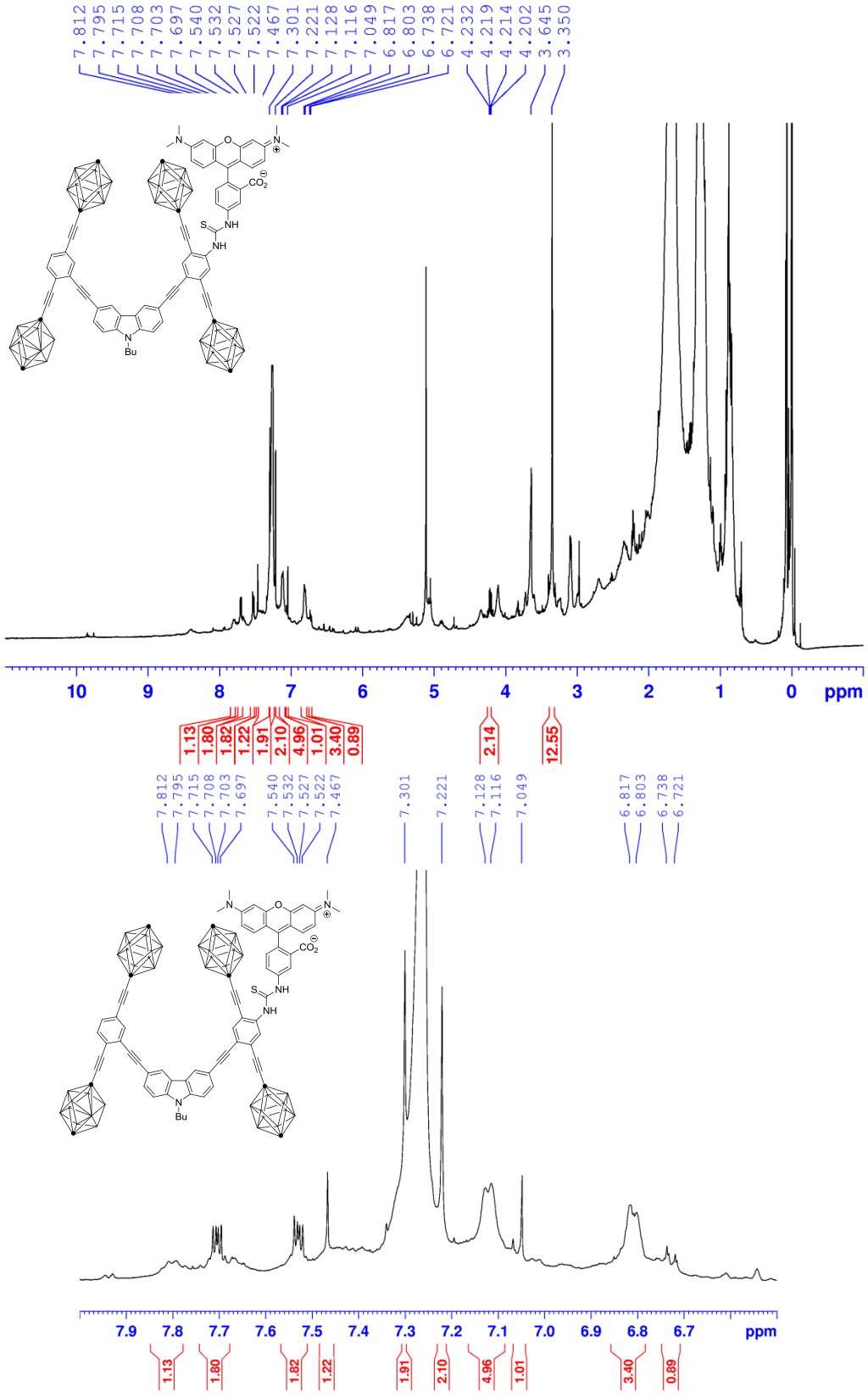

Figure S1.30. ^{1}H NMR spectrum of **29** (400 MHz, $CDCl_3$).

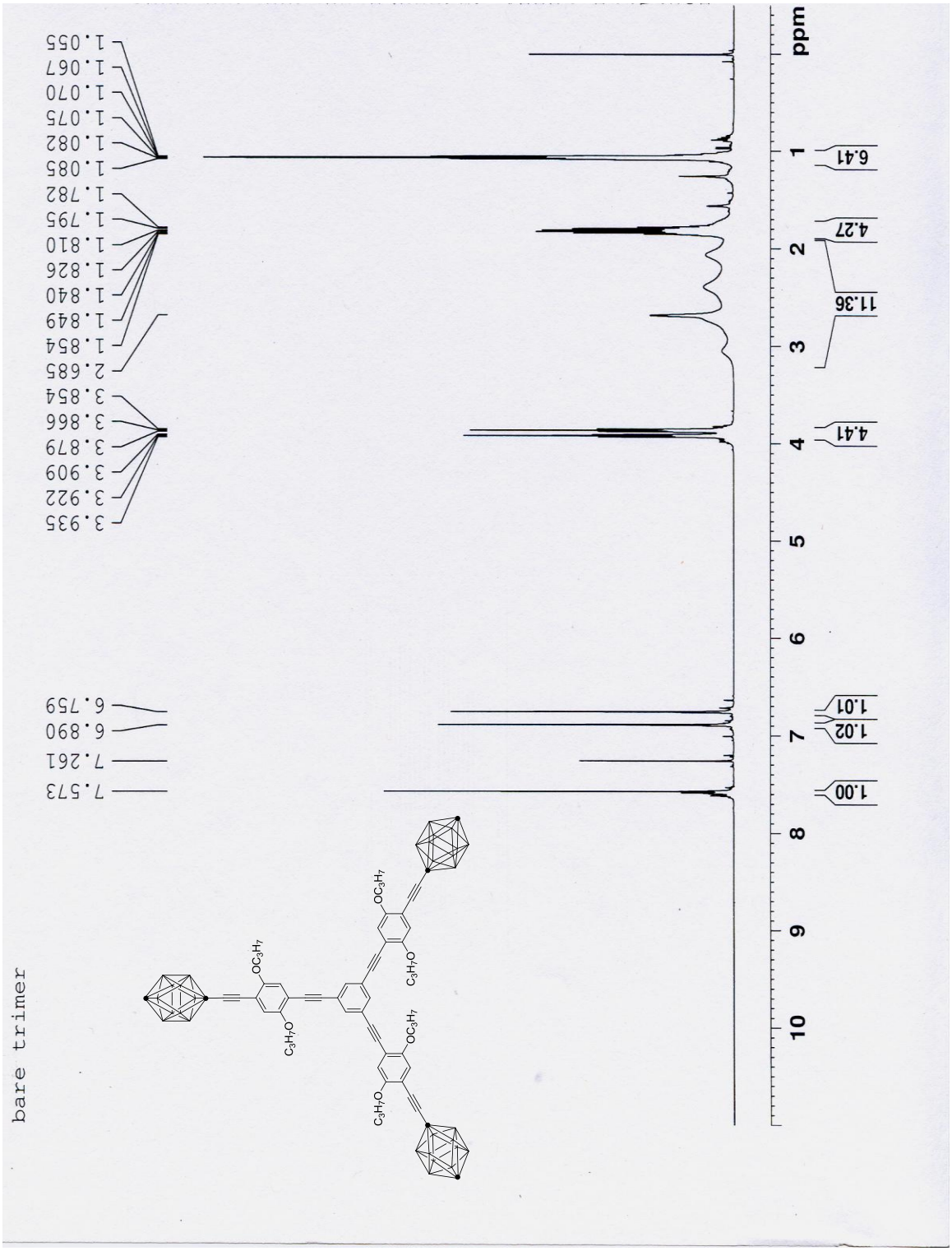

Figure S1.31. ^{13}C NMR spectrum of **29** (100 MHz, $CDCl_3$).

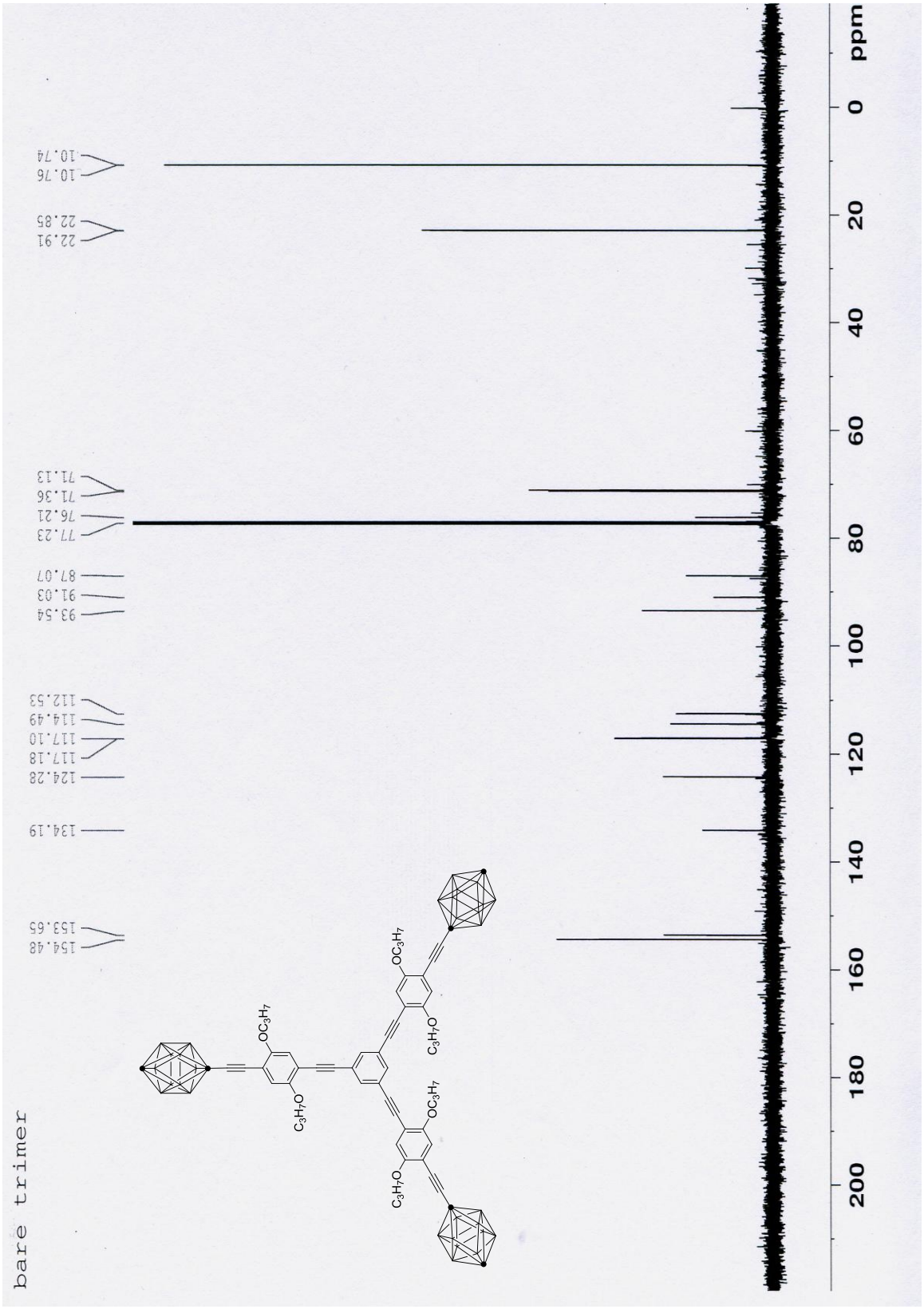

Figure S1.32. ^{1}H NMR spectrum of **30** (400 MHz, $CDCl_3$).

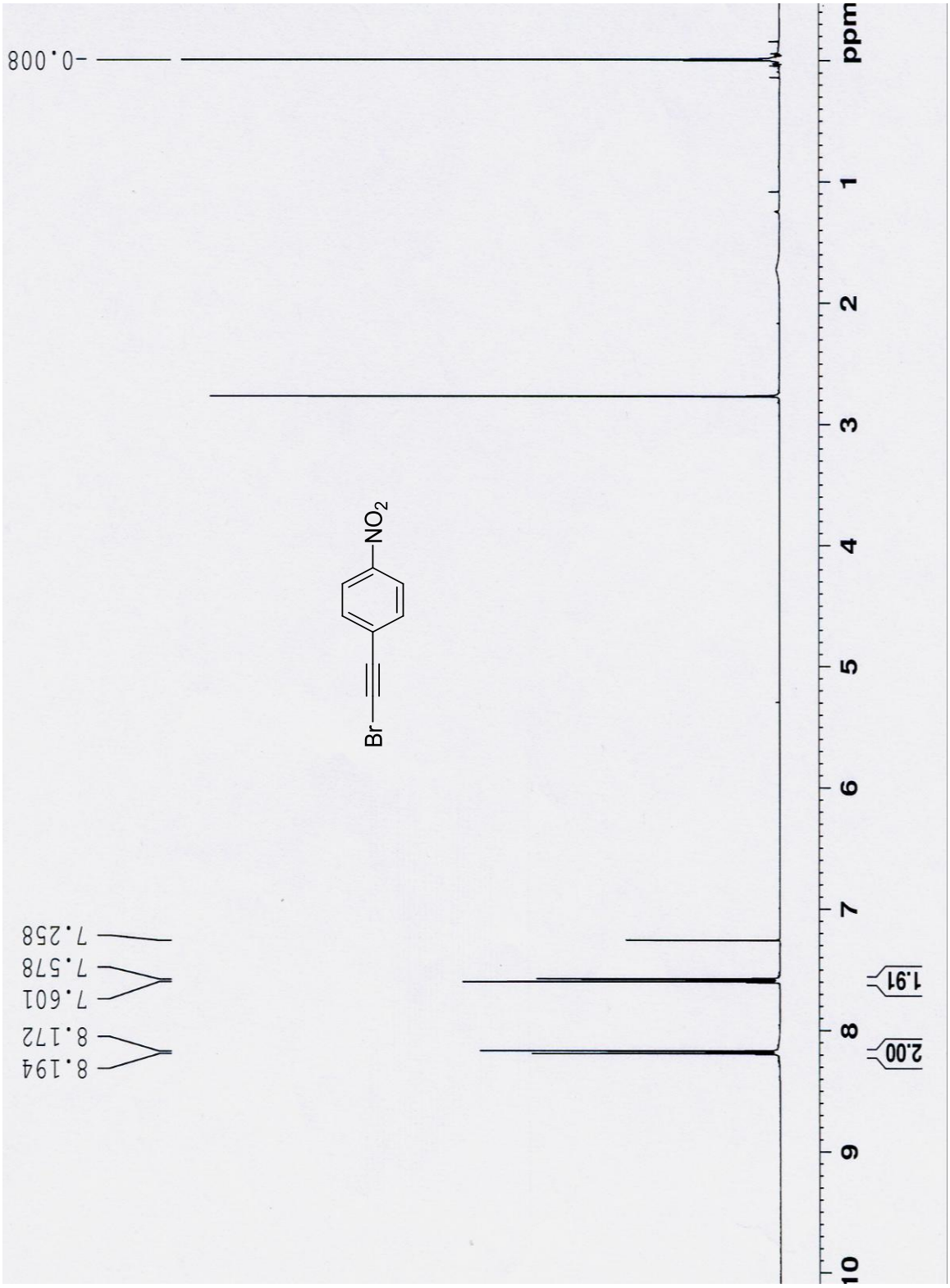

Figure S1.33. ^{13}C NMR spectrum of **30** (100 MHz, $CDCl_3$).

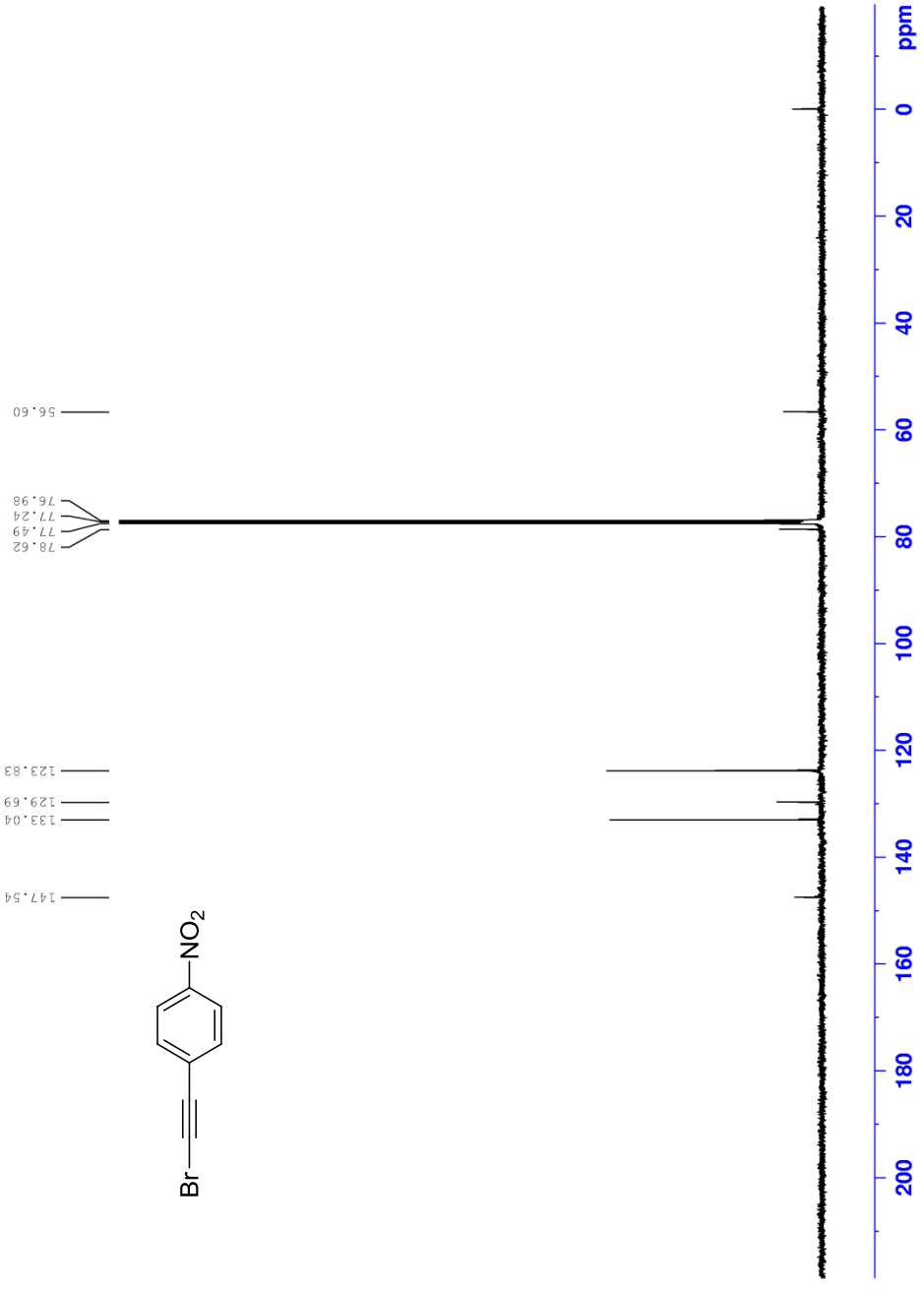

Figure S1.34. ^{1}H NMR spectrum of **31** (400 MHz, $CDCl_3$).

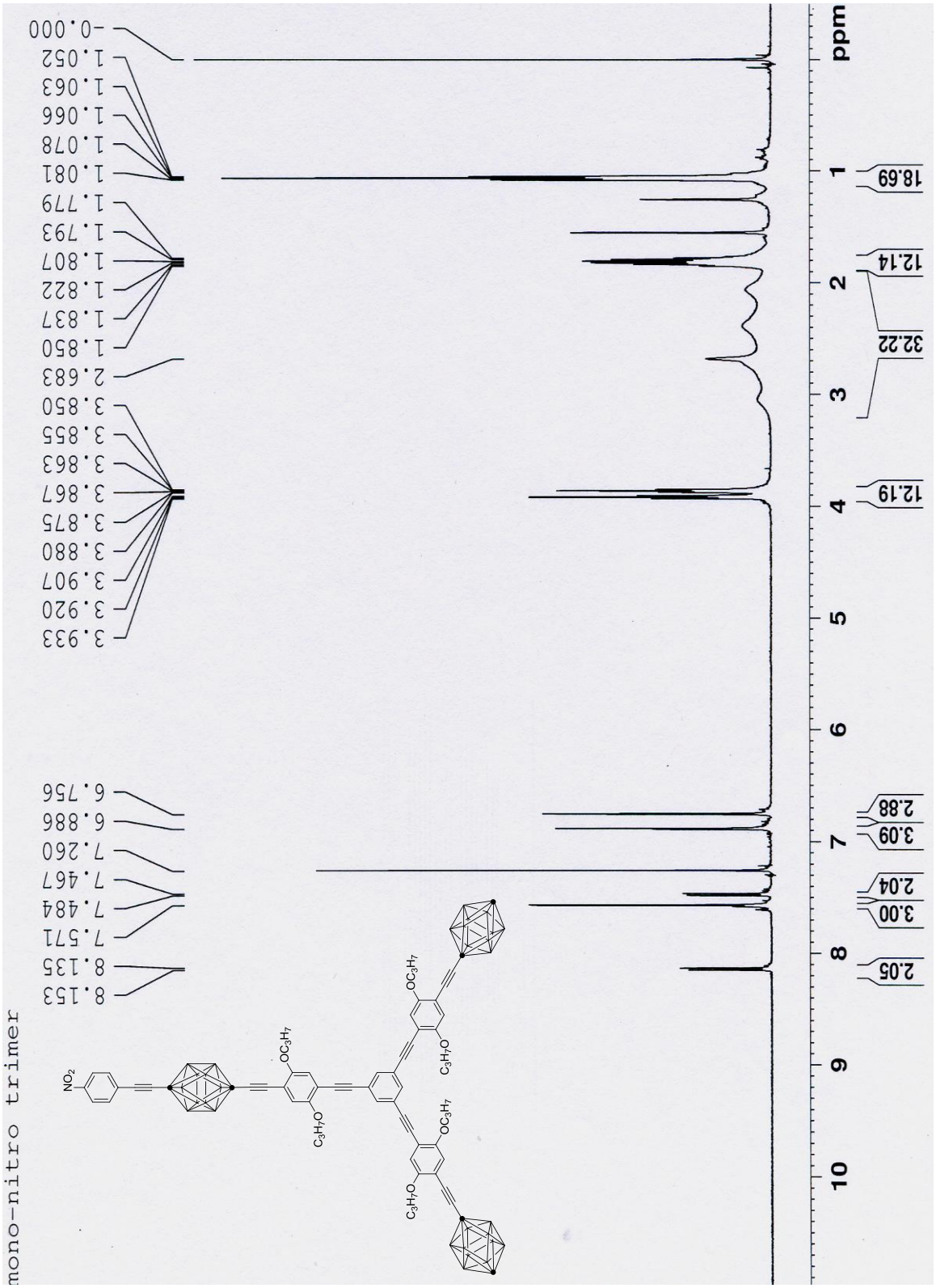

Figure S1.35. ^{13}C NMR spectrum of **31** (100 MHz, $CDCl_3$).

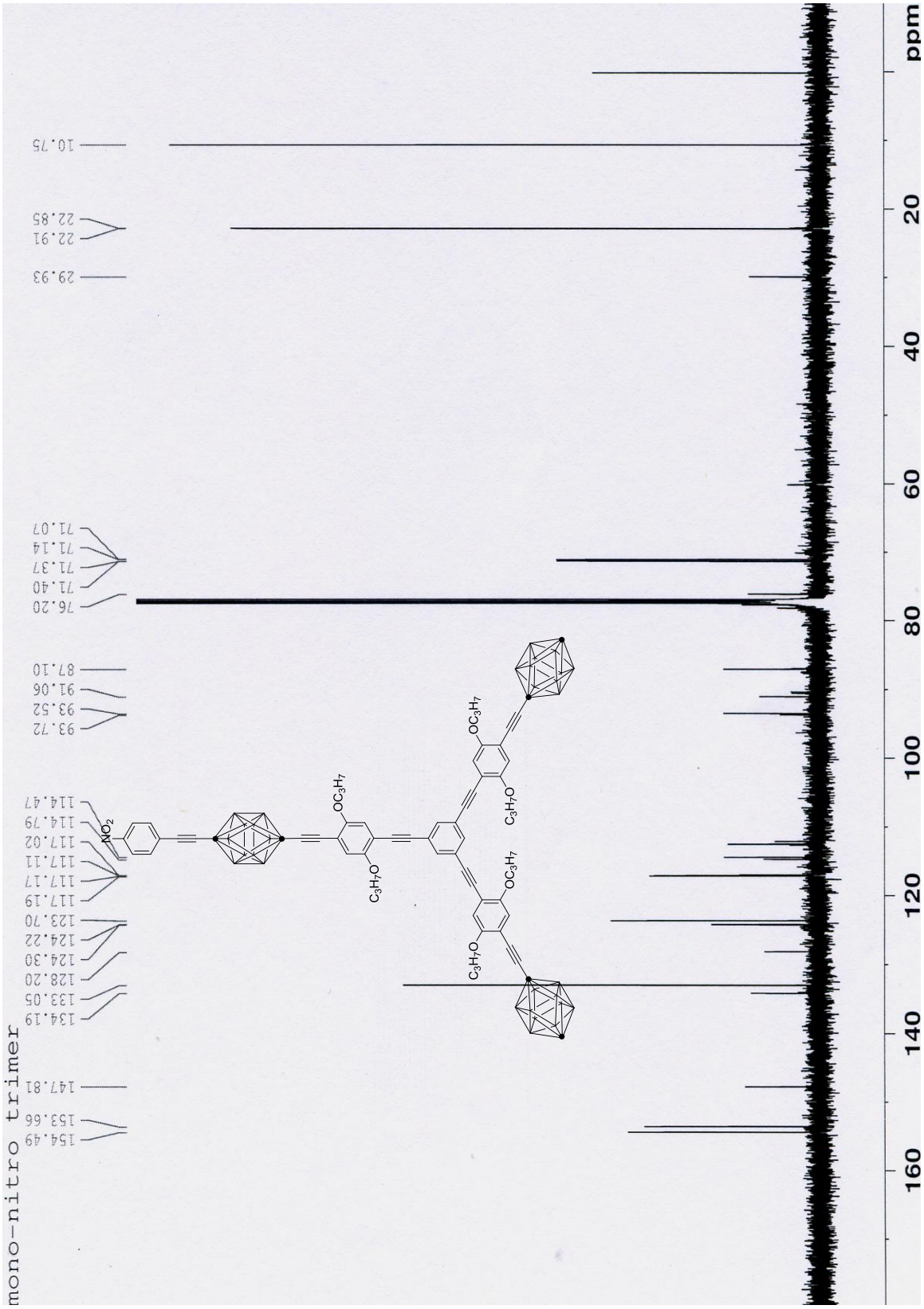

Figure S1.36. ^{1}H NMR spectrum of **32** (400 MHz, $CDCl_3$).

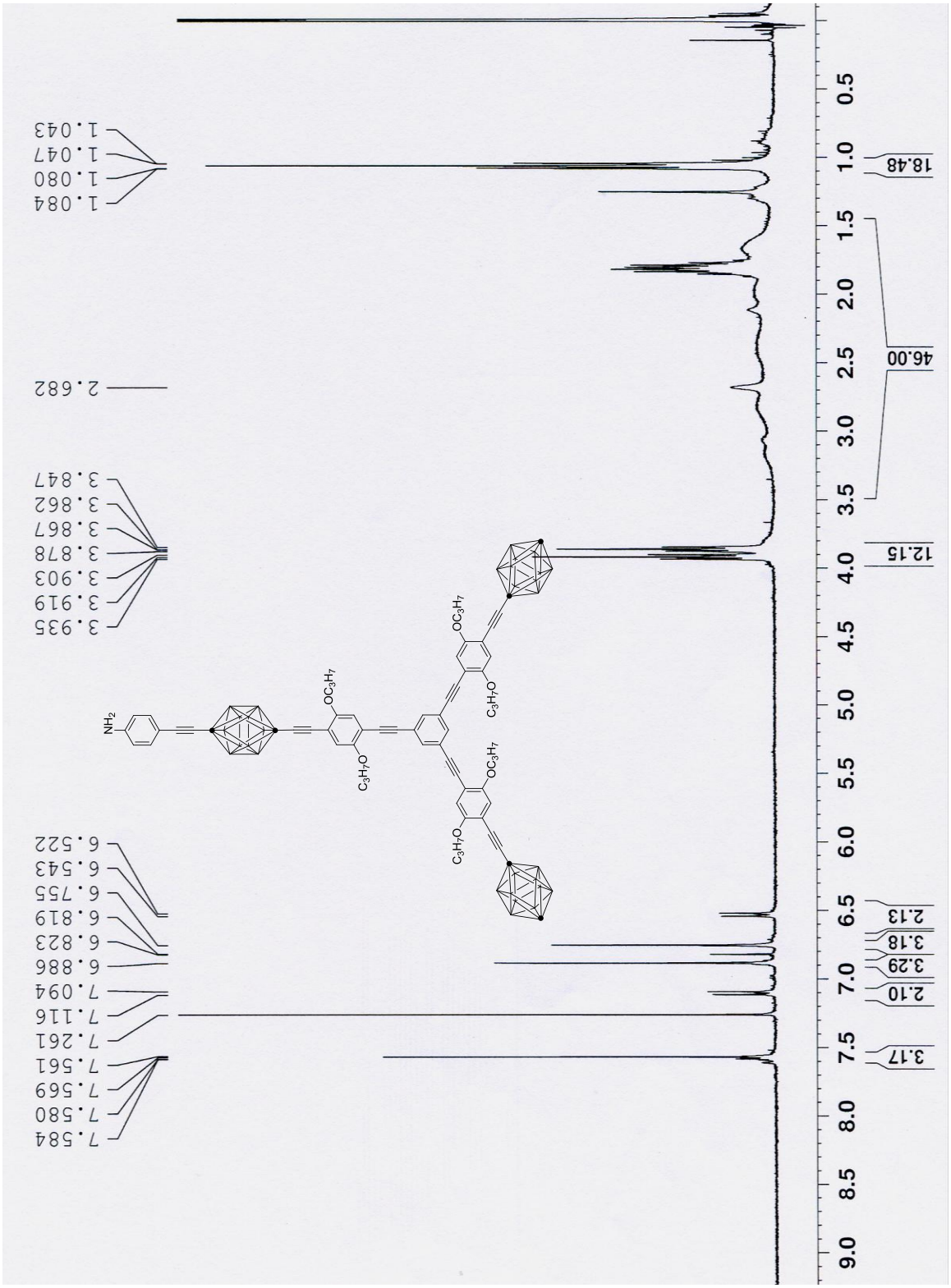

Figure S1.37. ^{13}C NMR spectrum of **32** (100 MHz, $CDCl_3$).

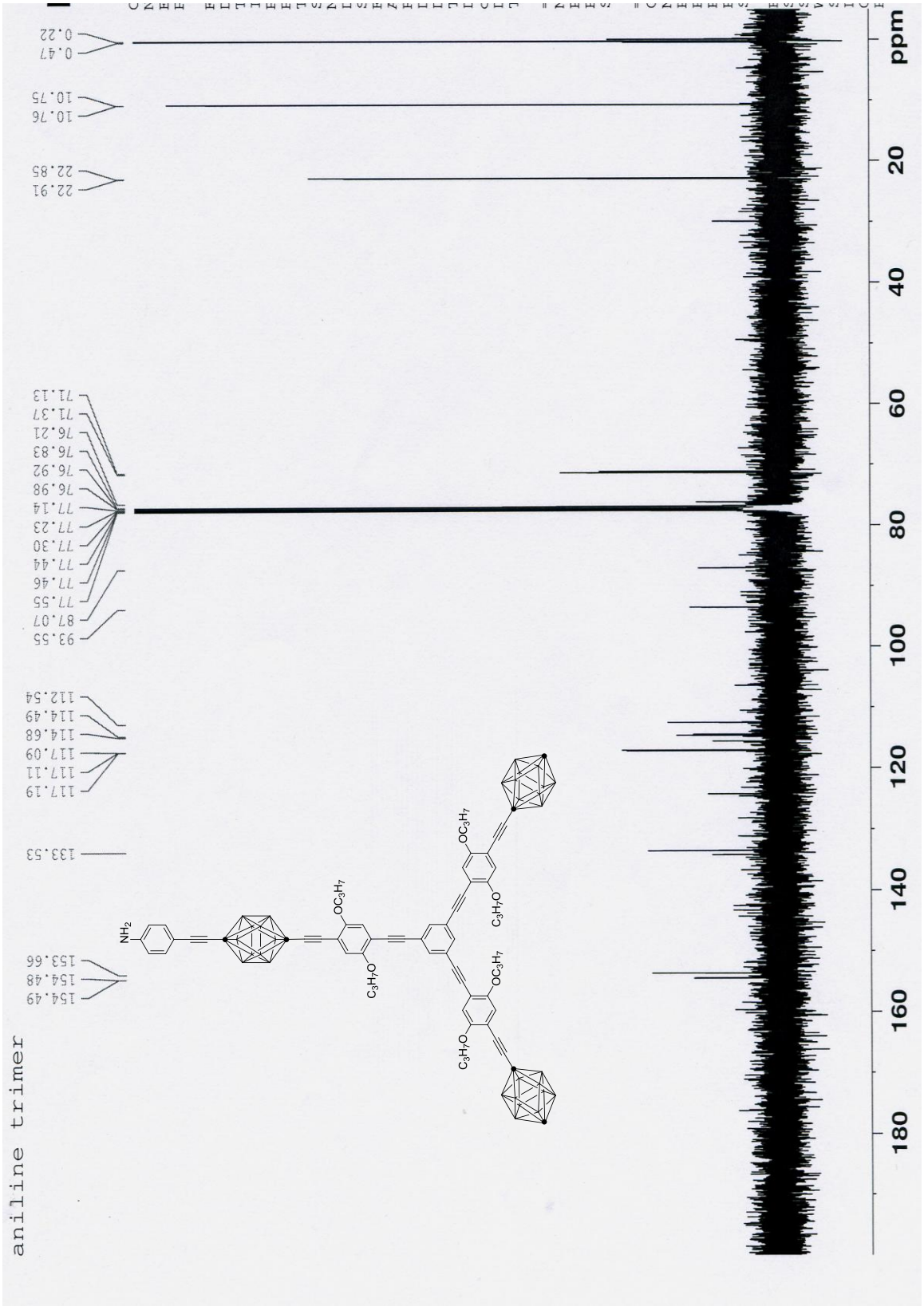

Figure S1.38. ^{1}H NMR spectrum of **4** (400 MHz, $CDCl_3$).

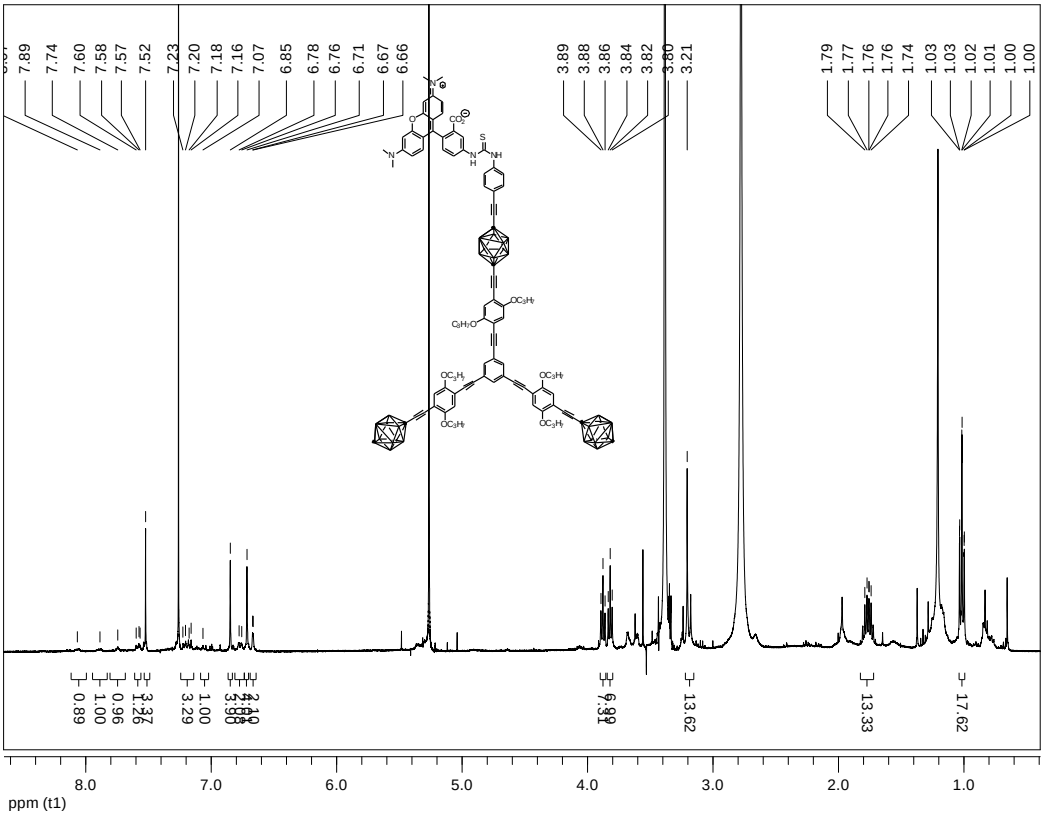

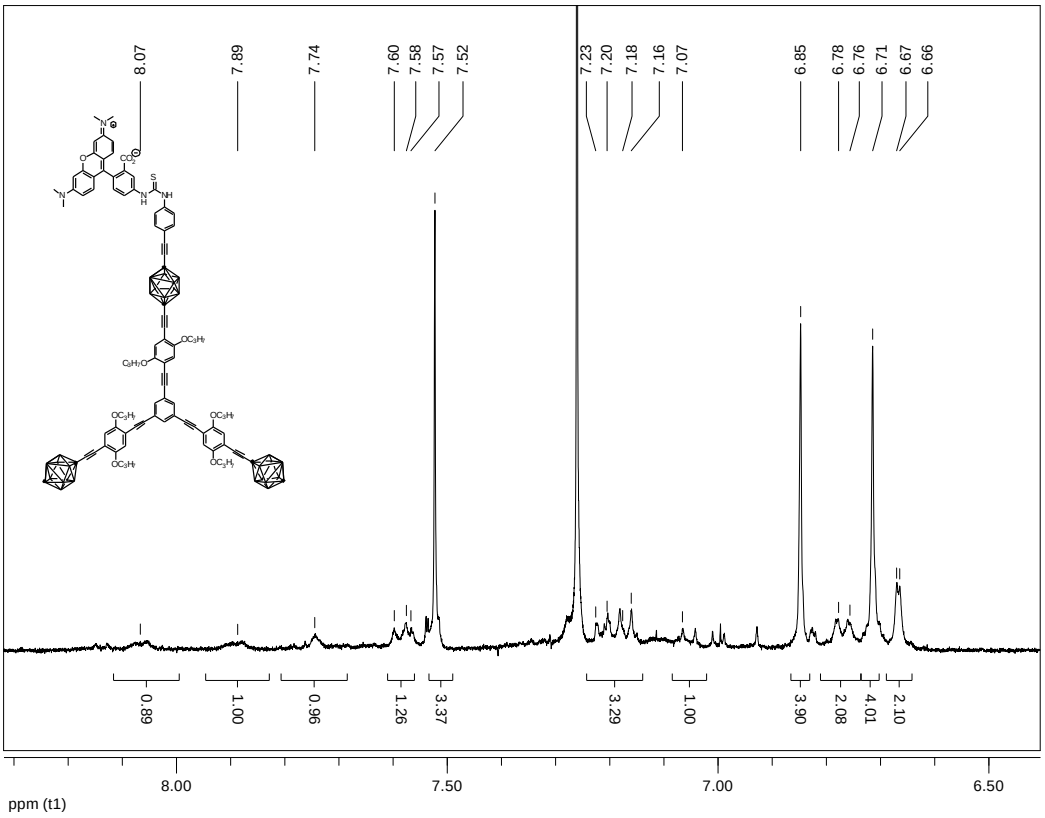

Figure S1.39. ^{1}H NMR spectrum of **34** (400 MHz, $CDCl_3$).

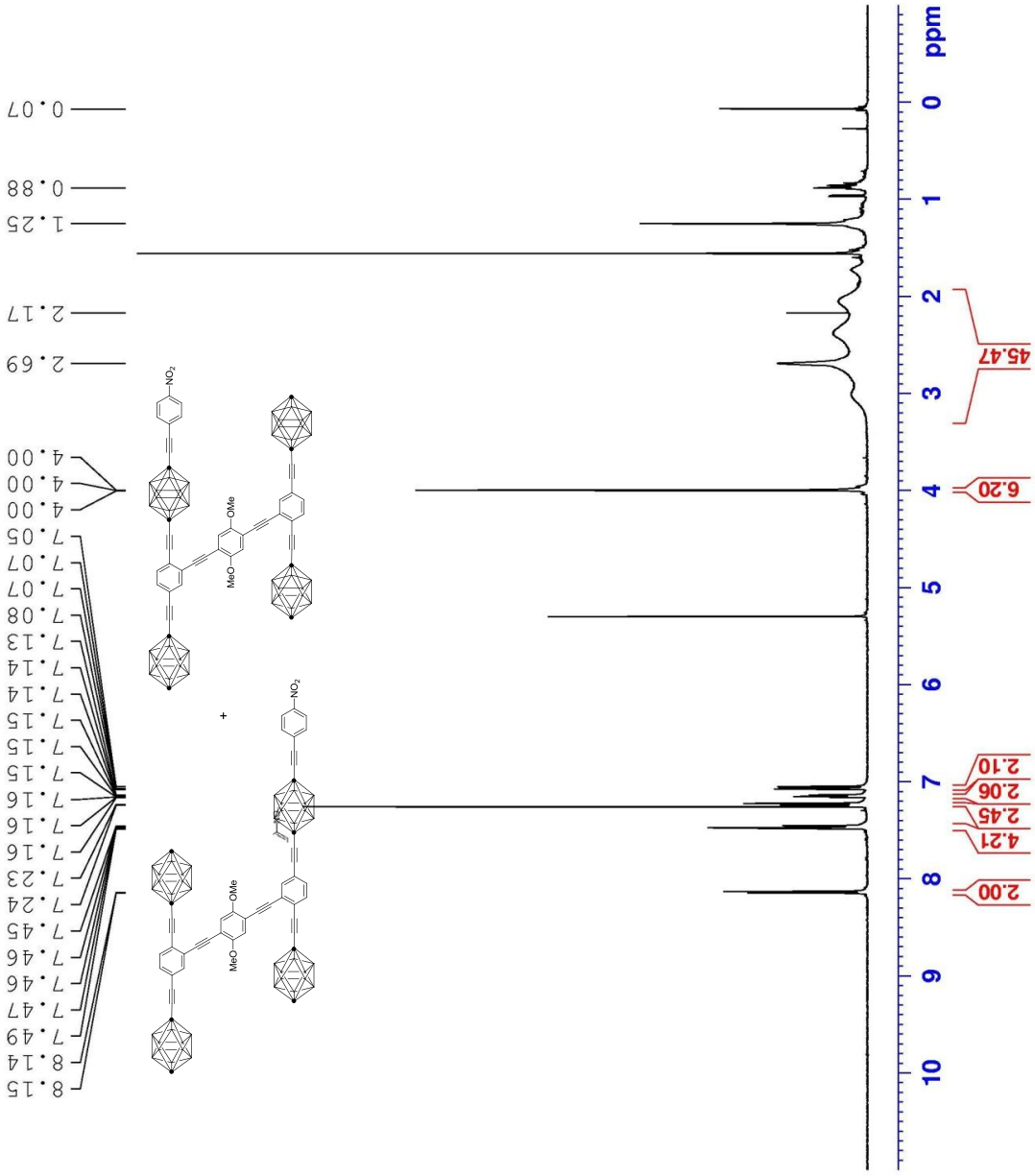

Figure S1.40. ^{13}C NMR spectrum of **34** (100 MHz, $CDCl_3$).

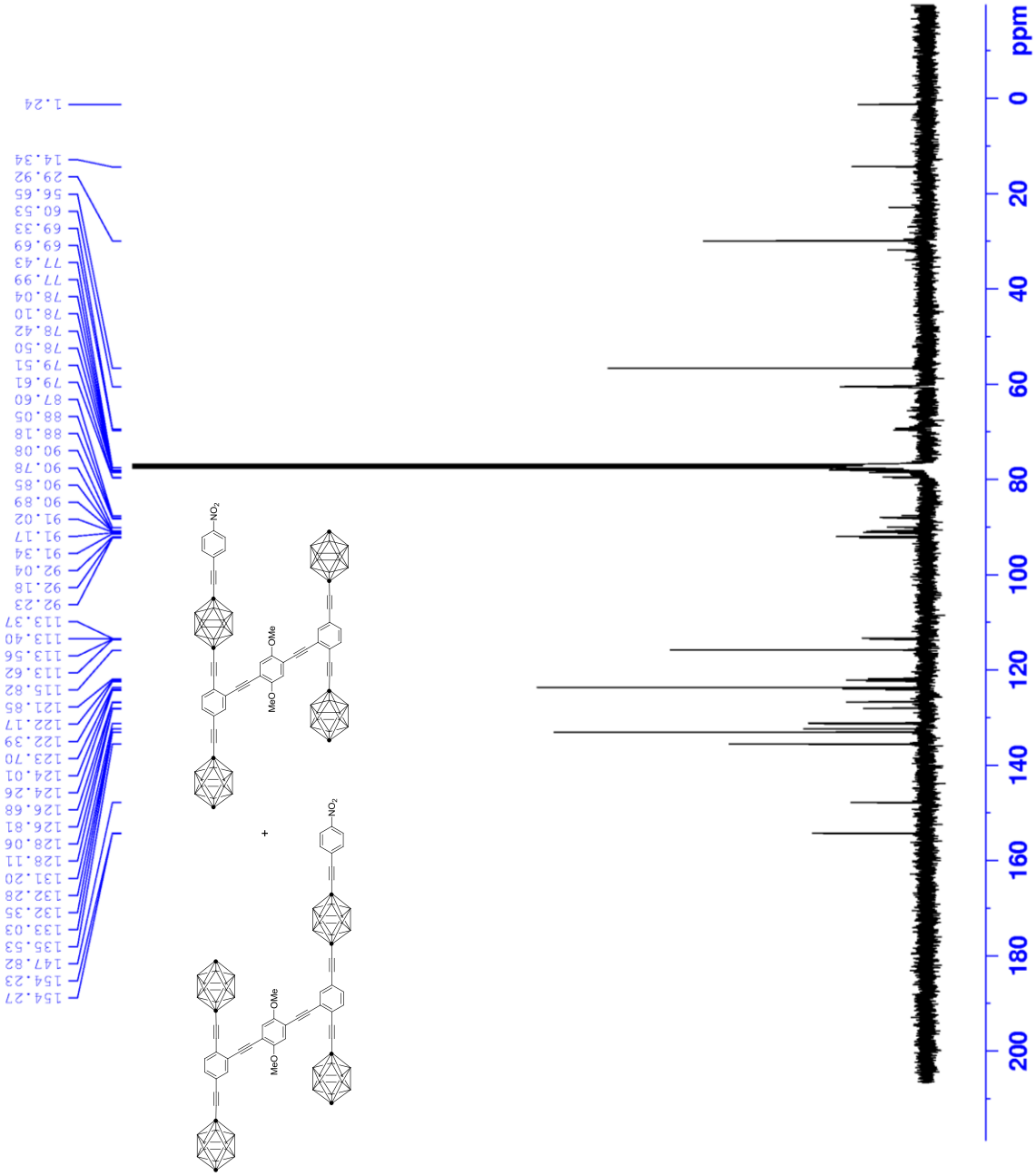

Figure S1.41. ^{1}H NMR spectrum of **35** (400 MHz, $CDCl_3$).

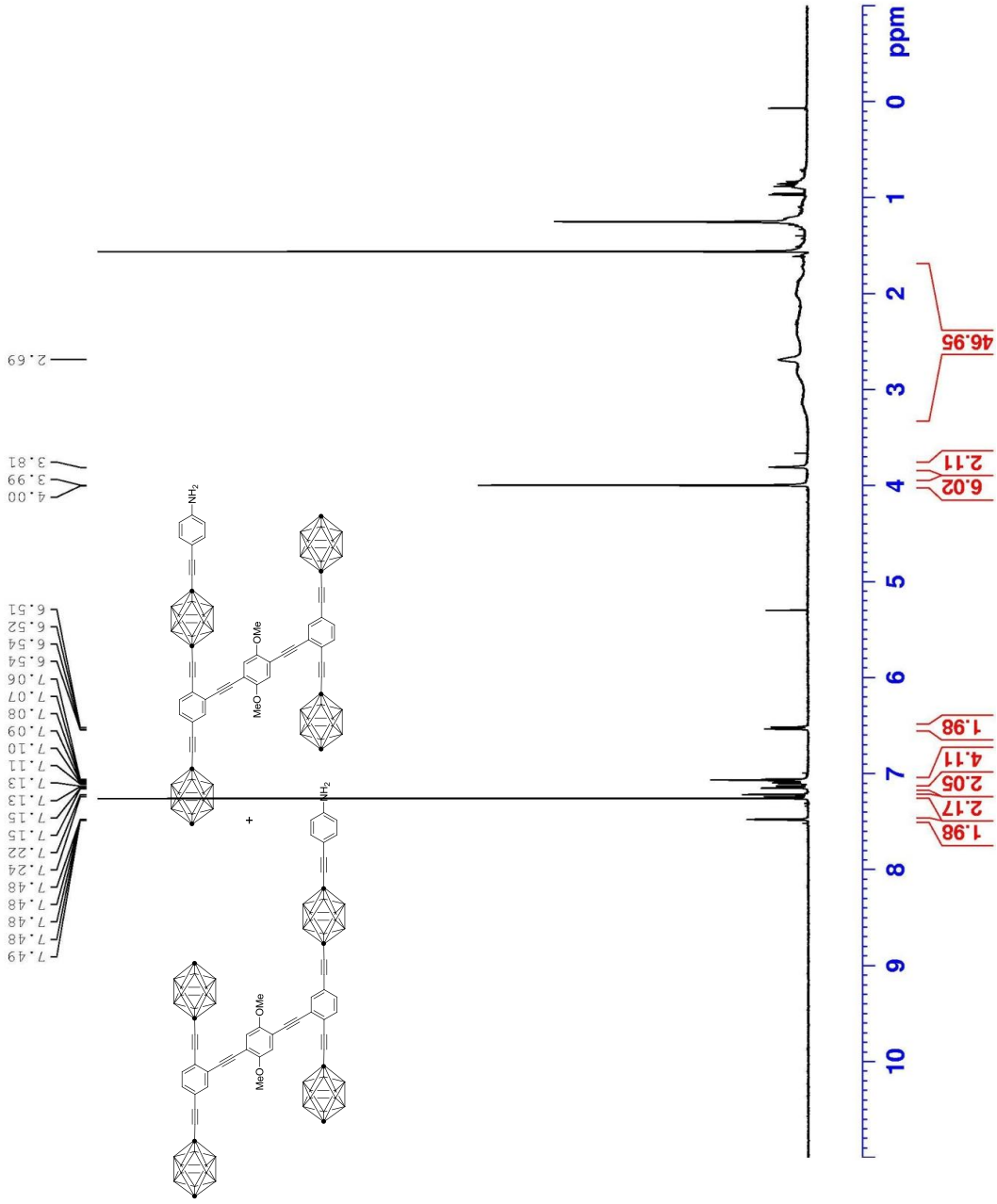

Figure S1.42. ^{13}C NMR spectrum of **35** (100 MHz, $CDCl_3$).

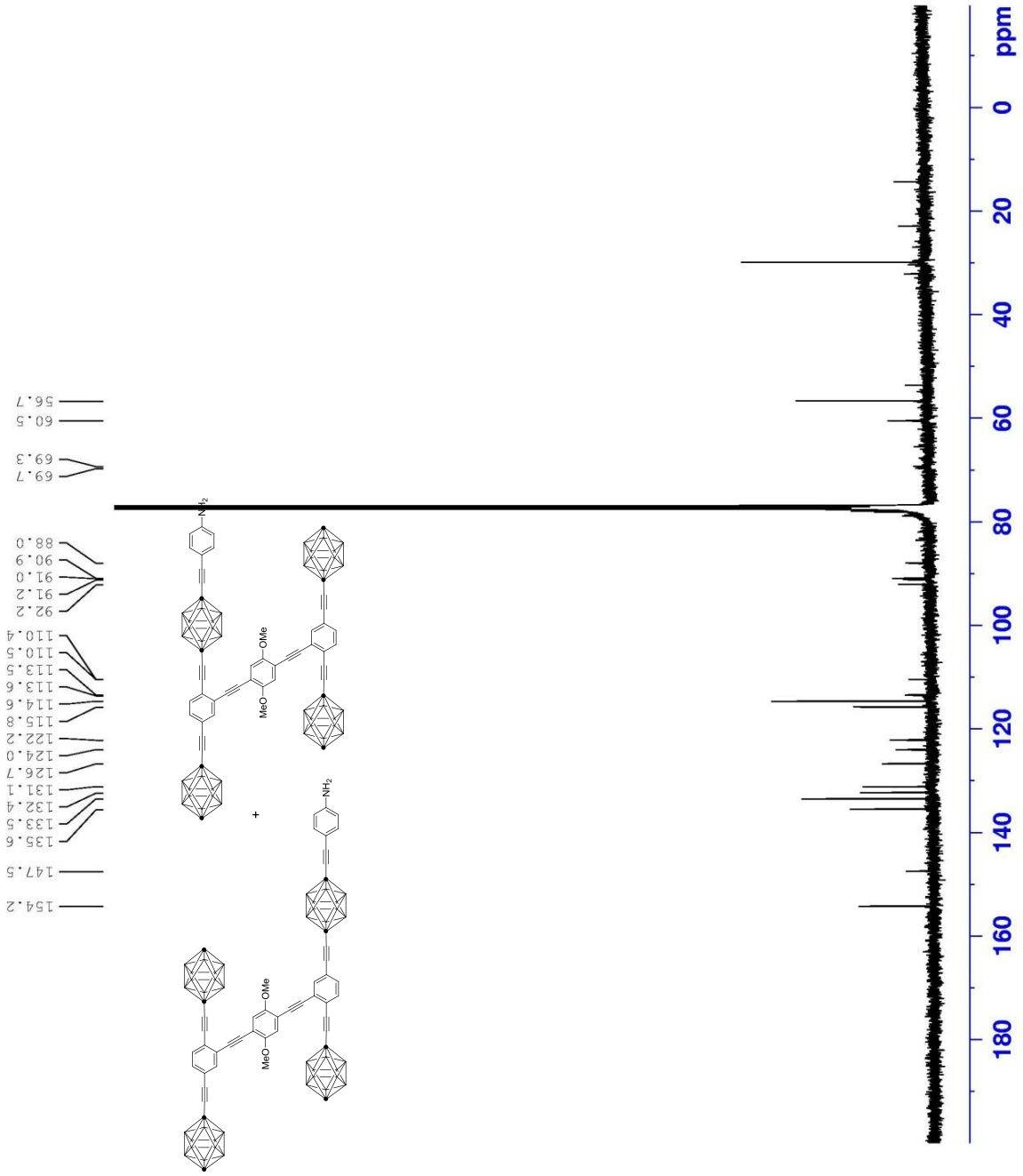

Figure S1.43. ^{1}H NMR spectrum of **5** (400 MHz, $CDCl_3$).

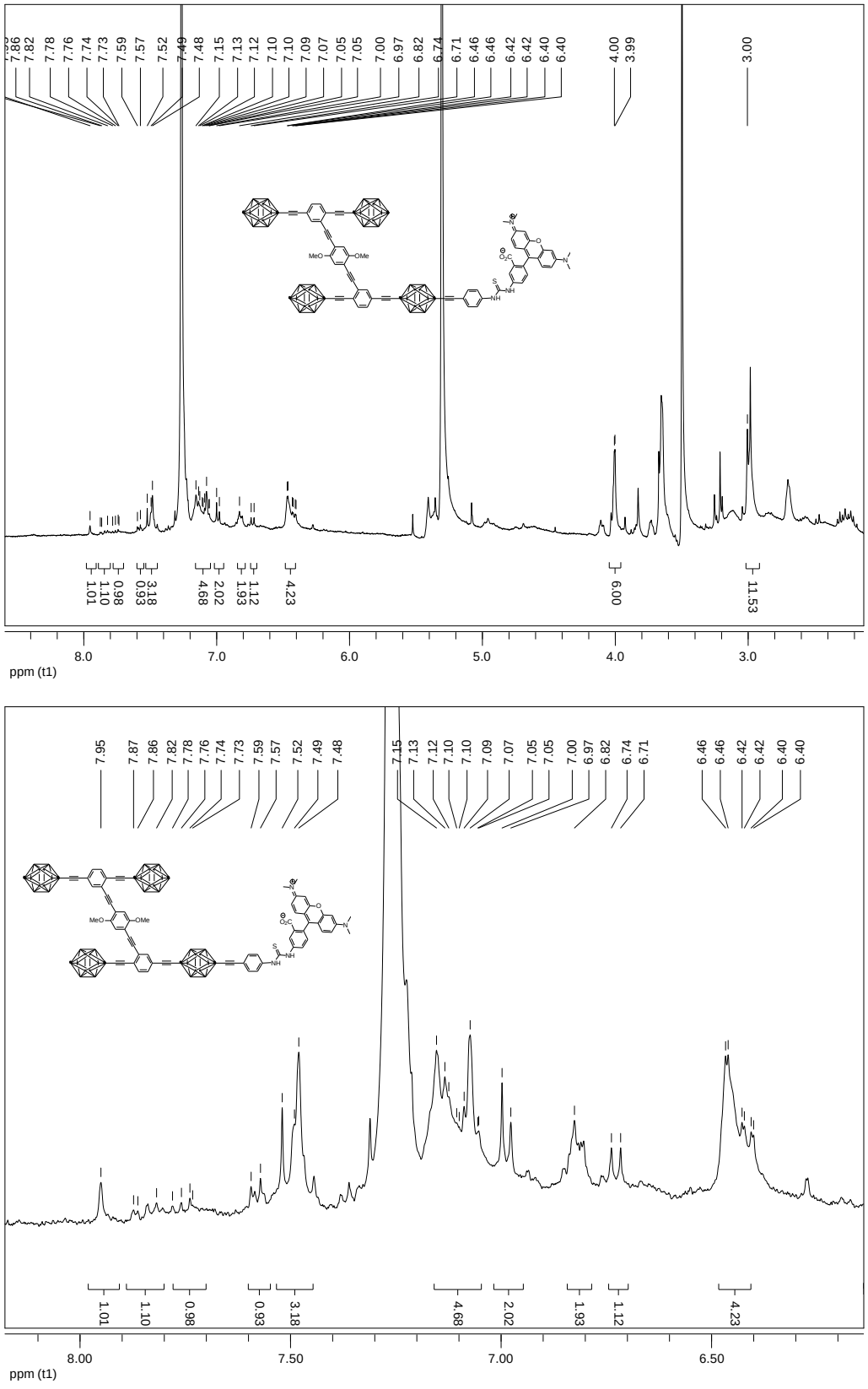

Supporting Information of

Chapter 2

Synthesis and Fluorescence Imaging of BODIPY-Based Nanocars

^{1}H and ^{13}C NMR spectra of new compounds

Time-lapse fluorescent images

AFM images of the different substrates

NMR Spectra

Figure S2.1. ^{1}H NMR spectrum of **5** (400 MHz, $CDCl_3$).

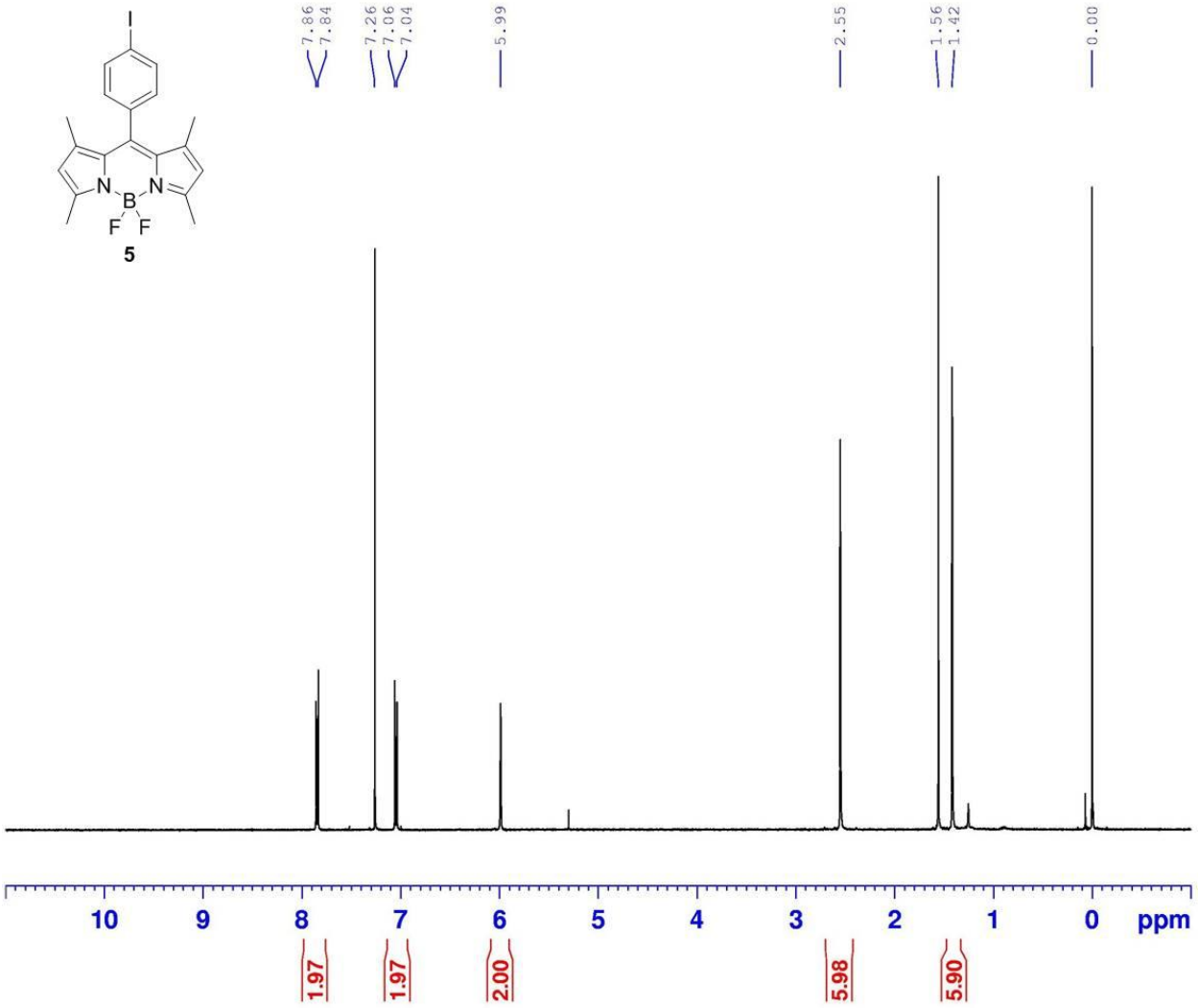

Figure S2.2. ^{1}H NMR spectrum of **6** (400 MHz, $CDCl_3$).

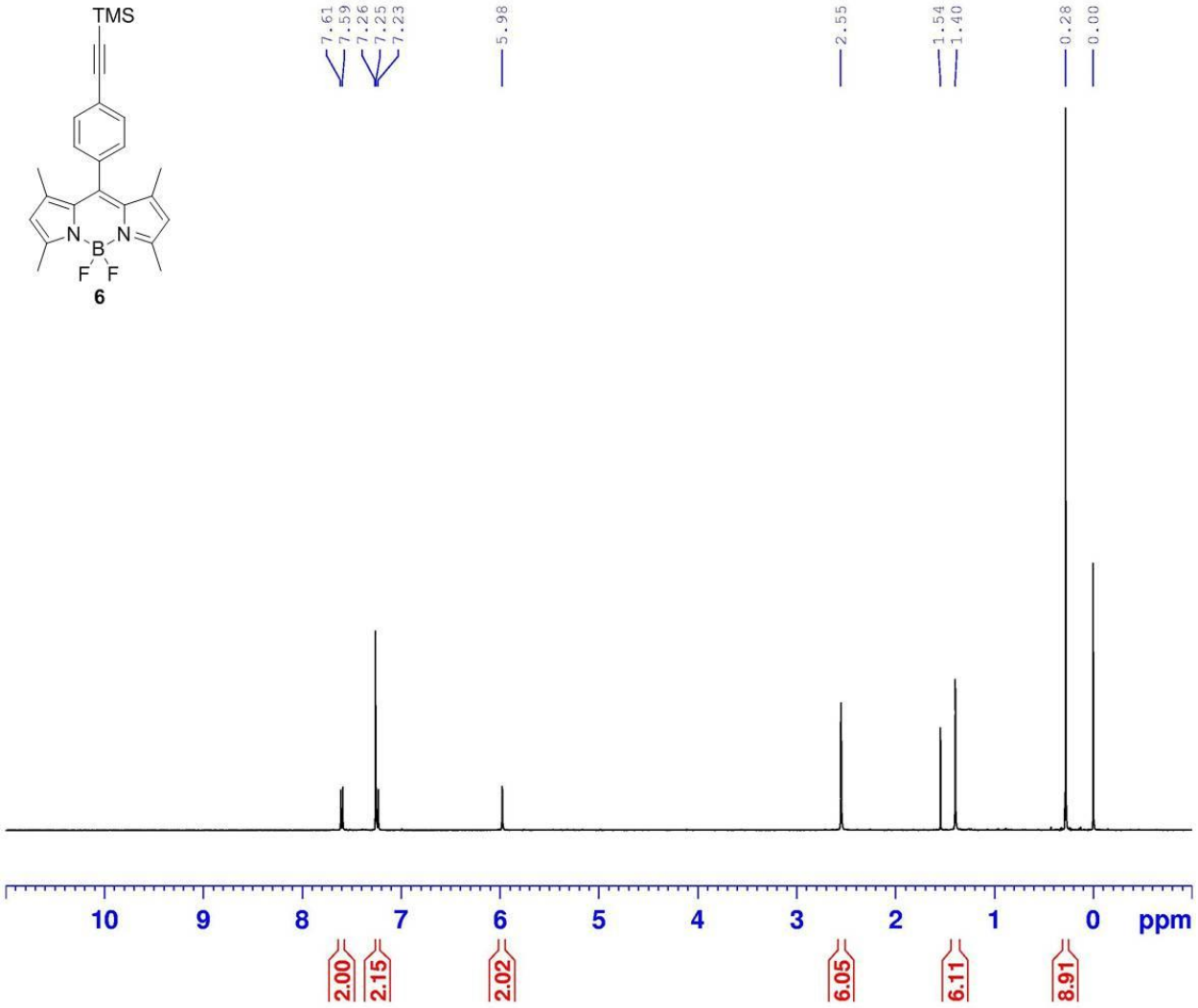

Figure S2.3. ^{13}C NMR spectrum of **6** (100 MHz, $CDCl_3$).

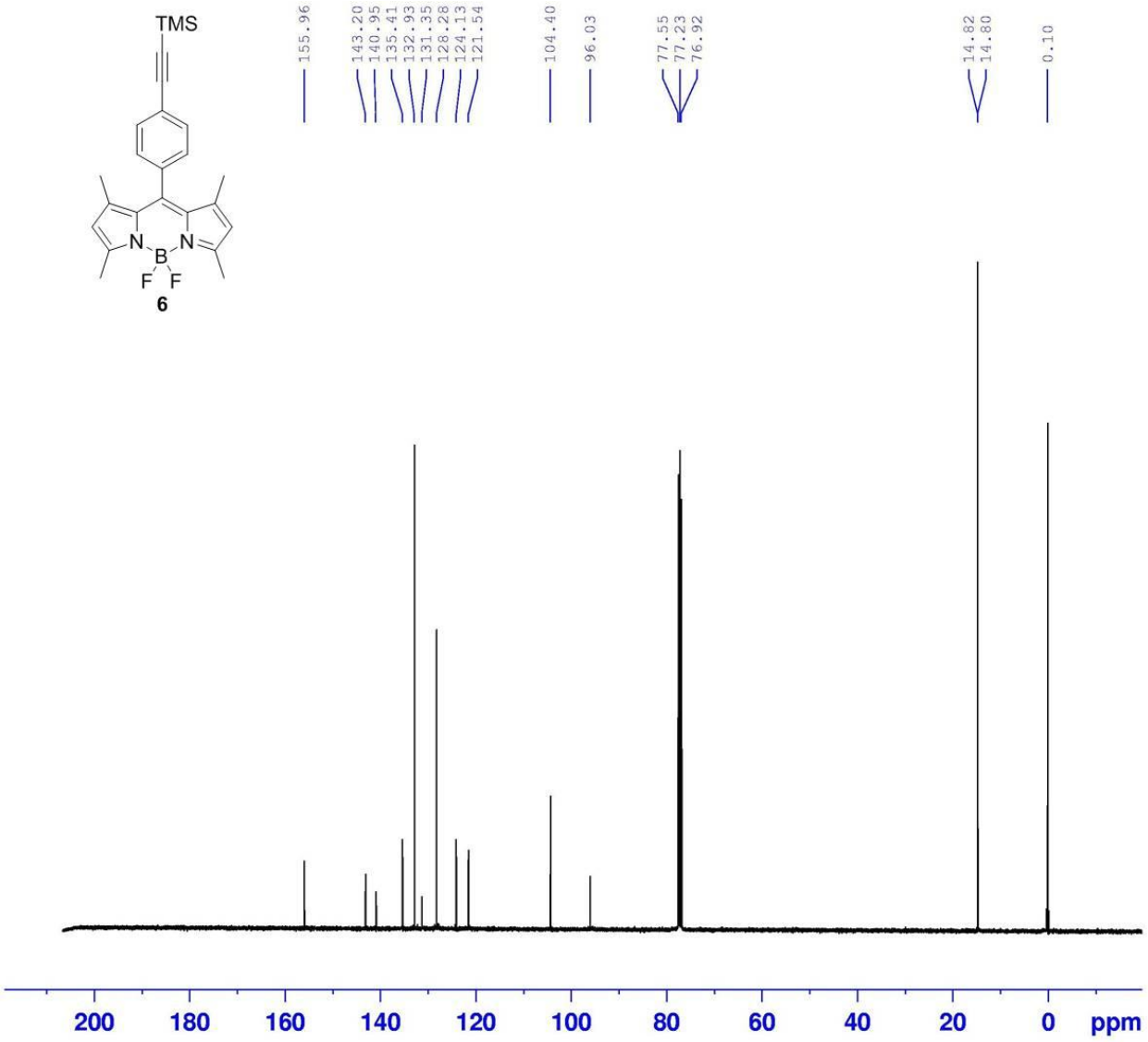

Figure S2.4. ^{1}H NMR spectrum of **7** (400 MHz, $CDCl_3$).

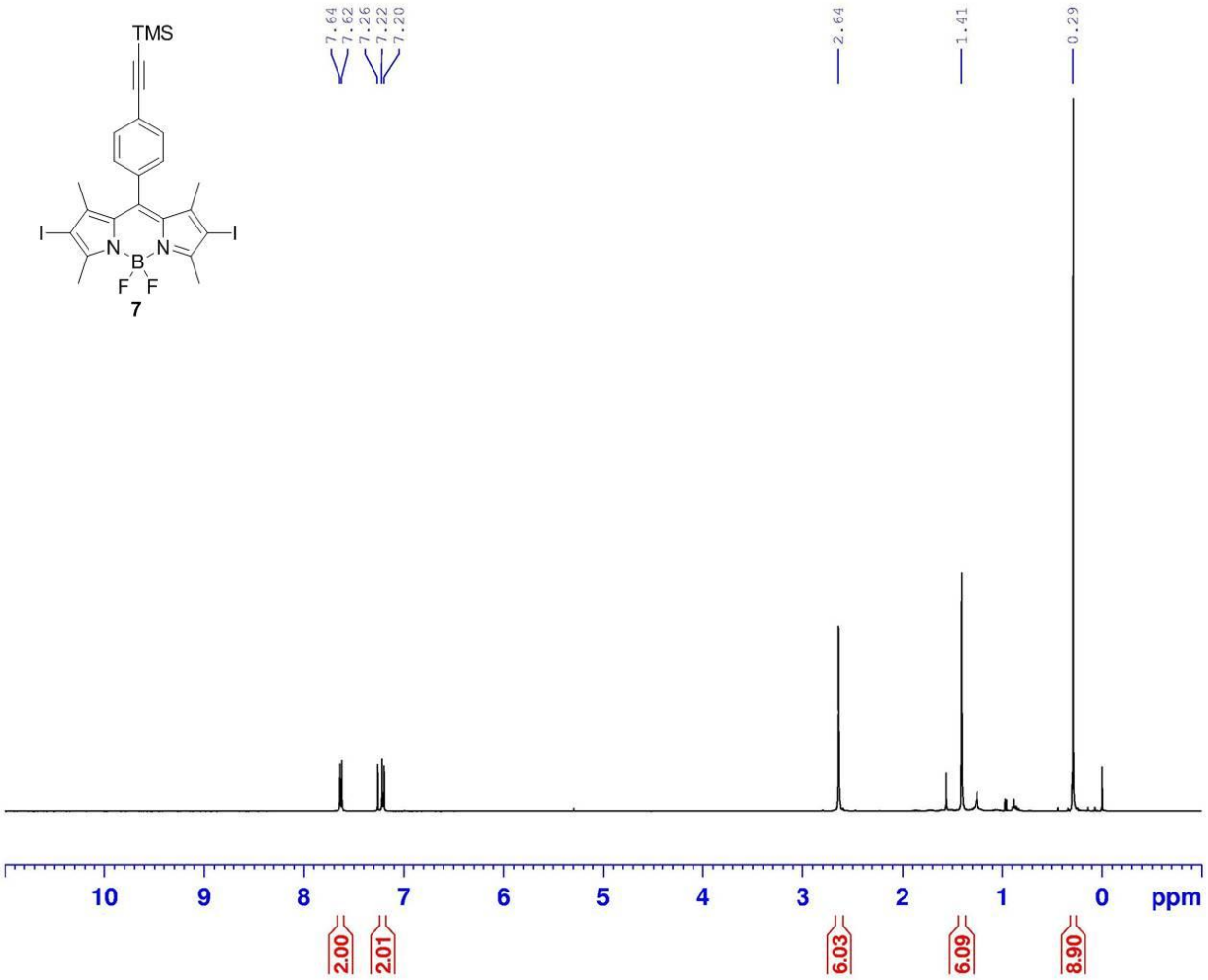

Figure S2.5. ^{13}C NMR spectrum of **7** (125 MHz, $CDCl_3$).

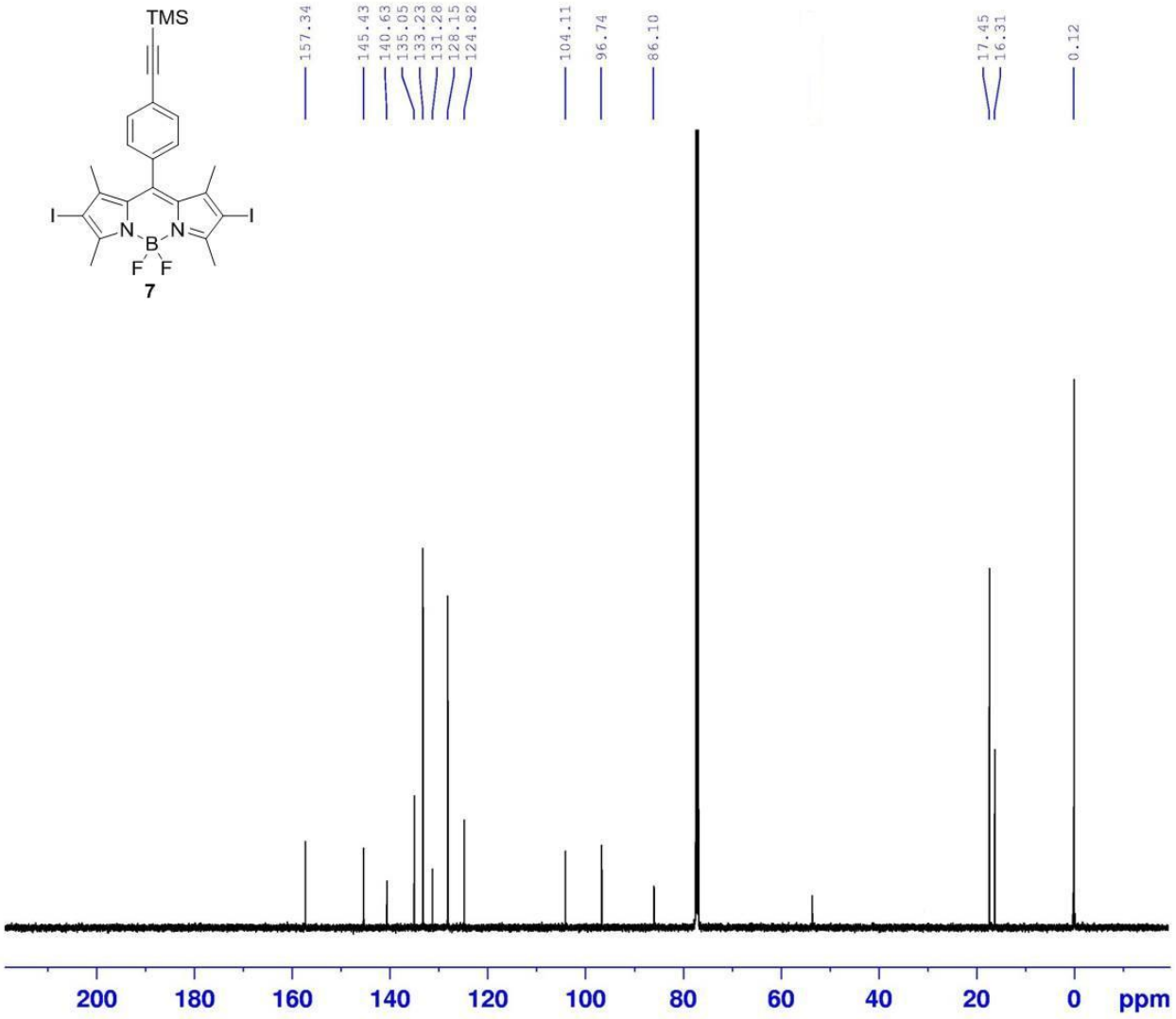

Figure S2.6. ^{1}H NMR spectrum of **9** (400 MHz, $CDCl_3$).

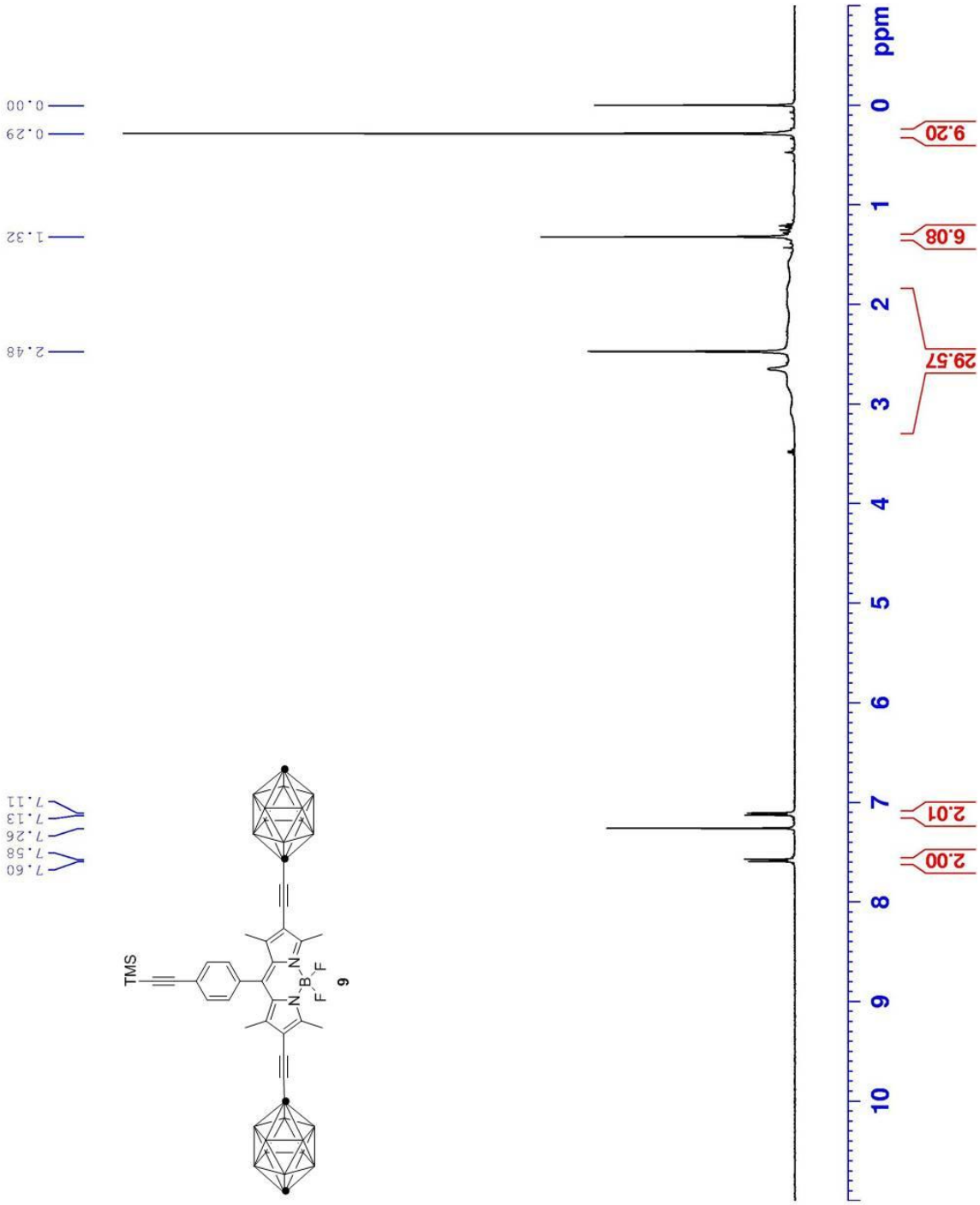

Figure S2.7. ^{13}C NMR spectrum of **9** (100 MHz, $CDCl_3$).

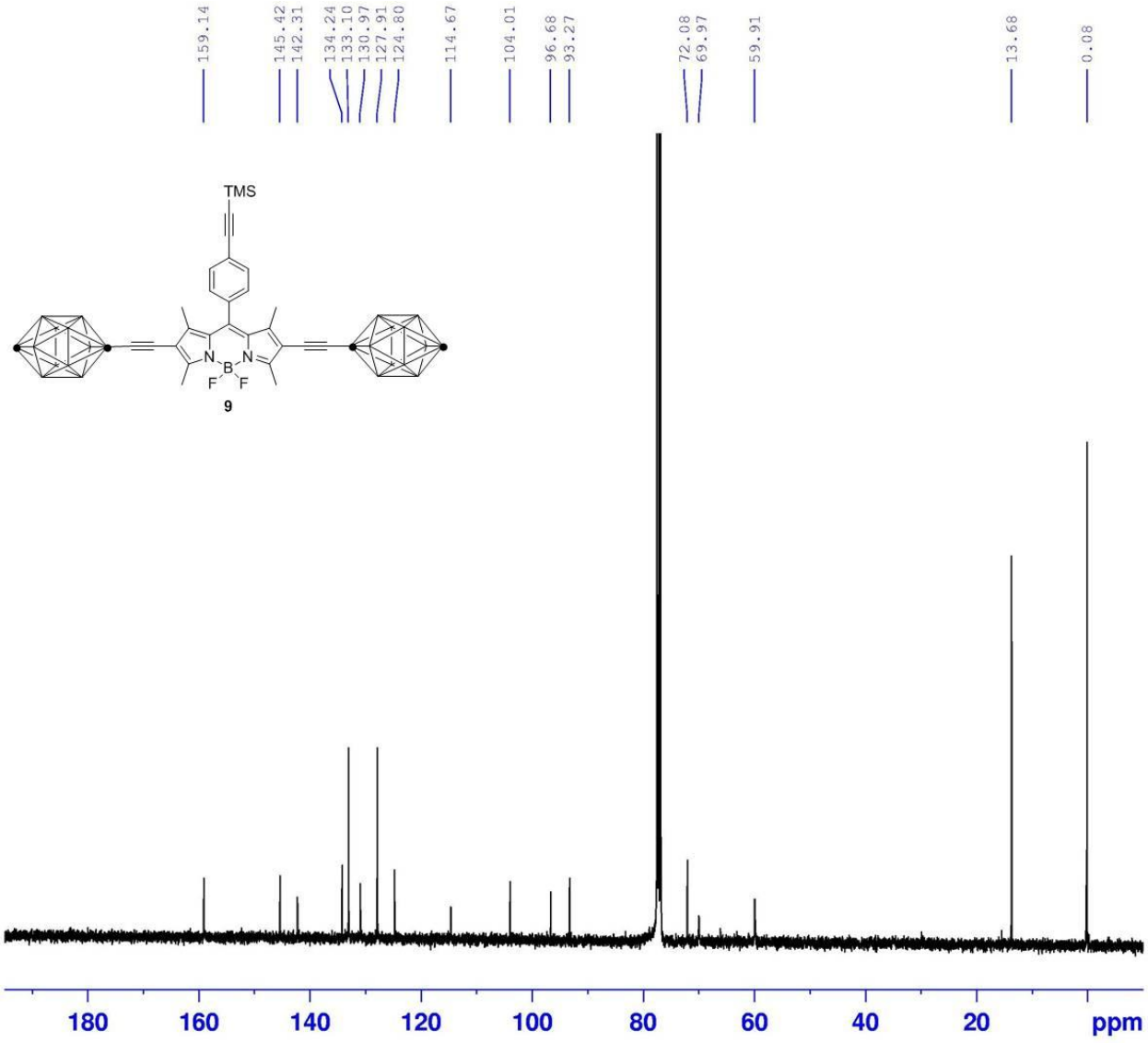

Figure S2.8. ^{1}H NMR spectrum of **10** (400 MHz, $CDCl_3$).

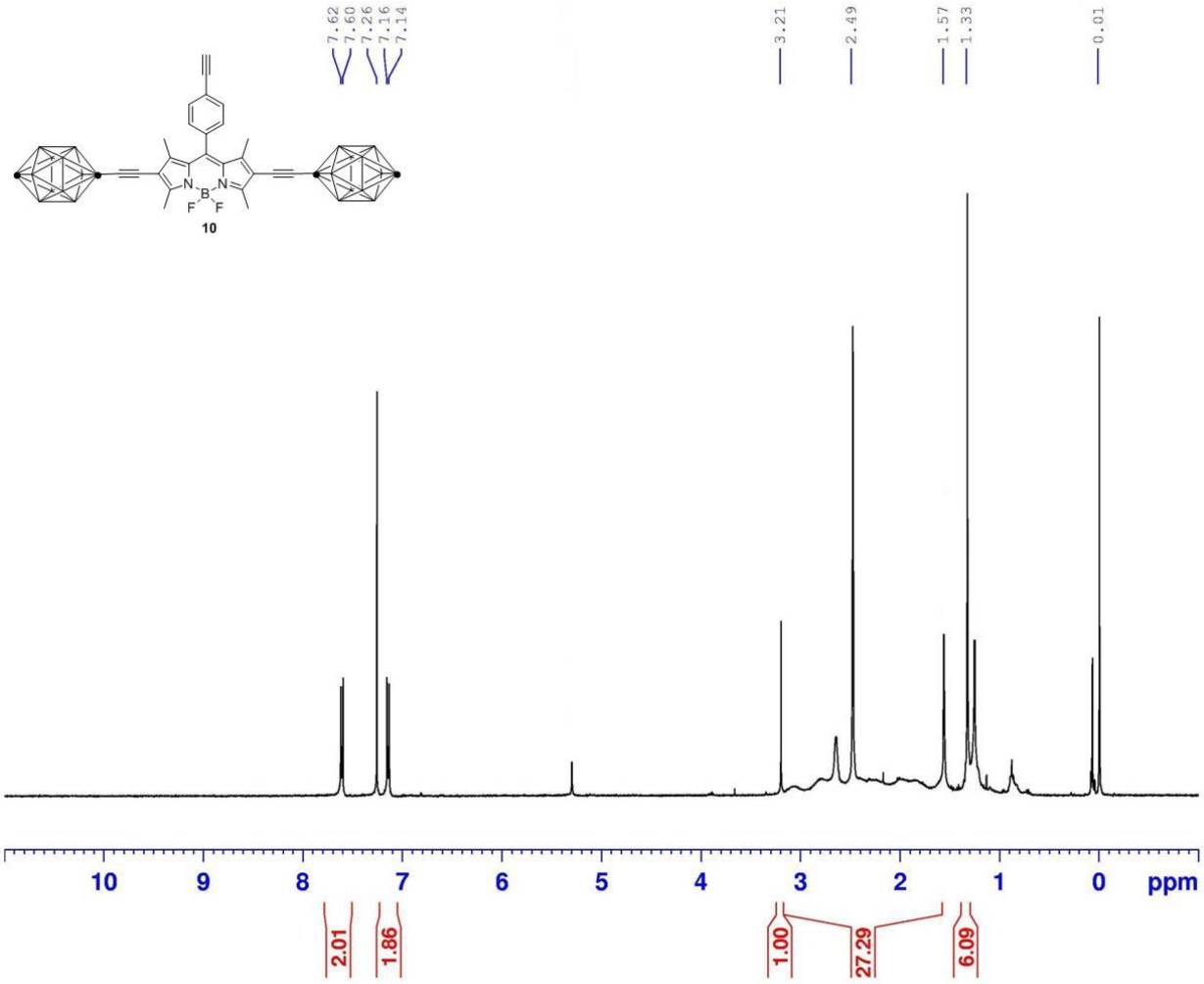

Figure S2.9. ^{13}C NMR spectrum of **10** (125 MHz, $CDCl_3$).

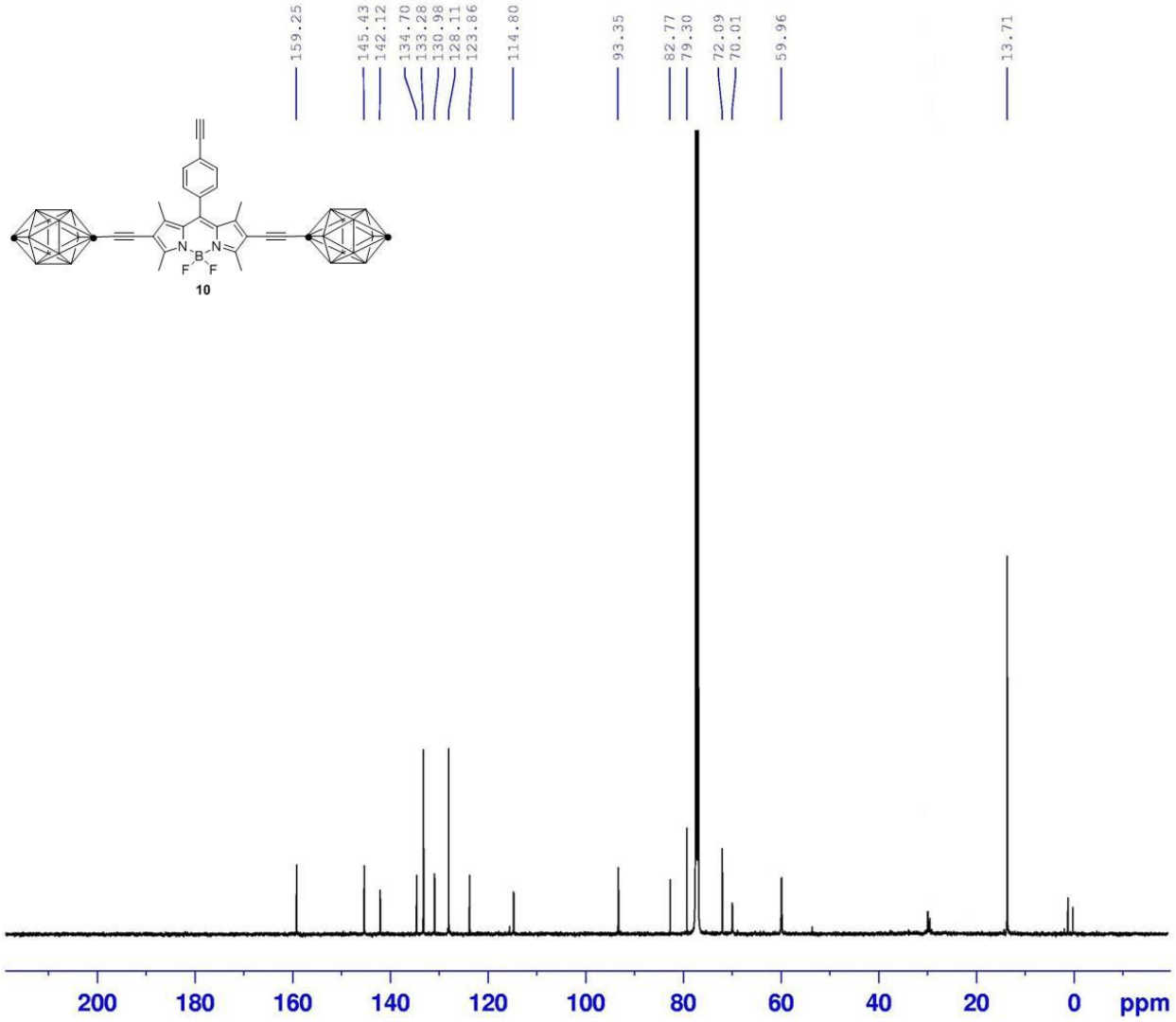

Figure S2.10. ^{1}H NMR spectrum of **1** (400 MHz, $CDCl_3$).

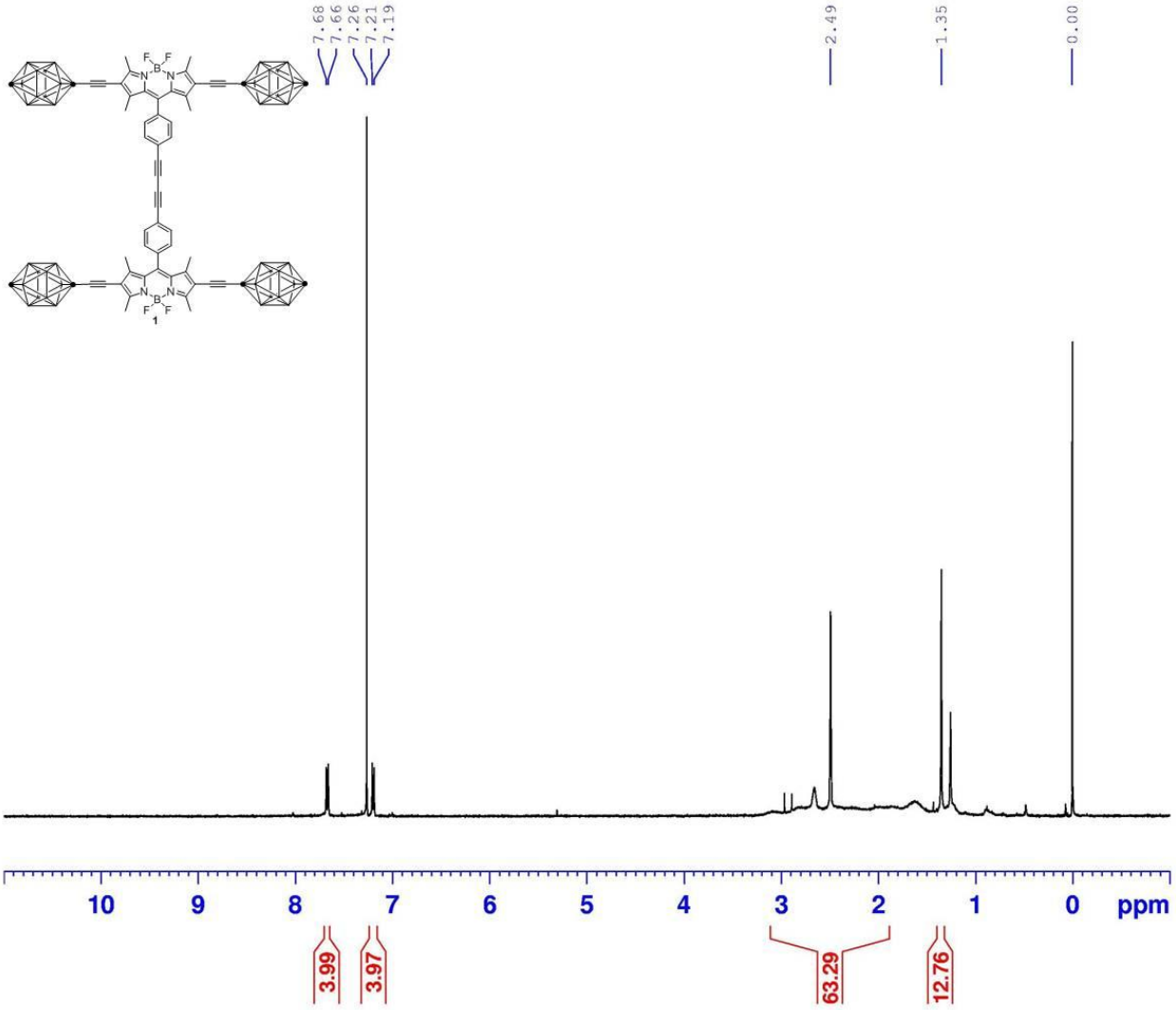

Figure S2.11. ^{13}C NMR spectrum of **1** (100 MHz, $CDCl_3$).

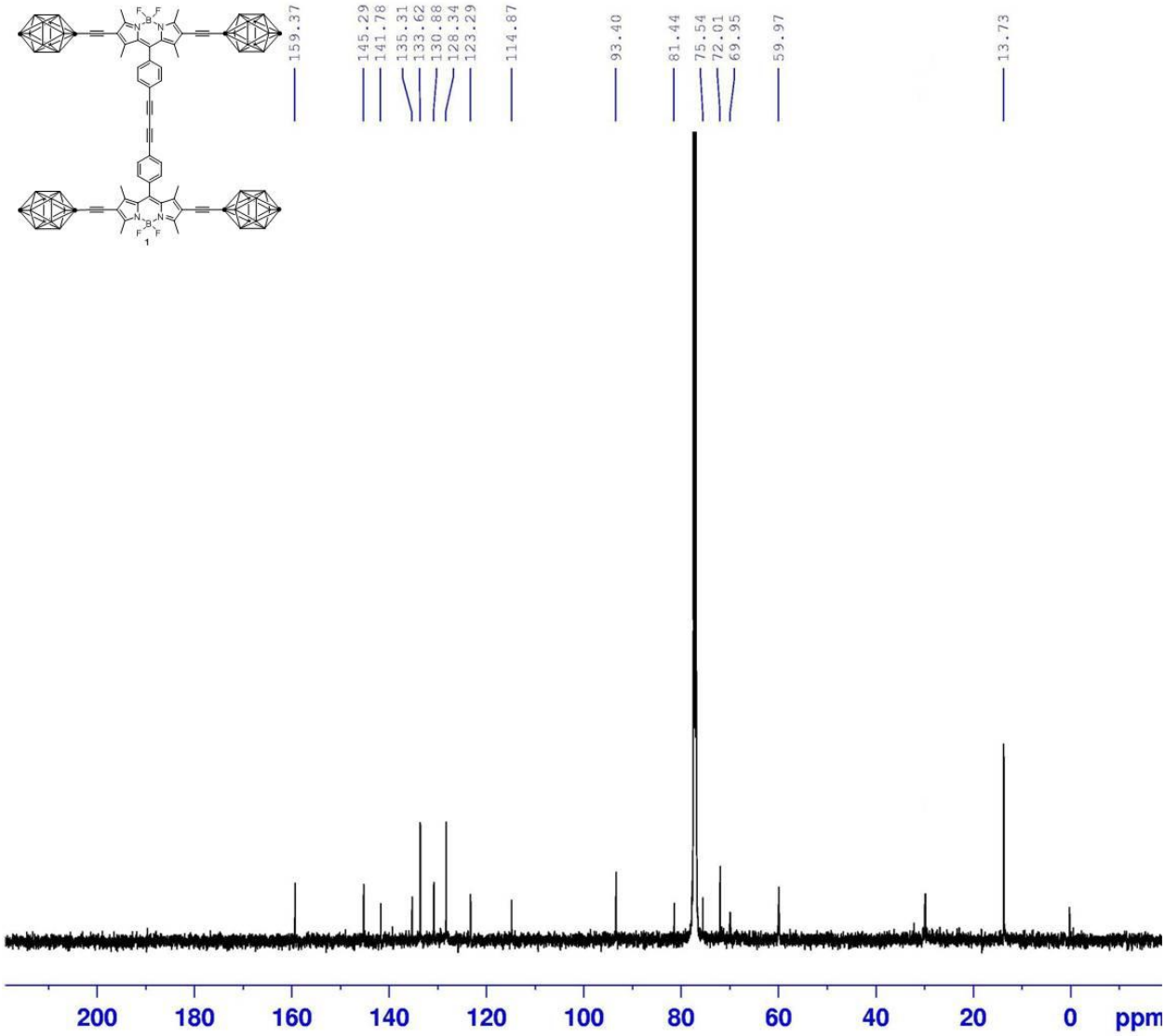

Figure S2.12. ^{1}H NMR spectrum of **2** (400 MHz, $CDCl_3$).

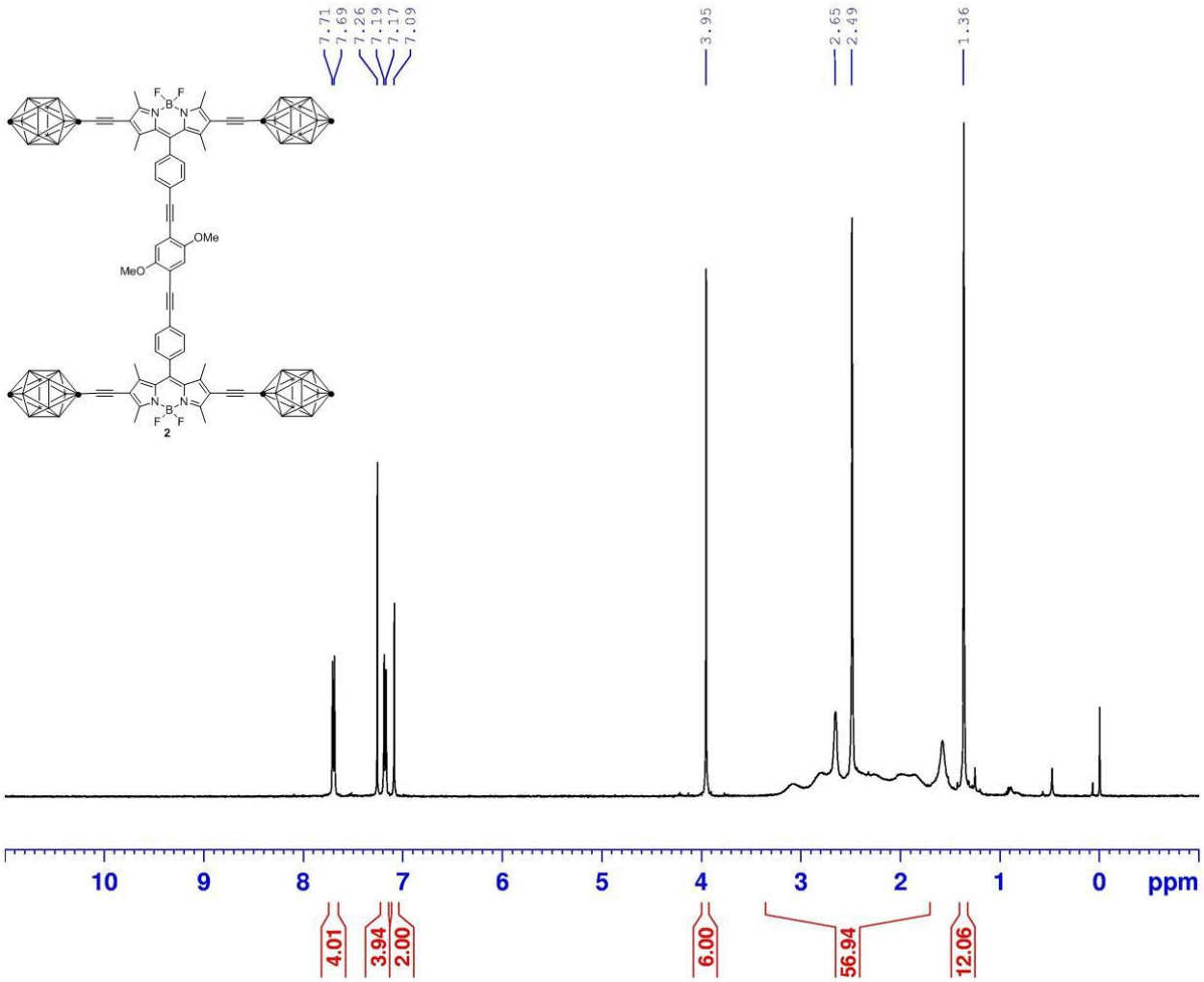

Figure S2.13. ^{13}C NMR spectrum of **2** (125 MHz, $CDCl_3$).

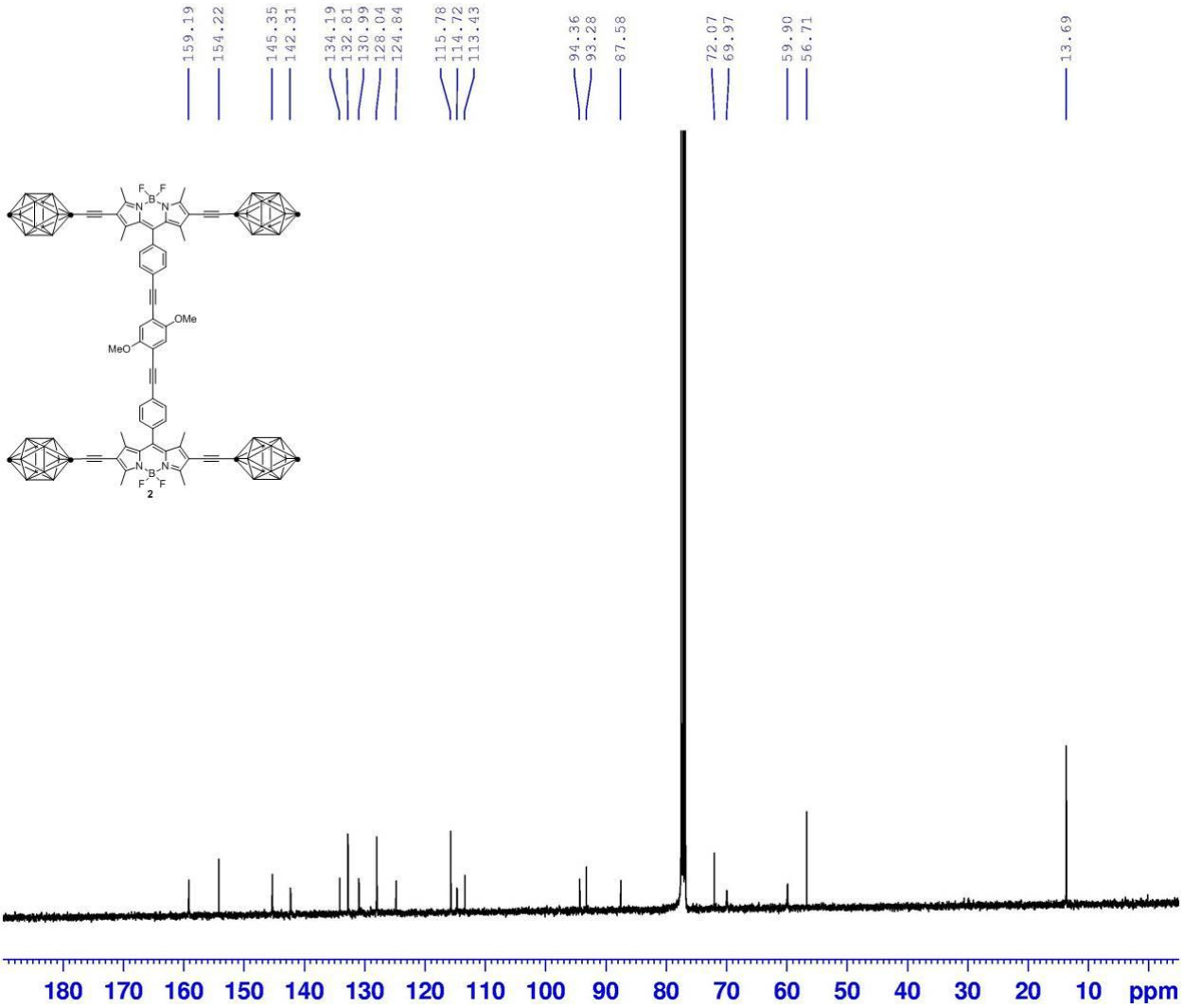

Figure S2.14. ^{1}H NMR spectrum of **3** (400 MHz, $CDCl_3$).

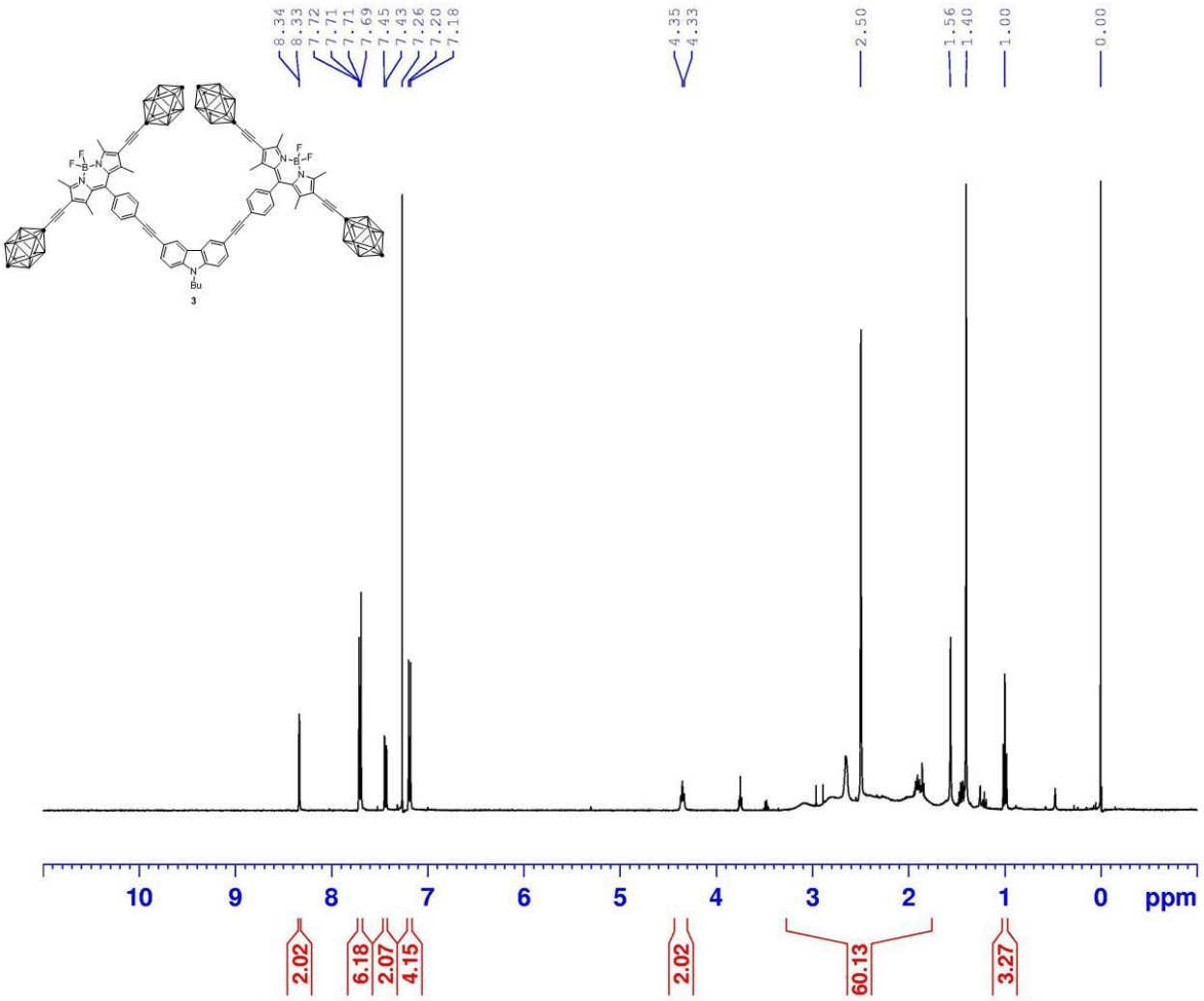

Figure S2.15. ^{13}C NMR spectrum of **3** (125 MHz, $CDCl_3$).

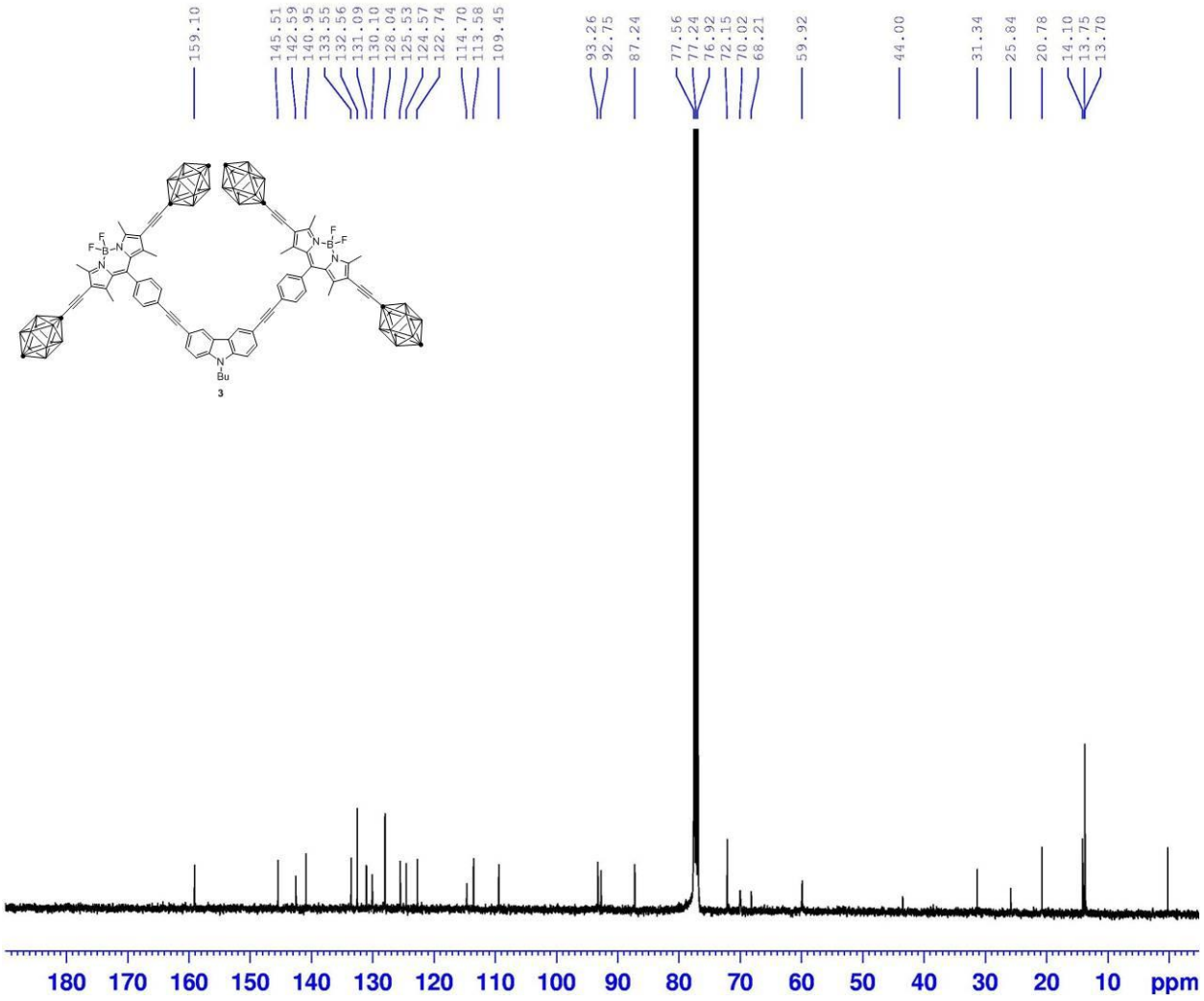

Figure S2.16. ^{1}H NMR spectrum of **13** (500 MHz, $CDCl_3$).

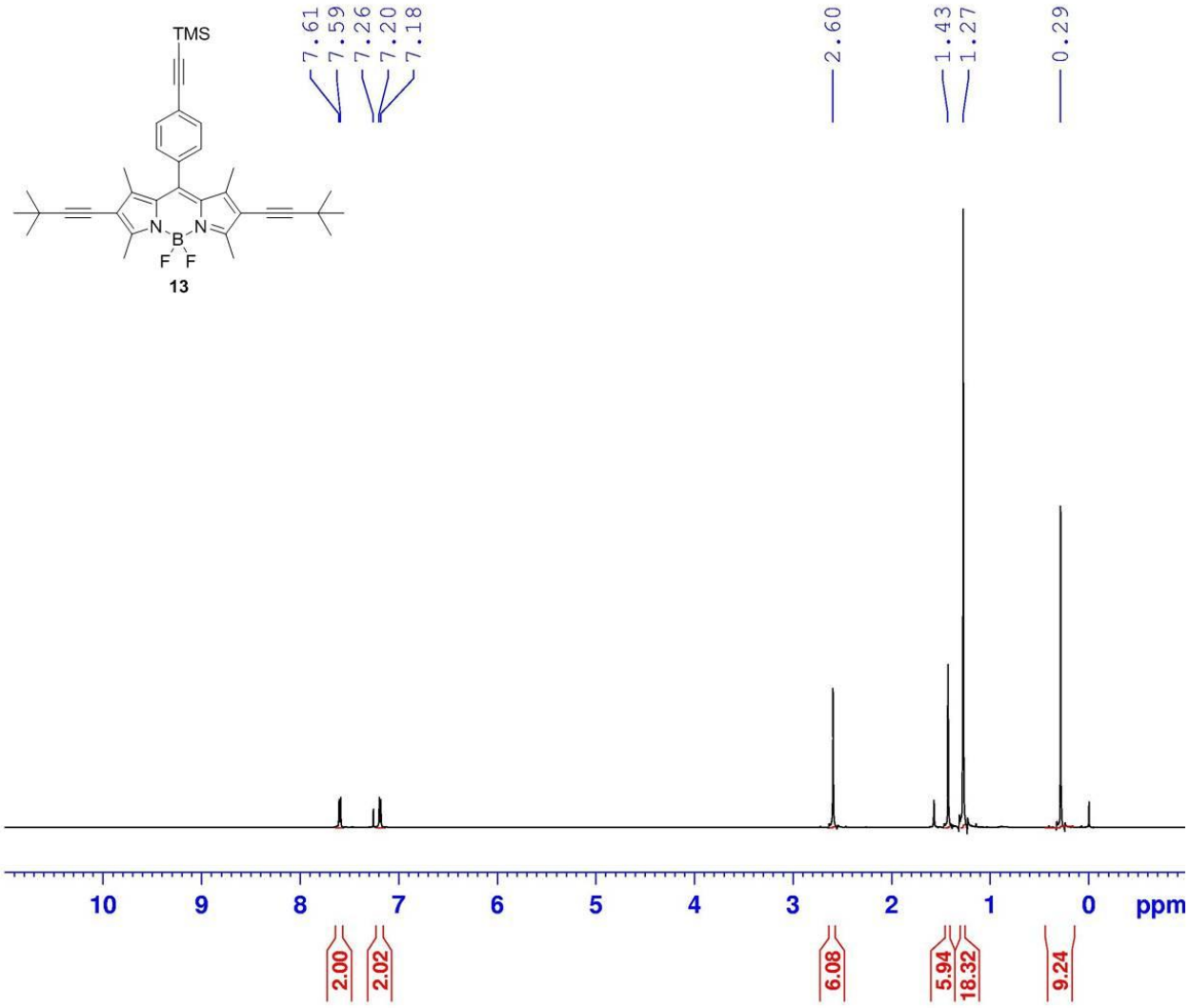

Figure S2.17. ^{13}C NMR spectrum of **13** (125 MHz, $CDCl_3$).

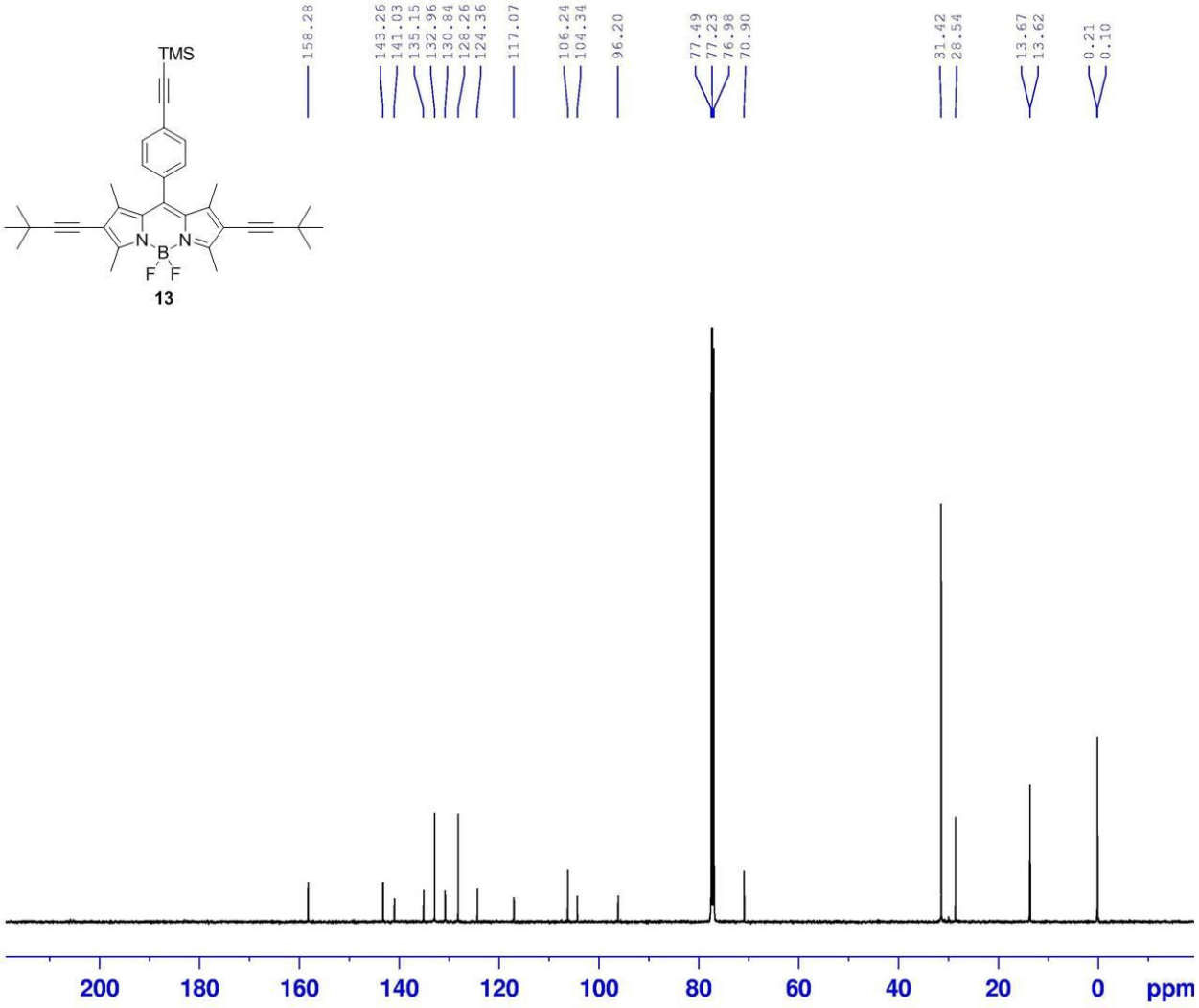

Figure S2.18. ^{1}H NMR spectrum of **14** (500 MHz, $CDCl_3$).

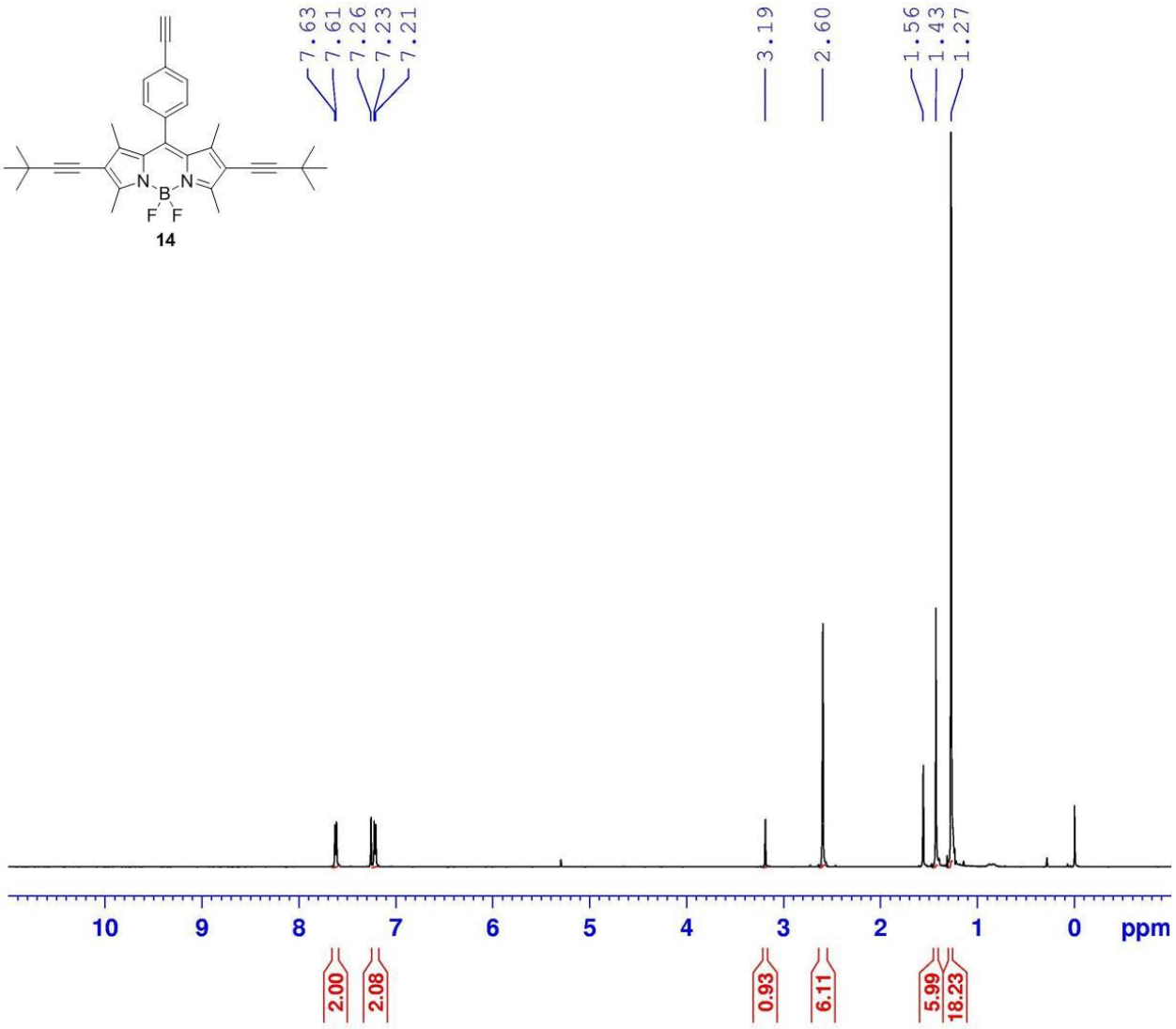

Figure S2.19. ^{13}C NMR spectrum of **14** (125 MHz, $CDCl_3$).

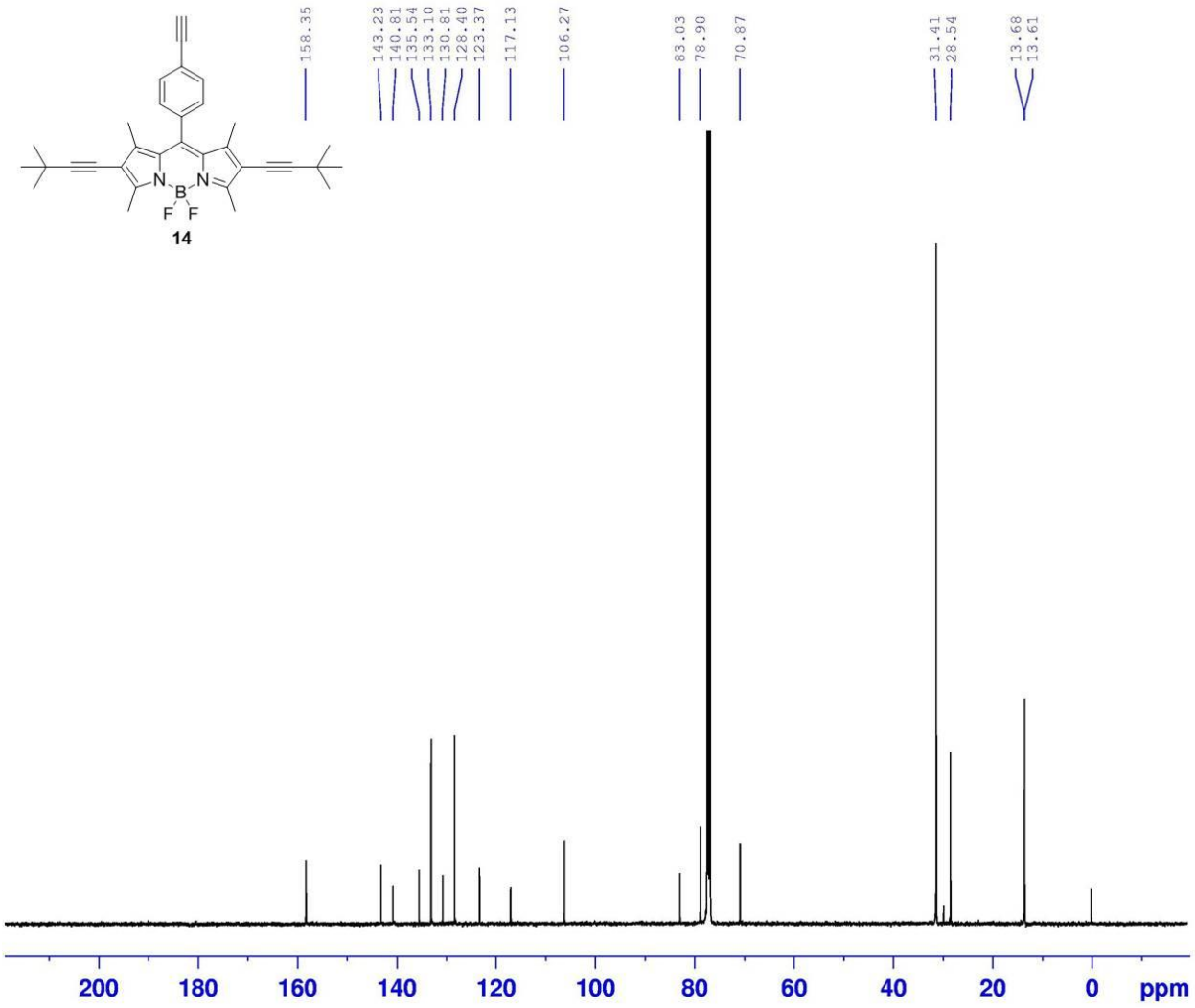

Figure S2.20. ^{1}H NMR spectrum of **4** (400 MHz, $CDCl_3$).

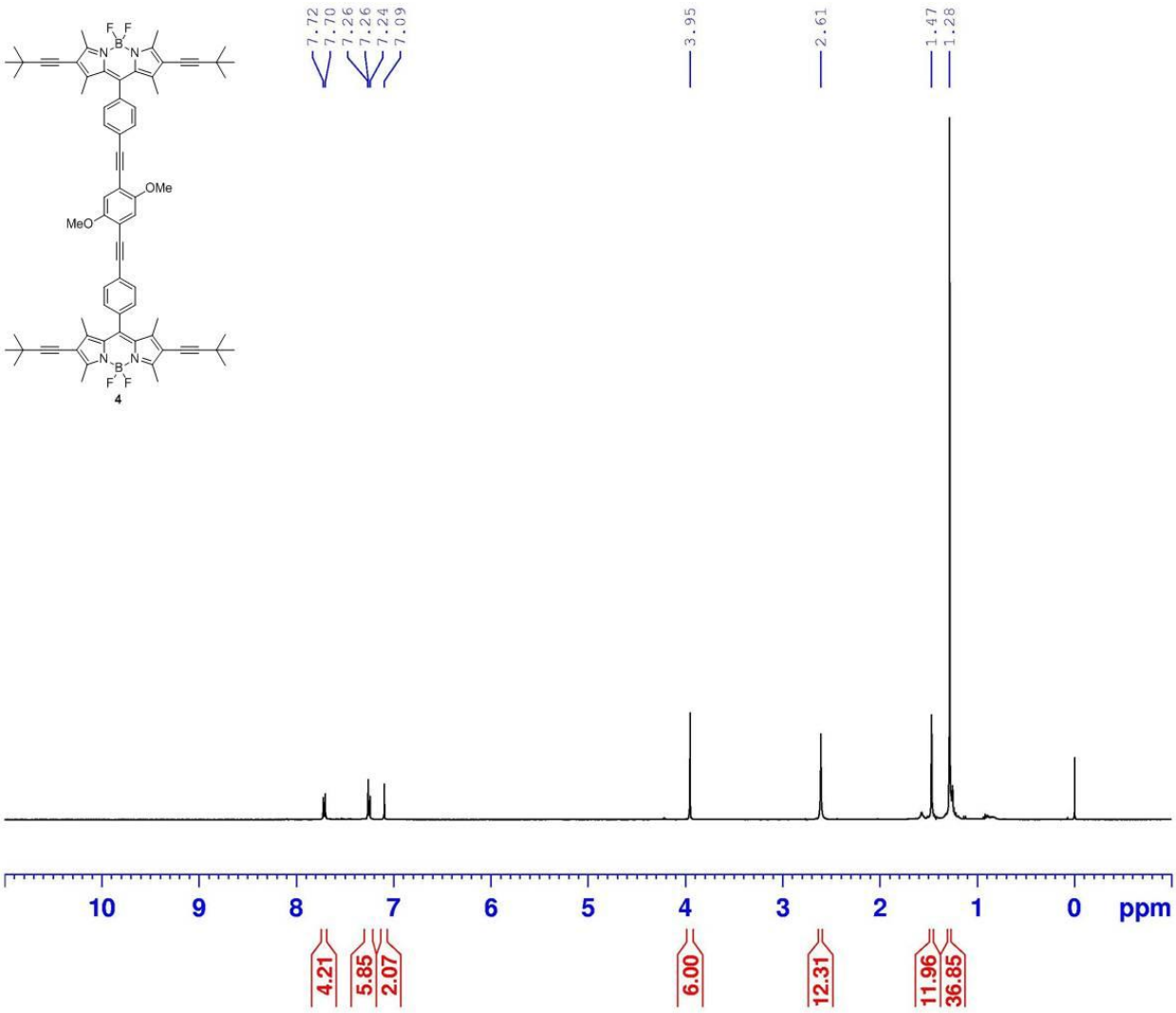

Figure S2.21. ^{13}C NMR spectrum of **4** (125 MHz, $CDCl_3$).

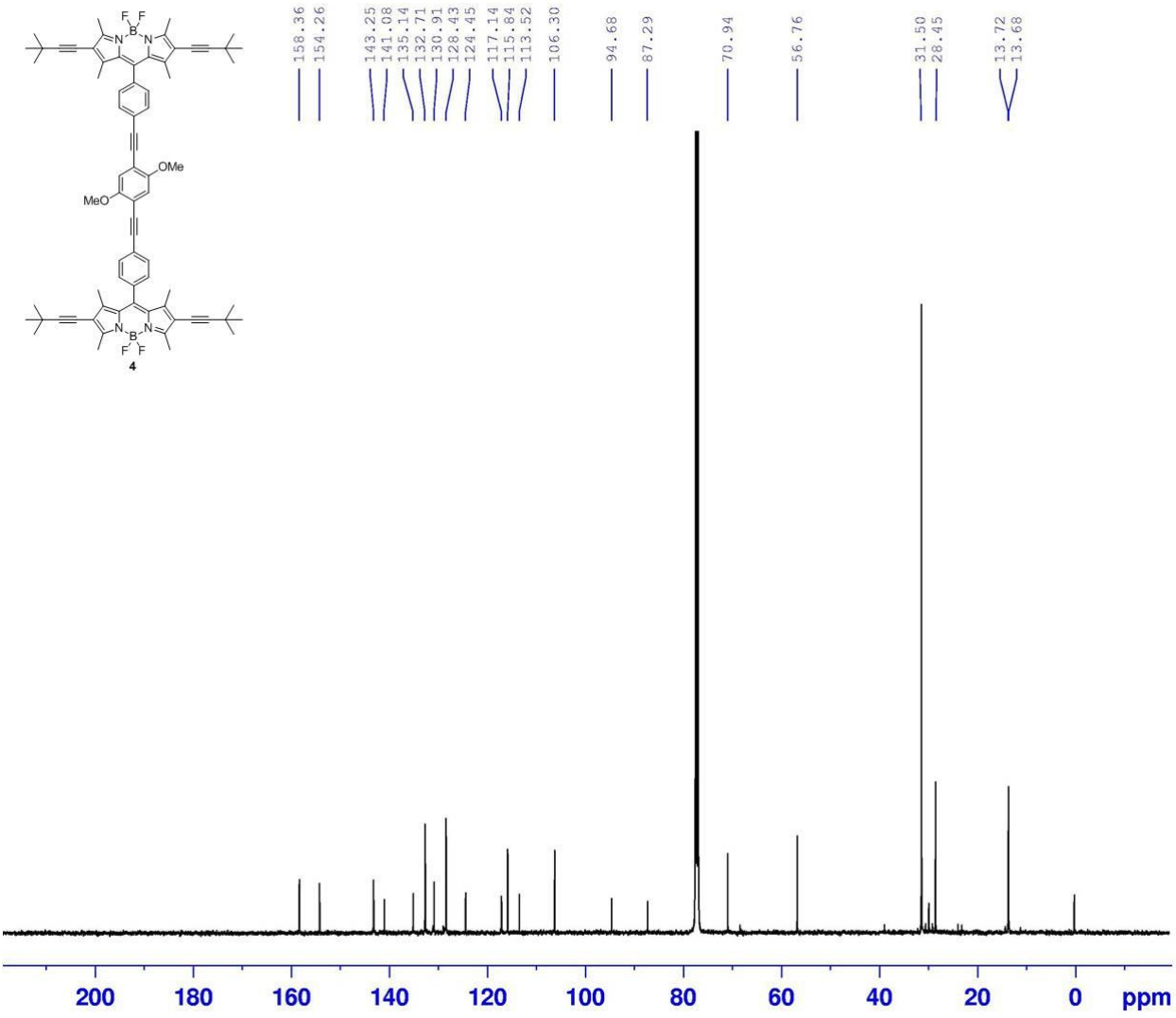

Figure S2.22. ^{1}H NMR spectrum of **15** (400 MHz, $CDCl_3$).

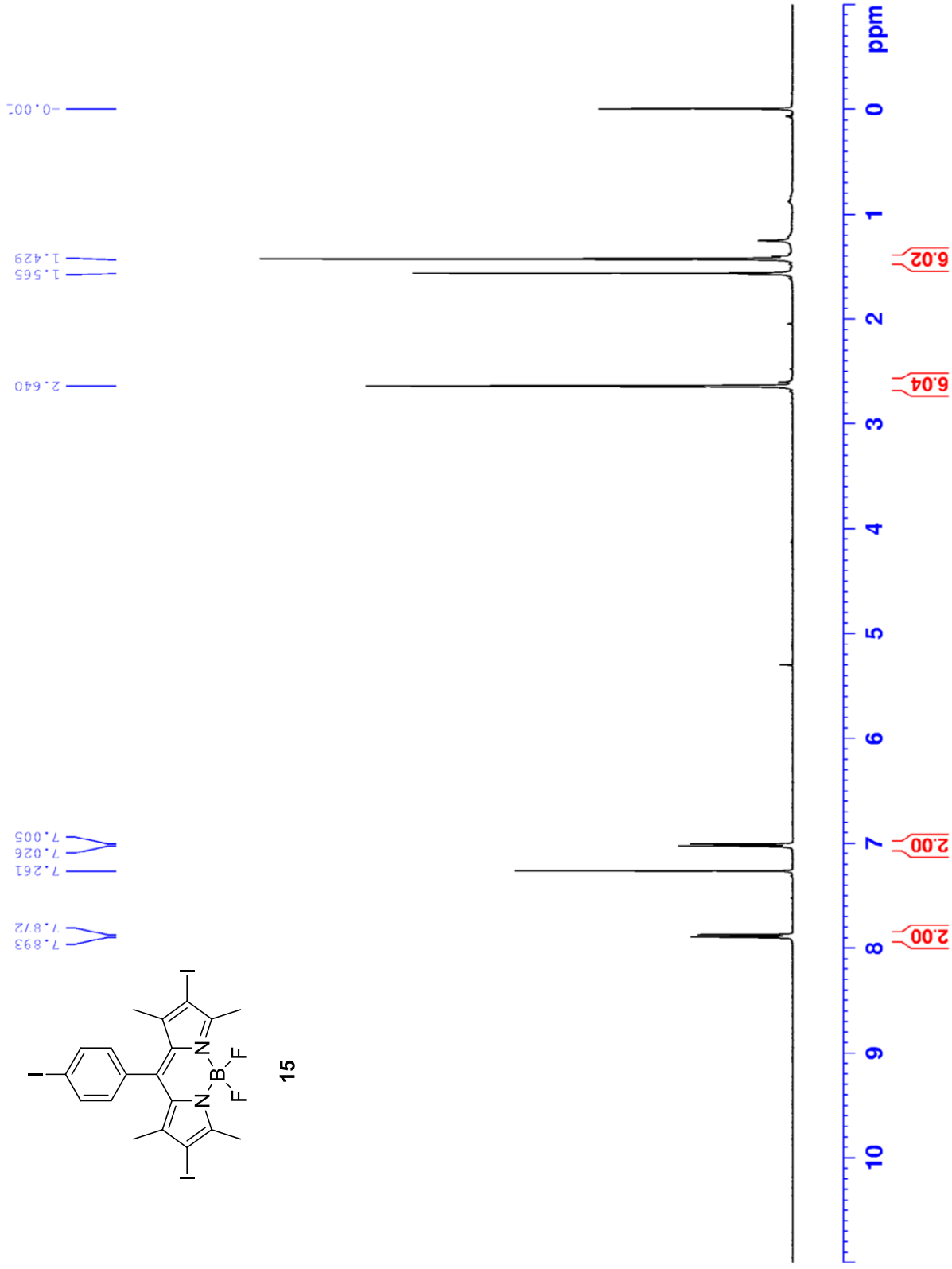

Figure S2.23. ^{13}C NMR spectrum of **15** (100 MHz, $CDCl_3$).

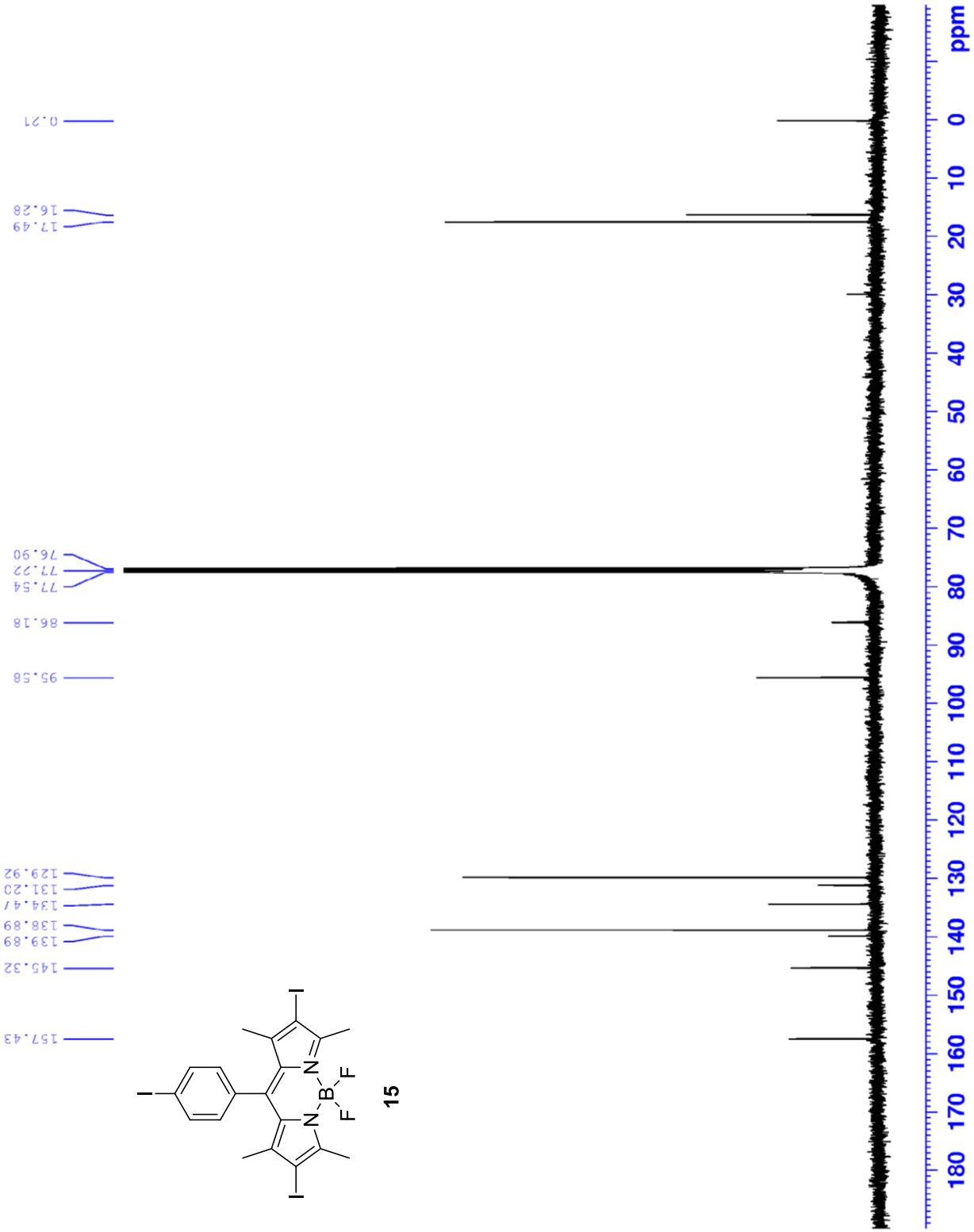

Figure S2.24. ^{1}H NMR spectrum of **16** (500 MHz, $CDCl_3$).

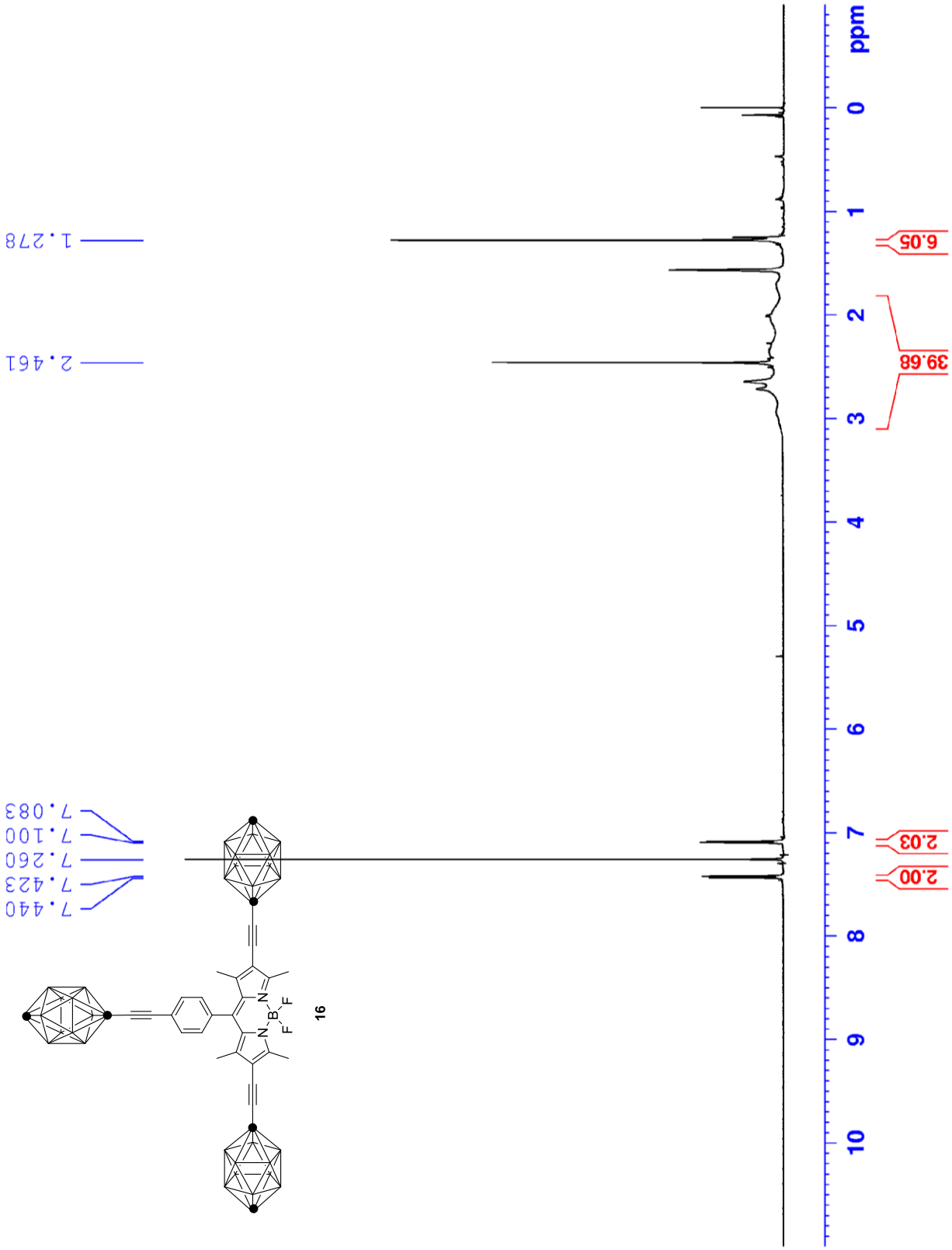

Figure S2.25. ^{13}C NMR spectrum of **16** (125 MHz, $CDCl_3$).

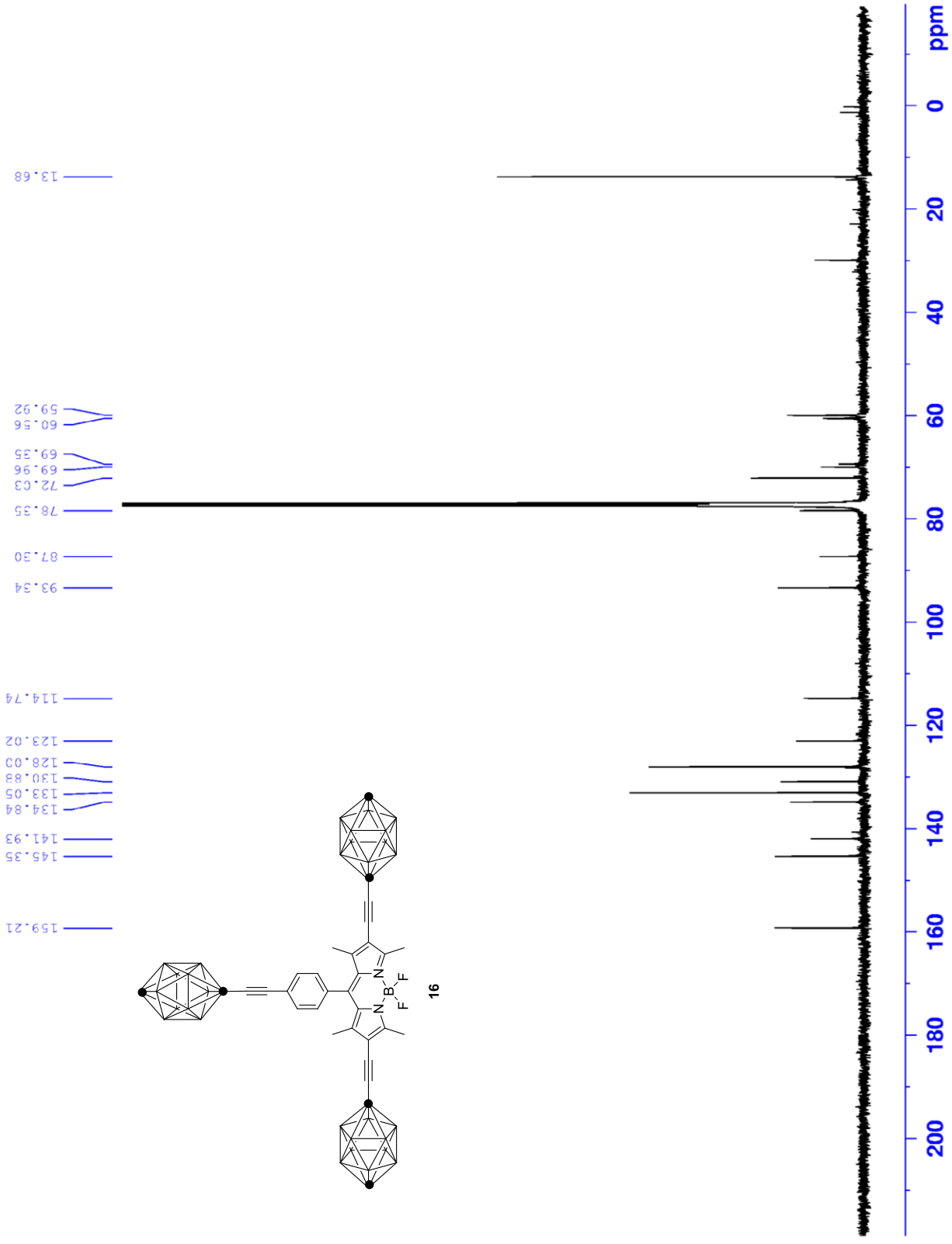

Time-lapse fluorescence images

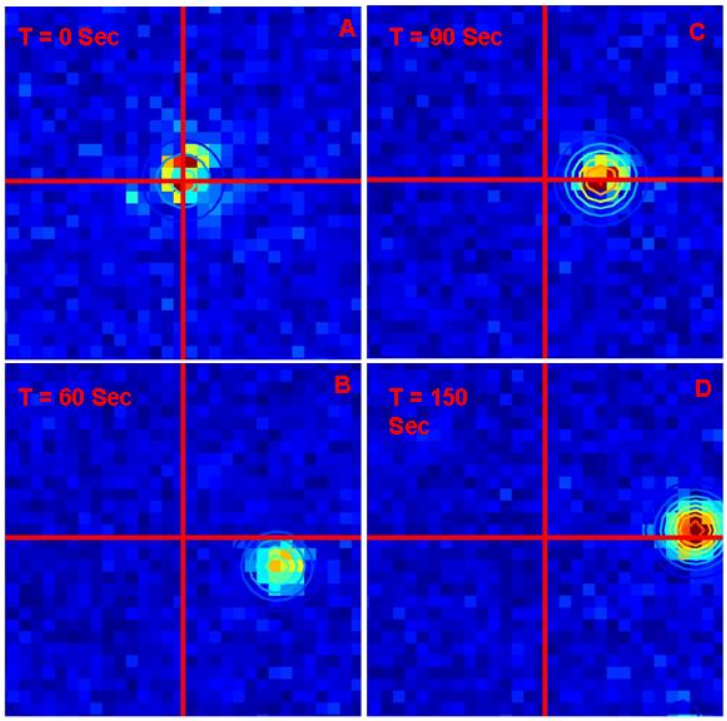

Figure S2.26. Time-lapse fluorescence images showing the movement of a single BODIPY-based nanocar **2** on plasma cleaned glass. Each image is 2.4 x 2.4 μm.

AFM images of different substrates

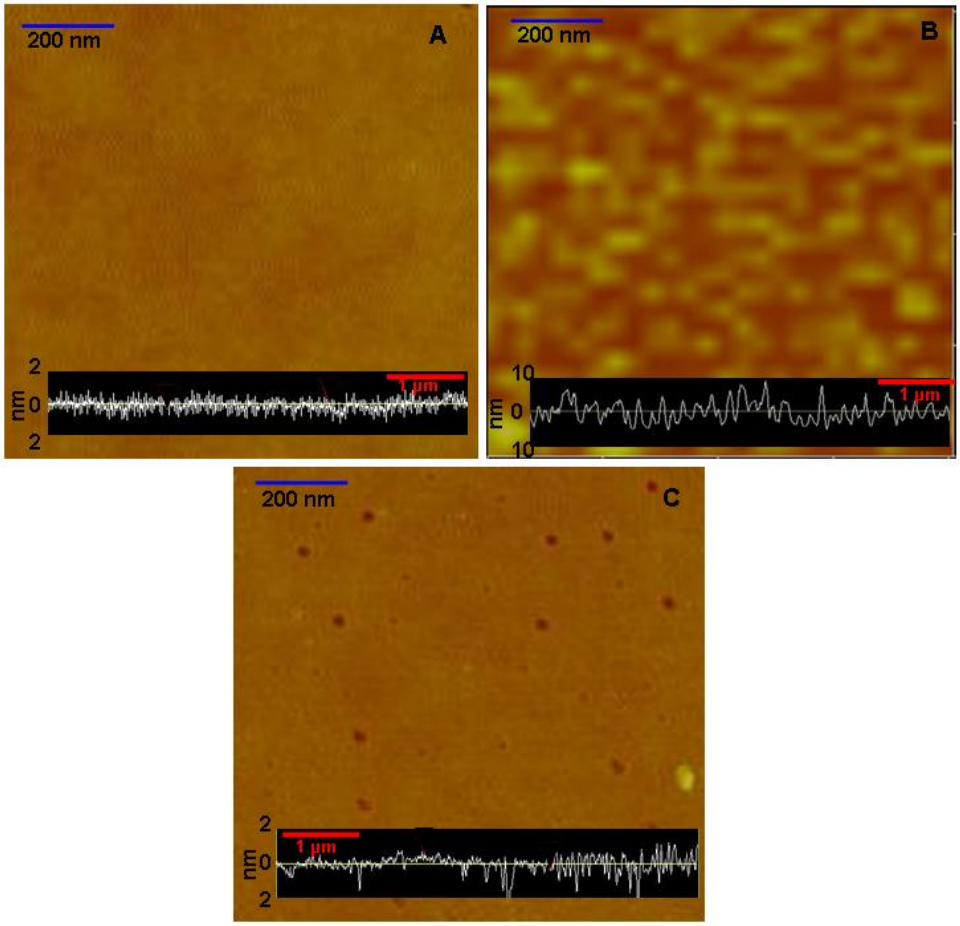

Figure S2.27. AFM images (1 µm x 1 µm) of plasma cleaned glass (A), etched glass (B), and Vectabond™ treated glass (C). The insets show line scans taken on each surface. The average surface roughness of these surfaces was measured to be 0.4 ± 0.1 nm (glass), 2.6 ± 0.2 nm (etched glass), and 0.5 ± 0.2 nm (Vectabond™ treated glass). Surface holes (dark spots) are seen for Vectabond™ treated surfaces, which are as big as 50 nm in diameter and 5 nm in height. They are most likely due to an uneven surface functionalization, but contribute at most 2-3 % to the total surface area.

Supporting Information of

Chapter 3

Toward Chemical Propulsion: Synthesis of ROMP–Propelled Nanocars

^{1}H and ^{13}C NMR of new compounds

Ring-Opening Metathesis Polymerization Results

Figure S3.1. ^{1}H NMR spectrum of **3** (400 MHz, $CDCl_3$).

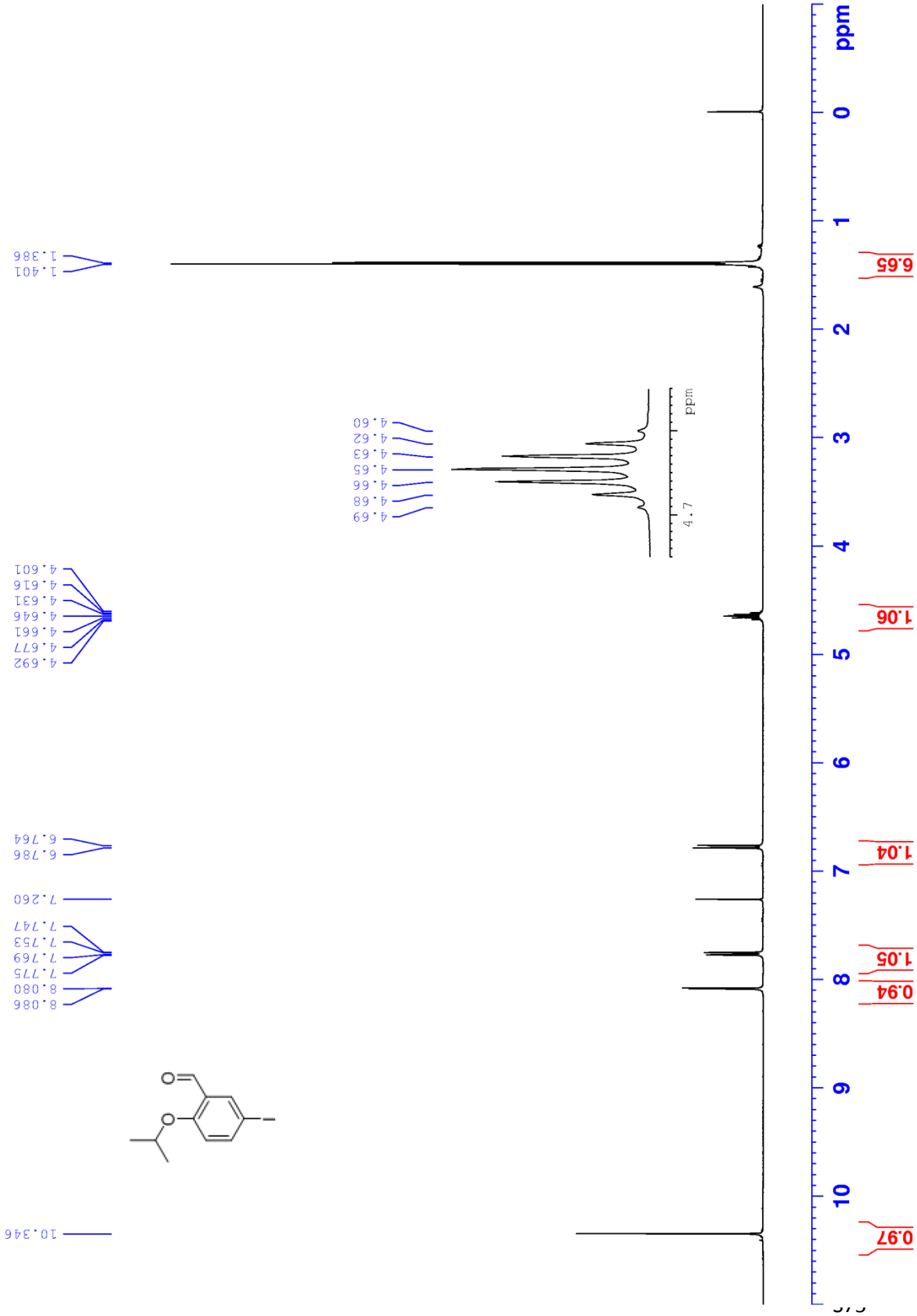

Figure S3.2. ^{13}C NMR spectrum of **3** (125 MHz, $CDCl_3$).

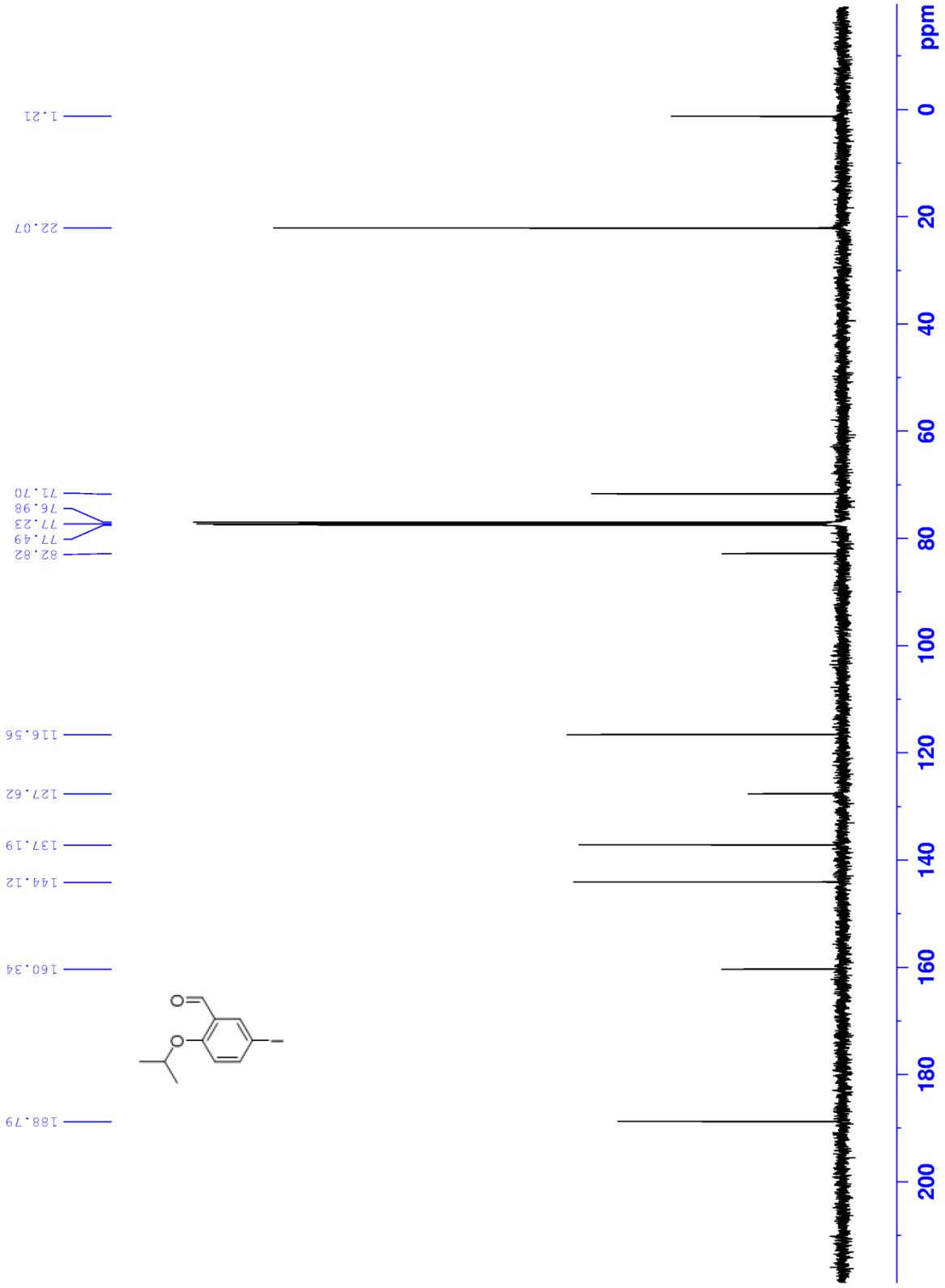

Figure S3.3. ^{1}H NMR spectrum of **4** (500 MHz, $CDCl_3$).

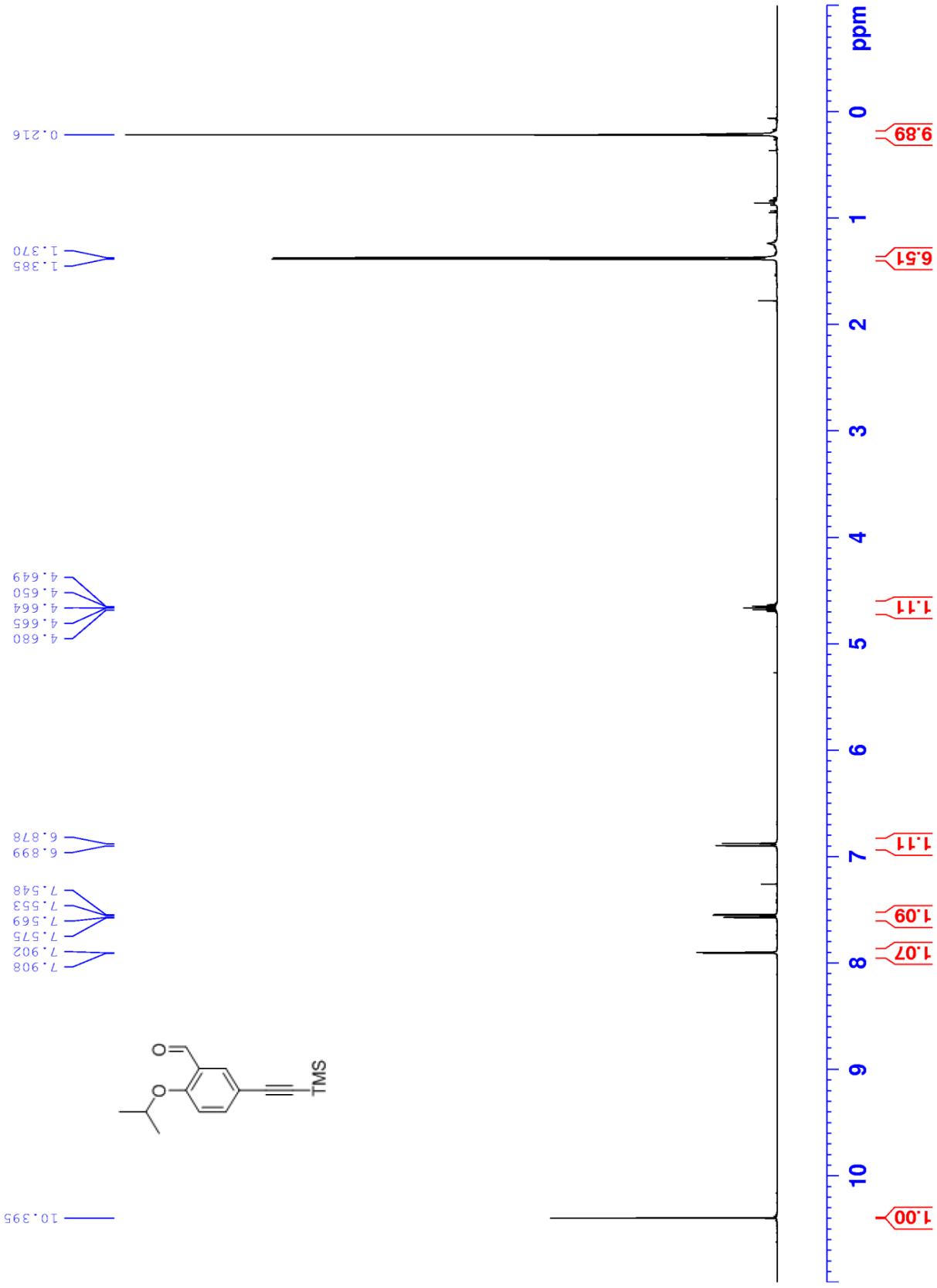

Figure S3.4. ^{13}C NMR spectrum of **4** (125 MHz, $CDCl_3$).

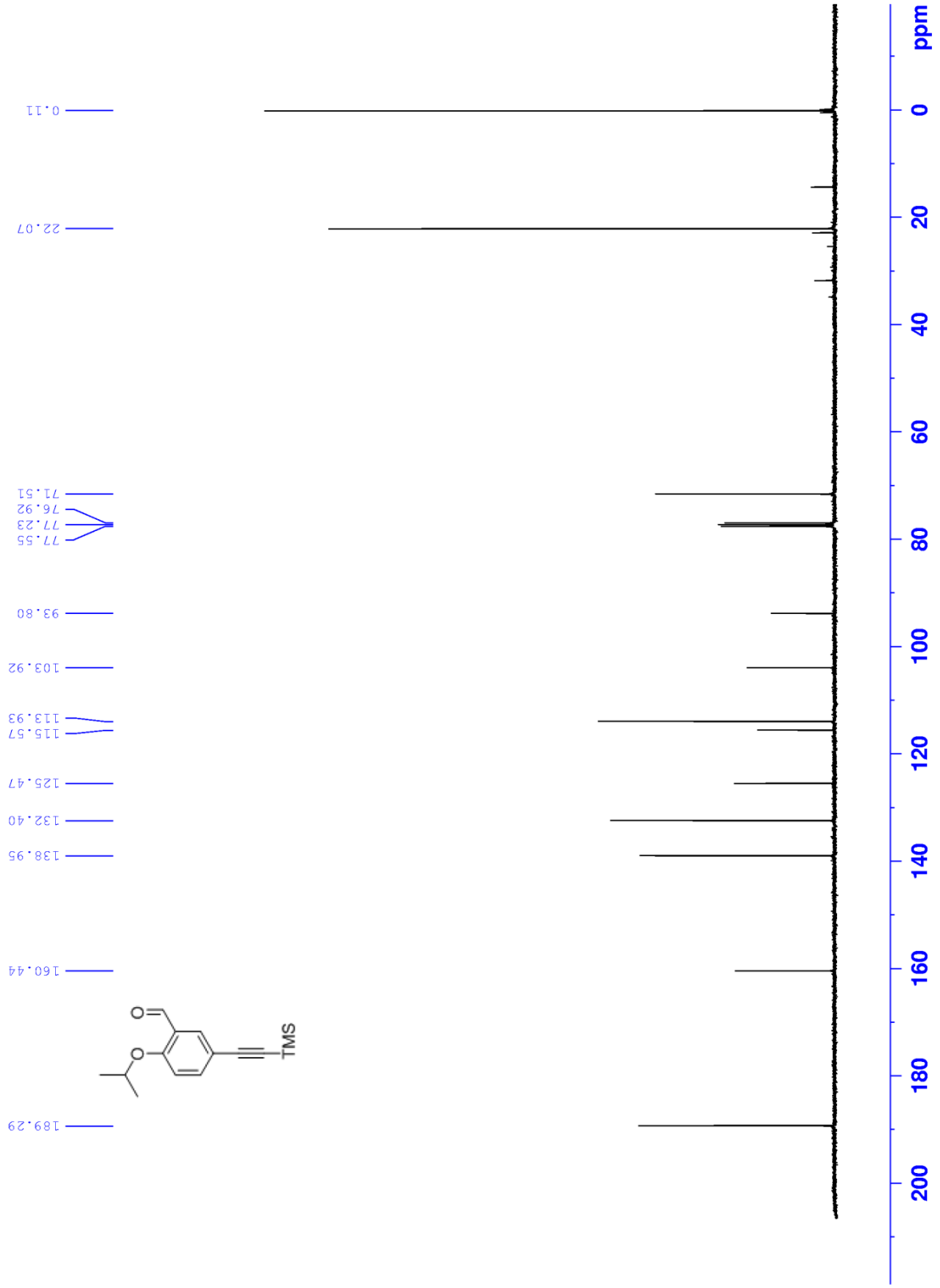

Figure S3.5. ^{1}H NMR spectrum of **5** (500 MHz, $CDCl_3$).

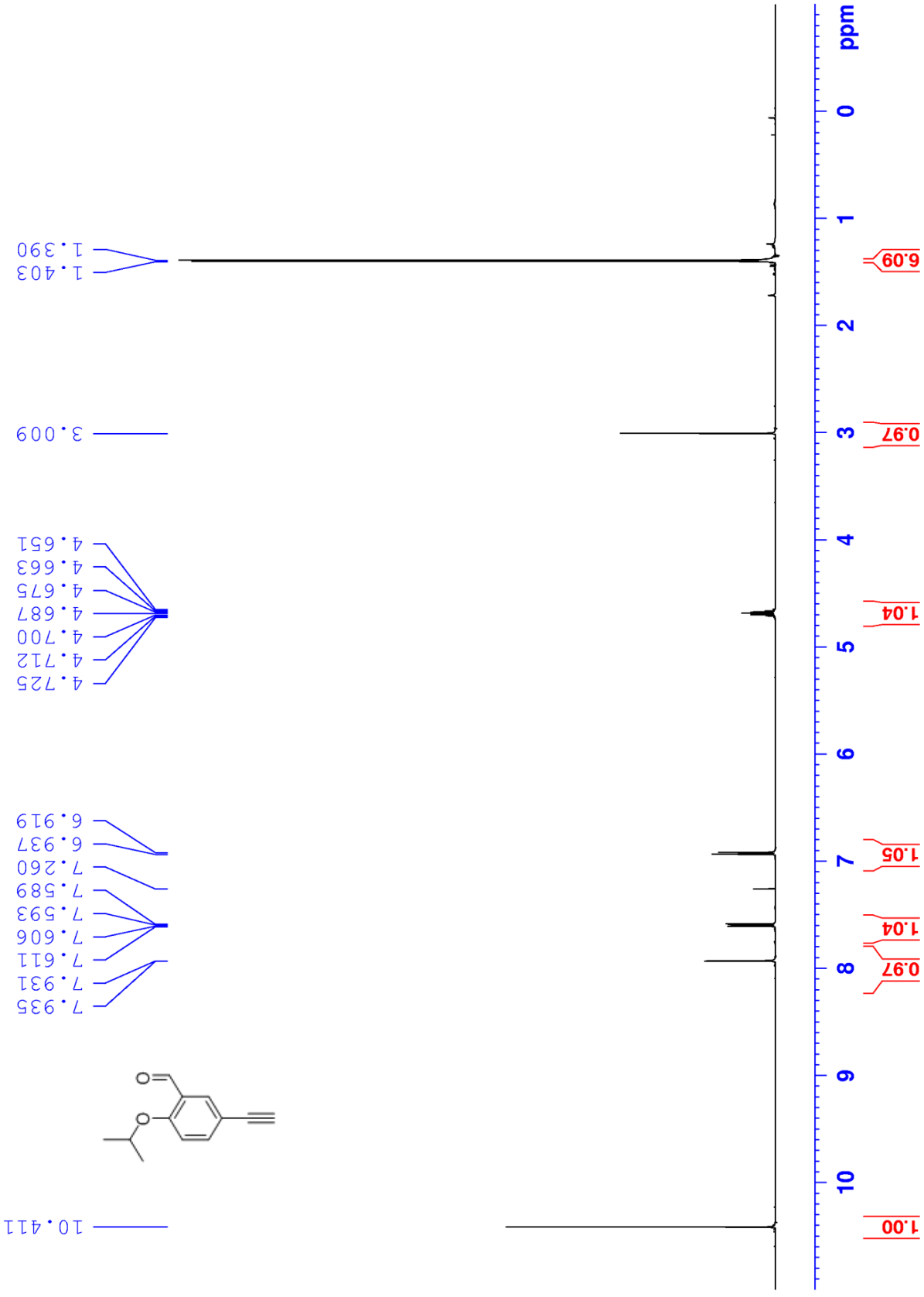

Figure S3.6. ^{13}C NMR spectrum of **5** (125 MHz, $CDCl_3$).

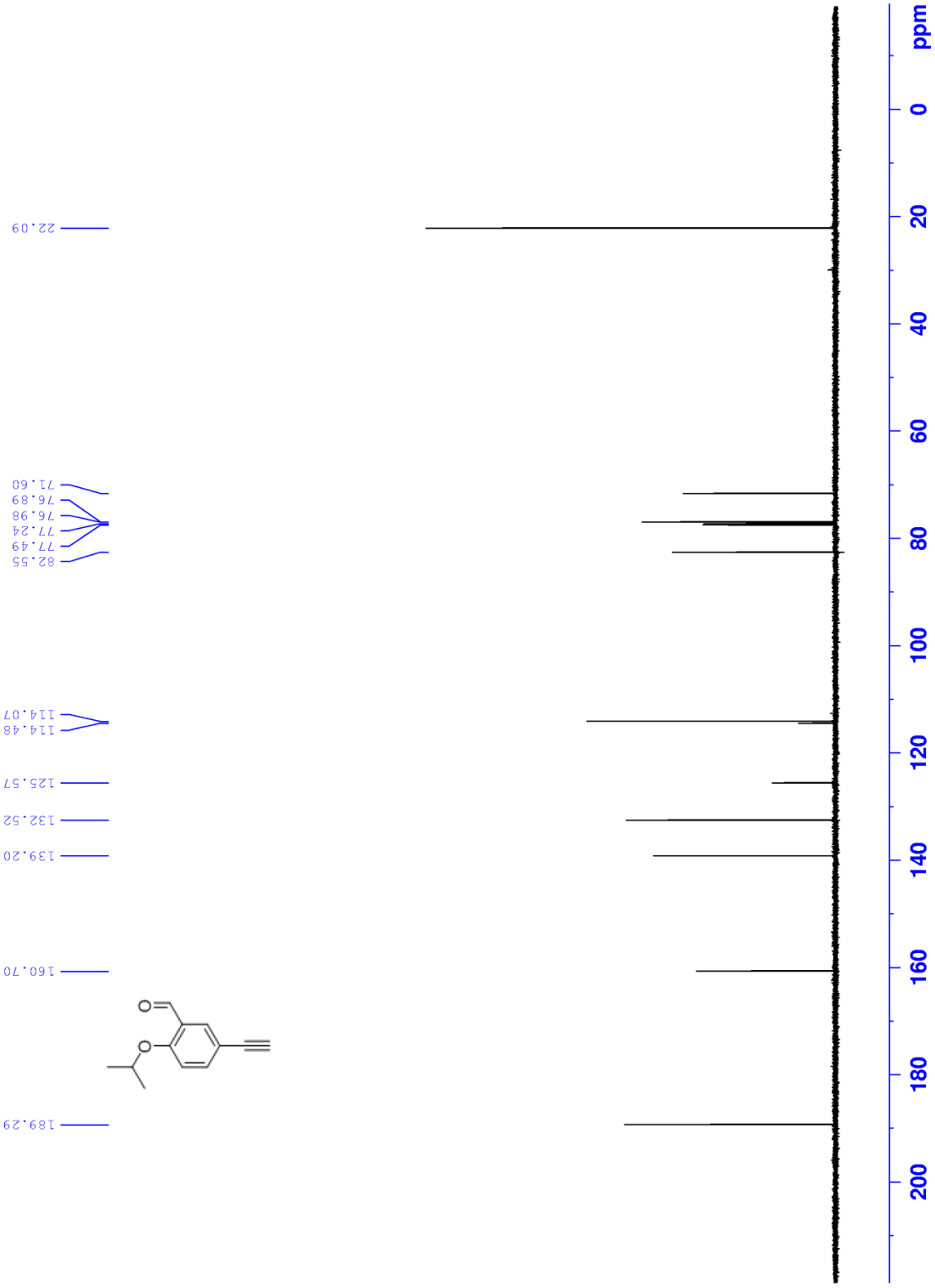

Figure S3.7. ^{1}H NMR spectrum of **8** (500 MHz, $CDCl_3$).

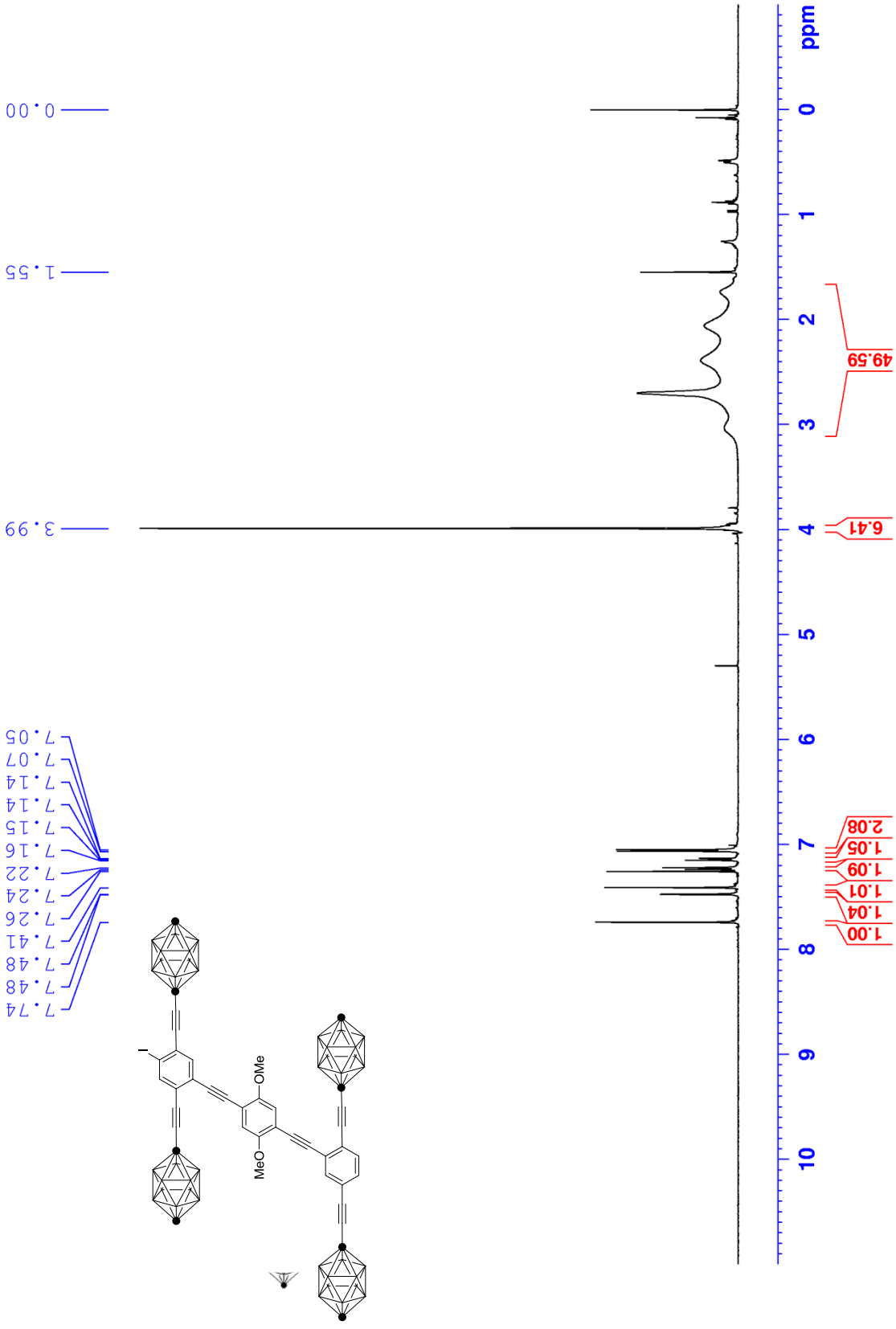

Figure S3.8. ^{13}C NMR spectrum of **8** (125 MHz, $CDCl_3$).

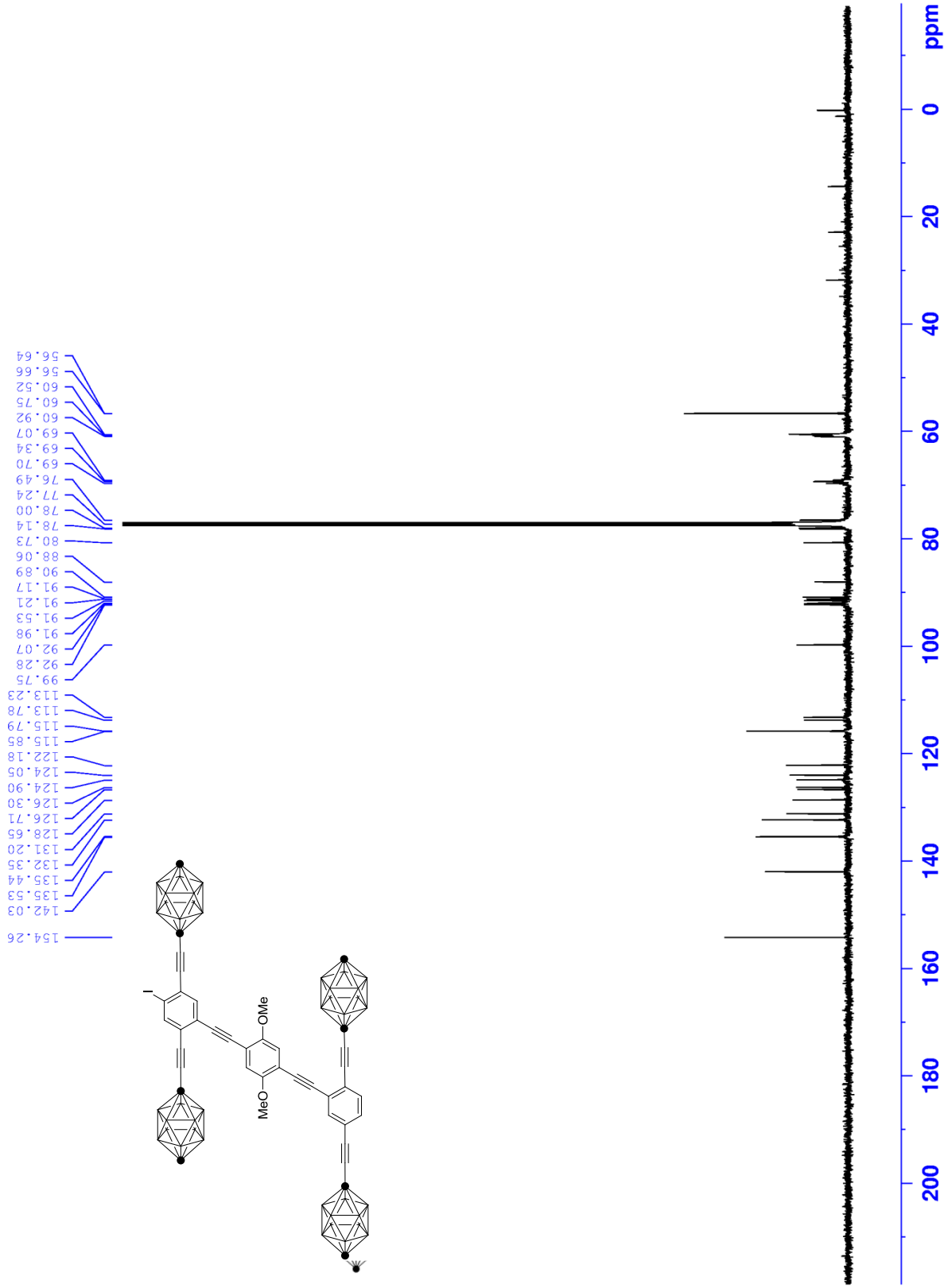

Figure S3.9. ^{1}H NMR spectrum of **9** (400 MHz, $CDCl_3$).

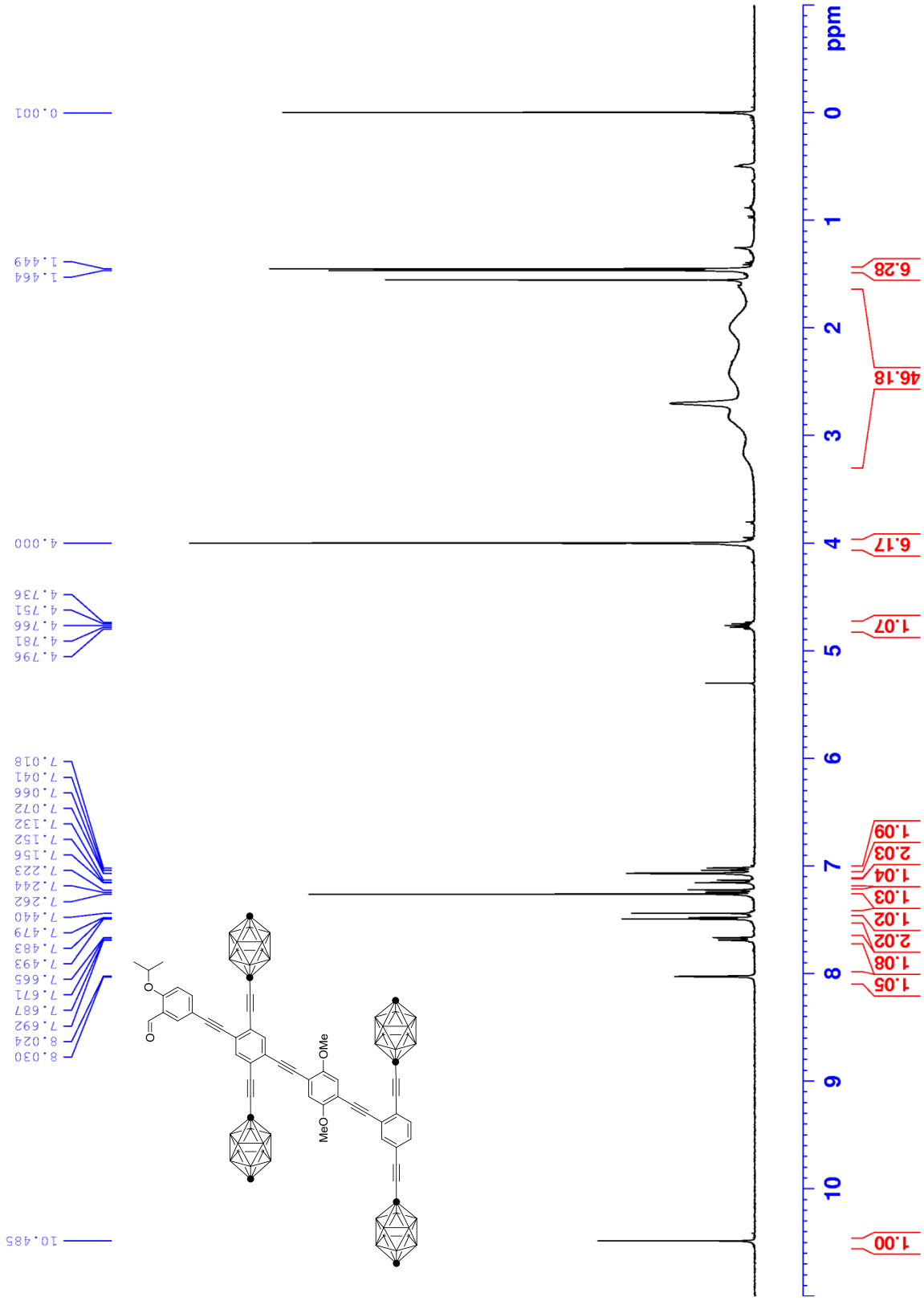

Figure S3.10. ^{13}C NMR spectrum of **9** (125 MHz, $CDCl_3$).

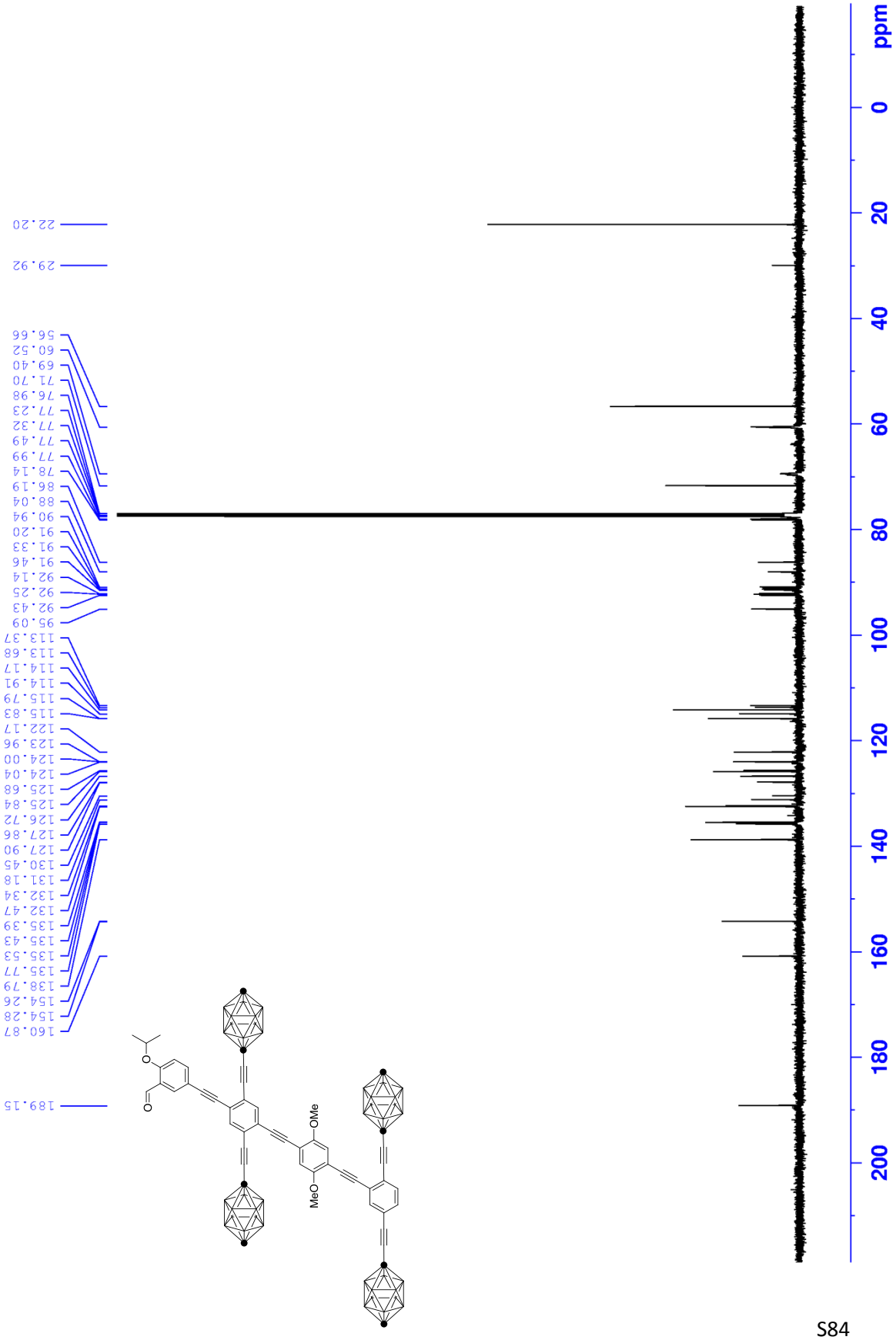

Figure S3.11. ^{1}H NMR spectrum of **10** (500 MHz, $CDCl_3$).

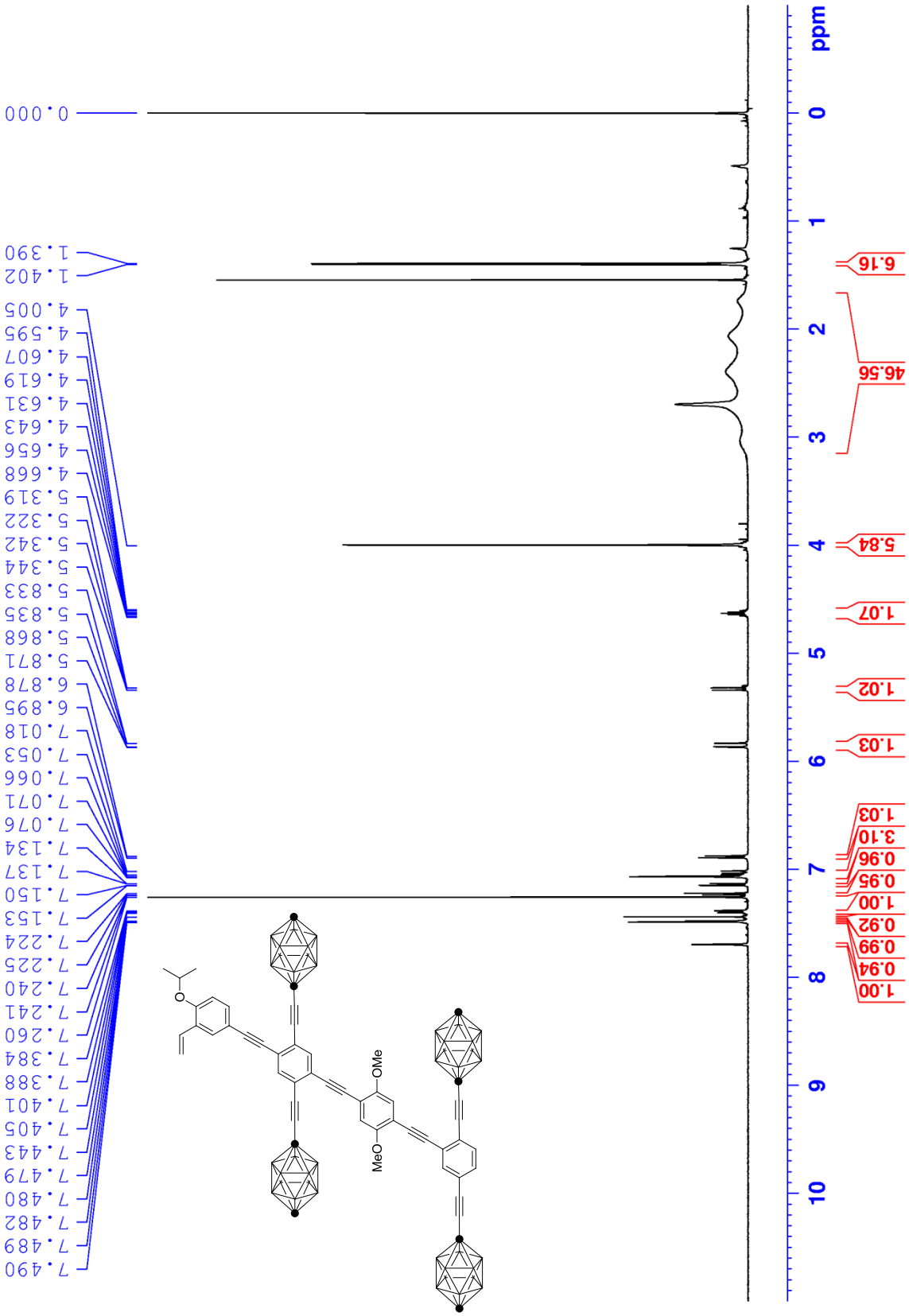

Figure S3.12. Amplification of ^{1}H NMR spectrum of **10** (500 MHz, $CDCl_3$).

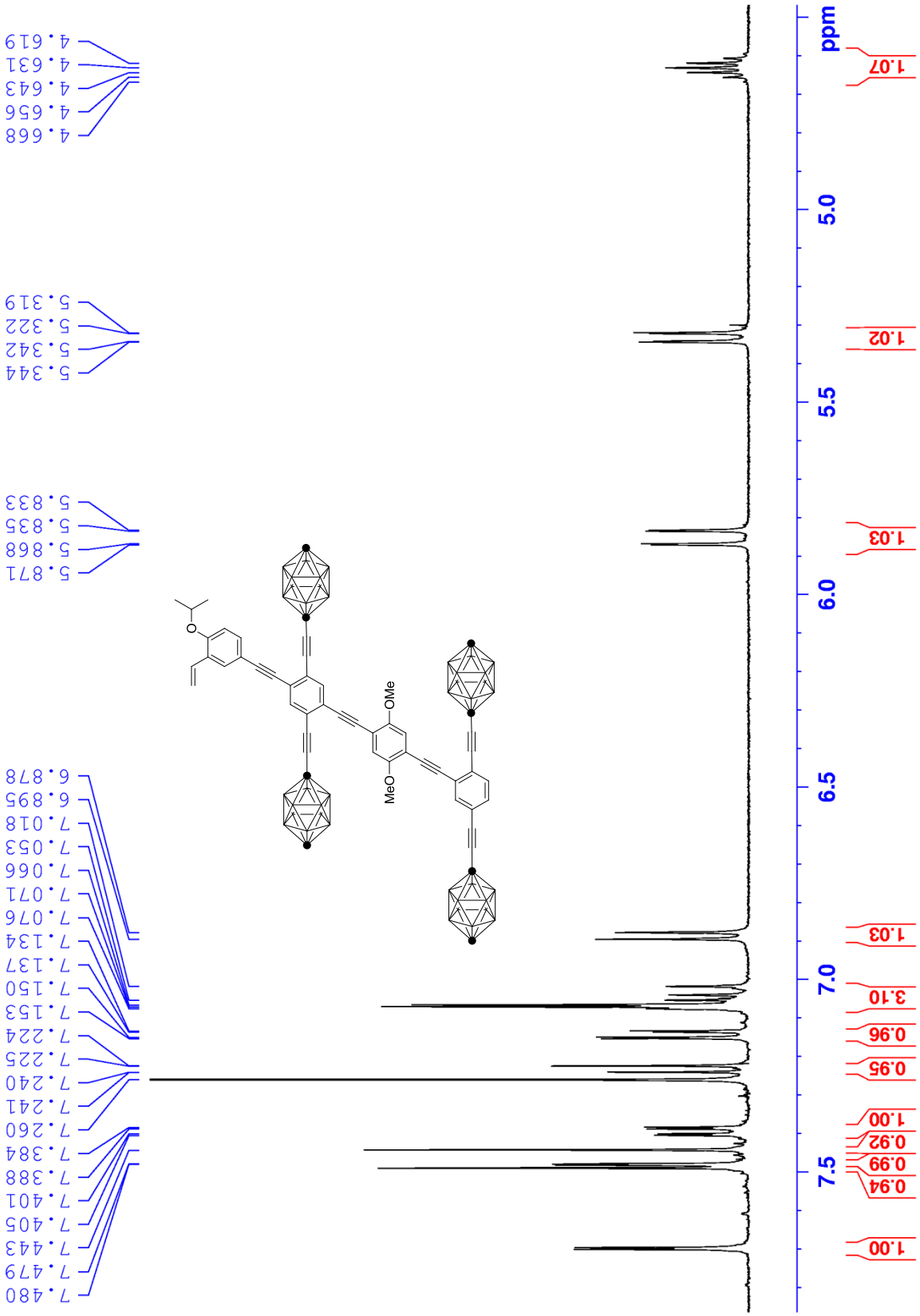

Figure S3.13. ^{13}C NMR spectrum of **10** (125 MHz, $CDCl_3$).

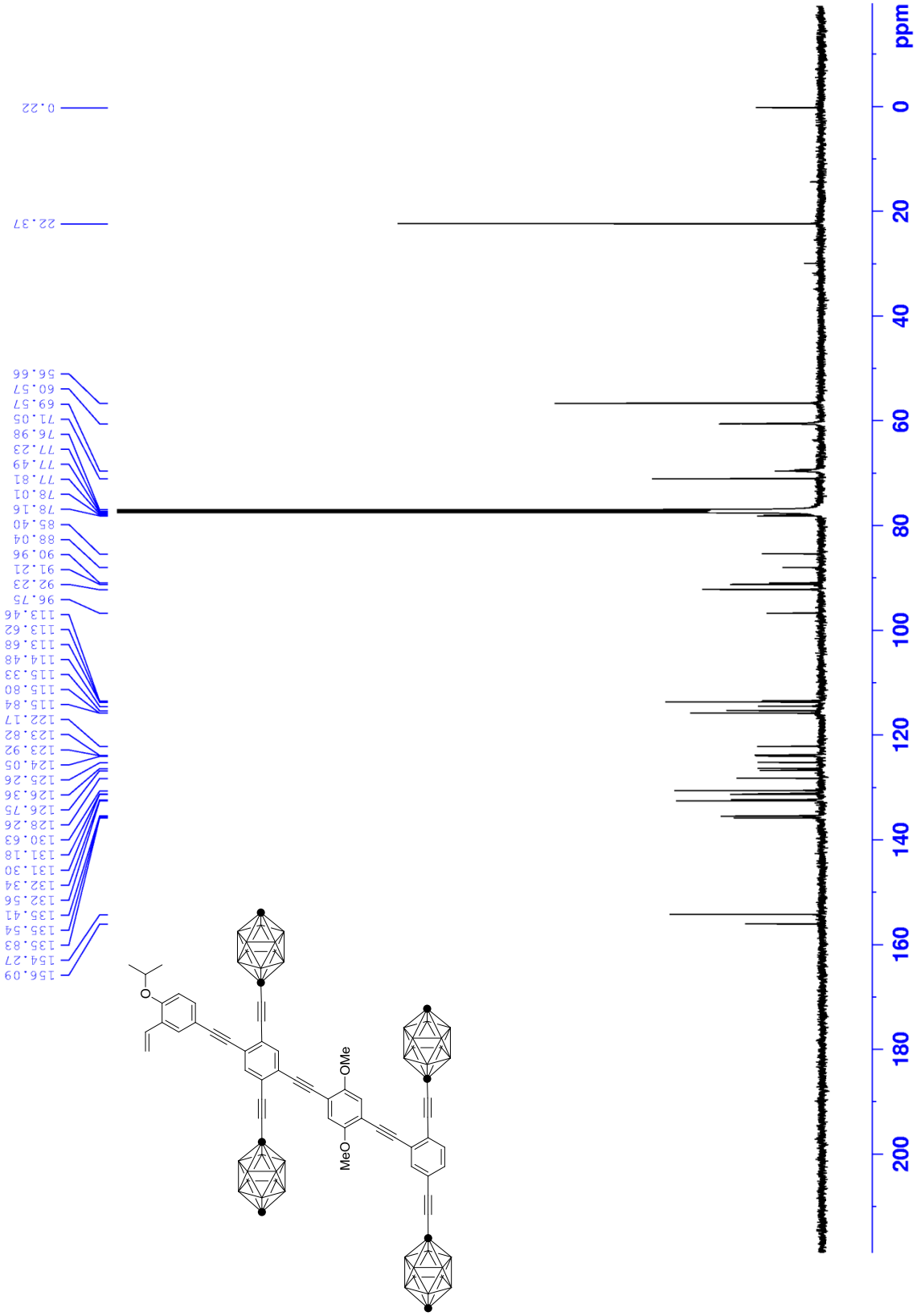

Figure S3.14. ^{1}H NMR spectrum of **1** (500 MHz, $CDCl_3$).

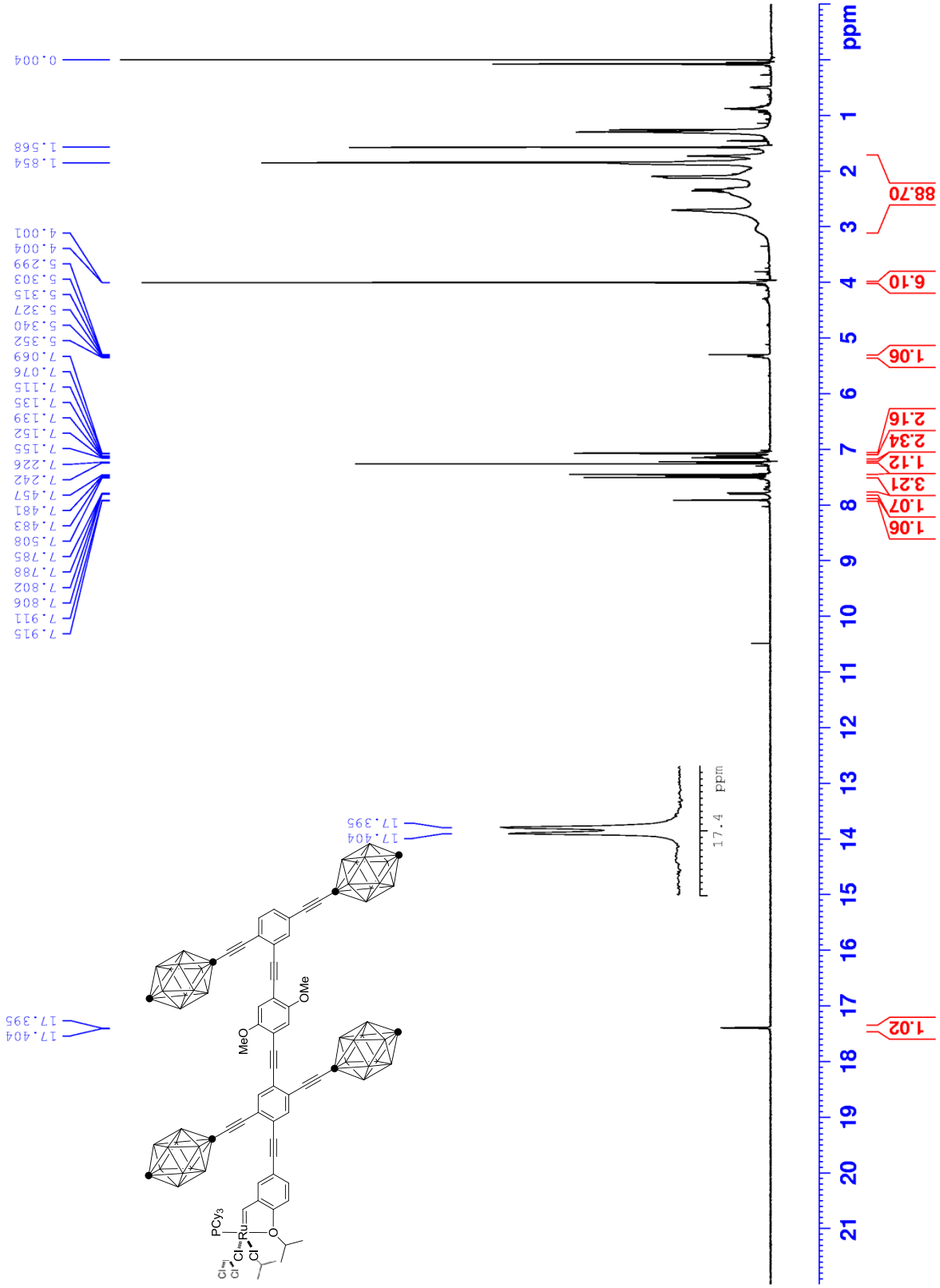

Figure S3.15. Amplification of ^{1}H NMR spectrum of **1** (500 MHz, $CDCl_3$).

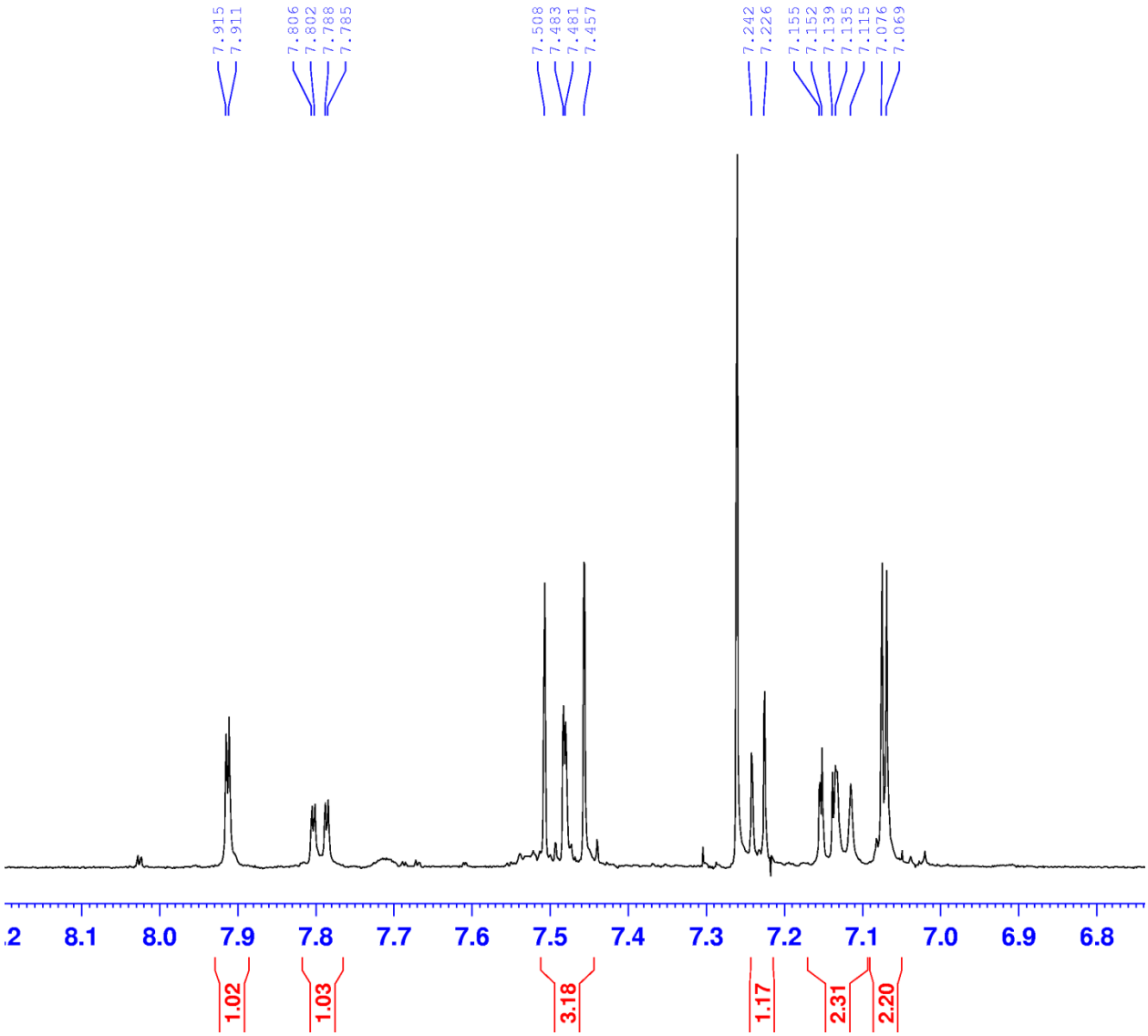

Figure S3.16. ^{13}C NMR spectrum of **1** (125 MHz, $CDCl_3$).

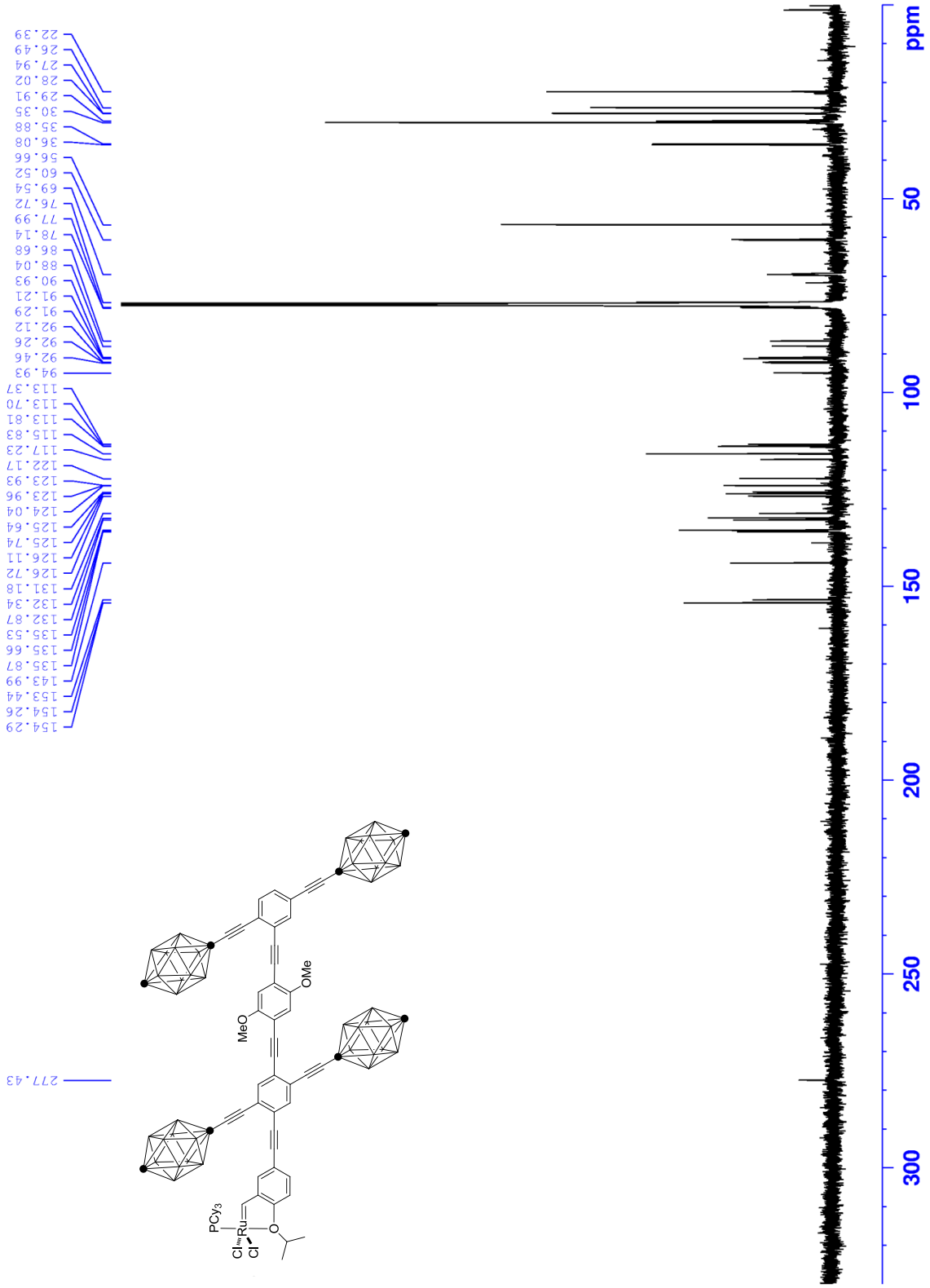

Figure S3.17. Amplification of ^{13}C NMR spectrum of **1** ($CDCl_3$).

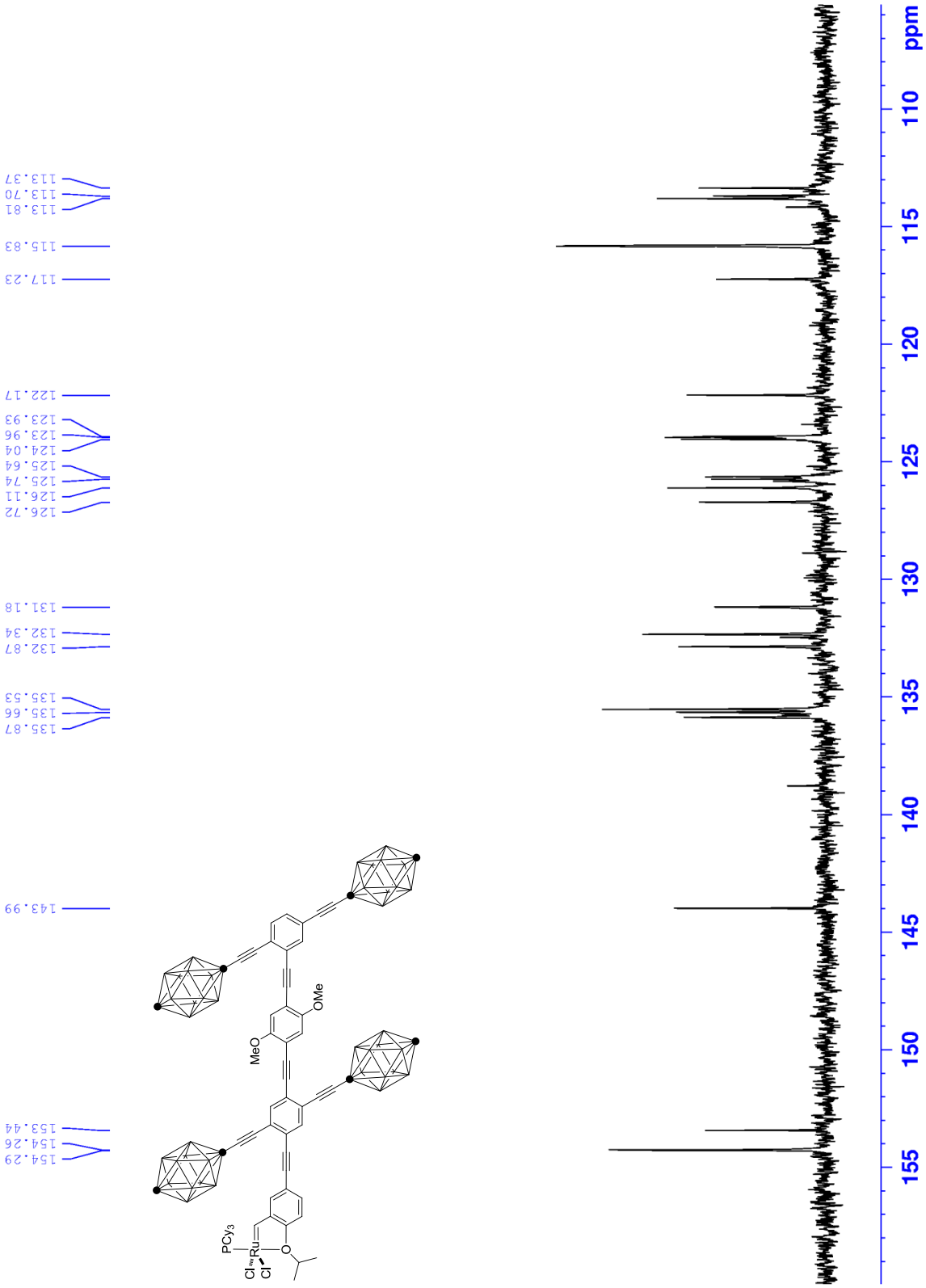

Figure S3.18. ^{31}P NMR spectrum of **1** (202 MHz, $CDCl_3$).

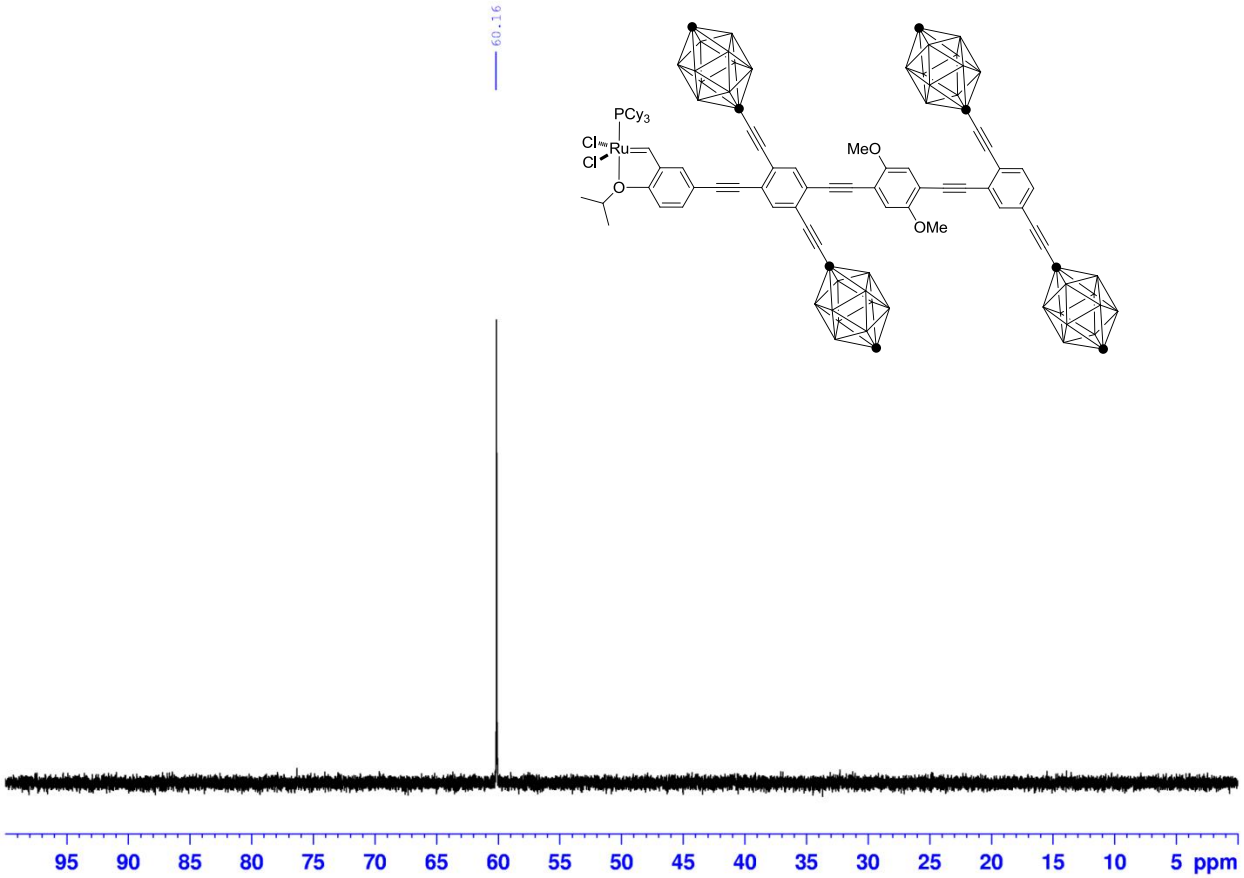

Figure S3.19. ^{1}H NMR spectrum of **2** (500 MHz, $CDCl_3$).

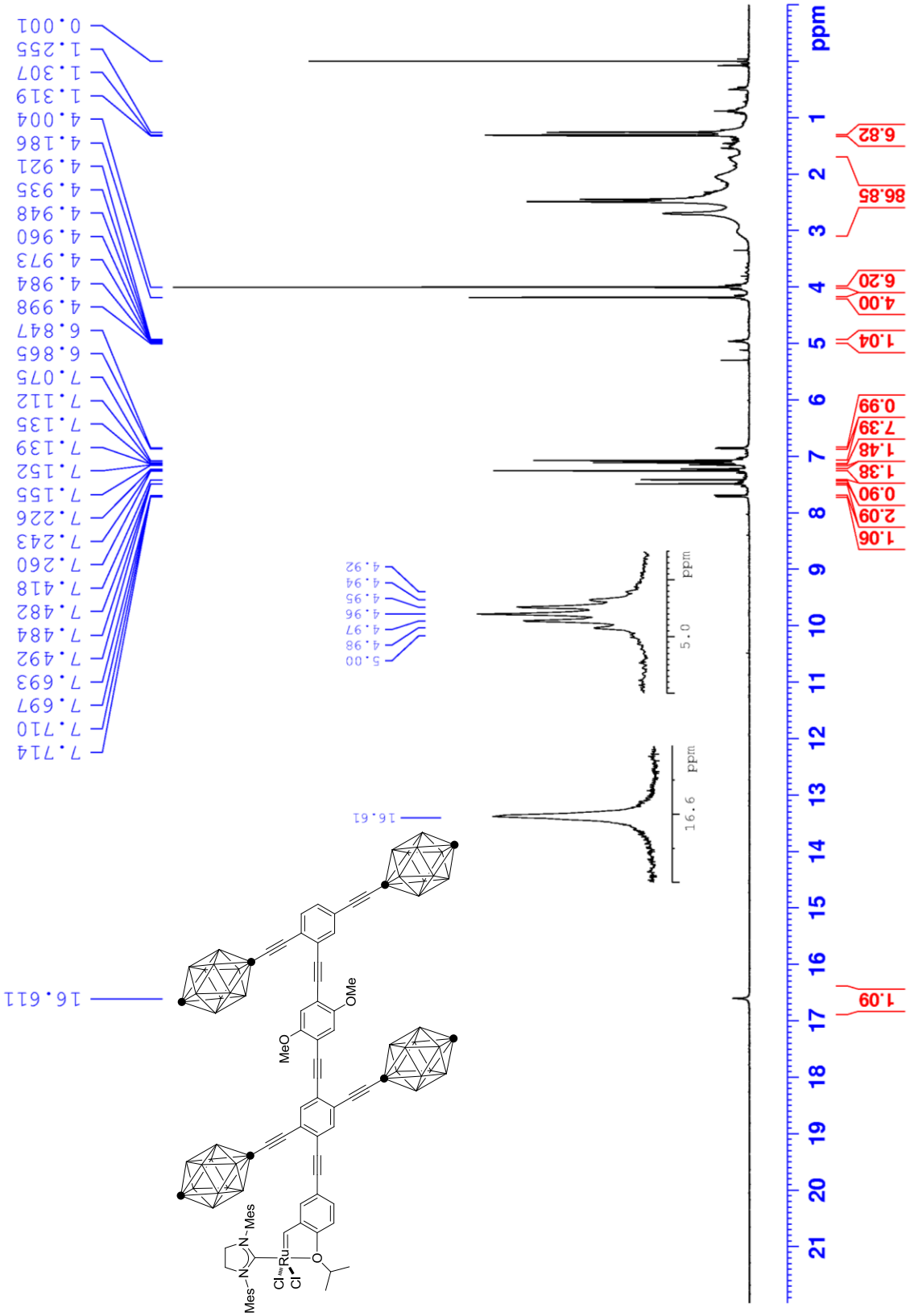

Figure S3.20. Amplification of ^{1}H NMR spectrum of **2** (500 MHz, $CDCl_3$).

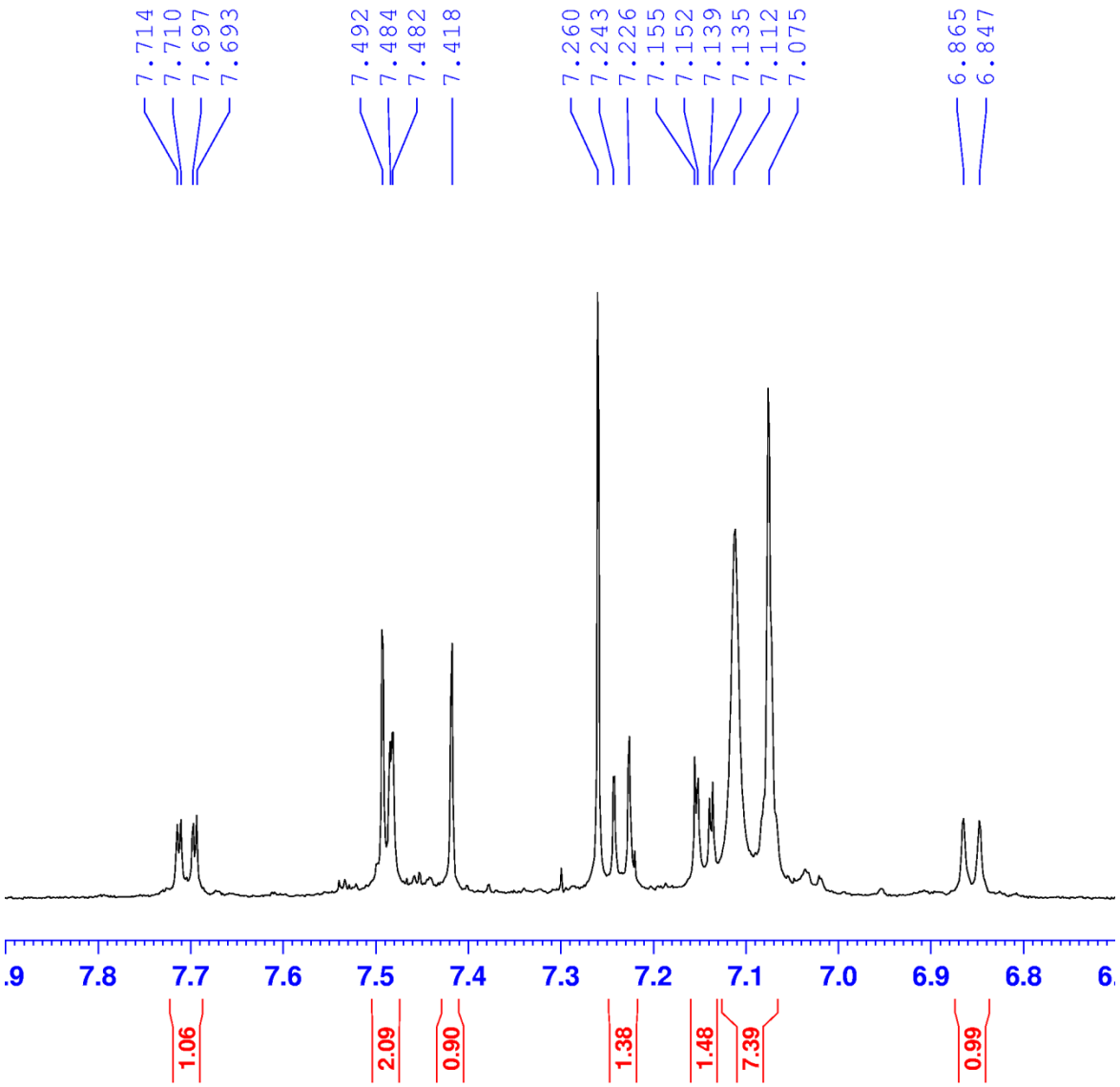

Figure S3.21. ^{13}C NMR spectrum of **2** (125 MHz, $CDCl_3$).

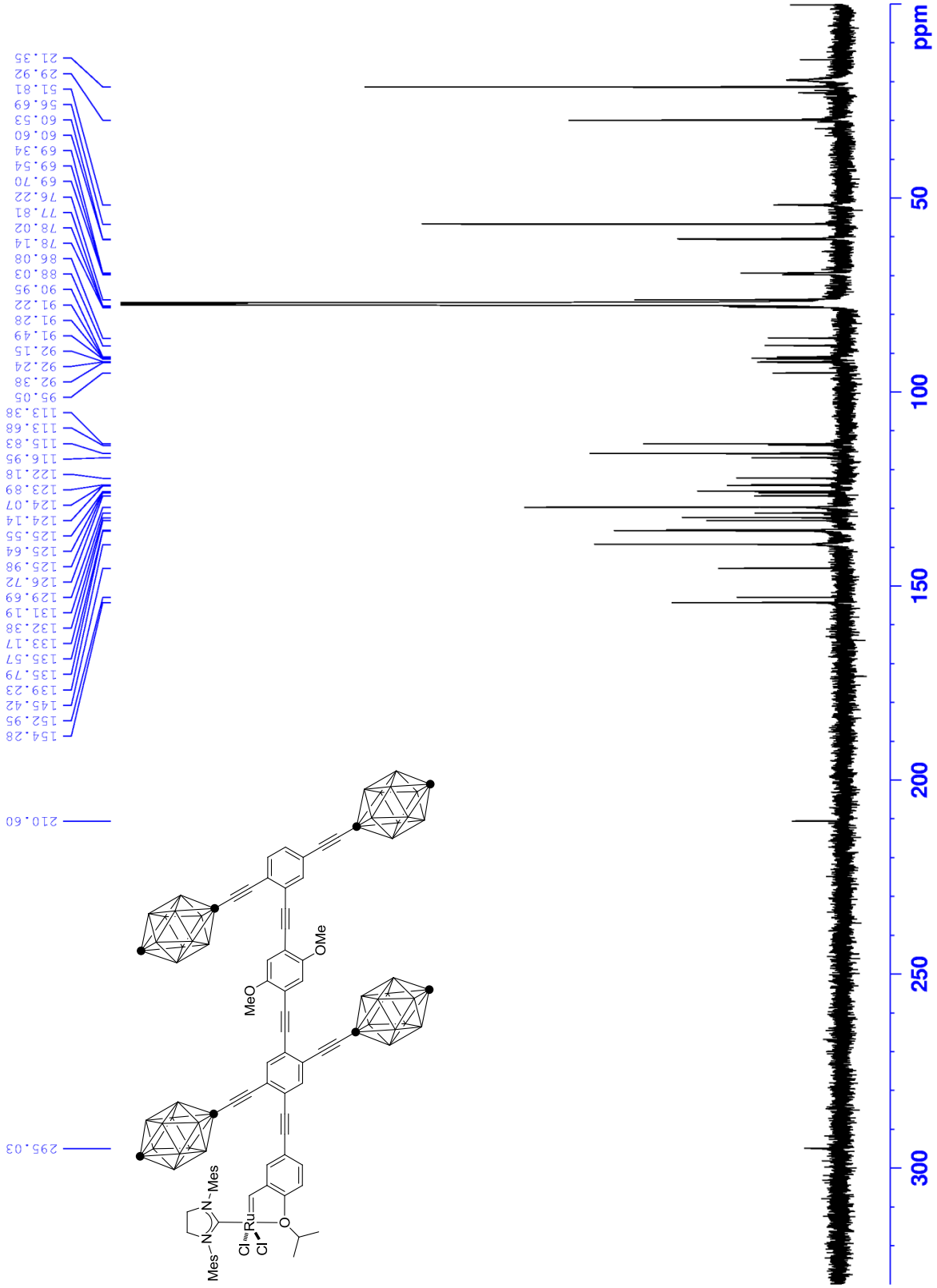

Figure S3.22. Amplification of ^{13}C NMR spectrum of **2** (125 MHz, $CDCl_3$).

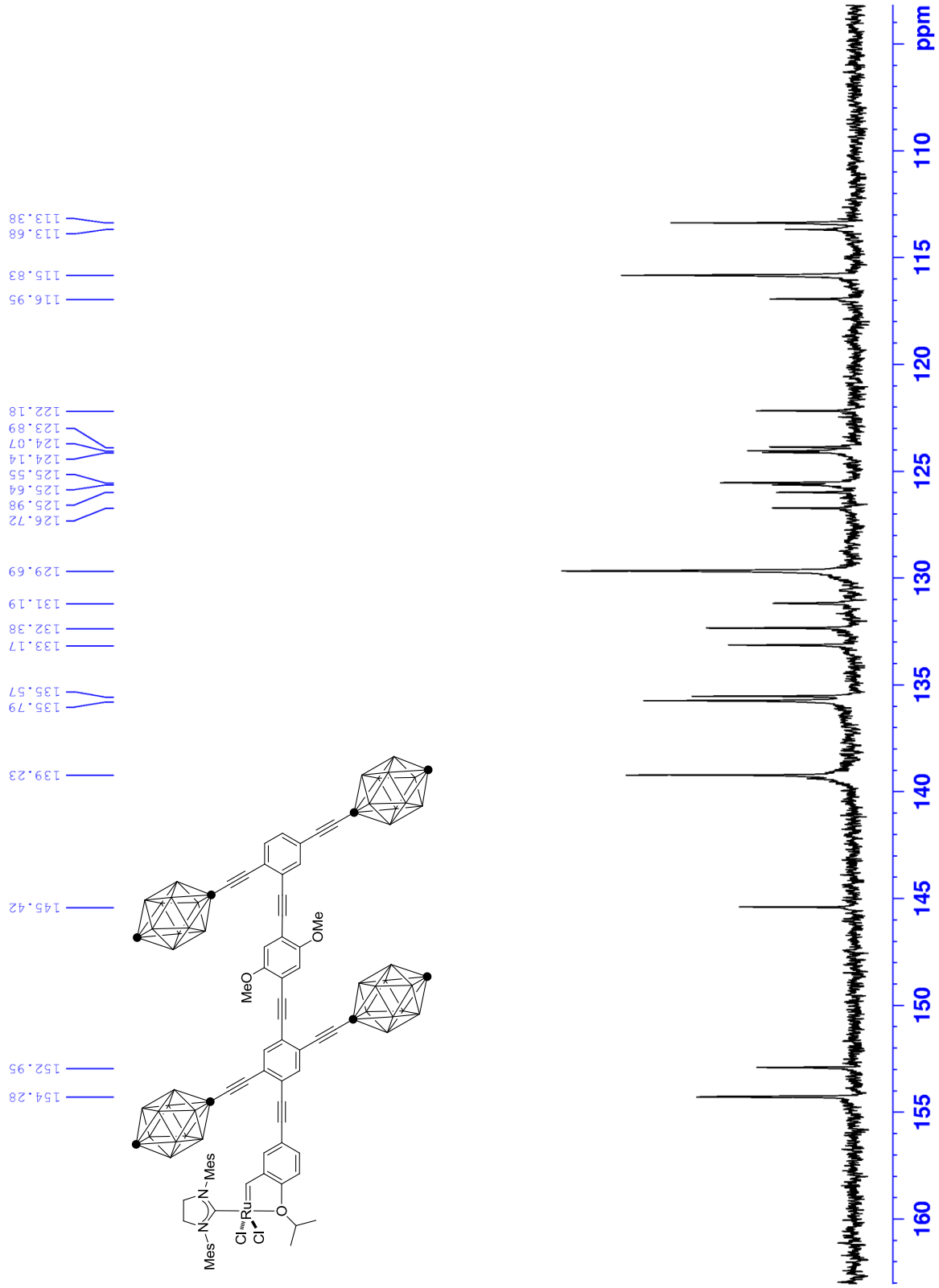

ROMP of 1,5 cyclooctadiene

Catalytic activity of 1. 102 μL of a 4.0 mM solution, 0.70 mL of CD_2Cl_2.

Table S3.1. Conversion to polymer product using **1**.

Time (min)	Conversion (%)
3.8	1.9
4.8	2.5
5.8	2.5
6.8	2.8
7.8	3.1
8.8	3.0
9.8	3.3
10.8	3.3
11.8	3.6
12.8	3.7
13.8	3.6
14.8	3.9
15.8	3.7
16.8	3.9
17.8	4.0
18.8	3.9
19.8	4.1
20.8	3.9
21.8	4.3
22.8	4.2

Time (min)	Conversion (%)
23.8	4.0
24.8	4.3
25.8	4.3
26.8	4.1
27.8	4.4
28.8	4.3
29.8	4.4
30.8	4.5
31.8	4.3
32.8	4.4
33.8	4.5
34.8	4.6
35.8	4.6
36.8	4.5
37.8	4.6
38.8	4.6
39.8	4.8
40.8	4.6
41.8	4.6
42.8	4.6
43.8	4.7
44.8	4.7
45.8	4.9
46.8	4.8
47.8	5.0

Time (min)	Conversion (%)
48.8	5.0
49.8	4.9
50.8	5.0
51.8	5.0
52.8	5.0
53.8	5.1
54.8	5.2
55.8	5.0
56.8	5.3
57.8	5.1
58.8	5.1
59.8	5.3
60.8	5.2

Catalytic activity of 2. 120 μL of a 3.3 mM solution, 0.68 mL of CD_2Cl_2.

Table S3.2. Conversion to polymer product using **2**.

Time (min)	Conversion (%)
3.0	99.4
4.0	99.8
5.0	99.9
6.0	99.9
7.0	100.0
8.0	100.0
9.0	100.0
10.0	100.0
11.0	99.9
12.0	100.0
13.0	100.0
14.0	100.0
15.0	100.0
16.0	100.0
17.0	100.0

18.0	100.0

In order to determine if our experimental setup was in good agreement with the standard system developed by Grubbs[4] and therefore producing comparable results, we measured the activity of catalysts **11** and 1**2**.

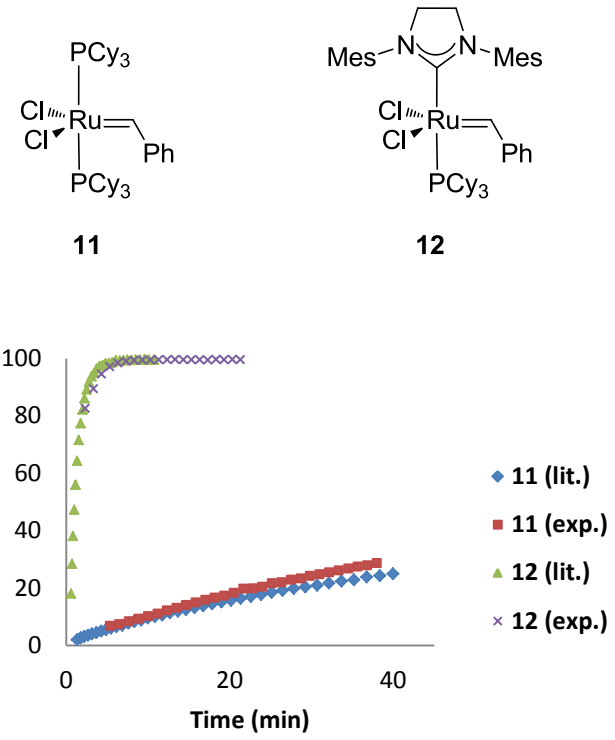

Figure S3.23. Observed polymerization (exp.) versus previously reported data (lit).

ROMP of norbornene with 1. A 3-neck 25 mL round-bottom flask equipped with a magnetic stir bar was charged with a solution of norbornene (35.3 mg, 0.37 mmol) in CH_2Cl_2 (6 mL). Complex **1** (100 µL of a 3.75 mM solution, 0.37 µmol) was added in one portion and the mixture was stirred 10 min at rt. The solvent was evaporated. The polymer was washed with MeOH to afford ring-opened polynorbornene (32.0 mg, 91%).

Supporting Information of

Chapter 4

A Polymerization-Propelled 'Nanosubmarine': Synthesis and Diffusion Studies

^{1}H and ^{13}C NMR spectra of new compounds

Figure S4.1. ^{1}H NMR spectrum of 4-ethynyl benzyl alcohol (400 MHz, $CDCl_3$).

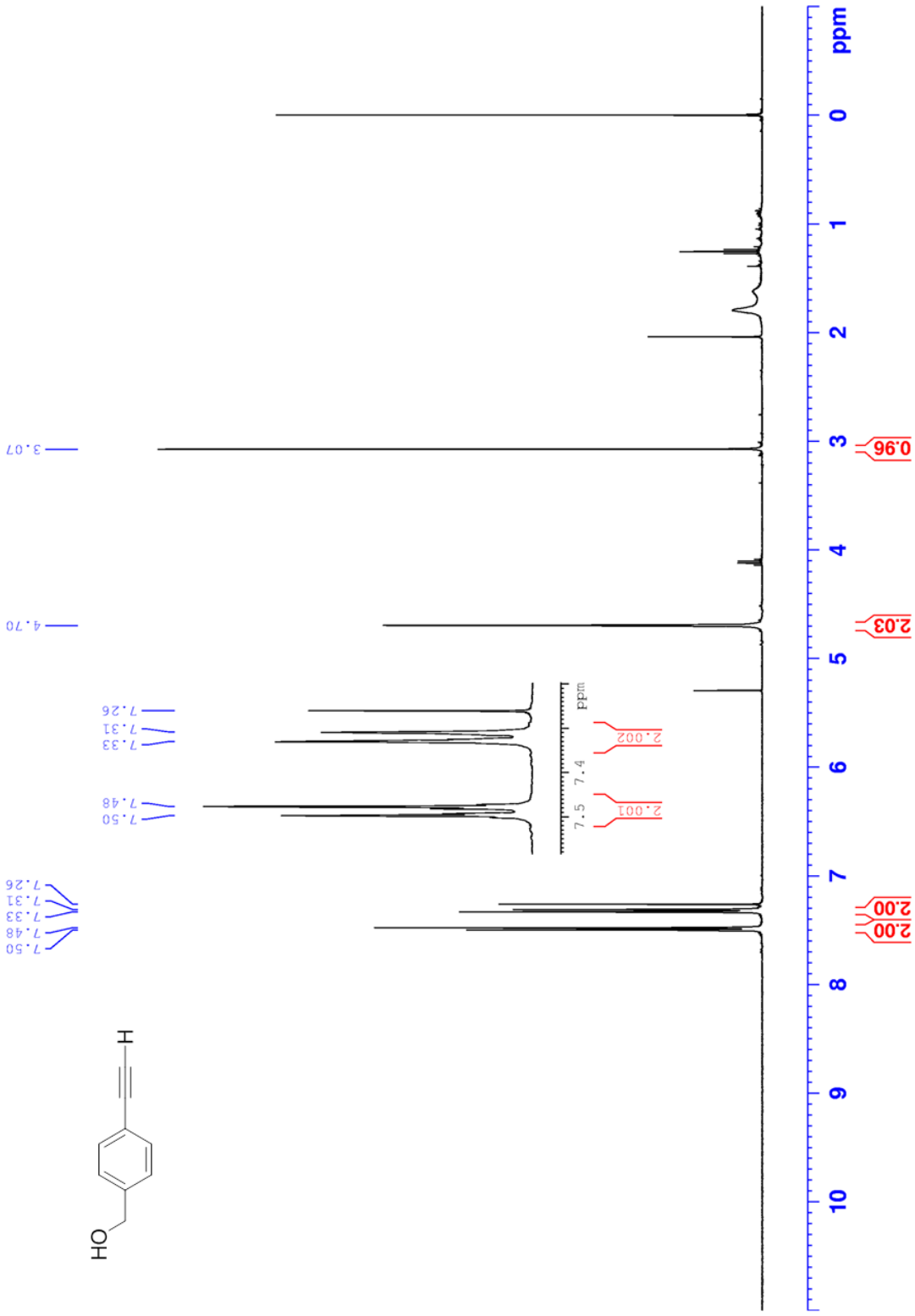

Figure S4.2. ^{1}H NMR spectrum of BODIPY **7** (400 MHz, $CDCl_3$).

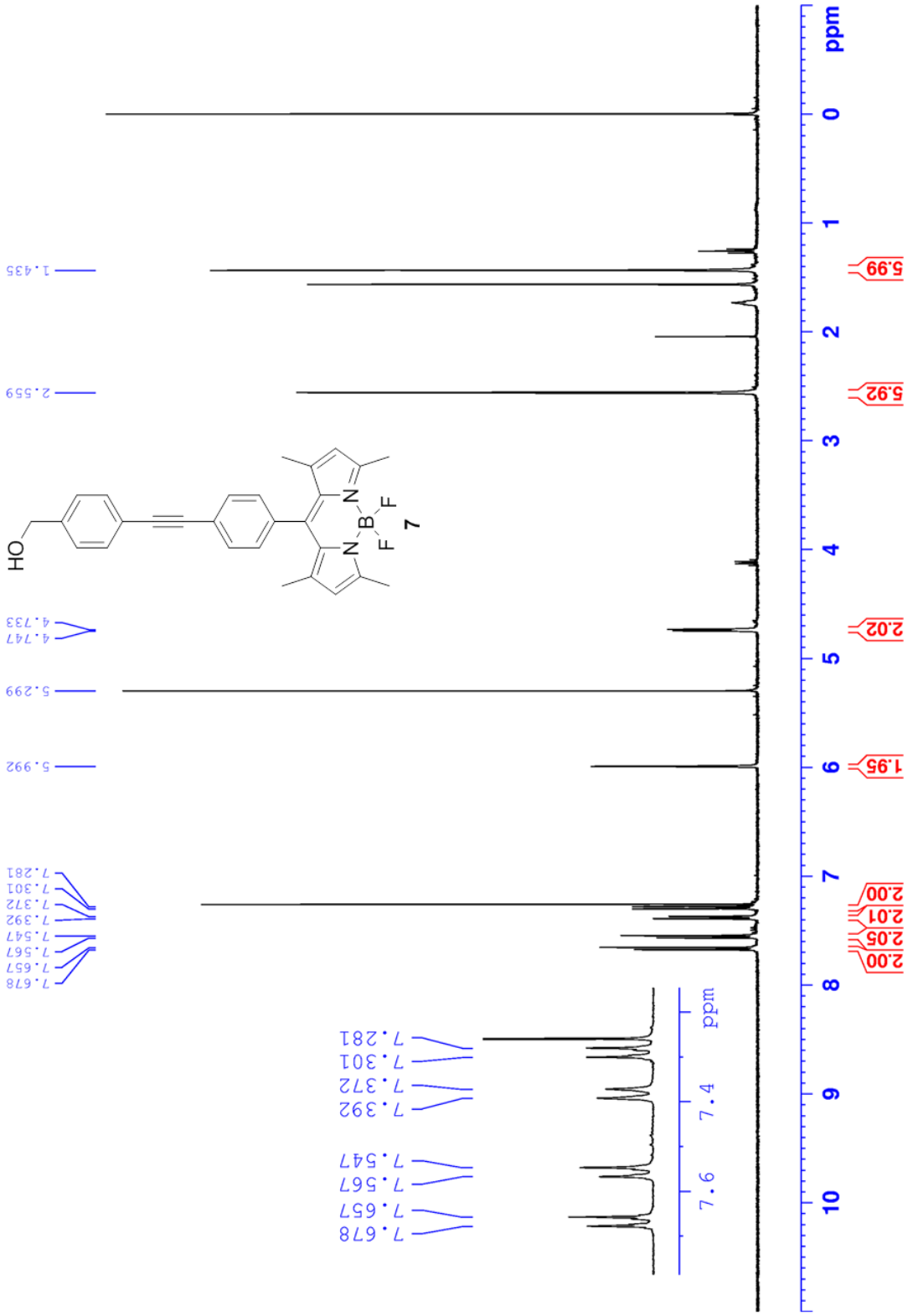

Figure S4.3. ^{13}C NMR spectrum of BODIPY **7** (100 MHz, $CDCl_3$).

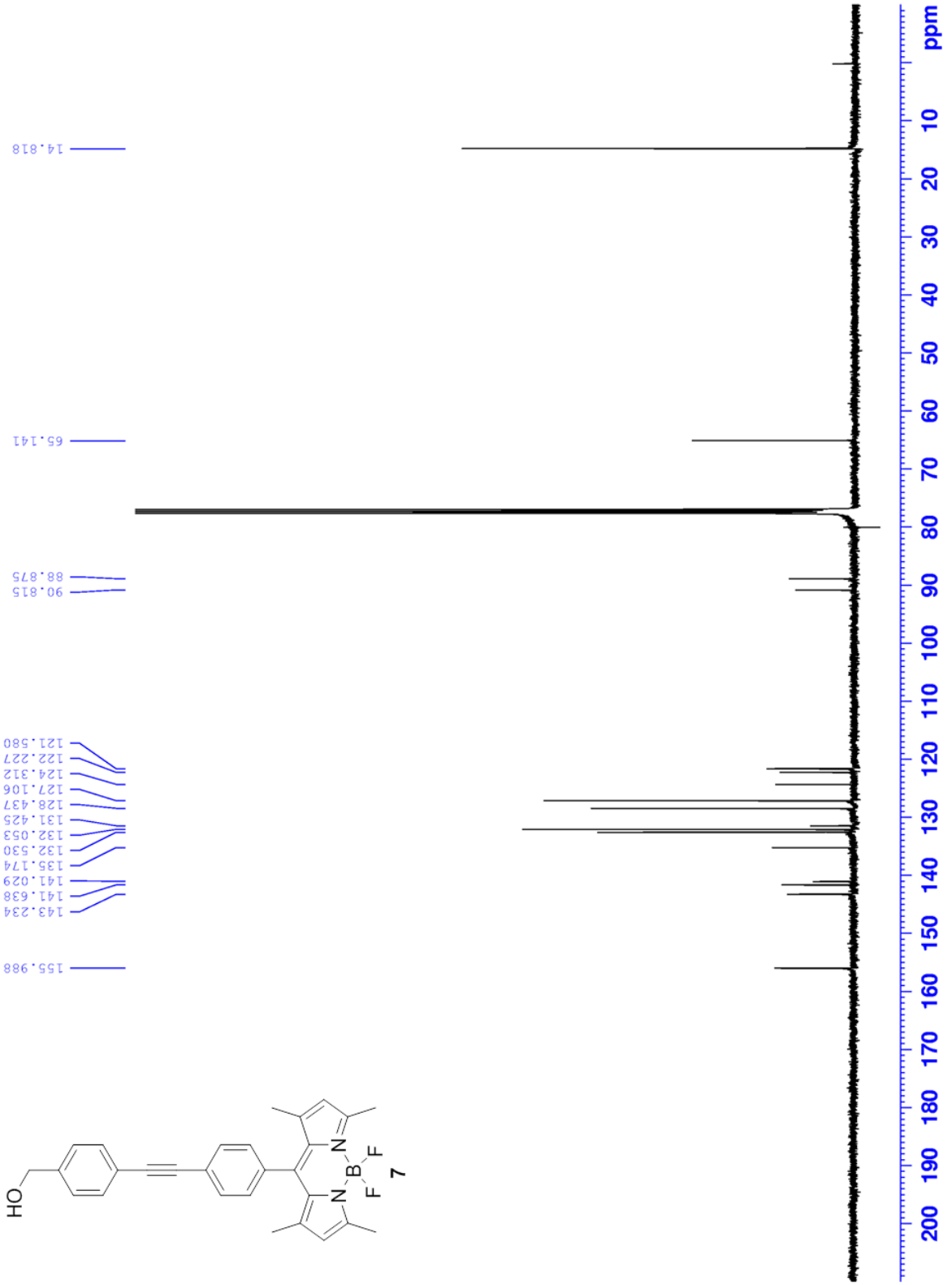

Figure S4.4. ^{1}H NMR spectrum of BODIPY **8** (400 MHz, $CDCl_3$).

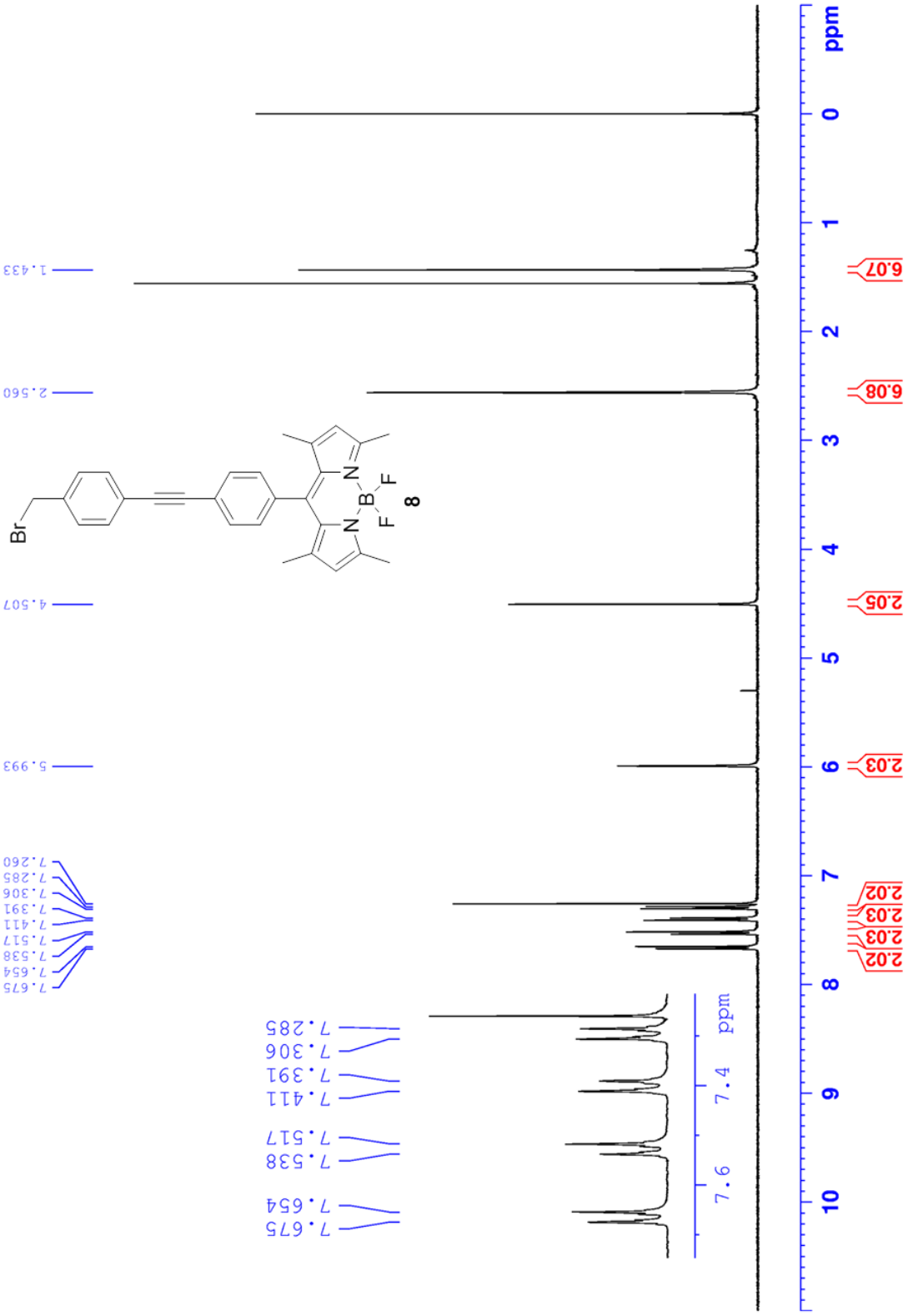

Figure S4.5. ^{13}C NMR spectrum of BODIPY **8** (100 MHz, $CDCl_3$).

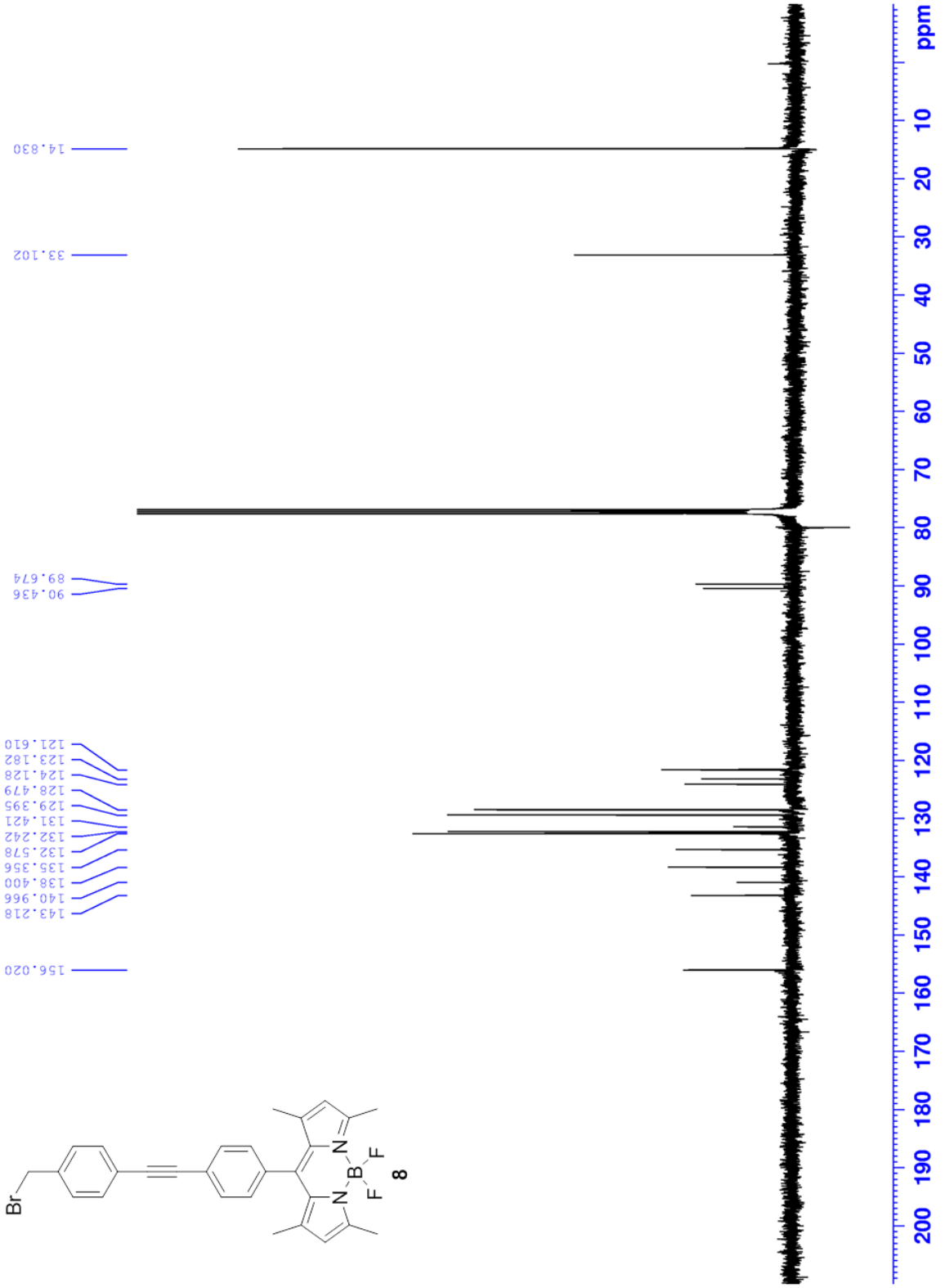

Figure S4.6. ^{1}H NMR spectrum of **4** (400 MHz, DMSO-d6).

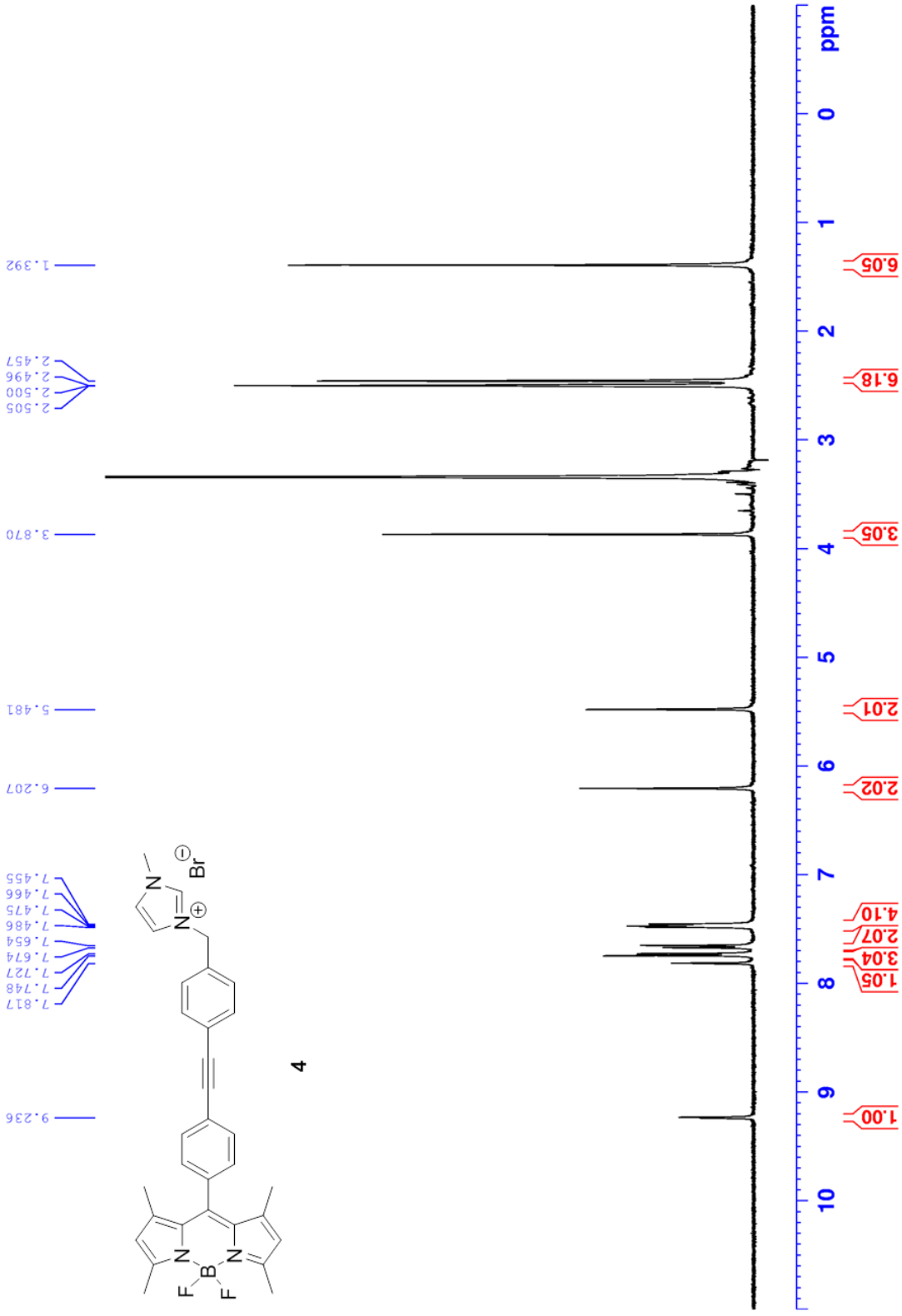

Figure S4.7. ^{13}C NMR spectrum of **4** (125 MHz, DMSO-d6).

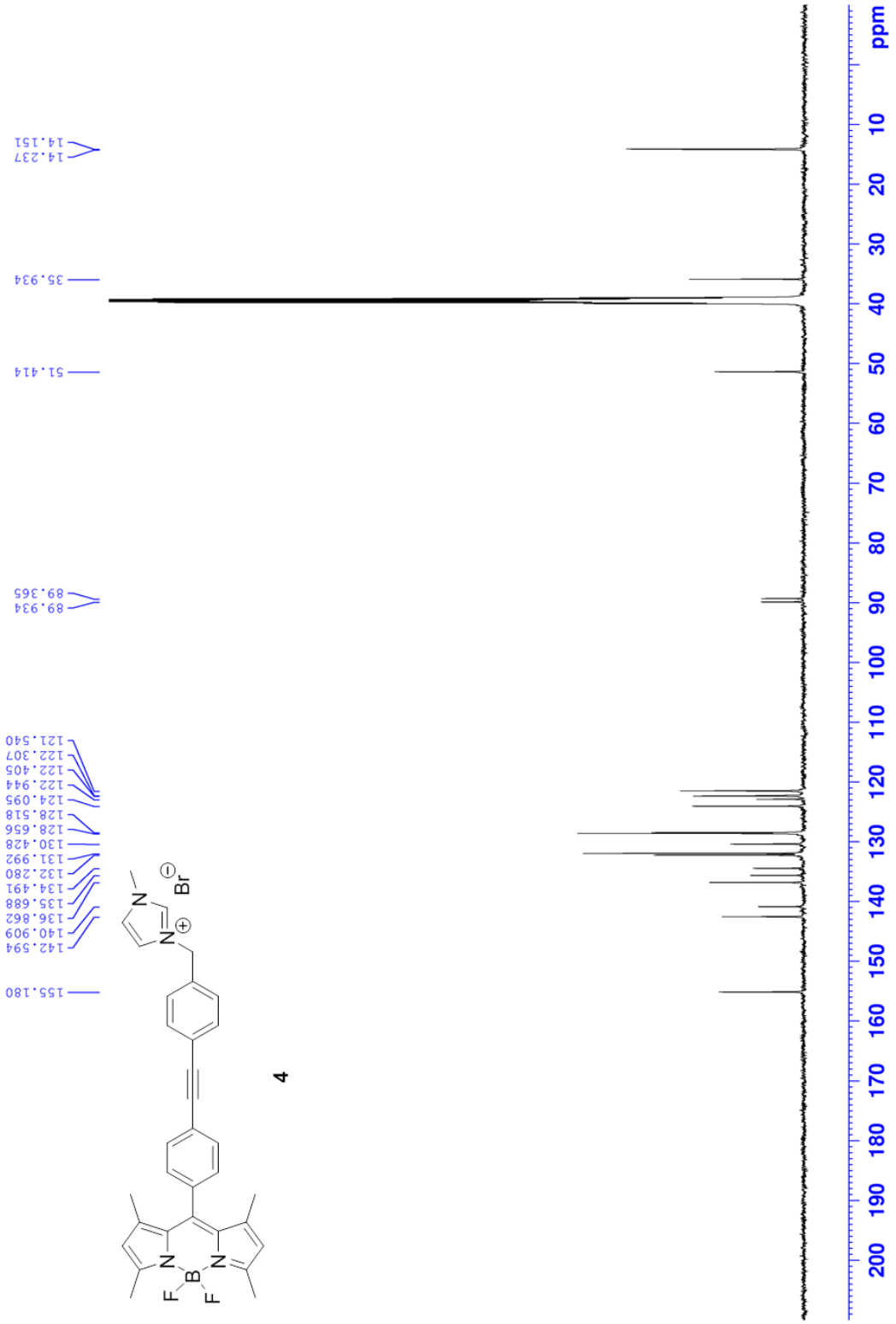

Figure S4.8. ^{1}H NMR spectrum of BODIPY **10** (400 MHz, $CDCl_3$).

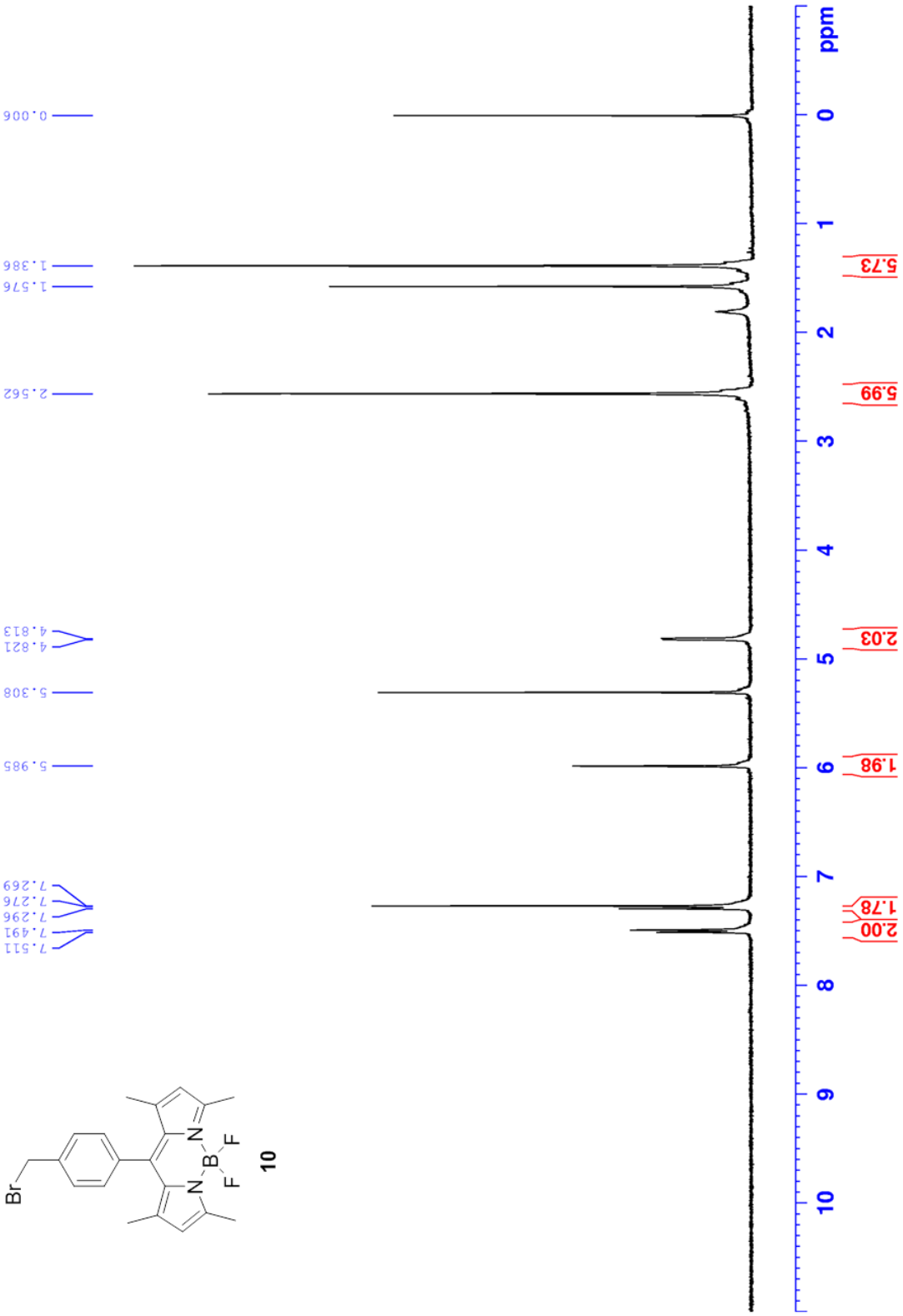

Figure S4.9. ^{13}C NMR spectrum of BODIPY **10** ($CDCl_3$).

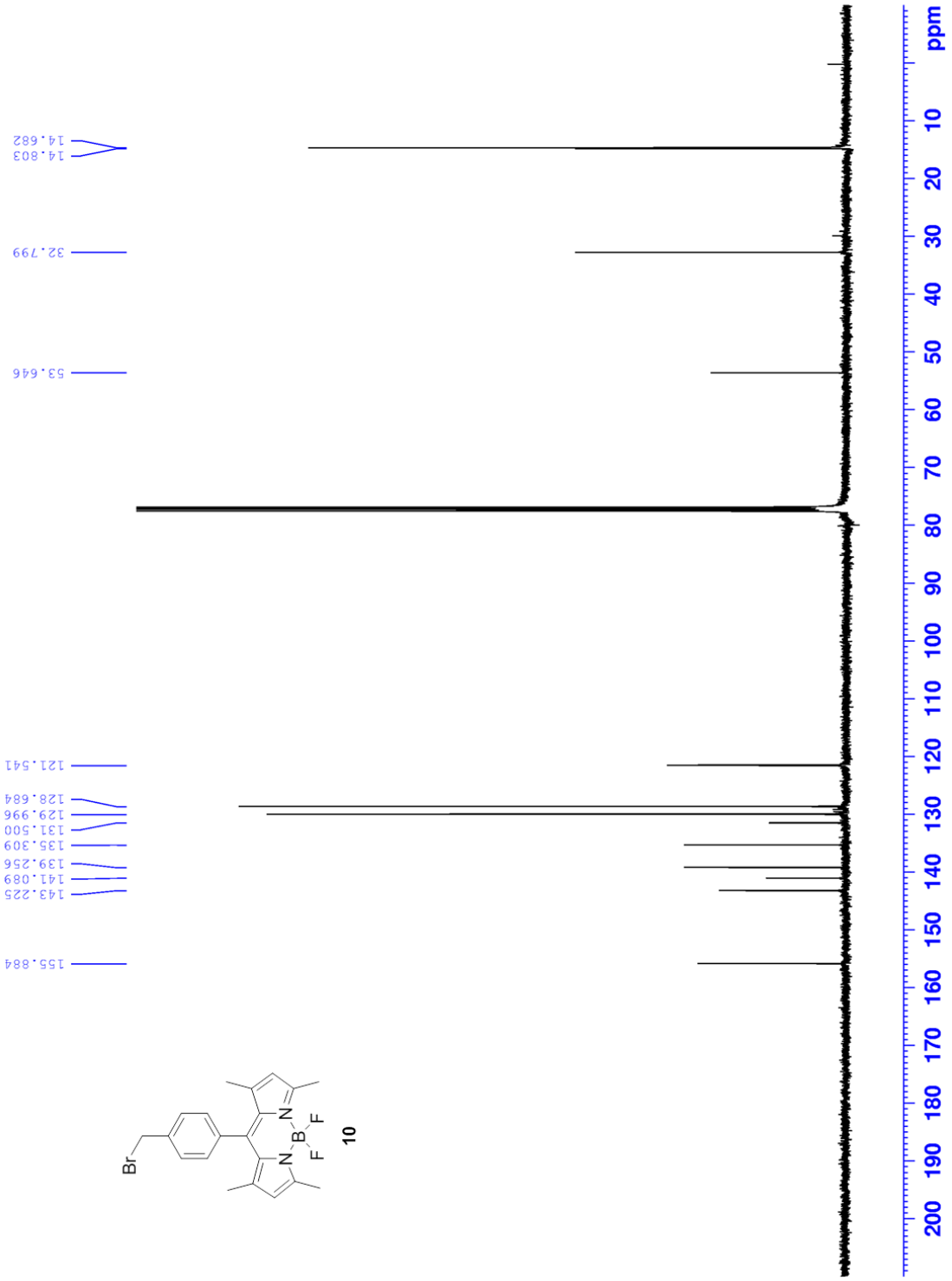

Figure S4.10. ^{1}H NMR spectrum of **5** (400 MHz, DMSO-d6).

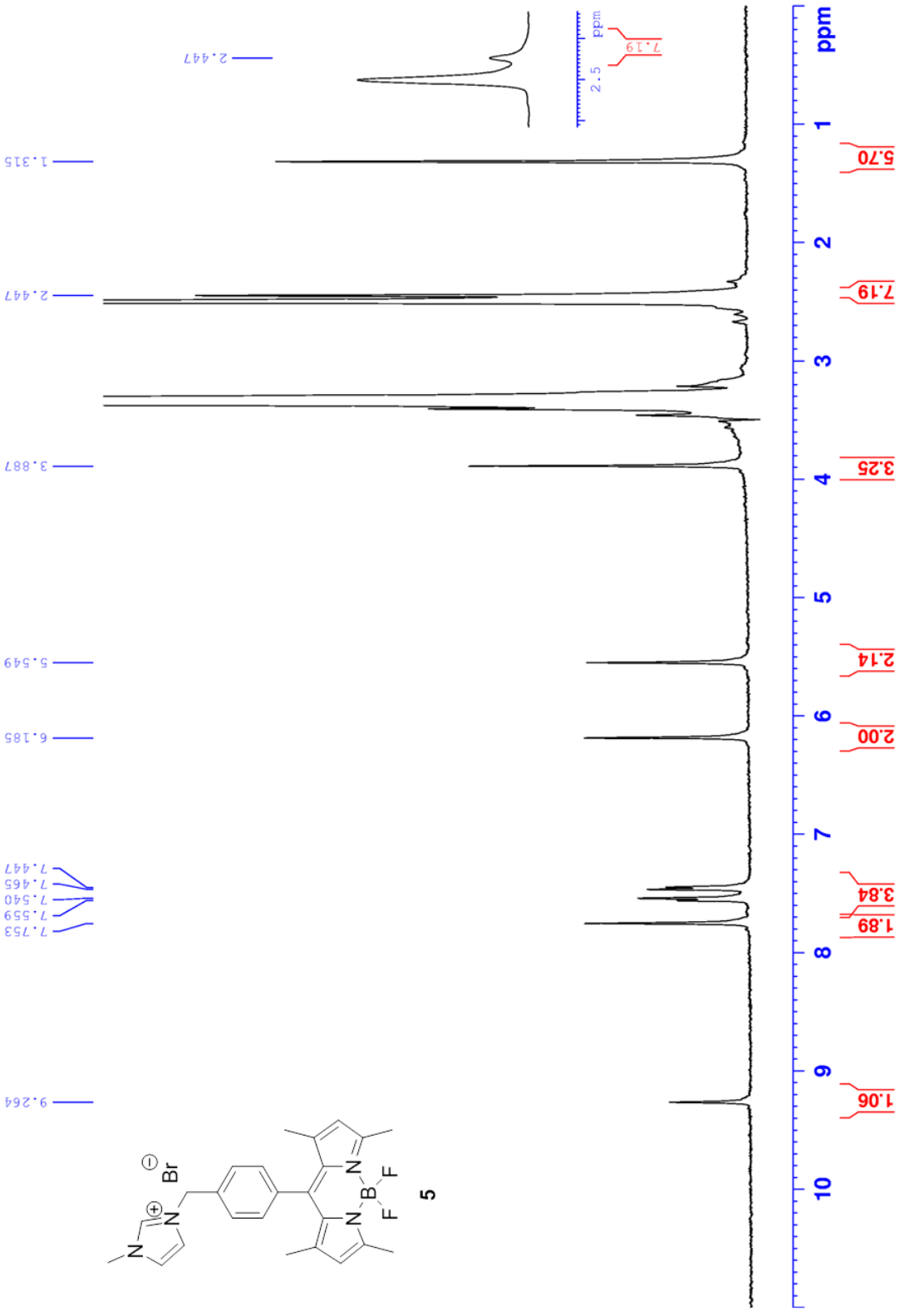

Figure S4.11. ^{13}C NMR spectrum of **5** (100 MHz, DMSO-d6).

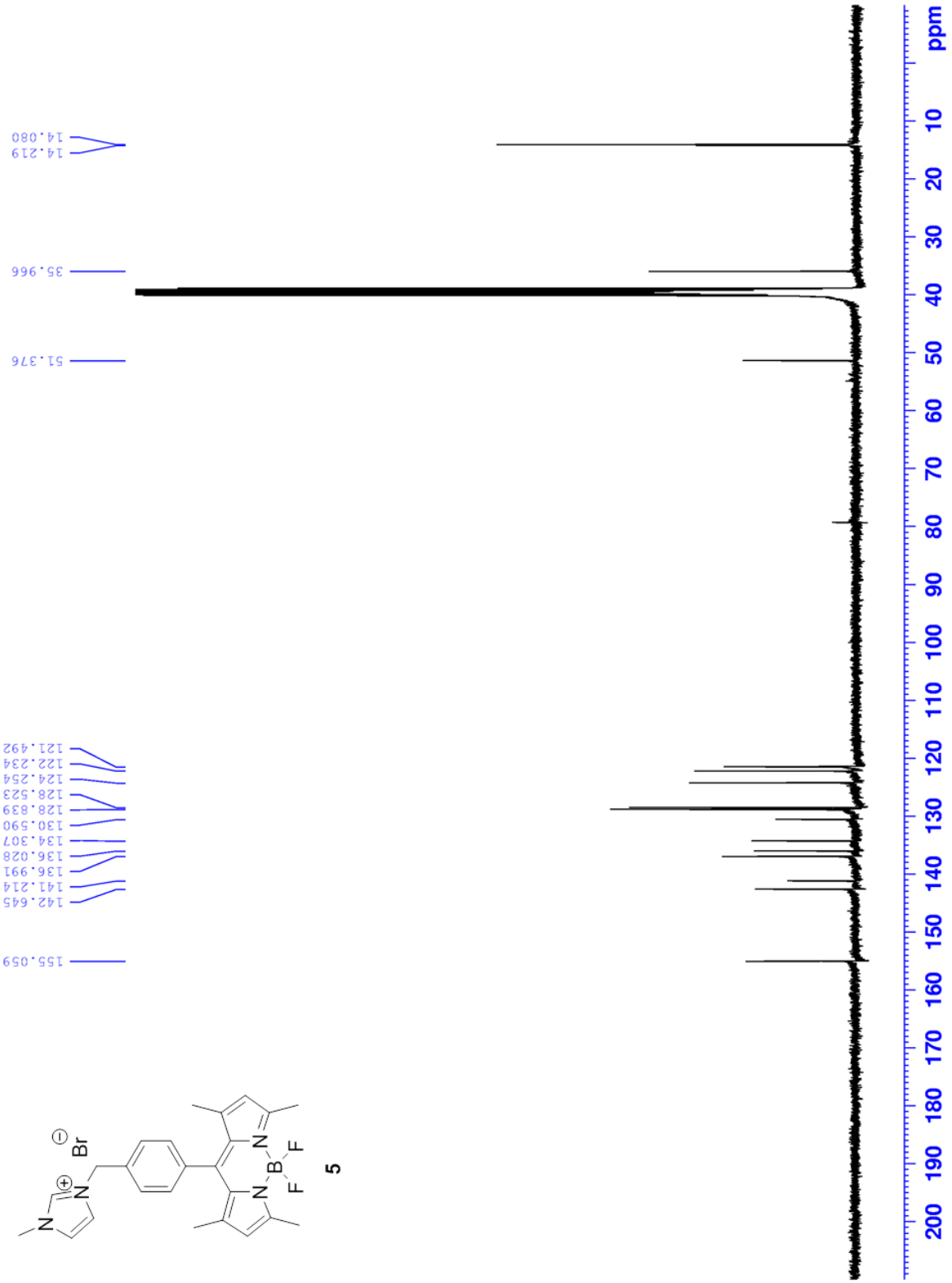

Figure S4.12. ^{1}H NMR spectrum of **13** (400 MHz, $CDCl_3$).

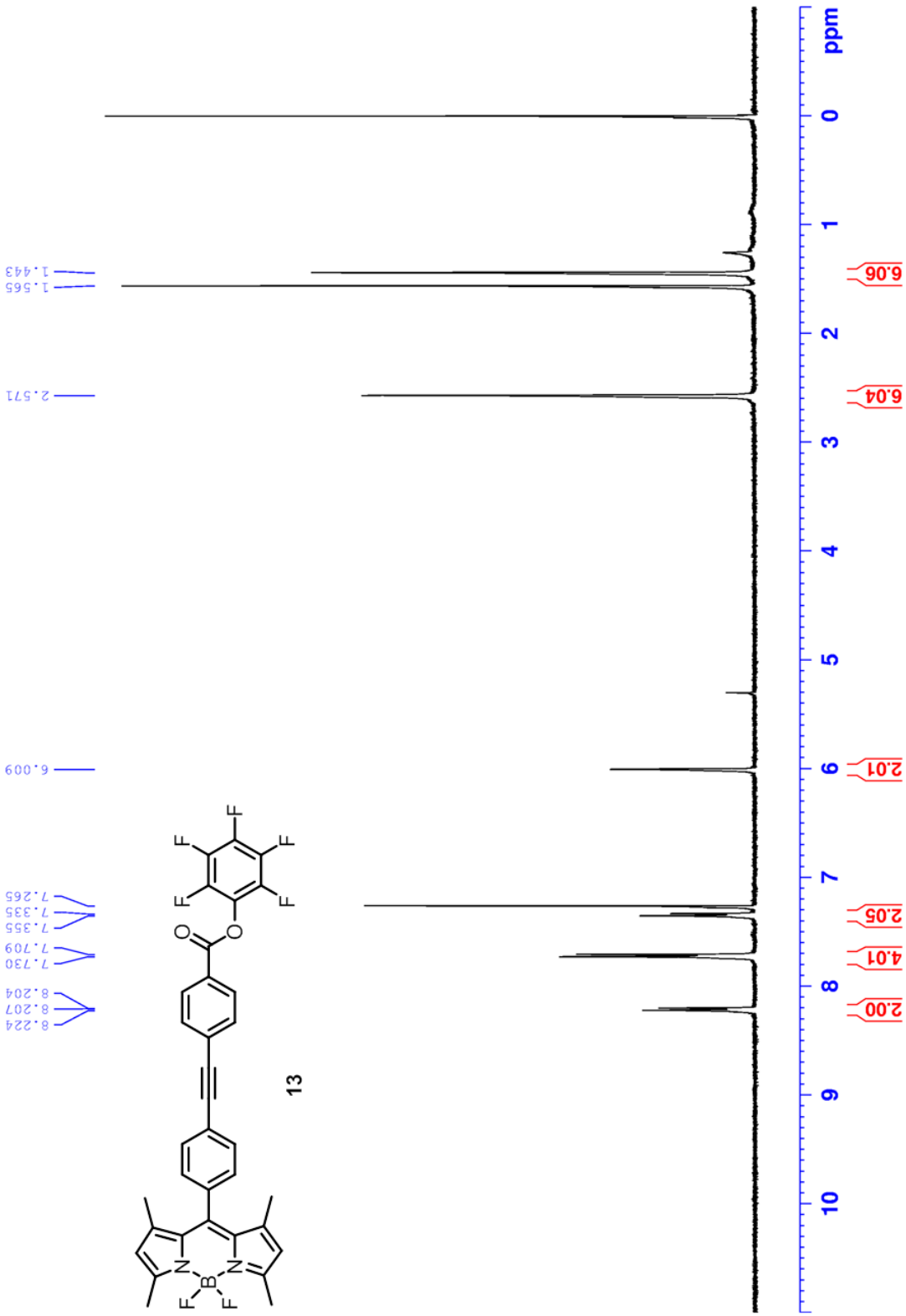

Figure S4.13. ^{13}C NMR spectrum of **13** (125 MHz, $CDCl_3$).

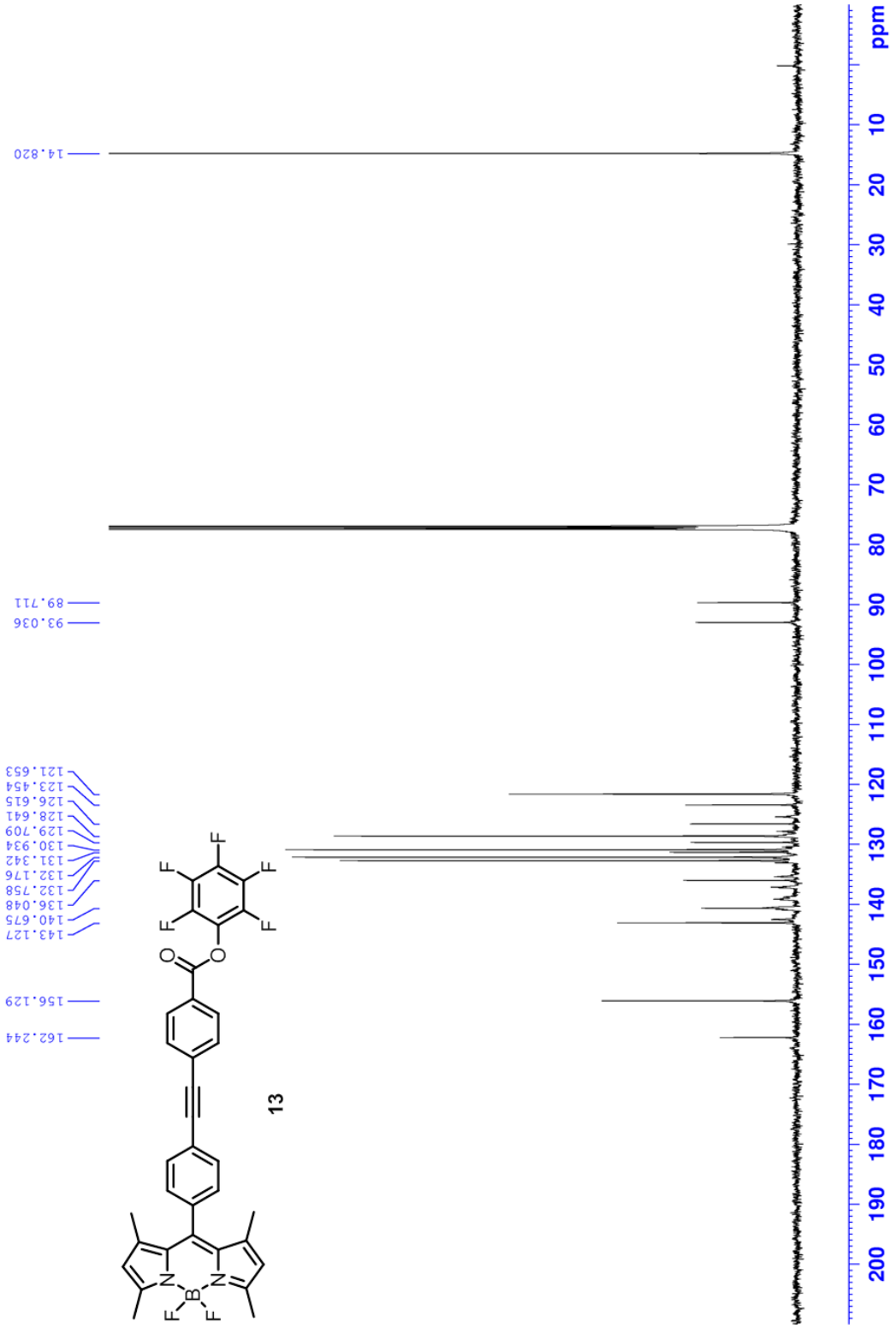

Figure S4.14. ^{1}H NMR spectrum of **12** (500 MHz, CD_2Cl_2).

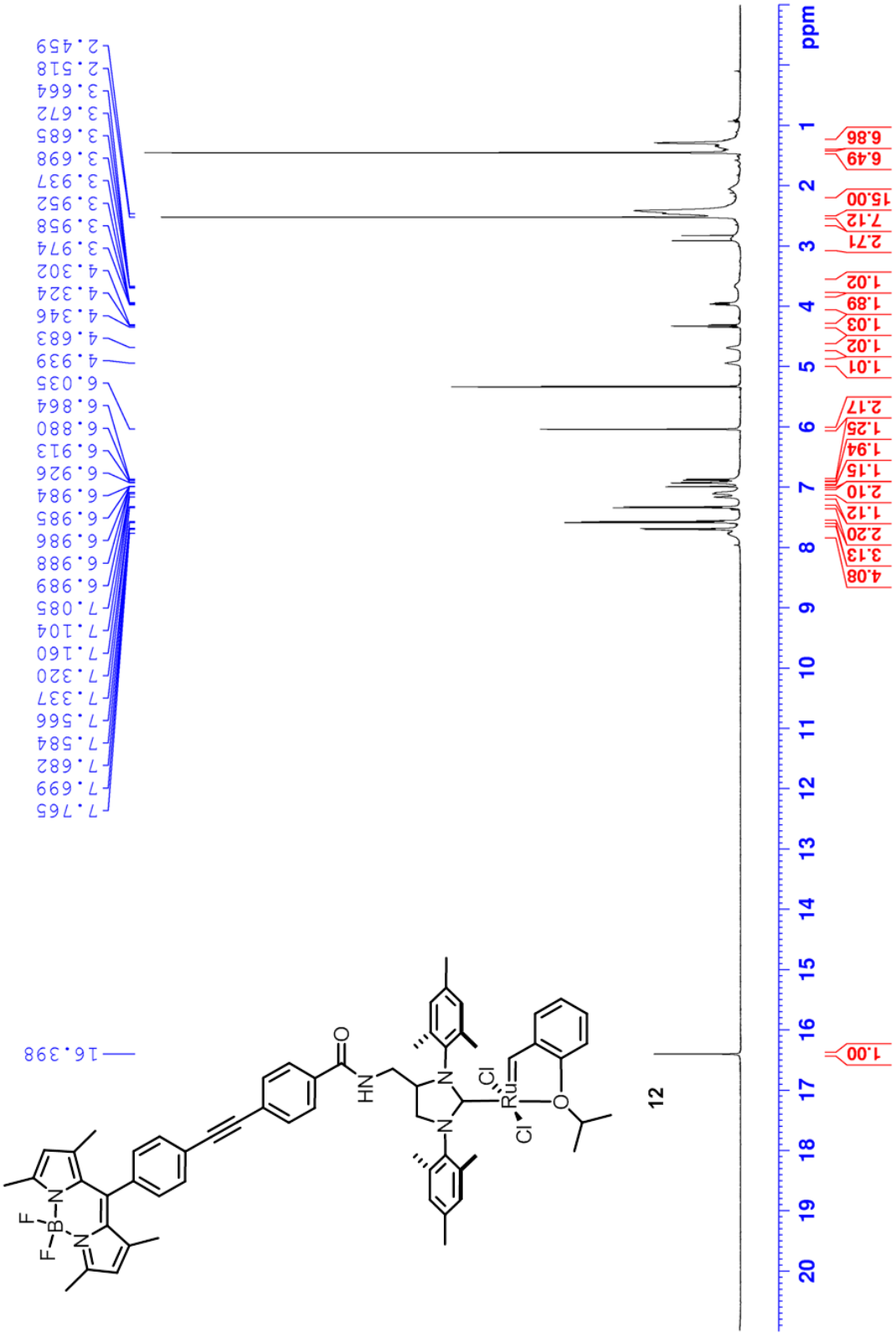

Figure S4.15. Amplification of 1 of ^{1}H NMR spectrum of **12** (500 MHz, CD_2Cl_2).

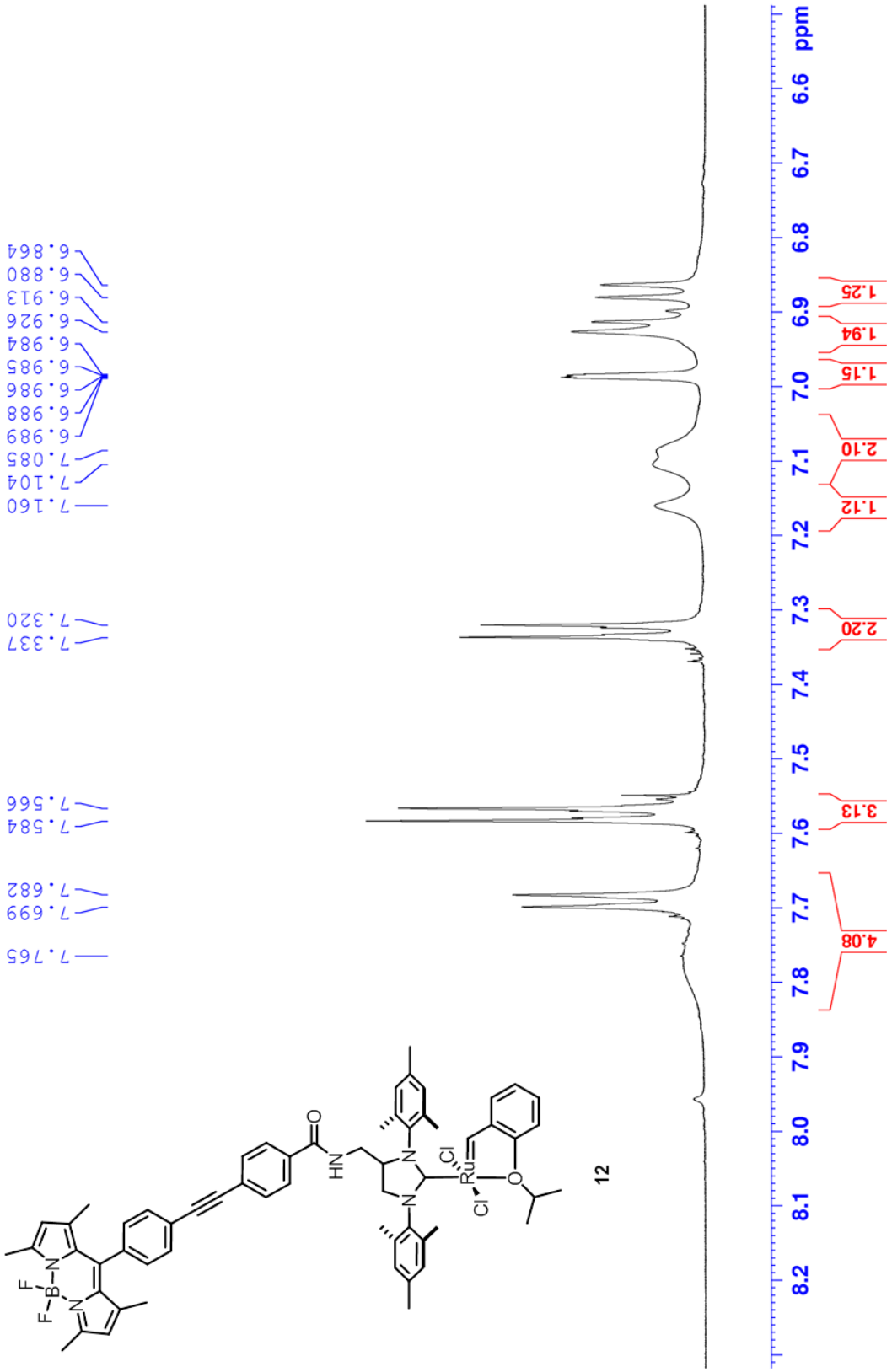

Figure S4.16. Amplification 2 of ^{1}H NMR spectrum of **12** (500 MHz, CD_2Cl_2).

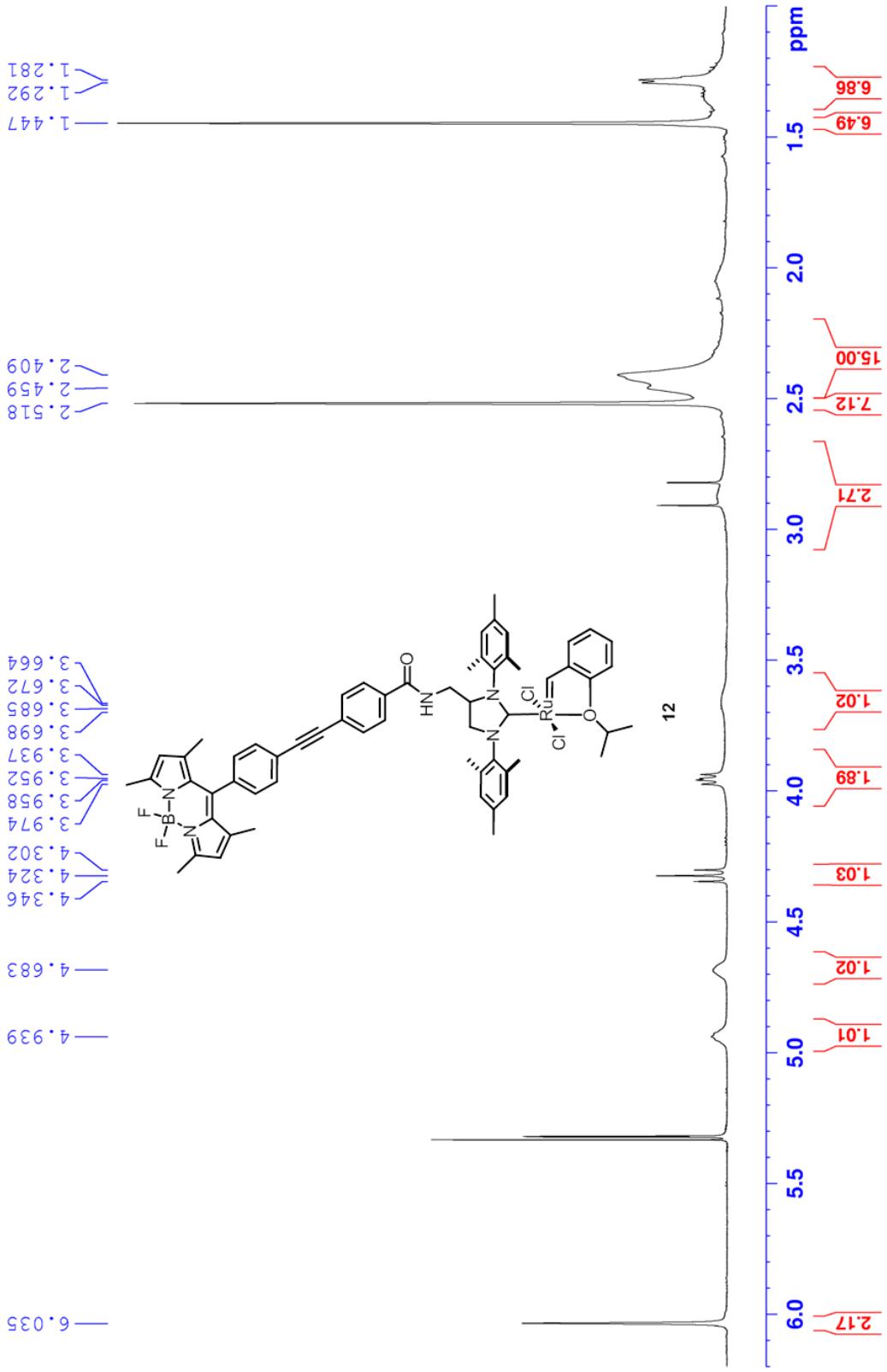

Figure S4.17. ^{13}C NMR spectrum of **12** (125 MHz, CD_2Cl_2).

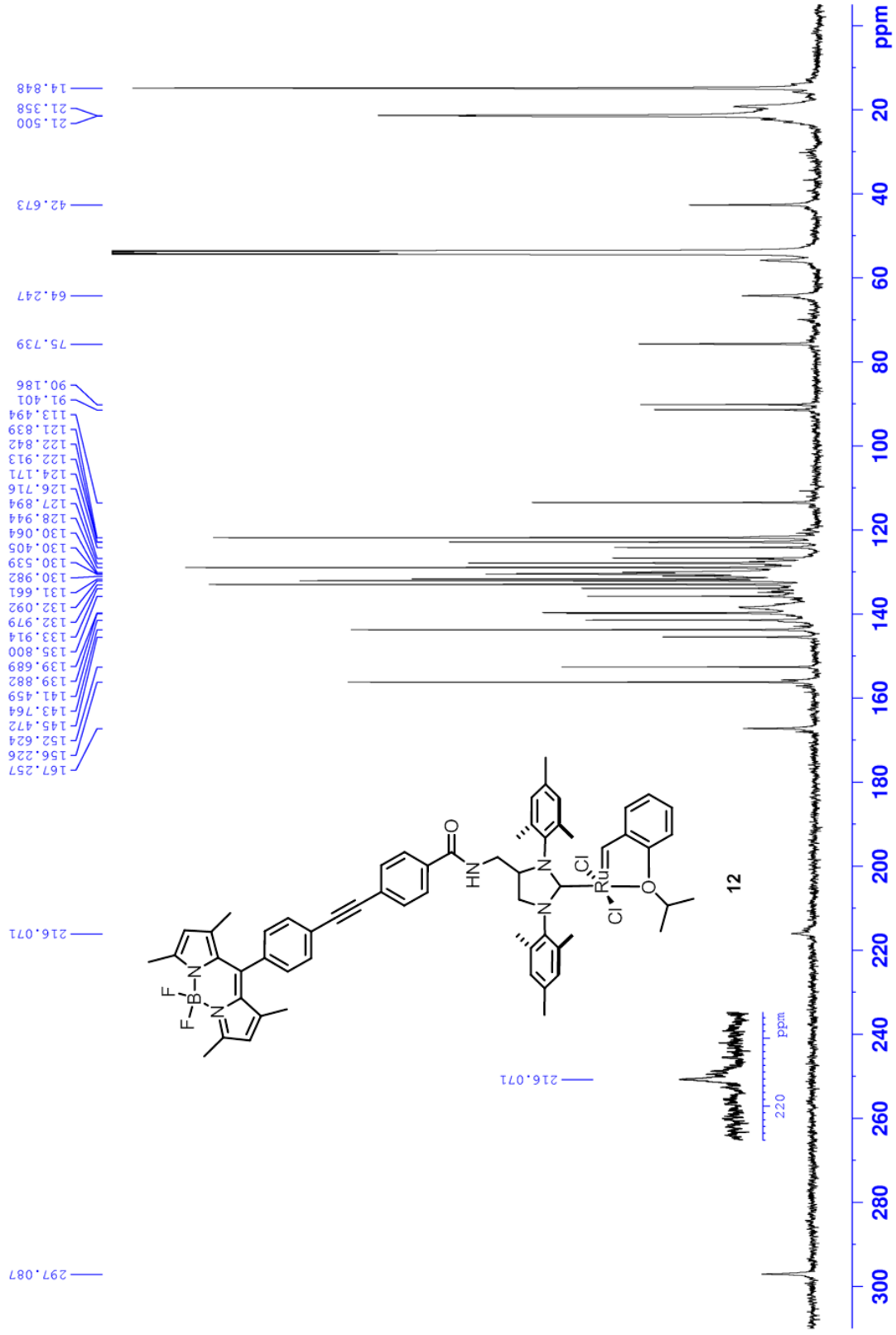

Figure S4.18. Amplification of ^{13}C NMR spectrum of **12** (125 MHz, CD_2Cl_2).